

Engineering Living Biomedical Devices

Mathematical and experimental tools for the rational design of cellular devices

Eva Gonzalez Flo

TESI DOCTORAL UPF / ANY 2020

Supervisor de la Tesi

Dr. Javier Macia Santamaria

Departament de Ciències Experimentals i de La Salut



Universitat
Pompeu Fabra
Barcelona

*“Success is a journey, not a destination.
The doing is often more important than the outcome.”*

— Arthur Ashe

ACKNOWLEDGEMENTS

Summarizing in a PhD dissertation three years of research, knowledge, personal and scientific challenges, efforts and struggle is not so easy. This had been a short but exciting period of my life. However, all started when I was in the last year of my bachelor degree when I discovered during my practicum in the Cell Signalling Research Group that I would like myself to combine experimental and computational tools to bring synthetic biology closer to society. However, at that time I couldn't have imagined that this decision would be accompanied by the starting of a new *lab: The Synthetic Biology for Biomedical Applications Lab*. Altogether, bringing the opportunity to start a lab from scratch, being involved in several research projects, teaching duties... that in turn allowed me to work closely with great professionals letting me grow professionally and personally. The following lines are just a small piece of gratitude to all of them.

Javier, supervisor, mentor, professor, company de *pyata* i psicòleg de tant en tant. Gràcies per donar-me l'oportunitat d'embarcar-nos en la bogeria d'un nou grup, per la confiança, la paciència i els aprenentatges durant tots aquests anys. També voldria tenir unes paraules pels prof. Francesc Posas i la prof. Laia de Nadal. Em van donar la confiança d'iniciar-me al laboratori quan encara era estudiant i tenia molt pocs coneixements sobre el món experimental i després hem seguit col·laborant en diferents projectes durant el doctorat. Gràcies per totes les ensenyances i consells.

Anna i Danny, papa i mama, gràcies, gràcies i gràcies. Per estar-hi sempre. Pels consells, per les "bronques", per confiar més que jo en mi mateixa..., per tot el que m'heu ensenyat i em seguiu ensenyat. Perquè el que el resultat d'aquesta tesi és també gràcies a vosaltres.

Començar un doctorat arrencant un laboratori de 0 no és el més habitual, i tampoc ho és ser l'única integrant d'un grup, però durant aquests anys el grup ha començat a créixer i ara escriure una dedicatòria es converteix en una feina més senzilla. La primera a incorporar-se va ser la *Sira*, qui va passar de ser l'estudiant que volia convertir-se en enginyera a ser la companya de *pyata* treballadora, confident i amiga: resumint el tàndem perfecte: *Zipi-Zape*. També una especial menció cap en Carlos, Marc grans compis de lab, de reflexions i de llargues tardes de feina i en Miquel i la Cristina pel seu suport tècnic i moral. Als nens, alguns dels estudiants en pràctiques que m'han deixat ensenyar-los com és el dia a dia del laboratori i que ara segueixen amb les seves carreres científiques i els hi desitjo els millors dels èxits: l'Èlia, el Nico, l'Elisenda Marta i l'Adrià. Ells també m'han ensenyat que la ciència va més enllà del treball diari a la *pyata* i que ensenyar és un art! Laia, Montse sense vosaltres el camí hagués estat mot diferent, us ho ben asseguro! Gràcies per ser-hi sempre, en els moments bons i en els dolents, pel vostre suport incondicional i els innumerables consells... Per ser el meu referent i acompanyar-me en aquest camí de la ciència des que era la millor becària que heu tingut. Arturo, gràcies per ensenyar-me com defensar-me al Lab per inculcar-me l'esperit crític i perfeccionista i... per aquells consells pre-PhD.

Podria dir que aquest doctorat no hauria sigut el mateix sense els meus *igemitas*. Vaig tenir el plaer de ser *advisor* de l'equip IGEM UPF-CRG2018. Van ser pràcticament dos anys molt intensos de treball científic però també de desenvolupament personal. Aquells que van ser prop meu saben que va ser una experiència dura, d'entrega al 100% però que ara, vist amb perspectiva va valer moltíssim la pena. Aquesta experiència em va ajudar a créixer molt científicament, però sobretot em quedo amb l'entusiasme, l'esforç, perseverança i lluita que em van desprendre els meus *nens*. Durant aquesta etapa també vaig tenir el plaer de poder treballar i aprendre de grans professionals. Gràcies Regina pel teu suport. M'agradaria fer especial èmfasi a les *iGEM Girls*. El vincle que es va crear és especial i únic, i allà on sigueu del món seguint la vostra carrera científica sabem que ens tenim les unes a les altres. També volia dedicar unes paraules als *compis* de vòlei: la Mar, la Paula, el Francesc i la Mònica. Ens haurem quedat sense trofeu, però hem passat molt bones i terapèutiques tardes a la platja! Agrair també als companys de passadís, especialment la Marta, el Marc i als Posas, que encara que hagueu marxat a l'IRB vam compartir moltes hores i records... i als integrants del programa *Systems Bionegineering* per les seves reflexions científiques i els bons moments durant tots aquests anys. També volia tenir un record pels membres del Complex System Lab, amb ells hi vaig passar molts estius quan estava a la carrera, i ... tenen part de culpa que ara estigui escrivint aquesta tesi, aprendre d'ells va ser un honor. Finalment agrair a la petita comunitat de predocs que arran dels *Docs en Lluita* s'ha creat: l'anti-retreat, les beersessions, festes de vòlei... sempre posant el toc de festa.

I també un etern GRÀCIES als meus amics. Aquells qui han hagut de patir les innumerables xerrades de ciència, els mals dies i les frustracions, però que han estat allà sempre i m'han ajudat a relativitzar la vida fora del lab: a les incondicionals de Masnou i als Charlies gràcies per formar també part d'aquesta aventura!

Agrair el finançament rebut per la Generalitat de Catalunya, que ha permès durant tres anys que em desenvolupes en l'àmbit de la recerca i de la docència.

Finalment volia donar les gràcies a l'Alexis, un petit gran artista, i al Jordi, per la portada d'aquesta tesi. Un toc artístic i original per posar el punt final d'aquesta etapa. GRÀCIES!

Dedicació, constància, esforç, frustració, capacitat de superació però sobretot esperit crític i reflexiu, humilitat, ganes d'aprendre diàriament i companyonia podrien ser les paraules que defineixen aquesta etapa. Resumir tres anys de recerca que posen punt final a la llarga etapa d'estudiant ha estat en si mateix una nova muntanya russa, com podria descriure aquests tres anys de tesi. Aquestes breus línies i reflexions, com bé una part dels capítols que trobareu a continuació han brollat des del confinament per la Covid-19; mentre el món quedava paralitzat per una pandèmia mundial.

ABSTRACT

The engineering of biology strives on the creation of biological devices concerning society-impact applications. In this PhD thesis, we developed mathematical and experimental tools for the standard and rational design of living devices for biomedical purposes, offering robust and reliable responses. By breaking-up cellular device complexity into functional modules, we have analysed how extracellular information is detected, processed and transformed thanks to re-engineering intrinsic cellular components. We show how the desired range of action of a biosensor could be tuned by modifying the relative levels from two-component receptors' biosensors. Regarding information processing, combining multicellularity and space permits to develop a 2D multi-branch approach inspired from printed electronics, allowing to perform logic computation by transferring device complexity into the geometrical arrangement. Sensing and processing capabilities have been applied as a *proof-of-concept* for the design of cellular devices for Diabetes Mellitus. Treating the cellular device closed-loop response as the fourth-functional module allowed to *in silico* decipher device characteristics on glycaemia regulation and design novel strategies based on dietary modulation, putting the manifest the need to combine both experimental and computational tools for living device application-based designs.

RESUM

L'aplicació de principis d'enginyeria en biologia permet somniar en l'ús de dispositius biològics per abordar problemes de la societat. Concretament, en aquesta tesi doctoral, s'ha abordat el disseny de dispositius biològics per aplicacions biomèdiques mitjançant la combinació d'eines experimentals i computacionals. La creació d'aquests dispositius demana d'un disseny racional que ofereixi respostes robustes i fiables. L'estudi de la creació de dispositius biològics s'ha fet seguint una aproximació modular, on s'ha analitzat com es poden re-enginyeritzar components cel·lulars per obtenir una resposta que s'adeqüi a l'aplicació requerida. Hem demostrat com podem modular el rang de detecció de la capa sensora a través de la modulació de l'element receptor de sensors bastats en dos components. Hem analitzat com integrar informació de diferents fonts de manera sistemàtica i robusta introduint com a nou element de computació l'espai i la divisió de tasques; tot desenvolupant un marc teòric i validant experimentalment per un seguit de funcions lògiques. Finalment, hem desenvolupat dispositius biològics que responen a molècules fisiològiques. Concretament, hem abordat el disseny de dispositius biològics pel tractament de la Diabetes Mellitus. Una primera validació experimental ens ha permès establir l'ús d'aquests dispositius *in vitro*. Seguidament, hem aprofundit en l'estudi de la seva aplicació mitjançant l'ús d'un simulador de pacient diabètic que ens ha permès el seu tractament virtual i l'anàlisi de les característiques del dispositiu per la regulació de la glicèmia. Finalment, hem explorat com la combinació dels dispositius cel·lulars amb la regulació del patró d'ingestes introdueix millores en els nivells de glucosa en sang. Posant de manifest el potencial que ofereix la creació d'una plataforma híbrida pel disseny de dispositius cel·lulars per una determinada aplicació.

PREFACE

Biological organisms are systems with highly sophisticated information processing tools. Evolution has endowed the ability to sense, process and respond to stressor signals and thus, to survive into a world plenty of information. The magic behind those processes relies on biological reactions involving genes, proteins, chemicals... Analogously, technology has translated and emulated those processes in electronic circuits to create devices developing complex computations foreseeing making our lives easier. Technological advances are also relevant in healthcare and endorsed to develop novel strategies centred on patients' needs and personalized medicine. Biomedical engineering and more specifically the development of biomedical devices allowed to bring healthcare outside hospitals, closer to the patients. However, limitations arouse when developing electronic sensors facilitating the detection of disease markers. The use of biological components, from an engineering point of view, has postulated to be integrated into such devices, giving rise to living technologies.

By following a modular approach, a living device could be seen as the combination of four-functional layers: i) the sensing layer, ii) the signal integration and computation layer, iii) the physiological output and iv) the closed-loop response. In this PhD thesis, we have developed strategies enabling the creation of rational, robust, automated and scalable ways for designing living biomedical devices, by combining mathematical and experimental tools, following the *design-build-test* cycle.

After an introductory chapter emphasising the brief but intense story of synthetic biology and how applying engineering principles to biology enables to strive on the creation of biological devices concerning society-impact biomedical applications, the following chapters are devoted to a deep exploration of the abovementioned four-functional layers defining a living device. *In chapter 2* we have analysed how we could benefit from the cellular ability to detect extracellular signals and developed a theoretical framework allowing the rational design of sensors characteristics for desired-based applications. *In chapter 3* we have analysed how sensorial information can be integrated to produce non-trivial responses. More specifically we took inspiration from printed electronics to design devices with the ability to perform logic computations. *In chapter 4* we have developed

a *proof-of-principle*, using *S. cerevisiae* as a model organism, of a cellular device for Diabetes Mellitus biomedical application. Extracellular glucose levels were sensed to stimulate the secretion of insulin hormone in a non-trivial dynamic, i.e. a time-pulsatile dynamic.

Nonetheless, designing a living biomedical device for a desired application demands its contextualization. To do so, in the case of biomedical applications, the tools offered from the field of systems biology are extremely useful. In chapter 5 a validated *in silico* platform allowed to test a living biomedical device closed-loop performance for Diabetes Mellitus treatment. We have explored the potential of using cellular devices engineered with a constitutive or glucose-dependent insulin production to regulate glycaemia in a diabetic virtual patient. The *in silico* studies showed that although postulating that a glucose-regulated insulin secretion device should account for a better glycaemia regulation, a time delay in insulin secretion compromises its performance. Hence, stressing the requirement of closed-loop analysis when designing cellular biomedical devices. On that line, an *in silico* platform was developed to explore a feed restriction strategy to overcome the lag-time of insulin secretion.

Our *in silico* analysis highlights the need of device contextualization for the translation of basic research towards society-need applications. Much is done in *SB* for the creation of devices with the ability to sense a wide range of signals: from pollutants to physiological markers or to integrate multiple signals in either analogue or digital circuits. However, despite the far-reaching potential of such devices, its implementation for specific applications is still a major challenge for the field.

The present PhD thesis has tested a diversity of model organisms that together with mathematical approaches served as a *proof-of-principle* platform for designing and building living biomedical devices. Hereby, our results represent a step forward on the rational design of robust, reliable and standard devices accounting for biomedical applications in line with the principles of the engineering of biology.

TABLE OF CONTENTS

ACKNOWLEDGEMENTS	iii
ABSTRACT	v
RESUM	vii
PREFACE	ix
TABLE OF CONTENTS	xi
LIST OF FIGURES	xiii
LIST OF TABLES	xvii
1 INTRODUCTION	3
1.1 Synthetic Biology brief story	3
1.2 The engineering of biology	11
1.3 Synthetic Biology Applications	17
1.4 Potential risks of Synthetic Biology	20
1.5 Living technologies and theranostics	21
1.6 Thesis Objectives	24
1.7 Thesis outline	27
2 TOOLS FOR SENSOR MODULE DESIGN	31
2.1 Applying engineering principles to cellular sensors	31
2.2 Objectives	39
2.3 Biosensor mathematical formalization based on two-component architecture	40
2.4 Model parameters determination	48
2.5 Predictive design of two-component biosensors	51
2.6 Dependence of sensitivity and operating range on receptor abundance ..	55
2.7 Experimental validation of the operating range	58
2.8 Discussion	60
2.9 Methodology	62
3 TOOLS FOR SIGNAL PROCESSOR MODULE DESIGN	71
3.1 Principles of cellular computation	71
3.2 Objectives	79
3.3 Design of a transistor-like modules	80
3.4 Design and characterization of a 2D surface	82
3.5 Transistor-like device for CS modulation	86
3.6 Logic computation based on a multi-branch topology	87
3.7 Experimental validation of two-inputs multi-branch topology	91
3.8 Discussion	93
3.9 Methodology	95

4	LIVING BIOMEDICAL DEVICE WITH TIME-DEPENDENT RESPONSES	103
4.1	Analyse responses for biomedical applications	103
4.2	Objectives	105
4.3	The use of hexose transporter promoters serves to create cells able to detect and respond to different extracellular glucose levels.....	106
4.4	Implementation of different minimal circuits to produce hormones in a glucose-dependent manner.	111
4.5	The affinity and sensitivity of circuits can be tuned by modulating extracellular wiring molecule levels	116
4.6	Implementation of a time-dependent single pulse behaviour by multicellular consortia.	124
4.7	Discussion.....	130
4.8	Methodology.....	132
5	DECIPHERING LIVING DEVICE CLOSED-LOOP PERFORMANCE	141
5.1	Cellular devices for Diabetes Mellitus treatment	141
5.2	Objectives	145
5.3	The virtual organism: Glucose insulin meal simulator.....	146
5.4	Experimental construction and characterization of cellular devices for insulin production	147
5.5	3D space definition for Diabetes Mellitus diagnosis criteria	155
5.6	<i>In silico</i> analysis of cellular implants in T1DM patients.....	161
5.7	<i>In silico</i> daily life meal ingestion simulations	170
5.8	Time Restriction Feed for glycaemia optimization	172
5.9	Discussion.....	180
6	DISCUSSION AND CONCLUSIONS	185
6.1	Living biomedical devices from intrinsic cellular components.....	185
6.2	<i>In silico</i> closed-loop living biomedical device performance.....	190
6.3	Final considerations	191
6.4	Main research findings	193
	SCIENTIFIC PUBLICATIONS	195
	BIBLIOGRAPHY	197
	ANNEX	233
	A. Two-component biosensors: unveiling the mechanisms of predictable tunability	233
	B. 2D BioPrintable Computational Circuits: modular topology for digital computation.	240

LIST OF FIGURES

Chapter 1	3
Figure 1.1 Synthetic biology number of publications per year since 1980 up to date.....	3
Figure 1.2 Bottom-up and top-down approaches for the disciplines of synthetic biology and systems biology.	4
Figure 1.3 <i>Negative feedback</i> , <i>repressilator</i> and <i>toggle switch</i> analysis of main device design characteristics.	5
Figure 1.4 Design-build-test cycle for synthetic biology.....	6
Figure 1.5 Synthetic biology engineering principles..	12
Figure 1.6 Design and modelling approach for systems biology and synthetic biology disciplines..	16
Figure 1.7 Living biomedical device modular approach..	22
Chapter 2	31
Figure 2.1 Schematically representation of the two-layered architecture of the sensor module.	32
Figure 2.2 Biosensor Transfer Function.	34
Figure 2.3 Two-component sensor.....	35
Figure 2.4 Biologic mechanisms to tune transfer functions features.	37
Figure 2.5 Schematic representation of two-component biosensor architecture..	40
Figure 2.6 Experimentally measured transfer functions of biosensors with different abundances of LuxR.	49
Figure 2.7 Model parameters <i>a</i> and <i>b</i> fitting.....	50
Figure 2.8 Relative promoters' strength characterization.	52
Figure 2.9 Model predictions of LuxR-dependent transfer functions.....	54
Figure 2.10 Mathematical determination of the biosensor operating range..	55
Figure 2.11 Mathematical determination of the biosensor operating range..	59
Chapter 3	71
Figure 3.1. Digital and analogue computation.	72
Figure 3.2 Processor computation based on different biological-elements.....	74
Figure 3.3 Processor computation based on different biological-elements.	75
Figure 3.4 Processor computation based on different biological-elements.	76
Figure 3.5 Processor computation based on different biological-elements.	78
Figure 3.6 Schematically representation of a transistor-like architecture.....	81
Figure 3.7 Cellular growth monitoring from RFP expression levels in the 2D surface..	83
Figure 3.8 <i>CS</i> diffusion profile trough the 2D surface.	84
Figure 3.9. <i>3OC6HSL</i> diffusion profile characterization.....	85
Figure 3.10 Experimental setup of a transistor-like circuit.....	86
Figure 3.11 Transistor-like device for <i>3OC6HSL</i> modulation.....	87
Figure 3.12 Multi-branch approximation for logic computation.	89
Figure 3.13 Relationship between the number of logic functions and topological complexity... ..	90
Figure 3.14 Experimental implementation of logic gates based on the multi-branch approach.. ..	92
Figure 3.15 Graphical representation of the Φ measurements obtained from the fluorescence surface scan.	100

Chapter 4

103

Figure 4.1 Schematically representation of the multicellular device comprising three layers. .	106
Figure 4.2 <i>a-factor</i> pheromone pathway.....	107
Figure 4.3 Design and characterization of glucose sensor cells.	109
Figure 4.4 Design and characterization of glucose sensor cells.	111
Figure 4.5 Characterization of output cells.....	112
Figure 4.6 Response of the effector cells in the alternate presence or absence the wiring molecule..	113
Figure 4.7 Design and implementation of multicellular consortia for glucose-responsive devices..	114
Figure 4.8 Design and implementation of multicellular consortia for glucose-responsive devices..	115
Figure 4.9 Mathematical model fitting	119
Figure 4.10 Fine-tune of <i>HIGH- glucose-consortium</i>	121
Figure 4.11 Fine-tune of a circuit's sensitivity	123
Figure 4.12 Fine-tune of a circuit's affinity.....	124
Figure 4.13 Single pulse dynamics in multicellular circuits.	126
Figure 4.14 Characterization of <i>HIGH-αCa</i> cell type and the <i>Modulator</i> cell.	127
Figure 4.15 Characterization of different elements in a circuit with a feed forward loop to generate a single pulse response..	130

Chapter 5

141

Figure 5.1 Historical evolution of diabetes management milestones.	142
Figure 5.2 Schematically representation of the Glucose-insulin meal simulator.	146
Figure 5.3 Schematically representation of a cellular device implanted in the organism simulator..	148
Figure 5.4 Schematically representation of insulin expression living devices.	150
Figure 5.5 Glucose-dependent SEAP expression of TXNIP-rINS6-SEAP cells. a) Glucose-dependent kinetics at different glucose concentrations. Cell cultures w.....	152
Figure 5.6 rINS6 mRNA dynamics measured with Real Time RT-PCR.	153
Figure 5.7 Insulin expression profiles for CMVp-rINS6 and TXNIPp-rINS6 cells.....	154
Figure 5.8 3-dimensional space for Fasting Glycaemia Test, Oral glucose Tolerance Test and Random Glucose Test.	157
Figure 5.9 3-dimensional space for Fasting Glycaemia Test, Oral glucose Tolerance Test and Random glucose Test.	158
Figure 5.10 3-dimensional space for <i>xy</i> -plane and virtual patient <i>p</i>	160
Figure 5.11 Plasma glucose levels for T1DM patients with different implants sizes constitutively producing insulin.	164
Figure 5.12 Evolution of glycaemic regulation based on constitutive insulin producer implants versus implant size.	165
Figure 5.13 Dependence between plasma glucose and insulin with implant size..	166
Figure 5.14 Dependence between plasma glucose levels with different implant sizes of glucose-dependent producer cells.	168
Figure 5.15 Evolution of glycaemic regulation based on glucose-dependent insulin producer implants versus implant size.	169
Figure 5.16 Dependence between plasma glucose and insulin with implant size..	170
Figure 5.17 Three meal ingestion plasma glucose and insulin levels with respect to implant size..	171
Figure 5.18 Schematically representation of the Evolutionary Algorithm procedure for time restriction feed optimization.....	173
Figure 5.19 Maximum and minimum plasma glucose levels evolution during algorithm iterations.	176

Figure 5.20 Plasma glucose levels for random and optimized feeding patterns..... 177
Figure 5.21 Glycaemia evolution applying glucose-dependent implant TRF-optimized pattern..
..... 178
Figure 5.22 Glycaemia evolution applying glucose-dependent implant TRF-optimized pattern for
three days..... 179

Annex **233**

Figure A. 1 Temporal evolution of the optical density OD. 239

LIST OF TABLES

Chapter 1	3
Table 1.1 Synthetic biology examples	10
Chapter 2	31
Table 2.1 Output readable proteins.....	33
Table 2.2 Theoretical and experimentally obtained R_T values associated with $K_{0.5}$ values.....	53
Table 2.3 Biobricks used in this study.	63
Table 2.4. Biosensors' genetic constructs.....	65
Table 2.5 Controls' genetic constructs.....	66
Table 2.6 Parameters used to fit the experimental biosensor transfer functions.....	68
Chapter 3	71
Table 3.1 Biobricks used in this study.	97
Table 3.2 Transistor-like modules genetic constructs.....	99
Chapter 4	103
Table 4.1 Model parameters for Sensor Cells.....	119
Table 4.2 Model parameters for Effector Cells.....	120
Table 4.3 Yeast strains used in this study.. ..	134
Chapter 5	141
Table 5.1 Model parameters.....	155
Table 5.2 Glucose test for T1DM diagnosis.. ..	155
Annex	233
Table A. 1 Genetic parts DNA sequence.	235
Table A. 2 Plasmid maps.	238
Table A. 3 Genetic parts DNA sequence.	243
Table A. 4 Plasmid maps.	244

CHAPTER 1

Introduction

Technology and life sciences are fields in rapid and constant evolution with envisioned shared objectives: trying to make life easier. First results could be seen in the area of biomedical devices, which emphasizes the synergies between them. Engineering technologies are disciplines with application-based design. In that sense, when thinking of combining engineering and technology with biology could sound too ambitious. However, since the beginning of the 2000, a new discipline arouses merging the profiles of physicists, mathematicians, engineers and biologists. Adding the knowledge on the biomedical sciences together with an engineering based-design approach allows fantasizing solving today's major challenges of modern medicine, namely, cancer or metabolic problems, among others, contributing a large list. The present PhD dissertation envisions to explore the ability of biological engineering approaches to strive on the creation of biological devices concerning society-impact biomedical applications. A modular methodology is tackled by studying intrinsic device properties and tangible device performance in an *in silico* biomedical application. As a case study, we would explore one society major challenge; glucose metabolism impairment. More concretely, we would explore the creation of biological devices following a synthetic biology approach.

Synthetic biology stands as a novel discipline with well-established roots envisioning today's biomedical challenges. During the following chapters, I would like to strengthen how synthetic biology and its engineering principles could be applied to design novel strategies upon biological devices. More specifically I would like to give insights and push a step forward on the design of biological devices by a combination of experimental knowledge and computational tools. Subsequent lines are encompassed on relating major aspects on synthetic biology as well as the engineering approaches governing the field.

1 INTRODUCTION

1.1 Synthetic Biology brief story

Synthetic Biology (SB) is a 21st century recent emerging discipline, still in its early years, in a constant change and evolution. As depicted in Figure 1.1, SB has reached a rapid increase in the number of publications from the year 2004.

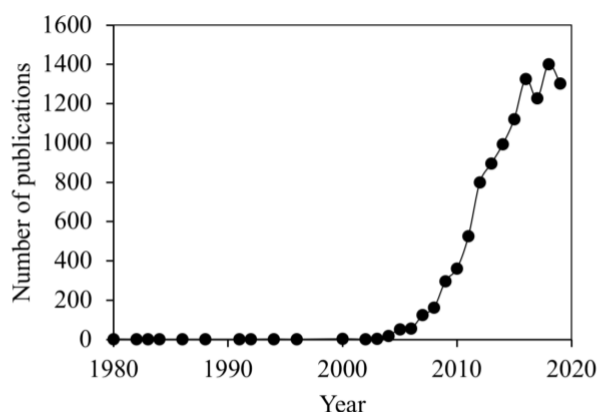


Figure 1.1 Synthetic biology number of publications per year since 1980 up to date. Data was obtained from Scopus Website in January 2020.

Although finding a general and accepted formal definition for SB remains a challenge [Jefferson et al., 2014; Landrain et al., 2013; Purnick & Weiss, 2009], it is feasible to find some common concepts in the broad spectrum of definitions, namely *DESIGN*, *CONSTRUCTION*, *NEW*, *NOVEL*, *DEVICES*, *ENGINEERING OF BIOLOGY*. Therefore, I would like to formalize a brief definition encompassing the present PhD thesis work. Synthetic biology discipline aims to apply engineering principles to tackle biological problems by designing or re-designing organisms with novel functionalities.

The emerging of the SB could not be explained without considering the technological advances concerning the biological science area of molecular biology. The discovery of the DNA sequence [Watson & Crick, 1953], the finding of natural genetic regulatory elements by Francois Jacob and Jacques Monod in 1961 [Monod & Jacob, 1961], together with the development of the first molecular cloning techniques during the 1970s-1980s,

could be understood as the elements enabling to establish the roots of SB. Technologies enable the growth of molecular biology promoting the emergence of systems biology. It was the first-time biologists and computer scientists began to combine experimentation and computation to reverse-engineer cellular networks [Ideker et al., 2001; Jeong et al., 2000; Westerhoff & Palsson, 2004]. First results indicate that biological systems were organized as modules comprising several hierarchies, similar to engineering designs. From that moment, it was thought, that a rational manipulation of biological systems could help to expand the field. From that, two main philosophies arose: the top-down approach of systems biology and the bottom-up approach envisioned for synthetic biologists.

Figure 1.2 represents the hierarchies approaching both systems and synthetic biology. Hereby, the systems biology approach goes from the smallest elements, e.g. DNA and proteins, into higher levels of organisation, giving insights into how organisms work. As stated in [Andrianantoandro et al., 2006] “Synthetic biologists design and construct complex artificial biological systems using many insights discovered by systems biologists and share their holistic perspective”. Both approaches are applied to study the functional organization of natural systems and to create artificial genetic circuits with high potential in biotechnology and health areas [Benner, 2003].



Figure 1.2 Bottom-up and top-down approaches for the disciplines of synthetic biology and systems biology. At the bottom of the pyramid are placed the smallest regulatory elements: DNA, RNA, proteins

and metabolites, circuits arouse as a combination of such biomolecules, which would configure or be integrated within cells, that together would configure tissues, organs up to the whole organism.

It was at the end of the 1990s, when a small group of engineers, physicists, and computer scientists began to migrate into molecular biology giving rise to the first synthetic genetic circuits that crash the field in the 2000s: the *negative feedback* by Becskel and Serrano [Becskel & Serrano, 2000] the *toggle switch* by Gardner *et al.* [Gardner et al., 2000], and *repressilator* by Elowitz and Leibler *et al.* [Elowitz & Leibler, 2000].

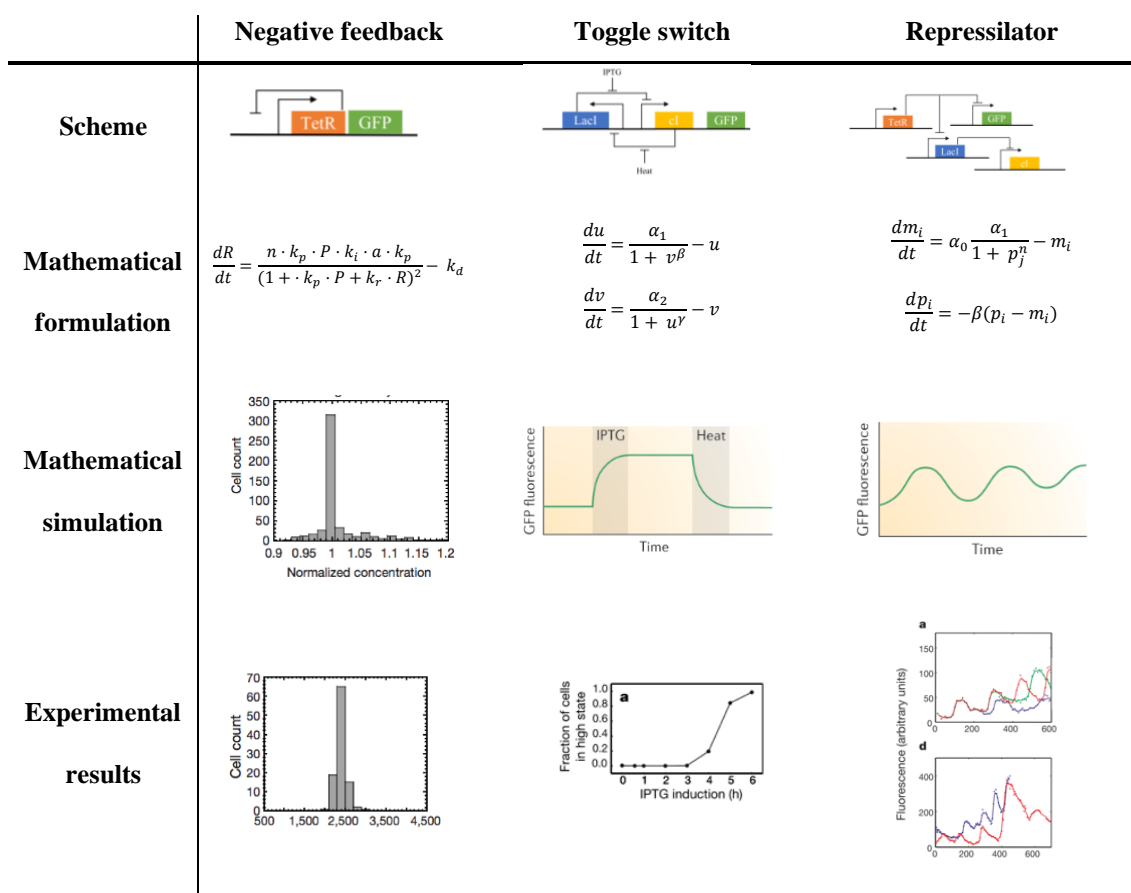


Figure 1.3 Negative feedback, repressilator and toggle switch analysis of main device design characteristics. Genetic circuits design is represented schematically by the combination of genes and proteins. The mathematical formalization of gene-protein interaction allowed to simulate and predict systems behaviour *in silico*. As a result, *E. coli* cells were engineered by the combination of characterized parts enabling to test systems behaviour *in vivo*. Extracted and adapted from [Becskel & Serrano, 2000], [Gardner et al., 2000] and [Elowitz & Leibler, 2000].

The first synthetic genetic circuits, as depicted in Figure 1.3, were designed following a very similar workflow. A mathematical formalization together with *in silico* simulations

allowed to define the architecture of the device followed by its translation into biological elements. Interestingly, designs were built from an analogous part library, i.e. protein-gene interaction by inducible promoter systems, monitor circuit's output with the expression of a fluorescent protein (e.g. Green Fluorescent Protein), and *E. coli* was used as a workhorse chassis. As a consequence of these seminal works the landmarks of SB were established: the philosophy behind the construction of synthetic organisms relies on the *design-build-test* workflow. As depicted in Figure 1.4 a combination of quantitative design, physical construction, experimental measurements, and hypothesis-driven debugging, remains as a characteristic feature of synthetic circuit construction [Hasty et al., 2001; Kærn et al., 2003].

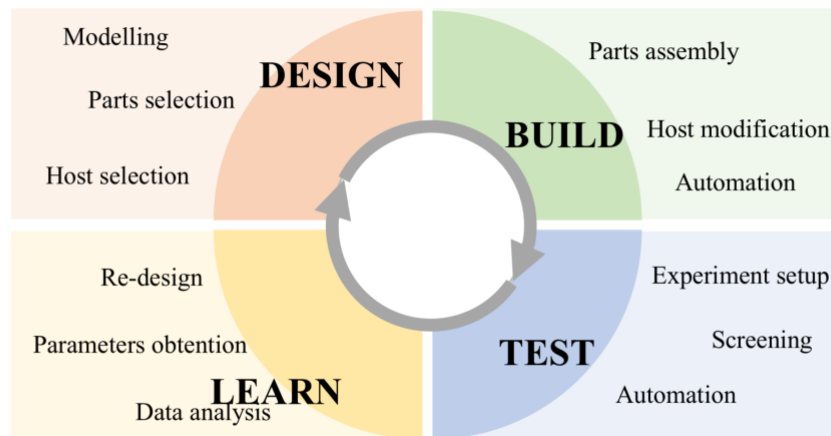


Figure 1.4 Design-build-test cycle for synthetic biology. A forth-step iterative workflow is depicted comprising a i) the design in terms of modelling and experimental characteristics, i.e. from genetic parts to model organism choice, ii) experimental assembly of genetic parts and host circuit integration is followed by iii) experimental test. From the experimental test phase knowledge is gained and enable to iv) learn in terms of model parameter obtention and desired device performance. Hence, re-designing from previous knowledge through iteration is followed until design behaviour satisfies researcher needs.

During the first years of birth, called the foundational years, several simple genetic circuits brought the light by being inspired from electronics, mimicking simple analogous functions based on electrical circuits [McAdams & Arkin, 2000; McAdams & Shapiro, 1995]. Remarkably are the first logic gates implemented by [Guet et al., 2002] combining

small regulatory elements that together with [R. Weiss et al., 2002] established the roots of transcriptional-based logic gates.

Noteworthy technologic milestones empowering the rapid growth within the first period are the development of DNA sequencing techniques [Sanger & Coulson, 1975] and the whole genome sequencing of model organisms *S. cerevisiae* and *E. Coli* [Blattner et al., 1997; Goffeau et al., 1996]. Therefore, allowing to create genetic circuits based on model organisms properties, for instance, the development of the first cell-cell communication based on quorum sensing [You et al., 2004], serving as a major footprint for prospective designs.

The mid-2000 and following years could be described as a slowing growing period, in which the field started to bring the engineering approaches mainly on the circuit engineering area. However, realizing that there were some breakthroughs needed to overcome, namely the time-costly *ad hoc* assembling of genetic parts and the lack of methodologies enabling to characterize genetic parts functionalities.

The first international conference on SB (Synthetic Biology 1.0) and the first iGEM competition, both held at the Massachusetts Institute of Technology (MIT), are understood as the footprints of the synthetic biology community. Scientists were committed to bringing the concepts and ideas of engineering to biological sciences in a standardized and automated fashion. Thus, efforts were made on creating modular parts and standardized protocols, further described in **section 1.2**. Remarkable achieved milestones include the creation of RNA-based circuits, introducing RNA molecules as novel regulatory elements in circuitry engineering [Bayer & Smolke, 2005; Isaacs et al., 2004]. On-going efforts on parts standardization allowed the creation of the first *AND* logic gate by the engineering of a T7 polymerase [Anderson et al., 2007].

Concerning cell-to-cell communication, the concept of multicellular circuits arouses, in which the coexistence of more than one engineered cellular type enables, for instance, the emergences of patterning [Basu et al., 2005] or light-sensible circuits [Levskaya et al., 2005]. However, one of the biggest milestones was achieved within the field of metabolic

engineering, in which engineering approaches enable the heterologous production of artemisinin precursors, one of the most used antimalarial drug [Martin et al., 2003; Ro et al., 2006], opening the door on the application and further commercialization for synthetic biology.

The advances made on engineering approaches together with time-maturation and the gained expertise of research groups stimulated a third period characterized by the scalability and rhythm of production. Hereby, it was exploited the use of permanent DNA modifications through DNA-recombinases [Friedland et al., 2009] or the expansion of RNA usage in synthetic circuits [Maung & Smolke, 2008].

When talking about RNA regulations, a must claim is the re-purpose of the CRISPR-Cas immunity system in bacteria as the “genome scissors”. *CRISPR* uses an RNA-directed DNA binding of the nuclease *Cas9* to detect and cleave DNA [Brouns et al., 2008]. These enormous advances could be better understood thanks to a new technological advance: the discovery of high-throughput DNA assembly methods [Gibson et al., 2009]. Here I want to point out that periods of higher productivity are preceded for novel technological landmarks, stressing out the synergies between technology and synthetic biology.

Through the following years up until now, we are facing a period entitled new era of SB [Sleator, 2014], in which applications arise. The aforementioned milestones together with the development of new DNA technologies enable SB to rapidly evolve towards driven-applications. Accordingly, I would like to point out some of the sub-areas synthetic biology that is evolving towards, mentioning the most remarkable works that would help to understand today's research and ambitions within the field. Briefly, I would like to point out in major lines the different moving fields as well describing the biggest achievements in Table 1.1.

1.1.1 Engineering biological parts

The engineering of biological parts enables, by modifying parts sequences, for instance by the expansion of the genetic code or directed evolution, to work towards the creation

of higher order synthetic gene circuits by means of orthogonal parts. Furthermore, protein engineering based on protein properties such as fluorescence or bioluminescence allowed gaining insights on protein behaviours inside cells.

1.1.2 Cell-based applications

Engineering *E. coli* and *S. cerevisiae* by way of illustration through enzymes overexpression, gene knock out or genetic incorporation from other species was studied towards optimization of metabolic pathways. On the other hand, whole cells have been explored as computation entities in which embedded synthetic genetic circuits allow to compute in Boolean logic. For explanatory purposes, implementation of logic gates by means of biological entities has been explored with DNA-recombinases, transcriptional modulators or RNA operators among others.

1.1.3 Genome engineering

As a result of the whole-genome sequencing, engineering tools had been developed, either inducing local modifications or at a whole genome-scale. Current techniques are TALEN, ZNF and the *CRISPR-Cas9*, and *MAGE* and *CAGE*, respectively. *De novo* DNA synthesis allowed to design and synthesize the *Saccharomyces cerevisiae* complete eukaryotic genome and bacterial *Mycoplasma mycoides* JCVI-syn1 to obtain the smallest genome of a self-replicating organism, JCVI-syn3.0, all together demonstrating the possibility of synthesizing genomes from scratch.

1.1.4 Cell free

Working with cells' transcription and translation machinery outside the host cell without encompasses cell-free systems. The first cell-free technology enables the creation of an Ebola virus detector. Cell-free systems are envisioned on allowing SB applications to move outside the lab without the associated problems of working with living organisms. Cell-free systems allowed the development of synthetic gene circuits, protein engineering or the creation of artificial cells.

Engineering biological parts	Reference
Tran/post transcriptional genetic circuits	[Hunsicker et al., 2009] [C. Y. Wu et al., 2015] [S. Meyer et al., 2016]
Protein engineering	[Brun et al., 2011] [Griss et al., 2014]
Expansion of the genetic code	[Diafa & Hollenstein, 2015]
Directed evolution	[Tizei et al., 2016] [Jäckel & Hilvert, 2010]
Cell-based	
Metabolic engineering	[Ajikumar et al., 2010] [Paddon et al., 2013]
Cellular computation	[Roquet et al., 2016] [Rinaudo et al., 2007]
Genome engineering	
Genome editing technologies	[Y. G. Kim & Chandrasegaran, 1994] [Moscou & Bogdanove, 2009] [Barrangou et al., 2007]
Genome scale engineering	[Gil et al., 2004] [H. H. Wang et al., 2009]
De novo DNA synthesis	[Annaluru et al., 2014] [Kosuri & Church, 2014] [Hutchison et al., 2016]
Cell free systems	
Genetic circuits	[Niederholtmeyer et al., 2015]
RNA-based gene switches	[Takahashi et al., 2015]
Ebola sensor	[Pardee et al., 2014]

Table 1.1 Synthetic biology examples.

1.2 The engineering of biology

During the foundational years of SB discipline, several drawbacks regarding the essentials were faced. Efforts were made to establish the principles governing the engineering of biology. SB was striking the biology field but creating knowledge and advances was a matter of standardization. SB was envisioned to be an engineering discipline; however, devices were accomplished mostly by following the trial and error philosophy encompassing the biological sciences.

Thus, applying engineering principles to biology would concern to establish a novel design framework. As an engineering discipline, biological elements, namely, genes, proteins, cells..., would be treated as standard, orthogonal and modular parts. Analogously, biological elements would be seen as a set of LEGO®-like pieces. As stated in LEGO®, each piece is well known by all the community, enabling to resemble different parts into different positions to obtain very broad different results. Comparatively, in synthetic biology, those pieces are codified by DNA sequences and are called genetic parts [Benner & Sismour, 2005]. As stated by D. Endy [Endy, 2005] “a DNA sequence is defined by the function that it encodes”. The sequential parts combinations permit the creation of sophisticated genetic circuits. However, the undesired *ad hoc* workflow for parts combinations until obtaining the required cellular function is currently a trend in SB, counteracting the idea behind LEGO®-like building blocks.

Hence, there was a true need to establishing an engineering framework governing the field in order to overcome the time, money and human resources of the *ad hoc* strategies. D. Endy proposed in 2005 to adapt 3 engineering-discipline concepts into SB [Endy, 2005], represented in Figure 1.5, namely *standardization*, *abstraction*, and *modularity*. The idea was reinforced by the community leading to major developments, which would be briefly described under the following sections. As the field has evolved, I would like to add a forth engineering concept: *design and modelling*. Altogether, envisioning the shift from *ad hoc* methodologies towards rational designs.

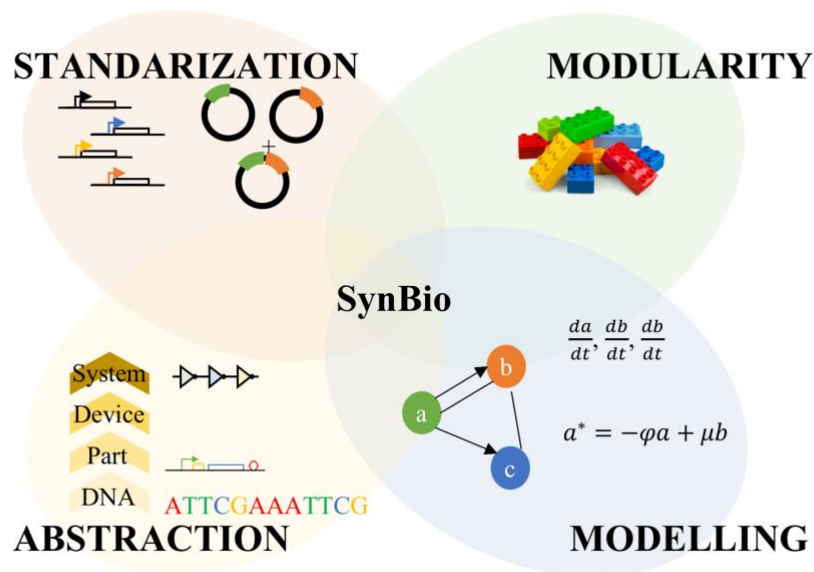


Figure 1.5 Synthetic biology engineering principles. **Standardization:** technical standards used by all SB community allowing to work towards the same direction, standards were settled from DNA sequences, plasmids, model organisms, measurements, environmental conditions, among others... **Abstraction:** consists of the breakdown of the system towards lower complexity hierarchies. De-coupling in simpler layers allows reducing systems complexity. **Modularity:** defining modules with defined functionalities allow to combine them in order to create novel devices. **Modelling:** a mathematical description of the aforementioned standard parts at any level of hierarchy allows the optimization of the design-cycle by means of mathematical predictions.

1.2.1 Standardization

Looking at the Cambridge dictionary definition of standardization we can define the concept as: “the process of making things of the same type all have the same basic features”.

Biological sciences have indeed well-established dogmas, the most relevant to SB being the DNA-RNA-PROTEIN [Crick, 1970]. However, within the biological engineering sciences, still under development, there is a lack of such dogmas. There is a need for establishing standards allowing the whole community to work towards the same guidelines. Efforts were made on defining parts functionalities, model organism chassis,

experimental measurements, and environmental conditions, among several experimental conditions. Intended to overcome the lack of standards emerged the Registry of Standard Biological Parts (<http://parts.igem.org/>), the Biobricks® and the assembly methods [Røkke et al., 2014].

1.2.1.1 Part Registry

The Registry of Standard Biological Parts is a public repository to store and catalogue collections of DNA sequences encoding for basic biological functions, the Biobricks®. The Registry of Standard Biological Parts has increased its Biobricks® collection to include over 12,000 parts, across 20 different categories (<http://parts.igem.org/>). Moreover, each new Biobricks® should require the experimental metadata allowing to capture the biological behaviour and context in which the Biobricks® are embedded. It includes information on the plasmid vector, the organism strain, and any relevant media or equipment conditions. The primary purpose of Biobricks® characterization data is to provide the necessary experimental data for predictive *in silico* biological modelling.

1.2.1.2 Biobricks®

Biobricks® are DNA sequences enabling a restriction-enzyme assembly standard [Shetty et al., 2008]. These DNA sequences confer the building blocks for the design and assemble of larger synthetic biological circuits from individual parts. Efforts were made to establish the way parts, devices, and systems are connected so that new designs will fit with old designs. Moreover, Biobricks® could be easily shared and combined to obtain several desired functionalities.

As a result, some tools for Biobricks® characterization were established: i) the use of RNA polymerase operations per seconds (PoPS) as the common signal carrier [Canton et al., 2008], ii) relative promoter unit (RPU) as a reference measurement standard [Kelly et al., 2009] and iii) the use of standardized restriction enzymes for cloning strategies [Røkke et al., 2014], as well as software tools enabling circuits' design, e.g. cell designer, AutoBio-CAD, RBS calculator.

1.2.1.3 Assembly

In 2003, Knight proposed the BioBrick® standard for the composition of biological parts [Speer et al., 2011]. The magic behind the assembly: two-by-two Biobrick® assembly results in a composite sequence being itself a new Biobrick®. Together with the *Registry of Standard Biological Parts* and the Biobricks® empowered the idea that genetic circuits could be assembled in an engineering perspective diminishing the problems associated with more traditional *ad hoc* molecular cloning approaches [Ellis et al., 2011].

1.2.2 Abstraction

When working with biological organisms, one has to bear in mind the existence of different levels of complexity, defining a set of hierarchies. Within a hierarchy, every part is embedded in a more complex system allowing to work at any level of the hierarchy without worrying about others. Designing new functions occurs at the top of the hierarchy in mind, however, it is implemented bottom-up.

As defined by E. Andrianantoandro *et al.* [Andrianantoandro et al., 2006], biological hierarchies were inspired by computer engineering, defining the layered elements as follows. At the bottom of the hierarchy, there is a minimal set of manipulable elements: DNA, RNA, proteins, and metabolites, analogous to the physical layer of transistors, capacitors, and resistors in computer engineering. The following layer comprises biochemical reactions between first layer elements, equivalent to engineered logic gates performing computations. A set of biochemical reactions are assembled into complex pathways as computer modules. The connection of the modules, together with its integration in a host cell, allows modifying the host cell behaviour in a programmable manner. Engineered cells are layered similar to computers, which can work independently executing complex functions or integrated into a population of communicating cells. Allowing to deal with the degree of complexity of biological systems.

1.2.3 Modularity

Once defined parts standardization at any of the hierarchy levels, the modularity principle could be introduced. In engineering, modularity encompasses defining functional-modules with inherent interchangeability ability. Modules could be defined at any hierarchy layer and ideally, should be independent on its context. Standardization of individual modules would allow its combination towards sophisticated devices. However, one has to bear in mind that biological organisms exhibit, more than expected, undesired interactions between layers.

1.2.4 Design and modelling

Design and modelling are two concepts that account together in a *design-build-test* workflow. Computational tools are used in a way to predict and optimize the behaviour of the desired circuits, devices or organisms prior to their construction. It could not be understood without the above-mentioned principles of abstraction, standardization, and modulation, conferring the difference towards biotechnology. Despite mathematical modelling and predictions are both used in the fields of synthetic biology and systems biology the purposes are quite different. Figure 1.6 is intended to graphically show the tendency of synthetic biology and systems biology towards the use of computational modelling. Whereas in systems biology modelling is used to a better understanding of biological systems, synthetic biologist uses to build novel functions of such biological systems. Nonetheless, sometimes the differentiation between both approaches is not as straightforward as stated, relying upon the pursued application.

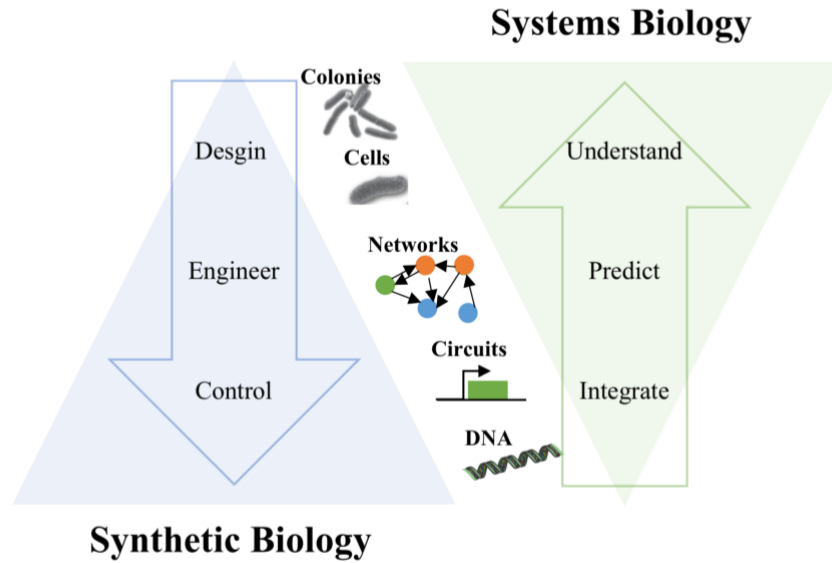


Figure 1.6 Design and modelling approach for systems biology and synthetic biology disciplines. **Synthetic biology** seeks to design and engineer cellular devices through genetic circuits. **Systems biology** envisions the integration of knowledge towards understanding and predicting cellular behaviours.

A mathematical model describes the components and interactions governing a system. Allows to describe the system behaviour and enable predictions. In essence, mathematical modelling is the formalization of all elements necessary for the implementation of a certain behaviour, while avoiding the unnecessary and complementary information. A trade-off between simplicity and complexity must be encountered when designing a model. Thus, models allow to i) describe a system behaviour, ii) explain the behaviour and iii) predict future behaviours. Once equations are built, either by experimental analysis or literature reviews parameter values are obtained, furthermore, additional mathematical analysis would reveal critical-behavioural parameters. Model predictions based on experimental data would suggest system re-design followed by a rational assembly of minimal parts. Hereby, following the synthetic biology approach workflow, mathematical models are used within the design and learn steps, as depicted in the workflow of Figure 1.4, minimizing the construction of devices by a trial-and-error methodology.

1.3 Synthetic Biology Applications

Synthetic biology has emerged and evolved towards an engineering discipline. During the first pages of the thesis I have emphasised the foundations and principles of the field, however, the rapid achievements and hype enabled researchers to develop towards society-based applications. The achievements within engineering cellular organisms with programmed-based circuits allow envisioning towards topics of social & economic interests. The very first application-based examples of SB could be found in its early years. Illustrative are the production of the antimalarial artemisinin by re-engineered metabolic pathways [Ro et al., 2006] or the development of the first whole-cell biosensors for heavy-metals detection [Amaro et al., 2011; Bousse, 1996].

I would like to have some lines on remarkable achievements within other areas, for instance, environmental, agriculture or industry among others. It is worth mentioning that achievements within very different applications are potentially transferable to the whole field.

1.3.1 Environmental applications

Bacteria exhibit very different forms of metabolism conferring adaptation towards a broad spectrum of environmental conditions. Since bacterial communities are evolved towards living in hostile environments, applying a SB approach upon them becomes trivial. - *Why not taking profit from the naturally evolved mechanisms enabling them to survive in hostile scenarios for environmental applications?* -

Heavy metals detections through engineered bacterial organisms had been the very first biosensors developed within SB principles [Bousse, 1996]. Bacteria have natural genetic sequences enabling to detect a broad range of heavy metals, e.g. Arg, Hg, S..., and allowing to adapt towards different environmental conditions [Sterritt & Lester, 1980]. By coupling them to reporter genes researchers were able to measure environmental contaminants, i.e. heavy metals [Trang et al., 2005], explosives residues' [Shemer et al., 2015] or pesticides [Sinha et al., 2014]. Moreover, using different pieces of metabolic

pathways enabling to reduce extracellular challenging conditions was exploited by synthetic biologists to trigger the removal of environmental pollutants [Urgun-Demirtas et al., 2006].

The re-engineering of existing metabolic pathways allowed the efficient production of chemicals, already produced in nature several attempts are found in producing biodegradable plastics [Somleva et al., 2008; S. Zhou et al., 2005]. Remarkably is the production of 1,4-butanediol (BDO) [Yim et al., 2011], non-natural chemical, for the production of plastics, rubber or solvents, by the construction of a new pathway with no “blueprint” in nature.

1.3.2 Energy applications

By coupling different species-enzymes to re-engineer metabolic pathways enable a broad range of energy-driven applications. Fuel production through the natural carbon cycle of microorganisms [Nakamura & Whited, 2003; Yim et al., 2011] has positioned as an industry greenish alternative. Furthermore, the use of microalgae has envisioned as an industrial-scale biofuel production [Singh et al., 2011].

1.3.3 Agriculture applications

Agriculture applications of synthetic biology are extremely related to metabolic engineering. Re-designing strategies of plant carbon metabolism allow increasing plant growth [A. P. M. Weber & Bar-Even, 2019]. Interestingly is the approach based on the CO₂ fixing enzyme ribulose-1,5-bisphosphate, extensively used or for instance, in order to change metabolism towards the C₄ carbon cycle [Schuler et al., 2016].

Due to reaching crops productivity limits, adding nutritional value within engineered plants is stated as a current alternative in the food supply. As a matter of exemplification, the Golden Rice Project aims to increase Vitamin A production in plant rice [Beyer, 2010]. Together with the above-mentioned microalgae strategy, photoautotrophic species

are envisioned as green cell factories due to their low cost a highly scalable biomass production [Fuentes et al., 2016; Reski et al., 2018].

1.3.4 Health applications

Synthetic biology has positioned as a new approach working towards most leading health problems. Engineering, -omics and biology principles confer several strategies encompassing drug discoveries, vaccine development or theranostics. Omics, computer aided design and *de novo* gene synthesis [Johnson et al., 2002] were used to create viral genomes in order to obtain attenuated viral vaccines [Mueller et al., 2010]. Metabolic engineering allowed to optimize naturally occurring drugs, e.g. antimalarial [Ro et al., 2006] or cancer drugs [Ajikumar et al., 2010] by combining host cell metabolic pathways with plant enzymes.

More remarkably are the systems derived from synthetic genetic circuits. Some of the achievements in cancer research or metabolic diseases are described. Transcriptional gene circuits were triggered to recognize protein domains from bacterial and viral infections [Tavassoli et al., 2008; W. Weber et al., 2008]. RNA circuits enabled the detection of changes in cell behaviours, thus, exploring the ability to fight towards cancer cells [Culler et al., 2010; Venkataraman et al., 2010; Wimmer et al., 2009]. Examples could be found on infectious diseases; bacteriophages were engineered to fight to biofilm infectious through cell-to-cell communication destabilization [T. K. Lu & Collins, 2007]. Other examples of simple genetic switches could be found for drug cancer screening for treating acute myeloid leukaemia in order to increase drug treatment effectiveness [Alloush et al., 2010] or early detection of liver cancer through the implementation of a LacZ-AND gate [Danino et al., 2015]. Engineering chimeric antigens to direct immune T-cells to recognise and destroy cancer cells following an AND gate logic, to so-called CAR-T cells therapy, has positioned as a novel theranostics for cancer disease. The FDA has approved, in the year 2007, the first CAR-T therapy based on the CD-19 targeted antigen [Kochenderfer & Rosenberg, 2013]. After obtaining patient T-Cells a viral vector is used to re-engineer the cells with a chimeric antigen receptor for its further amplification, i.e. in a bioreactor, and administered with lower doses of chemotherapy to the patient. Alternatively, cellular

encapsulation of synthetic gene circuits is stated as living implantable devices [Kemmer et al., 2010; Xie et al., 2016] Notably are the advances lead by Martin Fusseneger in ETH Zurich upon blood glucose regulation [Xie et al., 2016]. Glucose homeostasis was achieved in diabetic mice through the encapsulation of synthetic genetic devices regulating GLP-1 and insulin genes via the triggering of blue light stimulation or potential membrane depolarization, respectively.

Both CAR-T and encapsulated devices works established the roots of synthetic biological devices for theranostics: simple synthetic genetic circuits embedded in patients' cells that could act as prosthetics or drugs.

1.4 Potential risks of Synthetic Biology

Synthetic biology seeks to work towards real-world applications. As the field has recently advanced towards that objective, is it clear that concerns regarding safety and security as well as ethical questions. As a matter of awareness, I would like to point out what should be considered when trying to bring synthetic biology discoveries outside of the lab.

Living organisms can cause disease or environmental related problems, thus, in all areas in which microorganisms are manipulated there is the need to regulate the practices by legislation. The EU regulates through laws working with animals (**EU Regulation 1069/2009**), genetically modified organisms (**EU Directive 2009/41**), the release into the environment of genetically modified organisms (**EU Directive 2001/18**) or genetically modified food and feed (**EU Regulation 1829/2003**), among others.

Moreover, other important biosafety concerns in synthetic biology are i) the intentional or unintentional release of synthetic organisms into the environment, ii) horizontal gene transfer or iii) the induction of antibiotic-resistant organisms due to the use of antibiotic selective plasmids for organism engineering. The European Union has funded several research efforts on the environmental impact of a deliberate release of genetically engineered microbes concluding that the impact was approximately the same between genetically and non-genetically modified microbes.

Synthetic biology has moved towards trying to find novel strategies to fight with the current state of the art problems. Applications regarding reducing environmental contaminants, or modifying cells to fight against cancer are leading the field. However, the same cutting-edge technologies could be used, as exemplification, for bioterrorism activities. Information and tools for re-engineering organisms are world-wide open through internet databases and repositories, and the Do-It-Yourself (DIY) community is also spread worldwide. Making it much more difficult to regulate purposes and acts.

1.5 Living technologies and theranostics

Synthetic biology has moved forward the development of novel strategies towards biomedical problems. Examples are found in **section 1.3.4** with engineered CAR-T cells [Kochenderfer & Rosenberg, 2013] or encapsulated devices [Xie et al., 2016]. Up to date, the field of therapeutics has been led by biomedical devices: electronics or electro-mechanical technologies enabling the detection or monitoring of one or several biomarkers and treatment [Chan, 2008]. Along with the same path theranostics systems, which are implantable, integrated systems that can automatically diagnose a patients' disease and fantasize with an appropriate treatment if necessary [Crawley et al., 2014; Jeelani et al., 2014; Kojima et al., 2015], have reached an enormous interest. Both approaches would encompass the medical field towards a quickest, efficient and patient-centred care. However, in both, limitations awaken when developing the electronic sensors facilitating the detection of disease markers.

Accordingly, living technologies [Bedau et al., 2010] has positioned as a new technology combining both synthetic biology principles and biomedical devices rational design by using biological components instead of electro-mechanical ones, or by a combination of both [Froese, 2014]. Biomedical devices, inert or alive, could be described as a device able to obtain information through a sensor module, integrate the received information from sensors by applying programmed rules in the processor module, and translate the response upon the integrated information in the actuator module. See Figure 1.7a for a functional-module scheme.

Living systems *per se* could be seen as devices performing robust, sensitive and specific responses upon a broad range of biomedical signals. Synthetic biology approaches are applied to rationally design new living biomedical devices with standardized and modular architectures following the design of the electro-mechanical devices [B. Wang & Buck, 2012]. Figure 1.7b exemplifies how modules can be translated into a biological approximation giving rise to a living biomedical device.

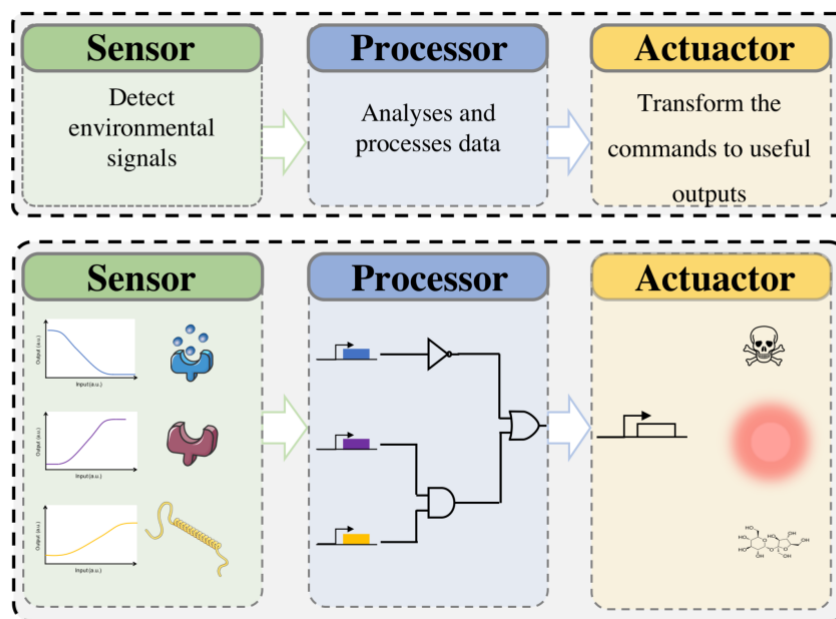


Figure 1.7 Living biomedical device modular approach. a) Schematically representation of the different modules comprising a biomedical device. b) Biological approximation of a living device. Adapted from [B. Wang & Buck, 2012].

Clear is the relevance of biomarkers detection for disease diagnosis [H.-J. J. Chang et al., 2017; Courbet et al., 2015], monitoring [Rawson et al., 1989; Struss et al., 2010] or treatment [Alloush et al., 2010]. Using cellular components or whole-cells as sensors encompass for an expansive library of biological markers. Whole-cell biosensors [Bousse, 1996] take advantage of the biological elements capable of detecting extra or intracellular signals. Upon a certain signal, cells activate their cellular machinery, i.e. signalling or metabolic pathways, allowing to produce the desired response, i.e. the cellular adaptation, apoptosis, mobility, among others [Owicki & Wallace Parce, 1992]. Thus, by applying the principles of engineering biology, identifying the DNA sequence

responsible to detect a particular signal e.g. a pathogen, extracellular or intracellular biomarker, would allow obtaining the components of the device sensor module.

Remarkably is the integration of sensorial information in a non-trivial fashion for biomedical disease monitoring, diagnosis and/or treatment. Elucidating the integration of sensorial information emerges as a critical point in the designing of living biomedical devices. Biological computation has postulated as the SB branch integrating multiple signal information and generating non-trivial responses. Most explored biological computation tools depict digital responses; however biomedical-application processor modules would also depict graded computation, i.e. analogue [Daniel et al., 2013; Manzoni et al., 2016; R. Sarpeshkar, 2014]. Processor module must i) to be set up with disease or biomedical application rules, ii) obtain sensorial information from the sensor module and, iii) apply the pre-defined rules to generate a response.

Based on processor responses, living biomedical device should either express a readable-output, for diagnosis purpose or act by producing a change in the physiological state, for treatment purposes. Further, living systems can continuously produce output molecules as long as they are supplied with sufficient nutrients and energy. Hence, living devices could be engineered by tacking profit of natural cellular responses such as changes in metabolic activity, gene expression profile, and pH as a response of inducer agent [Schultheiss et al., 2008; Tamsir et al., 2011], or by engineering *de novo* functionalities [Baeshen et al., 2014].

1.6 Thesis Objectives

Living technologies encompass the design of therapeutic strategies based on the engineering of biology approach. The use of cellular components for biomarker detection, the ability to design genetic circuits implementing programmed-based responses together with envisioned implantable cellular devices give rise to the PhD thesis main objective:

Apply engineering biology approaches to study the standard, robust, reliable and rational design of living biomedical devices enabling the fine-tune management of closed-loop biomedical applications.

We have envisioned to standardize the design of biomedical devices by breaking the device architecture in functional modules. Depicted in Figure 1.7 three main functional modules are defined. However, a fourth module considering the closed-loop behaviour is added in our approach. Our main methodological approach would be to consider both experimental and computational tools working together for establishing a framework that will help to design and construct such devices in a predictable manner rather than by costly trial and error approaches.

More specifically we challenged our devices to balance glucose levels in diabetic patients. Diabetes mellitus is a metabolic disorder causing unbalanced blood glucose levels due to defects on secretion or sensibility of the insulin hormone. Diabetes prevalence worldwide is 8.3%, i.e. about 387 M people are diabetic. It is expected a significant increase, up to 205 million new patients, in the year 2035. Diabetes is one of the fastest-growing health problems in the world as a consequence of lifestyle, lack of exercise, unhealthy diet, obesity and overweight [Association, 2010]. The relevance of the illness, the non-ideal treatment, and the uncertainty of the causes make diabetes an attractive problem being tackled from different strategies: electro-mechanical artificial pancreas [S. A. Brown et al., 2019], targeted drug delivery [Yu et al., 2015], artificial β -cell [Z. Chen et al., 2018], implantable living devices [Xie et al., 2016] or ingestible drug-delivery capsules

[Abramson et al., 2019]. I would like to emphasize, that despite research strategies have been trying, but with very little success, β -cell islet transplantation or stem-cells regeneration [Bouwens et al., 2013; Robertson, 2010; Fan Zhang & Tzanakakis, 2019] or the possibility of controlling on the patient's immune system to stop the destruction of pancreatic islets [Actobiotics, 2020; Lichtman et al., 2012], novel strategies rely on the principles of biomedical devices and theranostics.

Following a synthetic biology approach of *design-test-and build* we aim to tackle our main objective in a modular way. In that sense *two main objectives* with several specific sub-objectives are specified:

Objective 1: Explore the ability to create a living biomedical device using intrinsic cellular components.

Objective 1.1. Upon sensor module.

- Explore the ability to use of cellular sensors to detect external metabolites and disease-related signals within a range of interest.
- Explore the tunability of natural sensors by using a mathematical approach able to design and predict biosensors responses by means of minimal genetic engineering.

Objective 1.2 Upon signal processor module.

- Explore the ability to integrate multiple signals and produce non-trivial responses.
- Explore multicellularity and space conformations to minimize genetic engineering

Objective 1.3 Upon actuator module.

- Explore the creation of multicellular devices able to produce and secrete insulin and glucagon hormones.

Objective 2: Analyse living biomedical device performance in a close-loop environment via an *in silico* approach.

Objective 2.1. Upon biomedical device dynamics.

- *In silico* explore the ability of different device dynamics on glucose regulation based on real-experimental data.

Objective 2.2. Upon the patient daily-life routines.

- *In silico* explore the optimization of glucose regulation through a combination of an implantable cellular device and feed restriction patterns.

1.7 Thesis outline

The succeeding chapters are structured within the above-described objectives. Chapters 2,3 and 4 are devoted to exploring objective 1, and Chapter 5 explores objective 2. Chapter 6 encompasses the discussion.

More specifically, in **chapter 2**, the design of *sensor modules* is studied. Designing sensors responding to the application desired concentration range is explored within a combination of a mathematical framework and experimental validation in *E.Coli* model organism.

In **chapter 3** the *processor module* is deeply analysed. Multicellularity and signal information codification and de-codification in a chemical molecule are explored to integrate different input signals and produce non-trivial outputs. Research is done by exploiting the cell-to-cell communication of *E. coli* model organism.

In **chapter 4** we have explored by applying the sensor ability and the multicellularity approach to eukaryotic cells, i.e. *S. cerevisiae*, to detect and secrete physiological signals by engineering the production of secretable hormones in the *actuator module*. Moreover, we have implemented either simple input/output analogue responses or more complex time-pulsatile dynamics by modular reusability

Once insights on living device module-design had been explored longwise chapters 2 3 and 4; **chapter 5** aims to analyse living device characteristics, based on experimental data from engineered *HEK293T mammalian* cells, upon its implementation in an *in silico* closed-loop biomedical application.

Chapters 6 is dedicated to the discussion and conclusions of the main results among the different objectives in an individual and general perspective ending with the conclusions.

CHAPTER 2

Tools for sensor module design:

Two-component biosensors: unveiling the mechanisms of predictable tunability

The design and construction of living biomedical devices demand the study of extracellular signal detection. Throughout this chapter, we would benefit from cellular ability for signal detection and gain insights on how such responses could be used and modulated for desired applications. We developed a theoretical framework allowing the rational design of sensors for desired-based applications.

This work was developed in the *Synthetic biology for biomedical applications lab*, in collaboration with Dr. Javier Macia under the current project MINECO (2018-2020) “Printable Cellular Circuits”. Elisenda Alaball had also collaborated in the project during the development of her biomedical engineering bachelor thesis “Building genetic tuneable sensors” co-directed by Dr. Javier Macia and myself during the academic year 2018-2019.

As a result, the research main achievements described in this chapter have been published in [Gonzalez-Flo et al., 2020].

2 TOOLS FOR SENSOR MODULE DESIGN

2.1 Applying engineering principles to cellular sensors

Sensing information is a matter of life. Being able to detect surrounding conditions, processes, or physical properties allows environmental adaptation [Dincer et al., 2019]. Sensors are the ones in charge of information acquisition, surround us, and many processes successfully running around are measured and detected by sensors. A sensor is defined by The American National Standards Institute as "a device which provides a usable output in response to a specific measurand", i.e. a physical quantity, property, or condition which is measured. In general, sensors are based on a two-layered architecture: the first layer can detect an external magnitude, i.e. input, and the second one, the transducer, can translate the measurand into a measurable signal, i.e. output [Ento, 2006].

Cells are systems in continuous communication with the environment, detecting and adapting towards different environmental conditions by possessing and expressing a series of molecular recognition elements, e.g. receptors, ion channels, or enzymes, triggering the expression of adaptive mechanisms [Bousse, 1996; Pancrazio et al., 1999]. These molecules are usually sensitive to their corresponding analytes because of their native cellular mechanism [Owicki & Wallace Parce, 1992]. Applying engineering principles to intrinsic cellular sensors makes possible to re-design them to perform novel functionalities. Cells can be envisioned as autonomous measurement devices profiting from biological elements for specific stimulus recognition and quantification [Rawson et al., 1989]. Concretely, stimuli could be detected at either molecular, cellular or tissue level, providing real-time information related to the cell physiology or toxicology, for instance.

From that perspective, within the presented modular approach describing a living biomedical device, in Figure 1.7, in which we can distinguish the sensor, the processor and the actuator module [B. Wang & Buck, 2012], we zoomed into the sensor's module configuration. In the sensor module, as represented in Figure 2.1, the information is

acquired through a two-layered system based on the receptor-transducer interaction [Ento, 2006].

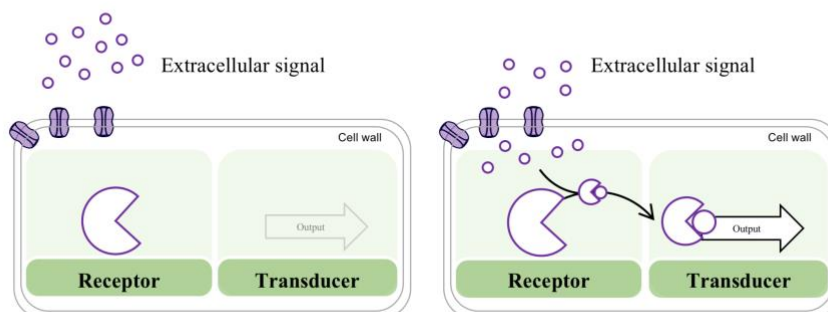


Figure 2.1 Schematically representation of the two-layered architecture of the sensor module. Two-layered components based biological components. The receptor layer comprises the detection of the external signal or stimuli through their interaction, binding or recognition and as a result, produces a change in the transducer by triggering the response signal, i.e. output.

The very-first synthetic biosensor described in Selifonova *et al.* [Selifonova et al., 1993] relies on the ability of bacteria to grow in environments rich in heavy metals. Deciphering the mechanisms allowing bacteria to adapt and survive to those extreme environmental conditions enabled the design of biosensors for heavy metals detection. Hence, biosensor design trusts on the detection of the biological mechanism involved in specific signal detection. Originally, such biological elements were mostly identified by chance. Later, part mining and high-throughput screenings had been one of the most useful tools allowing searches based on DNA sequence similarity [Johns et al., 2018] and by part labels on protein databases [Xue et al., 2014]. Other tools rely on directed evolution and mutagenesis followed by the subsequent characteristic screening [Beggah et al., 2008].

Despite sensor output signals could range from enzymes, DNA, antigens, antibodies, or biofilms as the reporter elements [Bousse, 1996], integrated into the processor module, Table 2.1 summarizes most of the used reporter systems with its main advantages and disadvantages. For simplicity, in the experimental setup presented in this chapter, we have selected a fluorescent-readable output, because of direct measurement due to non-substrate dependency. Nowadays laboratory technologies allow obtaining easy scalable,

stable and robust measurements of the fluorescent sensor output and help towards a deeper analysis of the sensor module.

Gene	Detection method	Advantages	Disadvantages	Reference
Lux	Bioluminescence	Easy measurement Rapid response	Thermal lability O ₂ requirement	[Hakkila et al., 2002]
Luc	Bioluminescence	High sensitivity Rapid response	O ₂ and ATP requirement Lower permeability	[Gutiérrez et al., 2015]
(G)FP	Fluorescence	No substrate High stability	Low sensibility High stability Lag time	[Sagi et al., 2003]
LacZ	Bioluminescence	High stability Nacked eye	Substrate dependent	[Mascher et al., 2004]
	Fluorescence			
	Colorimetry			
crtA	Colorimetry	Nacked eye	Substrate dependent	[Chong & Ching, 2016]

Table 2.1 Output readable proteins. Genes expressing reporter proteins from different detection methods are related to its corresponding advantages and disadvantages.

For any desired purpose, biosensor's response must fulfil application needs. This response is defined by the relationship between the input and the output upon different input concentrations (Figure 2.2), described by the so-called transfer function [Mukherji & Van Oudenaarden, 2009; B. Wang et al., 2011]. Several key features characterize the biosensor transfer function, shown in Figure 2.2, namely, the dynamic range (γ), the operating range, the sensitivity (σ), the affinity ($K_{0.5}$), the leakiness and the limit of detection. Leakiness stands for the output expression value without the presence of input. Lower limit of detection value is calculated through the first input/output variation. Operating range determines the signal region associating the maximal input sensitivity.

Sensitivity (σ) is defined as the output variation for a given change in the input. Dynamic range (γ) corresponds to the different range of output produced. Affinity ($K_{0.5}$) determines the input concentration needed to reach half the maximum output value.

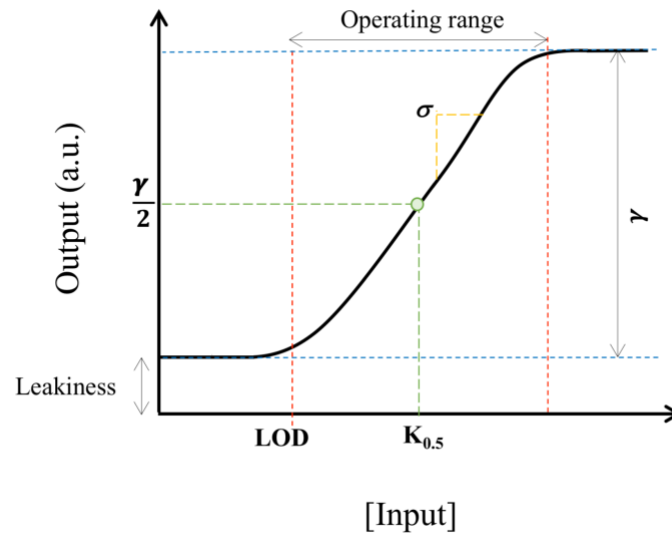


Figure 2.2 Biosensor Transfer Function. The transfer function of a biosensor enables the quantitative characterisation of the input concentration and the biosensor output. Biosensor leakiness is defined as the output expression in the absence of its input signal. The dynamic range is represented by γ and corresponds to the exhibited output range. Biosensor sensitivity (σ) is calculated as the transfer function slope of the operating range region. Affinity is parametrized by $K_{0.5}$ and calculated as the input signal giving the half maximal γ .

Nonetheless, using intrinsic sensors for designing living biomedical devices account for signal detection within biological relevant concentration ranges [Eugenia Inda et al., 2019]. However, occasionally, the biological concentration ranges are below real-world application needs [Mahr & Frunzke, 2016; Merulla & Van Der Meer, 2016; A. J. Meyer et al., 2019; Fuzhong Zhang et al., 2012] and exists the need for customizable biosensor performance [S.-Y. Chen et al., 2019; Jia et al., 2019].

One of the most commonly used biological systems to detect extracellular signals of interest are transcriptional factor (TF) based biosensors. Mainly, consist of a repressor or activator protein regulating the transcriptional activity of a specific promoter. Upon interaction with a small molecule or environmental signal, TFs undergo a conformational change allowing the transcription of genes downstream the regulated promoter. In

prokaryotes, the most abundant protein mechanism responsible for sensing and responding to aforesaid signals is the two-component system (TCS) [Stock et al., 2000]. Two-component systems are comprised of a receptor protein and its regulated promoter. Signal detection relies on the interaction of the two components mediated by the external signal to be detected, i.e. inducer. The external signal can bind the receptor protein, i.e. the first TCS component, and form a complex. Throughout the DNA Binding Domain (DBD) region, the complex is able to recognize a structural motif that regulates a DNA promoter region, i.e. the second TCS component. Once the complex is bound to the DBS, it triggers the expression of downstream promoter genes. Figure 2.3 schematically represents TCS architecture. Despite transcription factors encompass for a large family of proteins enabling signal detection, protein engineering is envisaged for novel libraries permitting further inducers detection [Taylor et al., 2016].

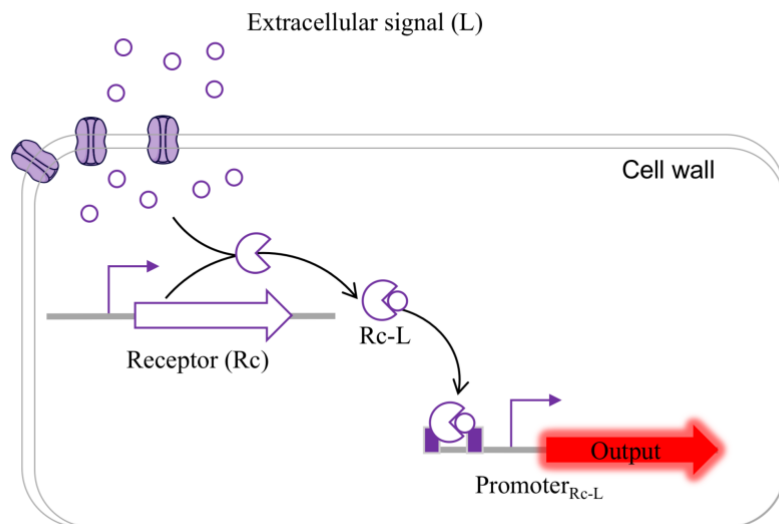


Figure 2.3 Two-component sensor. Extracellular signal (L) crosses the cellular wall and forms a complex with the Receptor protein, i.e. $Rc-L$. The complex recognizes the DNA Binding Domain (DBD) regulating the promoter region of the Promoter $Rc-L$, i.e. a positive regulable promoter only being active in the presence of the external signal L . Downstream the promoter region a fluorescence protein, e.g. red fluorescence, is expressed as a matter of detection.

Much has been done in the study of prokaryotic organisms to modulate biosensors' characteristics. Following the structure presented in Figure 2.4, the main engineering

approaches for modulating limit of detection, dynamic range, leakiness and sensitivity are briefly described.

2.1.1 Limit of detection

Limit of Detection (LOD) is important for use in real-life applications because molecules of interest are often present at very low concentrations. The intracellular concentration of the transcription factor regulating output gene expression plays a significant role in the minimal input concentration that can be sensed [Cayron et al., 2017; Eugenia Inda et al., 2019; Rössger et al., 2013; B. Wang et al., 2015]. Increasing the TF concentration allows modifying the LOD, as depicted in Figure 2.4a.

2.1.2 Dynamic range

Maximising the dynamic range is important for being able to reliably determine the result from a biosensor. Modifying the expression of the output protein, for instance by using different promoter strength [Y. Chen et al., 2018; Rössger et al., 2013] or different RBS sequences [Rubens et al., 2016; Wang et al., 2011], as depicted in Figure 2.4b, will alter the dynamic range. Moreover, positive signal amplification, for instance through genetic amplifiers or positive feedback loops [Nistala et al., 2010; B. Wang et al., 2014], enable to boost dynamic range.

2.1.3 Leakiness

Leakiness should be reduced to ensure biosensors performance. It could be acquired through the use of degradation tags on the output protein [Fernandez-Rodriguez & Voigt, 2016], mRNA antisense blocking the output protein [Brophy & Voigt, 2016], mutations on operator binding sites to reduce basal expression [Lee & Maheshri, 2012]. Effect on transfer function leakiness could be visualized in Figure 2.4c.

2.1.4 Sensitivity

Reliable and accurate biosensors need to be highly specific to the detected signal. Biosensor sensitivity could be improved by different methods such as directed evolution [Lönneborg et al., 2012] or involving high throughput screening of novel candidates to satisfy the demands of specific applications [H.-J. Chang et al., 2018; Yoo et al., 2013; Younger et al., 2017]. Figure 2.4d shows the effect on the transfer function.

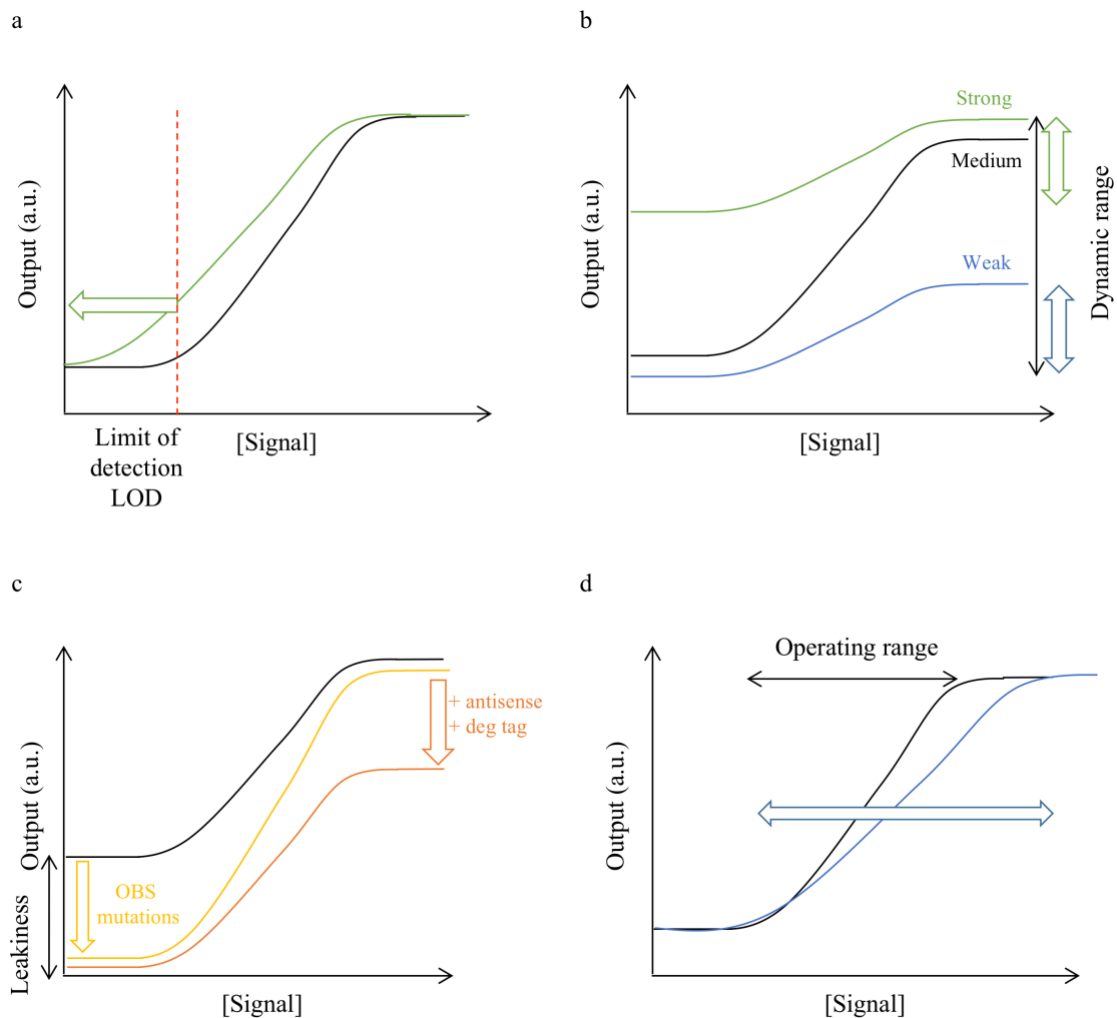


Figure 2.4 Biologic mechanisms to tune transfer functions features. **a)** Limit of Detection. The modulation of the intracellular concentration of the transcription factor, regulating output gene expression, allows to change the amount of input signal giving a detectable output response. **b)** Dynamic Range. Using appropriate DNA sequences ensuring stronger or weaker output gene expression allows modifying the dynamic range. **c)** Leakiness. Basal output expression in the absence of the inducer signal could be diminished by exploiting mRNA antisense molecules or protein degradation tags. Moreover, mutations on

the operator binding site could reduce output leakiness. **d) Sensitivity.** The range of input concentrations inducing a significant change in the output could be improved by directed evolution or high throughput screening.

Although different methods for tuning biosensor responses have been explored, the simplest strategy is based on the modulation of the abundance of the first TCS component, i.e. the receptor protein [Ang et al., 2013; Max Carbonell-Ballesteró et al., 2014; B. Wang et al., 2015]. The simplicity of this method, that allows specific modifications with minimal genetic manipulation, makes it suitable for designing synthetic bacterial sensors. However, despite the enormous experimental evidence, circuits are constructed following an *ad hoc* workflow: re-designing circuits until obtaining the desired behaviour. Hence, emphasising the fact that there is no formal theory that allows the design of customized biosensors in a systematic and predictable manner.

2.2 Objectives

By combining a mathematical and experimental approach:

We aim to develop a formal mathematical model able to predict the performance of synthetically designed biosensors based on two-component systems.

The *specific objectives* addressed within this chapter are:

- Mathematically describe the relationship between biosensor's features and the receptor abundance.
- Use the mathematical model to design biosensors with specific features in a predictable manner.
- Experimental validation of model predictions.

2.3 Biosensor mathematical formalization based on two-component architecture

The mathematical formalization allowing to describe the functional relationship between the abundance of the receptor protein and the main features of a two-component biosensor response is based on the architecture shown in Figure 2.5. As a *proof-of-concept*, the two-component biosensor comprising this study was based on the architecture of the well-known quorum sensing Lux system from *Vibrio fischeri*, which has been extensively used in synthetic biology [Ang et al., 2013; Garcia-Ojalvo et al., 2004]. In this system, the receptor protein, termed LuxR, is constitutively expressed and, in the presence of external molecules of 3-oxo-C6-homoserine lactone (*3OC6HSL*), the complex LuxR-3OC6HSL dimerizes and binds to the Lux promoter, thereby triggering the expression of a downstream gene, e.g. red fluorescent protein (RFP) that acts as a reporter [Fuqua et al., 1994].

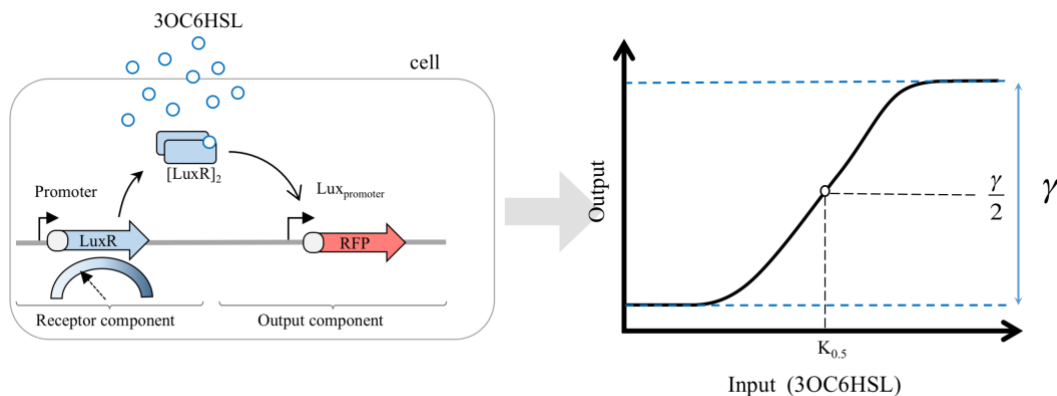


Figure 2.5 Schematic representation of two-component biosensor architecture. The first biosensor component, i.e. the receptor component, is responsible for the production of the receptor protein and consists of a terminator, a DNA promoter sequence (variable depending on the experimental setup), an RBS sequence (variable depending on the experimental setup), and the LuxR protein. The second biosensor component, i.e. the output component, can respond in an inducible way to the complex of LuxR and *3OC6HSL* due to the inducible Lux promoter. The DNA cassette consists of a terminator, the Lux promoter, an RBS and the output red fluorescent protein (RFP). The transfer function, defined as the relationship between input and output, is characterized by $K_{0.5}$ and γ .

In this model we take into consideration the following assumptions:

- The number of genes is constant.
- The average behaviour of a cell population can be described in a deterministic approach by a set of ordinary differential equations (ODEs).
- Transfer functions are measured at the steady state.
- The total amount of receptor protein R_T is constant because cell has reached the equilibrium between receptor protein synthesis and degradation.

2.3.1 Transcription Process

The external input L binds to the receptor protein forming an active transcription factor that triggers the synthesis of the output $mRNA$, which will be translated into the final output protein P . The ratio of $mRNA$ synthesis depends on the concentration of the transcriptional complex Q_P formed by the gene p and the transcription factor R_{2L} , which depends on i) the number of copies of the gene and ii) the transcription factor abundance. Hence:

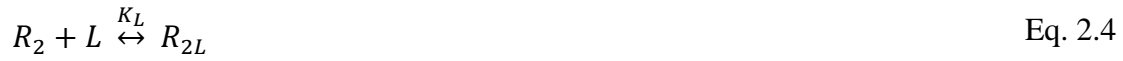
$$\frac{dmRNA}{dt} = \mu \cdot Q_p - \delta_{mRNA} \cdot mRNA + \mu_0 \quad \text{Eq. 2.1}$$

Where δ_{mRNA} represents the degradation rate of $mRNA$, μ is the transcription rate of the gene p regulated by the transcriptional complex Q_P and μ_0 is the transcription rate of the gene p in absence of the transcription factor, i.e. basal gene expression. Applying the rapid-equilibrium approximation and assuming that the number of gene copies is constant [Schuster & Holzhütter, 1994] Q_P can be calculated as:

$$Q_p = \rho \cdot R_{2L} \cdot Q \quad \text{Eq. 2.2}$$

Where ρ accounts for the binding and unbinding constant rates and Q is the number of free genes. In turn, the number of active transcription factor R_{2L} depends on the amount of free receptor proteins R and the concentration of input L . It is worth mentioning, that

typically in prokaryotic two-component systems receptor proteins dimerizes [Max Carbonell-Ballester et al., 2014]:



According to the rapid-equilibrium approximation, from Eq. 2.4 we can express:

$$R_{2L} = K_L \cdot R_2 \cdot L \quad \text{Eq. 2.5}$$

and

$$R_2 = K_B \cdot R^2 \quad \text{Eq. 2.6}$$

At steady state, we can consider $\frac{dmRNA}{dt} = 0$. In consequence, the concentration of *mRNA* at equilibrium is described as:

$$mRNA = \frac{\mu \cdot \rho \cdot K_L \cdot Q \cdot R_2 \cdot L}{\partial_{mRNA}} + \frac{\mu_0}{\partial_{mRNA}} \quad \text{Eq. 2.7}$$

Assuming that the number of genes is constant, we can express:

$$Q_T = Q + Q_P \quad \text{Eq. 2.8}$$

Here, Q_T represents the total number of gene copies, which is assumed constant. Using Eq. 2.2:

$$Q = \frac{Q_T}{1 + \rho \cdot R_{2L}} = \frac{Q_T}{1 + \rho \cdot K_L \cdot R_2 \cdot L} \quad \text{Eq. 2.9}$$

Hence:

$$mRNA = \frac{\mu \cdot \rho \cdot K_L \cdot Q_T}{\partial_{mRNA}} \cdot \left(\frac{R_2 \cdot L}{1 + \rho \cdot K_L \cdot R_2 \cdot L} \right) + \frac{\mu_0}{\partial_{mRNA}} \quad \text{Eq. 2.10}$$

Combining Eq. 2.10 with Eq. 2.6 we can express the concentration of $mRNA$ at the steady state as a function of the free receptor protein R .

$$mRNA = \frac{\mu \cdot \rho \cdot K_L \cdot K_B \cdot Q_T}{\partial_{mRNA}} \cdot \left(\frac{R^2 \cdot L}{1 + \rho \cdot K_L \cdot K_B \cdot R^2 \cdot L} \right) + \frac{\mu_0}{\partial_{mRNA}} \quad \text{Eq. 2.11}$$

Considering that the receptor protein can be found in different configurations, such as free protein R , free dimer R_2 , an active transcription factor form R_{2L} or as a part the transcription complex Q_P , we consider:

$$R_T = R + 2 \cdot R_2 + 2 \cdot R_{2L} + Q_P \quad \text{Eq. 2.12}$$

where R_T is the total relative amount of receptor protein in the cell, assumed constant. However, the number of copies of the gene p is significantly lower than the number of receptor proteins in their different configurations. We can assume that: $Q_P \ll R + 2 \cdot R_2 + 2 \cdot R_{2L}$, hence:

$$R_T \approx R + 2 \cdot R_2 + 2 \cdot R_{2L} \quad \text{Eq. 2.13}$$

Using Eq. 2.7 and Eq. 2.8 we get:

$$2 \cdot K_B \cdot (1 + K_L \cdot L) \cdot R^2 + R - R_T = 0 \quad \text{Eq. 2.14}$$

The positive solution of this equations gives:

$$R(R_T) = \frac{-1 + \sqrt{1 + 8 \cdot K_B \cdot (1 + K_L \cdot L) \cdot R_T}}{4 \cdot K_B \cdot (1 + K_L \cdot L)} \quad \text{Eq. 2.15}$$

that describe the relationship between R and R_T . In consequence,

$$R^2(R_T) = \frac{[-1 + \sqrt{1 + 8 \cdot K_B \cdot (1 + K_L \cdot L) \cdot R_T}]^2}{16 \cdot K_B^2 \cdot (1 + K_L \cdot L)^2} \quad \text{Eq. 2.16}$$

For large values of R_T , the function presented in Eq. 2.16 can be approximated to its asymptote described by:

$$R^2(R_T) \approx m \cdot R_T + n \quad \text{Eq. 2.17}$$

With

$$m = \lim_{R_T \rightarrow \infty} \left[\frac{R^2(R_T)}{R_T} \right] = \frac{1}{2 \cdot K_B \cdot (1 + K_L \cdot L)} \quad \text{Eq. 2.18}$$

and

$$n = \lim_{R_T \rightarrow \infty} (R^2(R_T) - m \cdot R_T) = 0 \quad \text{Eq. 2.19}$$

Finally,

$$R^2(R_T) \approx \frac{R_T}{2 \cdot K_B \cdot (1 + K_L \cdot L)} \quad \text{Eq. 2.20}$$

By introducing Eq. 2.20 into Eq. 2.11 we could obtain the expression of steady state $mRNA$ as a function of R_T :

$$mRNA = \frac{\mu \cdot \rho \cdot K_L \cdot Q_T \cdot R_T}{K_L \cdot \partial_{mRNA} \cdot (2 + \rho \cdot R_T)} \cdot \left(\frac{L}{\frac{2 \cdot \partial_{mRNA}}{\partial_{mRNA} \cdot K_L \cdot (2 + \rho \cdot R_T)} + L} \right) + \frac{\mu_0}{\partial_{mRNA}} \quad \text{Eq. 2.21}$$

2.3.2 Translation Process

Using a similar approach than used in the transcription process, we consider that the ratio at which the output protein P is produced depends on the concentration of $mRNA$ according to:

$$\frac{dP}{dt} = \omega \cdot mRNA - \delta_P \cdot P \quad \text{Eq. 2.22}$$

Here, δ_P represents the degradation rate of protein P .

At the steady state we can assume $\frac{dP}{dt} = 0$. Combining Eq. 2.21 with Eq. 2.22 we obtain the final expression:

$$P = \Gamma(R_T) \cdot \left(\frac{L}{K_{0.5}(R_T) + L} \right) + P_0 \quad \text{Eq. 2.23}$$

Here

$$P_0 = \frac{\mu_0}{\delta_{mRNA} \cdot \delta_P} \quad \text{Eq. 2.24}$$

$$\Gamma(R_T) = \frac{a_0 \cdot R_T}{b_0 + b_1 \cdot R_T} \quad \text{Eq. 2.25}$$

and

$$K_{0.5}(R_T) = \frac{a_1}{b_0 + b_1 \cdot R_T} \quad \text{Eq. 2.26}$$

With

$$\begin{aligned}
a_0 &= \frac{\omega \cdot \mu \cdot \rho \cdot Q_T \cdot K_L}{\delta_P} \\
a_1 &= 2 \cdot \delta_{mRNA} \\
b_0 &= 2 \cdot \delta_{mRNA} \cdot K_L \\
b_1 &= \rho \cdot \delta_{mRNA} \cdot K_L
\end{aligned}
\tag{Eq. 2.27}$$

The range of accessible values for $\Gamma(R_T)$ and $K_{0.5}(R_T)$ can be calculated considering the limit values of Eq. 2.25 and Eq. 2.26 when $R_T \rightarrow 0$ and when $R_T \rightarrow \infty$. As a result, values of $\Gamma(R_T)$ and $K_{0.5}(R_T)$ are constraint to:

$$\Gamma(R_T) \in \left(0, \frac{a_0}{b_1}\right) \tag{Eq. 2.28}$$

$$K_{0.5}(R_T) \in \left(0, \frac{a_1}{b_1}\right) \tag{Eq. 2.29}$$

2.3.3 Relative protein concentration Θ and relative dynamic range $\gamma(R_T)$

Values of $\Gamma(R_T)$ cannot be directly measured but indirectly obtained through output fluorescent levels. The linear relationship between $\Gamma(R_T)$ and fluorescent levels depends on non-genetic factors such as emission efficiency of fluorescent proteins or the gain of the spectrofluorometer used. To address this issue, we can normalize Eq. 2.23 to the maximum value $\left(\frac{a_0}{b_1}\right)$. Hence,

$$\theta = \gamma(R_T) \cdot \left(\frac{L}{K_{0.5}(R_T) + L}\right) + \theta_0 \tag{Eq. 2.30}$$

Where

$$\theta = \frac{P}{\frac{a_0}{b_1}} \tag{Eq. 2.31}$$

$$\theta_0 = \frac{P_0}{\frac{a_0}{b_1}} \quad \text{Eq. 2.32}$$

and

$$\gamma(R_T) = \frac{\Gamma(R_T)}{\frac{a_0}{b_1}} \quad \text{Eq. 2.33}$$

Here $\gamma(R_T)$ represents the relative dynamic range of the biosensor. Using Eq. 2.25, Eq. 2.33 can be expressed as:

$$\gamma(R_T) = \frac{b_1 \cdot R_T}{b_0 + b_1 \cdot R_T} \quad \text{Eq. 2.34}$$

It is worth mentioning that the relative dynamic range $\gamma(R_T)$ is independent of the non-genetic factors previously mentioned.

As a result of our mathematical formalization, the relative expression of the reporter protein Θ produced upon an external input concentration L is described by:

$$\theta = \gamma(R_T) \cdot \left(\frac{L}{K_{0.5}(R_T) + L} \right) + \theta_0 \quad \text{Eq. 2.35}$$

Here, θ_0 represents the basal expression of the reporter protein in the absence of inducer, i.e. $L=0$, $\gamma(R_T)$ corresponds to the relative dynamic range, and $K_{0.5}(R_T)$ is the biosensor activation threshold, which is defined as the concentration of external input L that gives the half-maximal response. Both terms depend on R_T , according to:

$$\gamma(R_T) = \frac{b_1 \cdot R_T}{b_0 + b_1 \cdot R_T} \quad \text{Eq. 2.36}$$

and

$$K_{0.5}(R_T) = \frac{a_1}{b_0 + b_1 \cdot R_T} \quad \text{Eq. 2.37}$$

where a and b are model parameters.

2.4 Model parameters determination

To experimentally validate the mathematical model and its predictions, a library of genetic devices that act as biosensors were constructed and used as a *proof-of-concept*. Table 2.4 summarizes the set of genetic constructs analysed (constructs C1-C4). Each biosensor was designed to work at different LuxR concentrations by the exploitation of constitutive promoters with variable strengths.

To experimentally determine model parameters a_1 , b_0 and b_1 the transfer function of each device, i.e. the relationship between input L (*3OC6HSL*) and output Θ (RFP) at the steady state, was measured (Figure 2.6) and γ and $K_{0.5}$ were experimentally determined. Values of γ were calculated by dividing RFP levels by the maximum RFP value, which corresponds to that obtained with construct C1 (Table 2.4) at the maximum induction level, i.e. $L=10 \mu\text{M}$.

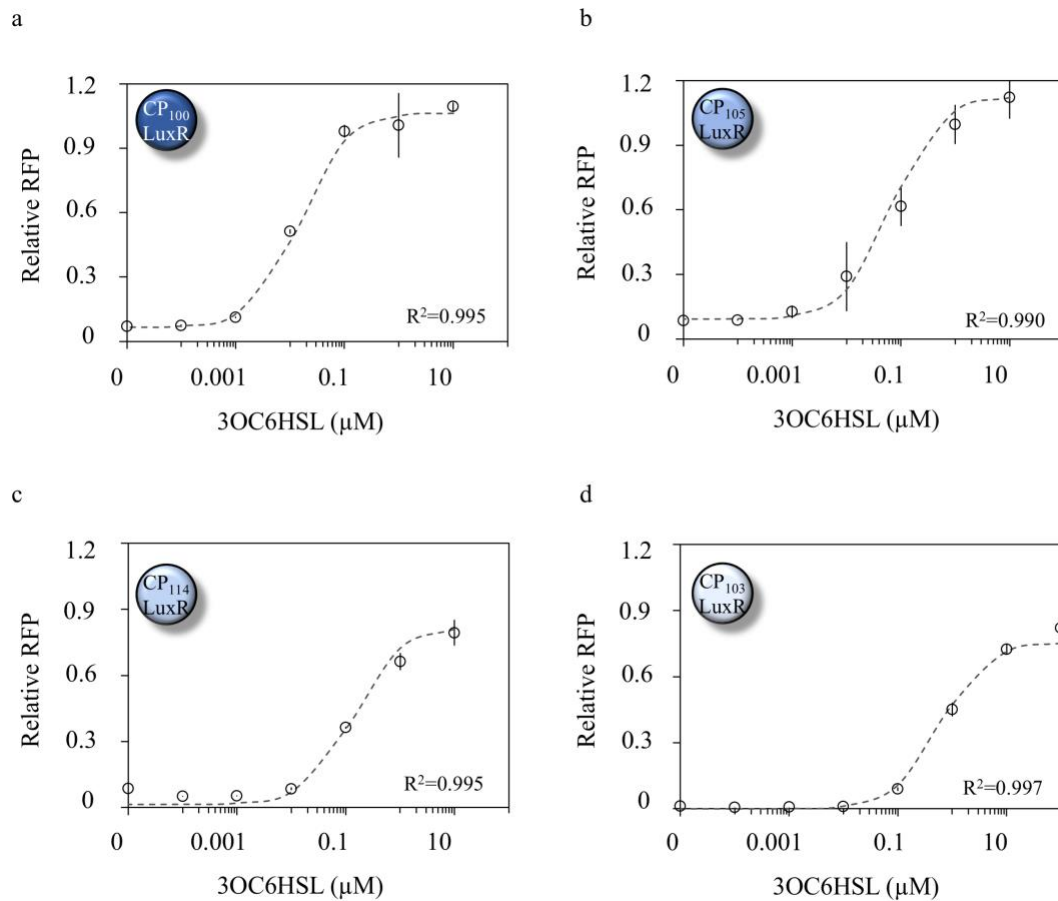


Figure 2.6 Experimental transfer functions of biosensors with different abundances of LuxR. The relationship between input *3OC6HSL* concentration and output RFP level was measured for constructs C1-C4 from Table 2.4. Relative RFP values were obtained by dividing RFP levels by the maximum RFP value, which corresponds to the maximum induction level, i.e. $L=10 \mu\text{M}$ of construct C1. **a-d)** Dots correspond to experimental values and the dashed lines to the experimental fitting. The error bars shown in the figures are the standard deviation of four independent experiments. Fitting parameters are shown in Table 2.6. Pearson test was applied to the experimental values and experimental fitting obtaining the correlation coefficients R^2 .

To determine the dependence of γ and $K_{0.5}$ on the relative concentration of LuxR, first it was necessary to determine the relative LuxR abundances. The relative receptor levels were calculated by measuring the strengths of the different constitutive promoters upstream of LuxR in constructs C1-C4 (Table 2.4). To that end, a new set of genetic constructs (C8-C11 in Table 2.5), in which each constitutive promoter was individually located upstream of the reporter protein RFP, was built. Experimental measures of RFP allows determining the relative activity of each promoter [Kelly et al., 2009]. We used

the strongest characterized promoter, i.e. promoter J23100 in construct C8 (Table 2.5), as a reference to calculate the relative activity of each different promoter.

Figure 2.7a shows the relative RFP expression level. Finally, we assumed that the relative abundance of LuxR can be directly estimated from the relative promoter activity located upstream LuxR [B. Wang et al., 2015]. Figure 2.7b-c show the dependence of $K_{0.5}$ and γ , respectively, on the relative abundance of LuxR. Lastly, Eq. 2.36 and Eq. 2.37 were fitted to experimental values and the model parameters a_1 , b_0 , and b_1 were determined. *Matlab R2016a* least-squares analysis software was used for fitting the parameters. Parameter values obtained were: $a_1 = 35 \mu\text{M}$, $b_0 = 20$, and $b_1 = 2.6 \cdot 10^3$. It is worth mentioning that, according to the model equations, model parameters define all set of biosensors based on the combination of receptor protein and its corresponding promoter regulating the output expression.

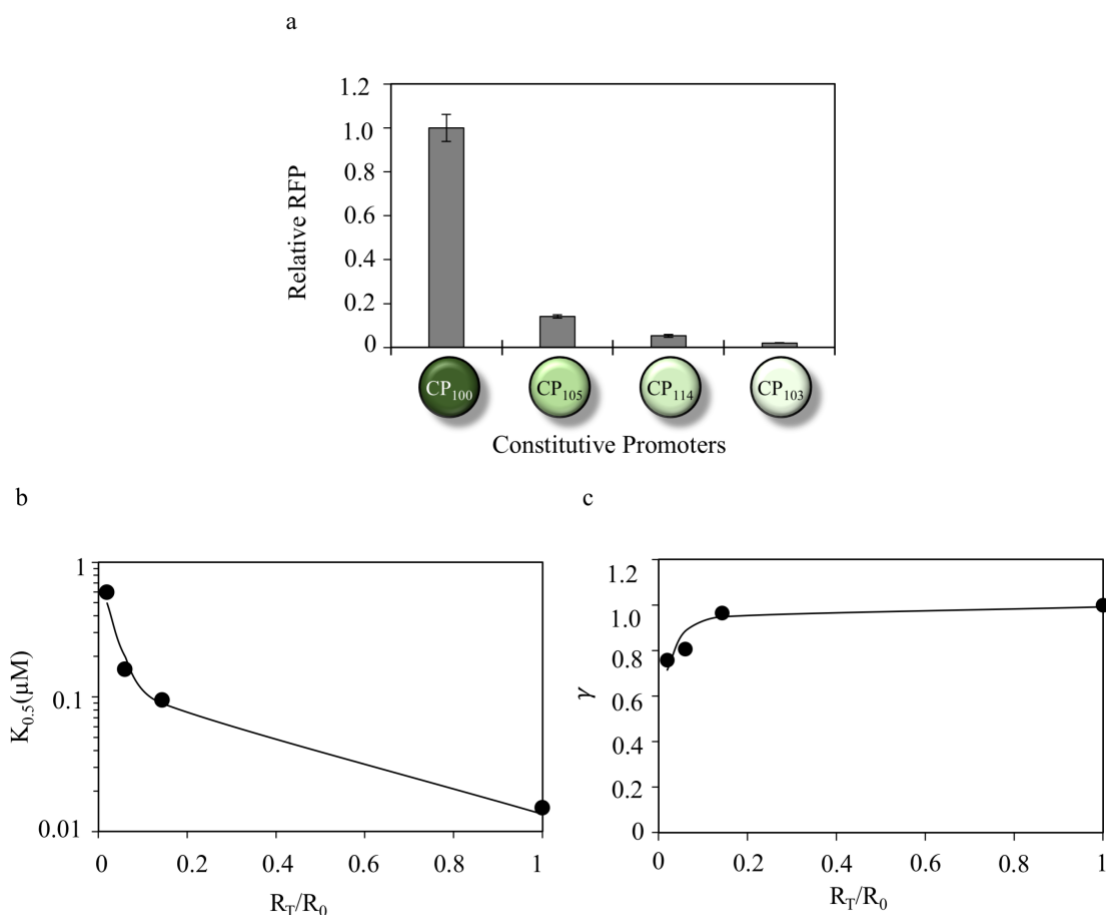


Figure 2.7 Model parameters a and b fitting. a) Experimental characterisation of relative RFP expression from the constitutive promoters expressing different levels of LuxR (constructs C8-C11 in table Table 2.5).

RFP levels are indicated relative to those expressed from the J23100 promoter, which was assigned an arbitrary value of 1. Data are shown as means \pm SD from four independent experiments. **b)** *3OC6HSL* biosensor affinity ($K_{0.5}$) with respect to relative variations in LuxR expression levels. $K_{0.5}$ corresponds to the concentration of external input L that gives the half-maximal response. Dots correspond to the experimental values obtained from the relative transfer functions from Figure 2.6. The solid line corresponds to the fitted mathematical Eq. 2.37. Relative receptor abundance is obtained from the relative activity of the promoters' characterization located upstream LuxR. **c)** Relative dynamic range γ with respect to relative variations in LuxR expression levels. Dots correspond to the experimental values obtained from the relative transfer functions from Figure 2.6. The solid line corresponds to the fitted mathematical Eq. 2.36. Relative receptor abundance is obtained from the relative activity of the promoters' characterization located upstream LuxR.

2.5 Predictive design of two-component biosensors

The above-defined model describes the dependence of $K_{0.5}$ on the relative abundance of the receptor protein R_T , which enables the design of two-component biosensors with predefined $K_{0.5}$ values. $K_{0.5}$ defines both the activation threshold and the operating range of the sensor. Thus, two-component biosensors with predefined $K_{0.5}$ values can be designed straightforwardly by calculating the relative R_T levels necessary to implement a given value of $K_{0.5}$ using the following equation:

$$R_T(K_{0.5}) = \frac{a_1}{b_1 \cdot K_{0.5}} - \frac{b_0}{b_1} \quad \text{Eq. 2.38}$$

To test the model predictability, we built a set of genetic constructs with different affinities $K_{0.5}$ expressing the receptor protein upon different promoters, either constitutive (promoter CP_{J23112} and P_{TET}: C5-C6 in Table 2.4) or inducible (construct C7 Table 2.4). It should be mentioned that the inducible system was implemented using the L-arabinose dependent promoter P_{B_{ad}} [Khlebnikov et al., 2000].

First, we characterized the relative activity of the different promoters involved in biosensors C5-C7. For this goal, we built a set of genetic constructs expressing an RFP under each promoter (constructs C12-C14 in Table 2.5). The experimental characterization of these promoters is shown in Figure 2.8.

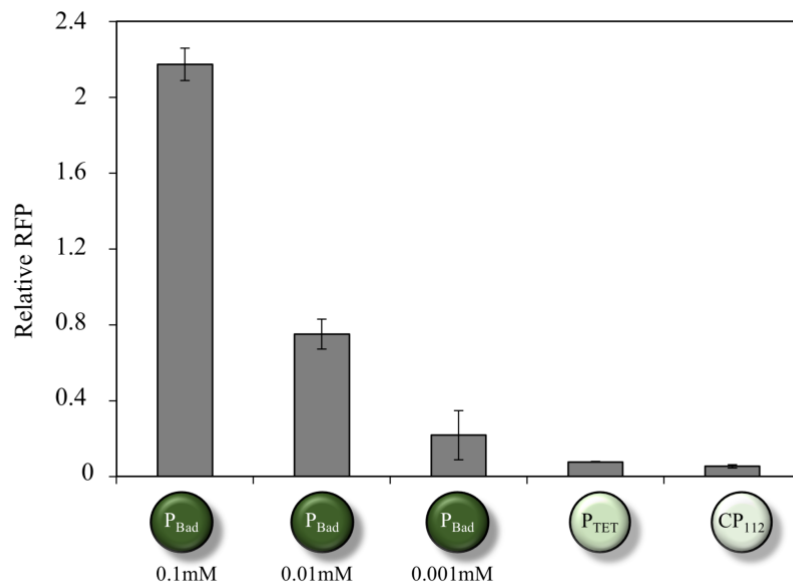


Figure 2.8 Relative promoters' strength characterization. Experimental characterization of the relative RFP expression from the constitutive promoters expressing different levels of LuxR (constructs C12-C14 in Table 2.5). RFP levels are indicated relative to those expressed from the J23100 promoter, which was assigned an arbitrary value of 1. Data are shown as means \pm SD from four independent experiments.

From these results, it was possible to estimate R_T values directly from the relative promoters' activity. Finally, using Eq. 2.35, Eq. 2.36 and Eq. 2.37 it was possible to calculate the theoretical transfer function for each biosensor C5-C7 using the estimated R_T values. In the case of the C7, based on the arabinose dependent promoter, theoretical calculations of transfer functions were performed considering three different arabinose concentrations, i.e. 0.1mM, 0.01mM and 0.001mM. The biosensor transfer functions theoretically calculated were compared with experimental measures.

Table 2.2 summarizes and compares the theoretical R_T values required to implement different $K_{0.5}$ values with those obtained experimentally from the relative promoter activity of constructs C12-C14.

Genetic Construct	$K_{0.5}$	Theoretical R_T levels	Experimental R_T Levels
CP ₁₁₂ LuxR	$4 \cdot 10^{-1} \mu\text{M}$	0.02	0.05 ± 0.02
P _{tet} LuxR	$1.5 \cdot 10^{-1} \mu\text{M}$	0.088	0.07 ± 0.02
P _{Bad} LuxR + 0.001mM arabinose	$6 \cdot 10^{-2} \mu\text{M}$	0.26	0.21 ± 0.09
P _{Bad} LuxR + 0.01mM arabinose	$10^{-2} \mu\text{M}$	0.89	0.75 ± 0.26
P _{Bad} LuxR + 0.1mM arabinose	$5 \cdot 10^{-3} \mu\text{M}$	2.7	2.17 ± 0.35

Table 2.2 Theoretical and experimentally obtained R_T values associated with $K_{0.5}$ values. By fixing several $K_{0.5}$ values the theoretical relative R_T levels haven been calculated using Eq. 2.37. The theoretical R_T levels are compared with the experimental characterization of the relative promoter strength for constructs C5-C7 from Table 2.4. Coefficient $R^2 = 0.99$ correspond to correlation between experimental and theoretical values of R_T levels.

Figure 2.9a-e show the good agreement between the theoretically calculated and the experimentally measured transfer functions. Moreover, Figure 2.9f shows the experimental values of $K_{0.5}$ for the whole set of genetic constructs analysed in this work (C1-C7) superimposed on the theoretical curve described by Eq. 2.37. It should be mentioned that theoretical predictions accurately describe the experimental behaviour independent of the particular genetic system used to express LuxR at the required relative level. This fact indicates that abundance of the receptor protein R_T is the key regulatory factor, independently of the specific genetic system used to produce R_T .

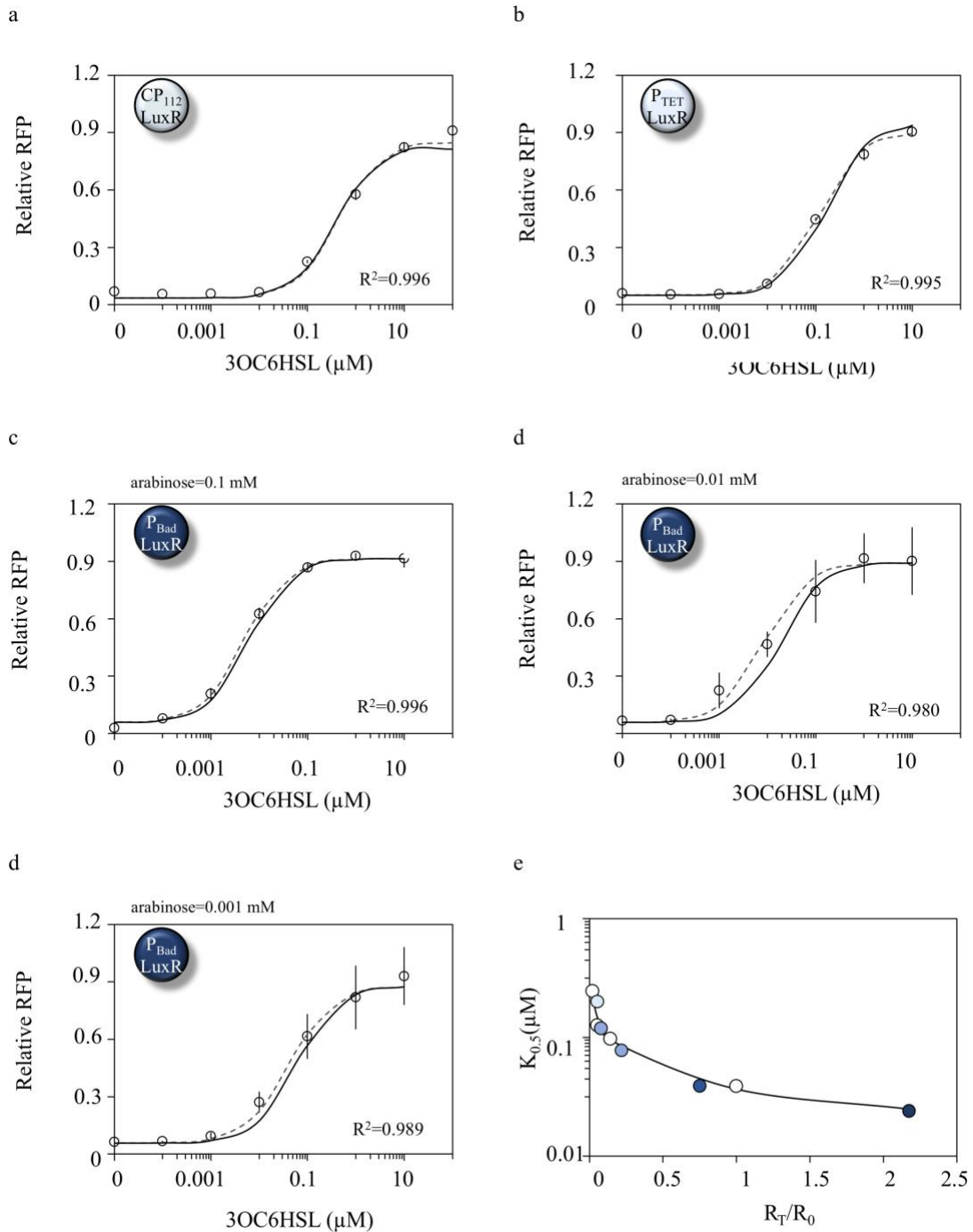


Figure 2.9 Model predictions of LuxR-dependent transfer functions. a-e) The relationship between input *3OC6HSL* concentration and output RFP level was measured for constructs C5-C7 from Table 2.4. The relative RFP values were obtained by dividing RFP levels by the maximum RFP value, which corresponds to the maximum induction level, i.e. $L=10 \mu\text{M}$ of construct C1. Dots correspond to experimental values and the error bars are the standard deviation of four independent experiments. The dashed lines correspond to the experimental fitting with parameters in Table 2.6. The solid lines represent the predicted transfer functions. Pearson test was applied to the experimental and model predicted transfer

functions obtaining the correlation coefficients R^2 . **f**) Crosses are the experimental values of $K_{0.5}$ corresponding to genetic constructs C1-C4 used to determine model parameters. The solid line represents theoretical predictions of $K_{0.5}$ according to Eq. 2.34 with fitted parameters. Circles are experimental values of $K_{0.5}$ corresponding to: C12, C13, C14 (0.001mM) C14 (0.01mM) and C14 (0.1mM) ordered from lower to higher R_T/R_0 values.

2.6 Dependence of sensitivity and operating range on receptor abundance

One of the most important features of a biosensor is the so-called sensitivity, σ . Biosensor sensitivity can be defined as the output variation for a given change in the input [Banica, 2012]. It should be mentioned that, for biosensors that display a nonlinear response, the value of σ is different for each input concentration L .

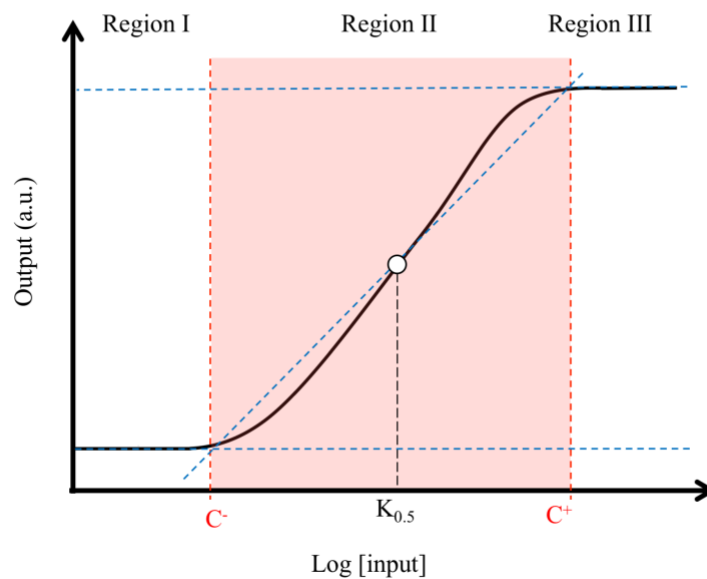


Figure 2.10 Mathematical determination of the biosensor operating range. Schematic representation of the three different determined sensor regions and the geometrical method proposed to define the optimal operating range. The dashed blue-lines represent depict the maximum and minimum output response values and the tangent to Θ at $C^* = \log(K_{0.5})$. The points of intersection of the blue dashed lines determine the upper and lower bounds, *i. e.* C^+ and C^- , of the optimal operating range.

Our theoretical analysis and experimental data show that two-component biosensor transfer functions have three well-defined regions, with different sensitivities, as represented in Figure 2.10. At low and high L concentrations (Regions I and III) the output θ shows no significant dependence on the input, i.e. $\sigma \approx 0$. However, there is a significant increase in biosensor sensitivity within Region II that corresponds to the optimal biosensor operating range, i.e. the range of input concentrations that induce a significant change in the output [Hicks, M., Bachmann, T.T., Wang, 2019]. For further mathematical analysis of this phenomenon, we defined parameter C as:

$$C = \log(L) \tag{Eq. 2.39}$$

Hence, Eq. 2.35 can be rewritten as:

$$\theta = \gamma(R_T) \cdot \left(\frac{10^c}{K_{0.5}(R_T) + 10^c} \right) + \theta_0 \tag{Eq. 2.40}$$

With this reformulation, changes in L are parameterized by changes in C and the behaviour of Eq. 2.40 presents a quasi-linear dependence with respect to C in Region II. As a consequence, sensitivity in this region can be approximated to:

$$\sigma = \frac{d\theta}{dC} \tag{Eq. 2.41}$$

i.e.

$$\sigma = \frac{\gamma \cdot K_{0.5}(R_T) \cdot 10^c + \ln(10)}{(K_{0.5}(R_T) + 10^c)^2} \tag{Eq. 2.42}$$

With $K_{0.5}(R_T)$ defined by Eq. 2.38. According to Eq. 2.40, a biosensor response has maximum sensitivity, i.e. $\frac{d\sigma}{dC} = 0$, at $C^* = \log(K_{0.5})$, which corresponds to $L=K_{0.5}$.

Here, we propose a mathematical determination of the Region II, i.e. the range of concentrations in which biosensor response exhibits higher sensitivity. This range can be

determined by the upper and lower bounds, C^+ and C^- , which are defined by the intersection of the tangent to Θ at $C^* = \log(K_{0.5})$, with the maximum and minimum values of the transfer function, respectively. Figure 2.10 shows a representation of this geometrical definition. The tangent line can be described by:

$$f = \left. \frac{d\Theta}{dC} \right|_{C^*} \cdot C + f_0 \quad \text{Eq. 2.43}$$

Using Eq. 2.40 and considering that at C^* the tangent line intersects the response curve at half maximum amplitude, i.e. $f = \frac{\gamma}{2}$, we can write:

$$f = \frac{\gamma \cdot \ln(10)}{4} \cdot C + \frac{\gamma}{2} [2 - \ln(10) \cdot \log(K_{0.5}(R_T))] \quad \text{Eq. 2.44}$$

Finally, the range of input concentrations in which the biosensor has higher sensitivity can be defined by $f(C^-) = 0$ and $f(C^+) = \gamma$. By imposing these conditions, C^+ and C^- can be defined as:

$$C^\pm = \frac{\log(K_{0.5}(R_T)) + \ln(10) \pm 2}{\ln(10)} \quad \text{Eq. 2.45}$$

Hence, the optimal operating range of the biosensor corresponds to the interval of input concentrations $L \in (10^{C^-}, 10^{C^+})$, in which the transfer function of the biosensor exhibits higher sensitivity. In this interval, the transfer function can be approximated to a linear dependence of Θ on $\log(L)$ described by:

$$\Theta \approx \frac{\gamma \cdot \ln(10)}{4} \cdot C + \frac{\gamma}{2} [2 - \ln(10) \cdot \log(K_{0.5}(R_T))] + \Theta_0 \quad \text{Eq. 2.46}$$

2.7 Experimental validation of the operating range

The whole set of biosensors from the presented study, described in Table 2.4, were submitted to the theoretical calculation of the operating range from the beforehand described mathematical framework in **section 2.6**. Hence, aiming to obtain an experimental validation.

Results containing experimental transfer function values along with the theoretical calculation of the operating range, i.e. Region II delimitation by C^+ and C^- thresholds, from Eq. 2.45, are shown in Figure 2.11. Furthermore, we have calculated the percentage of the experimental exhibited operating range captured from the mathematical formalization. Results reveal that our mathematical definition of the operating range captured at least 71.2% of the dynamic range of the biosensors within the region defined by Eq. 2.45 (see Figure 2.11). It is worth mentioning that these results indicate that the operating range of two-component biosensors can be determined from $K_{0.5}$ value, which in turn depends on the R_T levels. In consequence, modifying the R_T levels it is possible to tune the operating range of a given two-component biosensor.

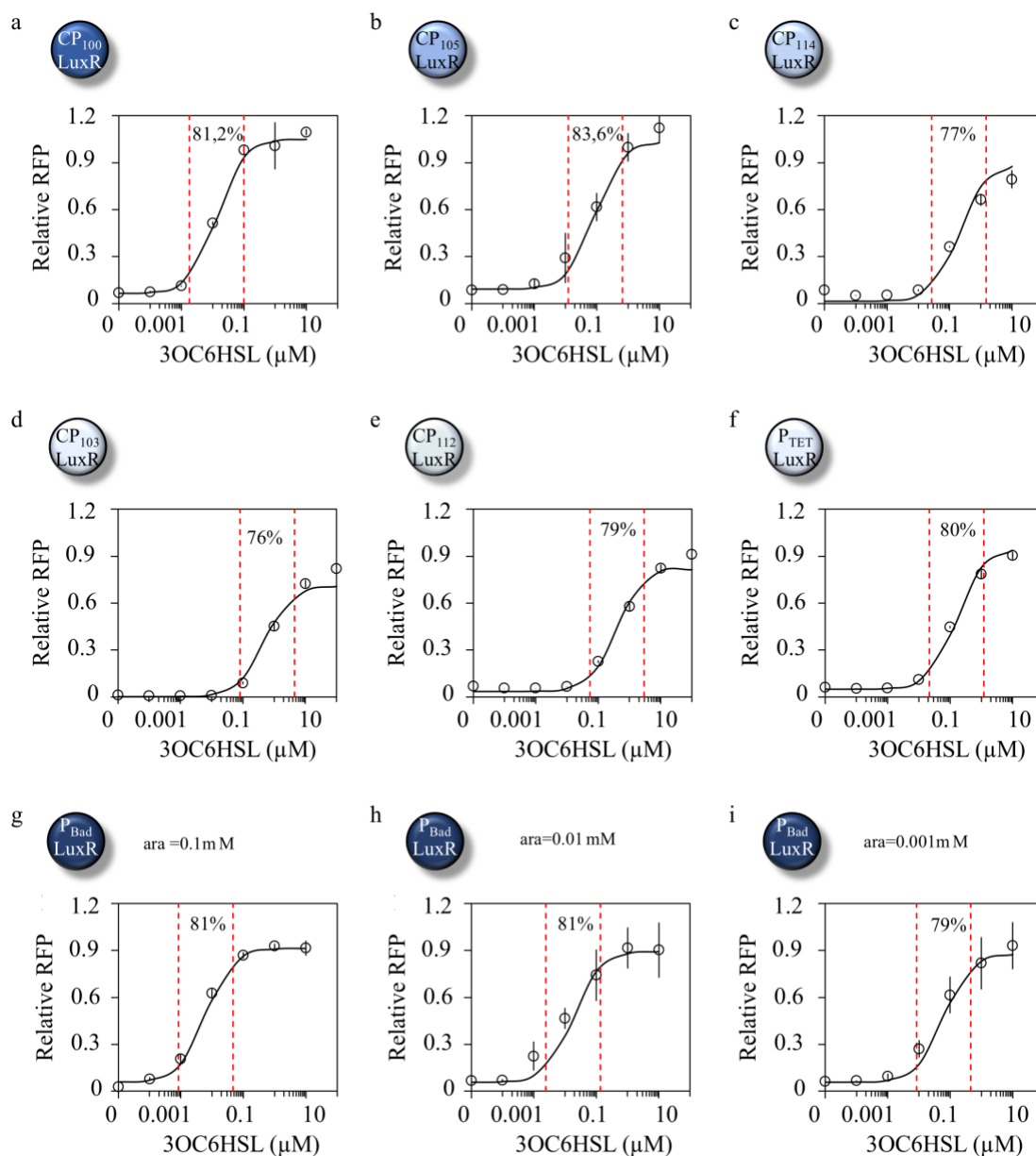


Figure 2.11 Mathematical determination of the biosensor operating range. a-i) The relationship between input 3OC6HSL concentration and output RFP level was measured for constructs C1-C7 from Table 2.4. Relative RFP values were obtained by dividing RFP levels by the maximum RFP value, which corresponds to that obtained with construct C1 (at the maximum induction level, i.e. $L=10$ μM). Dots correspond to experimental values and the solid lines represent the predicted transfer functions. The error bars shown in the figures are the standard deviation of four independent experiments. The red dashed lines correspond to the C^+ and C^- obtained from Eq. 2.45. The optimal operation range was calculated according to Eq. 2.46. Percentage values indicate the dynamic range captured by the mathematically defined optimal operating range.

2.8 Discussion

The design of genetic devices according to the fundamental principles of engineering is a big challenge in synthetic biology. It is necessary to develop tools and mathematical frameworks that help to design and construct such devices in a predictable manner rather than by costly trial and error approaches [Kwok, 2010; Lucks et al., 2008]. Focusing on biosensor designs, many studies have been devoted to engineering new cellular devices by exploiting natural sensors present in cells [Carpenter et al., 2018]. However, biosensors have to work within an adequate operating range for the development of a specific application. It is therefore sometimes necessary to tune natural systems in terms of activation threshold, sensitivity, operating range and dynamic range. In this study, we performed our analyses using one of the most abundant sensor systems in prokaryotes, the two-component sensor systems. We explored the possibility of adapting the two-component biosensor response by modulating the abundance of the main component, i.e. the receptor protein. To address this issue, we developed a mathematical model that determines the relationship between biosensor features and the abundance of receptor proteins. We further built a library of two-component biosensors based on the well-known Lux system [Williams et al., 2008]. As a first step, we analysed only the effect of receptor abundance on $K_{0.5}$ and γ by introducing different constitutive promoters, with different strengths, upstream of the receptor protein. The experimental results, which were consistent with previously published data [Ang et al., 2013; B. Wang et al., 2015], showed a clear correlation between threshold activation, parameterized by $K_{0.5}$, the relative dynamic range γ , and the sensitivity σ with LuxR relative concentrations. Experimental results were used to fit the model and determine its parameters. Interestingly, once the parameters were determined, the mathematical model allowed predicting the biosensor transfer function for a given abundance of the receptor protein. To validate these predictions, we built several genetic systems in which LuxR relative levels could be modulated by changes in the promoter or the RBS, or by the addition of an extracellular effector. The relationship observed between $K_{0.5}$, representing the activation threshold of the biosensor, and the relative abundance of LuxR protein is remarkable. Notably, $K_{0.5}$ could be increased by up to two orders of magnitude by regulation of LuxR levels, independently of the method used to regulate receptor concentration. However, the

dynamic range γ did not exhibit a strong dependence on LuxR abundance, meaning that transfer functions could be shifted towards greater or lower values of *3OC6HSL* without a major impact on the dynamic range. It is worth mentioning that the model derivation assumes that the abundance of receptor protein is large enough to consider a linear relationship between the concentrations of monomeric and dimeric forms of the receptor protein. This assumption can limit the applicability of the model to those situations in which receptor protein concentrations are very low. However, experimental results demonstrated that even for promoters with very low activities (construct C11 in Figure 2.7a) the theoretical calculations properly describe the experimental data, suggesting that the model is of general applicability for a broad range of genetic architectures.

Particularly notable were the results of the analysis of biosensor sensitivity. Due to the nonlinear response of the genetic systems, it is not possible to determine a single numerical value for their sensitivity. Despite showing a different sensitivity at each input concentration it was possible to distinguish two regions of low sensitivity, i.e. one at low and one at high-input concentrations, and a high sensitivity region at intermediate-input concentrations. Interestingly, the intermediate-input concentration region determines the input ranges that induce the maximal output variation, which corresponds to the optimal operating range of the biosensor. We have proposed a new method that allows the theoretical calculation of such a range of input concentrations. Furthermore, our model contemplates calculating the abundance of receptor protein necessary to adjust this optimal operating range to a given input range. Experimental results show good agreement with our theoretical predictions, thus validating our model.

Future work should be devoted to exploring the feasibility of using the currently developed model for predictable biosensor designs in other systems based on similar two-component architecture. Recent studies have demonstrated the application of synthetic biology biosensors in environmental monitoring [H.-J. J. Chang et al., 2017; Rinken & Kivirand, 2019], bioproduction [Pandi et al., 2019; Rogers & Church, 2016], biomedical applications in diagnostics [W. Zhou et al., 2014] and health monitoring [Mimee et al., 2018]. However, an ability to detect relevant inputs is not sufficient for the construction of commercial cell-based biosensors. Relevant input detection should be coupled with

output detection within the appropriate range of input concentrations for each specific application. We aimed to overcome the above limitations by developing a theoretical and experimental framework that explains the relationships between the main features of biosensor components.

2.9 Methodology

2.9.1 Strains, media and growth conditions

Top10 E. coli strain was used for cloning and expression experiments (F- *mcrA* Δ (*mrr*-*hsdRMS*-*mcrBC*) ϕ 80*lacZ* Δ M15 Δ *lacX74* *nupG* *recA1* *araD139* Δ (*ara-leu*)7697 *galE15* *galK16* *rpsL*(StrR) *endA1* λ -).

E. coli were grown in Lysogeny Broth (LB) at 37 °C and selected with the appropriate antibiotics corresponding to the transformed plasmid. Antibiotics were purchased from Sigma and used at the following concentration: chloramphenicol: 35 μ g/ml, kanamycin: 35 μ g/ml and ampicillin: 50 μ g/ml.

Bacterial strains were preserved in LB glycerol 20% (v/v) at -80 °C. Single colonies obtained from streaked glycerol stocks were inoculated and the cells were grown overnight at 37 °C with shaking (200 revolutions per minute (rpm)). Overnight cultures were diluted into fresh LB (1/100 dilution) and grown for 5 hours until the exponential phase, OD660 \approx 0.4.

Induction media consisted of LB kanamycin and the appropriate inducer or inducer combination: *3OC6HSL* (N-[-ketocaproyl]-L-homoserine lactone; Cayman Chemical Company, USA) and arabinose (L-(+)-Arabinose 98%, Sigma Aldrich, USA). Different *3OC6HSL* concentrations were prepared from an initial stock of 4·10⁻²M. Serial dilutions in LB kanamycin, providing final concentrations ranging from 10 μ M to 0.001 μ M, were prepared the day of the experiment. Different arabinose concentrations were prepared from an initial stock of 0,74 M. Serial dilutions in LB kanamycin, providing

final concentrations ranging from 0.1 mM to 0.001 mM were prepared the day of the experiment.

2 μ l of diluted cultures were loaded into a 96-well microplate (Nunc, ThermoFisher Scientific, USA) and induced in a final volume of 200 μ l. Growth curves are shown in Figure A. 1.

2.9.2 Molecular cloning and parts

Construction of the genetic sensors by cloning was carried out using the Biobrick assembly method and parts from the Spring 2018 iGEM distribution (<http://parts.igem.org>). DNA sequences are in Table A. 1.

Name	Part Registry Code	Plasmid
Terminator	BBa_B0014	pSB1C3
Weak RBS	BBa_B0033	pSB1C3
Medium RBS	BBa_B0030	pSB1C3
Strong RBS	BBa_B0034	pSB1C3
Constitutive promoter 1	BBa_J23100	pSB1C3
Constitutive promoter 2	BBa_J23105	pSB1C3
Constitutive promoter 3	BBa_J231114	pSB1C3
Constitutive promoter 4	BBa_J23103	pSB1C3
Constitutive promoter 5	BBa_J23112	pSB1C3
Ptet promoter	BBa_R0040	pSB1C3
Arabinose-inducible promoter	BBa_I0050	pSB1C3
LuxR receptor protein	BBa_C0061	pSB1C3
Red Fluorescent Protein	BBa_E1010	pSB1C3
Lux inducible promoter	BBa_R0061	pSB1C3

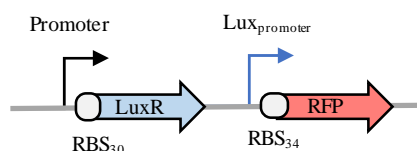
Table 2.3 Biobricks used in this study.





2.9.3 Biosensor genetic architectures

All the constructs analysed in this chapter were built by combining Table 2.3 parts using 3A assembly. Table 2.4 and Table 2.5 show the genetic structures of the different constructs. Biobrick cloning was performed using an assembly kit (Ginkgo Bioworks, USA). All constructs were included in the Biobricks high copy number plasmid (pSB1AK3) and were transformed using a chemical method. Sanger sequencing confirmed all genetic constructs. Plasmid maps are available in Table A. 2.

2.9.3.1 Biosensors

-LuxR-Terminator-Plux-RBS-RFP architecture was cloned downstream different DNA sequences, i.e. Promoter+RBS, with different expression levels.



Cell	Reference	Genetic Structure
	C1	B0014 + J23100 + B0030 + C0061 + B0014 + R0061 + B0034 + E1010+ B0014
	C2	B0014 + J23105 + B0030 + C0061 + B0014 + R0061 + B0034 + E1010 + B0014
	C3	B0014 + J23114 + B0030 + C0061 + B0014 + R0061 + B0034 + E1010 + B0014
	C4	B0014 + J23103 + B0030 + C0061 + B0014 + R0061 + B0034 + E1010 + B0014




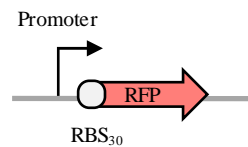

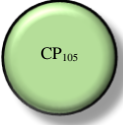

	C5	B0014 + J23112 + B0030 + C0061 + B0014 + R0061 + B0034 + E1010 + B0014
	C6	B0014 + R0040 + B0033 + C0061 + B0014 + R0061 + B0034 + E1010 + B0014
	C7	B0014 + I0500 + B0030 + C0061 + B0014 + R0061 + B0034 + E1010 + B0014

Table 2.4. Biosensors' genetic constructs.

2.9.3.2 Controls

Genetic architecture comprising **Terminator-Promoter-RBS** was designed to obtain different RFP output expressions. Anderson promoters (i.e. J23 constitutive promoters) upstream a medium RBS and inducible P_{Bad} were used as a mechanism for different protein expression levels.



Cell	Reference	Genetic Structure
	C8	B0014 + J23100 + B0030 + E1010 + B0014
	C9	B0014 + J23105 + B0030 + E1010 + B0014
	C10	B0014 + J23114 + B0030 + E1010 + B0014

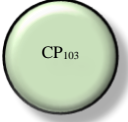

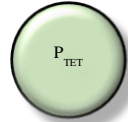

	C11	B0014 + J23103 + B0030 + E1010 + B0014
	C12	B0014 + J23112 + B0030 + E1010 + B0014
	C13	B0014 + R0040 + B0033 + E1010 + B0014
	C14	I0500 + B0030 + E1010 + B0014

Table 2.5 Controls' genetic constructs

2.9.4 Fluorescence assays for gene expression determination

Incubation for in vivo measurements was carried out by transferring 2 μ l of the overnight diluted cultures to 200 μ l of LB kanamycin induction media into a flat bottomed 96-well microplate. LB without cells was also incubated as a background control for both fluorescence and absorbance.

Gene expression induced by a wide range of *3OC6HSL* and arabinose concentrations over time was monitored by quantification of the RFP. The bacterial cultures were incubated and induced on a Synergy MX microplate reader (BioTek Instruments, USA) and measurements were taken every 30 min for 20 h. Conditions for fluorescence measurements of the red fluorescent protein (RFP) were: excitation: 578 \pm 9 nm, emission: 616 \pm 9 nm, with a gain of 50.

Sample (S) absorbance and fluorescence (f) readings (OD_{660} (S) and f (S), respectively) were corrected using respective signal background (B) controls (OD_{660} (B), f (B)). Averaged data were obtained from three independent experiments. As previously





described [Chappell et al., 2013], reporter protein θ was calculated according to the expression:

$$\theta = \frac{f(S) - f(B)}{OD_{660}(S) - OD_{660}(B)} \quad \text{Eq. 2.47}$$

The value θ corresponds, with a factor of proportionality, to the concentration of the RFP protein per cell.

2.9.5 Experimental fitting model parameters

Matlab R2016a least-squares analysis software was used for fitting the parameters to experimental results according to the Hill equation $\theta = \varphi \cdot \left(\frac{L^n}{\omega + L^n} \right) + \varphi_0$. Table 2.6 shows fitted parameters for each construct, i.e. C1-C7, and the computed correlated coefficient R^2 .

Cell	Construct	φ	φ_0	ω (μM)	n	R^2
	C1	1	0.06	$1.5 \cdot 10^{-2}$	0.99	0.99
	C2	1.04	0.09	$9.5 \cdot 10^{-2}$	0.98	0.99
	C3	0.8	0.01	$1.6 \cdot 10^{-1}$	0.99	0.99
	C4	0.76	0	$6 \cdot 10^{-1}$	1	0.99




	C5	0.81	0.03	$3.7 \cdot 10^{-1}$	1.01	0.99
	C6	0.86	0.05	$1.4 \cdot 10^{-1}$	0.99	0.99
	C7 (ara=0.1mM)	0.86	0.06	$5 \cdot 10^{-3}$	1	0.99
	C7 (ara=0.01mM)	0.84	0.05	$1.5 \cdot 10^{-2}$	0.98	0.98
	C7 (ara=0.001mM)	0.82	0.06	10^{-1}	0.97	0.99

Table 2.6 Parameters used to fit the experimental biosensor transfer functions.

CHAPTER 3

Tools for signal processor module design:

2D BioPrintable Computational Circuits: modular topology for digital computation

Working on the design and construction of living biomedical devices claims on the study and analysis of extracellular signal detection, followed by signal integration to perform desired responses. This chapter focuses on how sensed signals can be integrated to produce non-trivial responses. More specifically, a multi-branch approach implementing digital computations, inspired by printable electronic circuits, was designed by exploiting multicellularity and space. *E. coli* mimicking the core-elements of transistors were built to validate our design. This work was developed in the *Synthetic biology for biomedical applications lab*, in collaboration with Dr. Javier Macia and Sira Mogas, under the current project MINECO (2018-2020) “Printable Cellular Circuits”.

3 TOOLS FOR SIGNAL PROCESSOR MODULE DESIGN

3.1 Principles of cellular computation

Cutting-edge technologies foreseeing unprecedented progress in our society are based on the development of devices performing complex computations. Internet and cell phones are the more evident examples; however, technology has revolutionized the way we learn, communicate or even though we treat diseases. In light of this, generating non-trivial responses affording programmed rules permit to integrate information gathered from sensor modules. Computation is an information processing approach, where multiple inputs signals, either analogue or digital, are integrated into an output [Harder, 1959].

Palpable is the role of computation in electronics, where multiple signals are integrated, assembled or otherwise processed. Nonetheless, computation is also an intrinsic property of living systems. Natural systems rely on integrating multiple external signals for environmental adaptation [Nurse, 2008]. Understanding how biological systems compute [Hopfield, 1994] has sped the development of a novel SB discipline: cellular computation. Engineering living organisms using rational design, from the abovementioned engineering approaches, has envisaged the performance of complex computations with molecules and cells as a substrate. Enormous potential encompasses the development of cellular computers due to its autonomous performance relying on the intrinsic sensorial machinery. Hence, applications ranging from environmental approaches up to complex diseases are envisioned [Y. Y. Chen et al., 2012]. Nevertheless, fostering society-need applications requires for living machines to depict reliable, scalable, robust and predictable behaviours [Kwok, 2010].

The design and implementation of biological devices with computation capability have been inspired by electronics. Electronic circuits are physical devices encoding information in electrons flow. Individual components altering such flow are connected by physically separated wires, and due to an appropriate assembly, are capable to perform

complex operations. In that sense, either digital or analogue operations could be implemented.

Living organisms operate analogously *per se* [Rahul Sarpeshkar, 1998] and analogue computation is further envisioned to tackle the demands of complex society-applications due to the need for fine-tuning graded responses [Daniel et al., 2013; Purcell & Lu, 2014], Yet, circuits performing analogue computation are not as standardized as digital ones due to the lack of precision [T. Song et al., 2016] and output response variability [R. Sarpeshkar, 2014]. For that reason, up to now, although being a challenge for circuit design [Vaidyanathan et al., 2015], computation has been afforded by transforming the analogue behaviours of the biological elements into a digital response (Figure 3.1a). Therefore, signals are treated as binary: logic state “1” is defined when the signal is present or it’s above a certain threshold, and logic state “0” is defined when the signal is not present or it’s below a certain threshold, computing in a discrete set. Digital operations rely on the logical combination of the signals to be integrated. All possible input combinations with their corresponding output are represented in the so-called truth table. (Some examples of one-input and two-input truth tables are shown in Figure 3.1b).

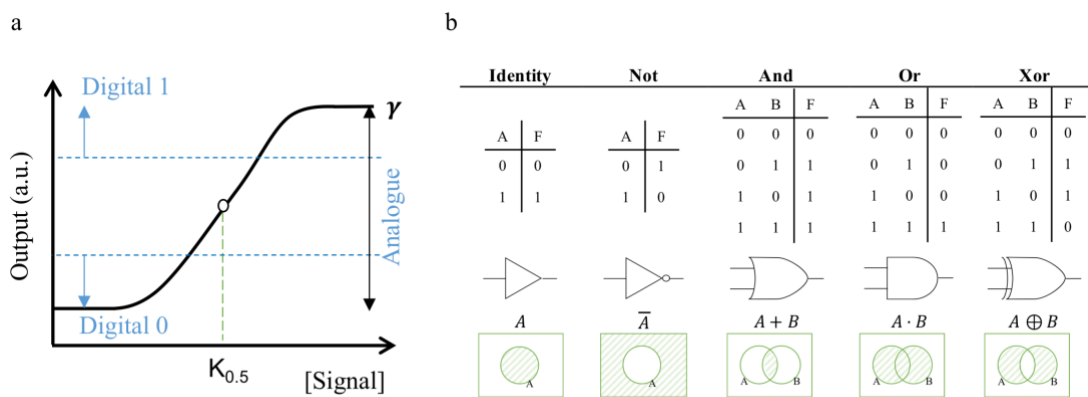


Figure 3.1. Digital and analogue computation. a) An analogue signal is digitalized by defining two different thresholds. Responses above the threshold are considered as a digital 1 and responses below as a digital 0. b) One-input and two-inputs logic gates representation. For each logic gate the truth table, Venn diagram and Boolean algebra formulation are depicted.

Several efforts on finding the biological substrate to perform logic computation are related in the subsequent **sections 3.1.1 to 3.1.5**. Throughout, exploring different

biological strategies that had allowed to assemble the roots of standard and robust cellular computation devices.

3.1.1 Devices based on transcriptional regulations

From the first Lac operon regulation mechanism [Monod & Jacob, 1961], insights were gained on protein mechanisms to modulate DNA sequences. Natural transcription regulators such as LacI, TetR, cI, cAMP, and AraC [Terpe, 2006] had been broadly used to implement logic gates. Moreover, these well-known systems have been used, for instance, for generating *AND* gates based on protein splitting [Moon et al., 2012; Shis & Bennett, 2013; B. Wang et al., 2011] as depicted in Figure 3.2a, or accounting for more sophisticated DNA architectures using CRISPR or TALEN [Lienert et al., 2013; Nielsen & Voigt, 2014] allowing the creation of *AND* logic circuits operating in eukaryotes. Despite, computations at the DNA level is widely used, such approach requires for large time periods to produce the expected output.

3.1.2 Devices based on DNA recombination

Computation based on DNA recombination uses recombinases as a tool to modify DNA. Recombinases recognize distinct DNA sequences that are placed flanking a sequence of interest. Recombinases can excise or flip the DNA of interest depending on the relative orientation of a short, directional DNA sequence [Groth & Calos, 2004]. Recombinases (Figure 3.2b) have been broadly used to build synthetic logic circuits for DNA-encoded memory storage [Farzadfard & Lu, 2014; Siuti et al., 2014].

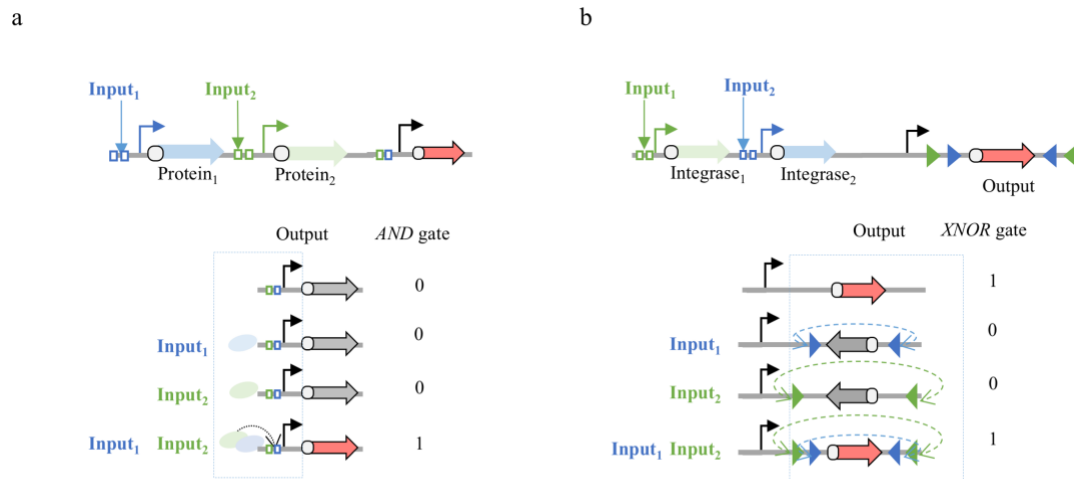


Figure 3.2 Processor computation based on different biological-elements. a) Transcriptional regulation. Schematic representation of an *AND* logic circuit from split protein transcription factor. Two different input signals trigger the expression of the two units that bind to trigger output production. Adapted from [B. Wang et al., 2011]. **b)** DNA recombination. Schematic representation of an *XNOR* logic circuit implemented with serine recombinases. Recombinases were induced by two different input signals: signal 1 triggers the expression of the green recombinase whereas signal 2 triggers the expression of the blue one. Recombinases attach to the triangular coloured motifs triggering the inversion of the output production either by one or both elements. Adapted from [Siuti et al., 2014].

3.1.3 Devices based on post-transcriptional regulations

Multiple computational devices have been built based on RNA regulators. For instance, in prokaryotic organisms, mRNA translation can be prevented by introducing a stem-loop structure that hides the ribosome binding sequence (RBS) from the translational machinery. The expression of a small RNA sequence allows unfolding the stem-loop structure in the mRNA, exposing the RBS for ribosome access [Green et al., 2017; Isaacs et al., 2004], as is exemplified in Figure 3.3. Other alternatives, such as targeting mRNAs for degradation introducing miRNAs [B. D. Brown et al., 2007; Xu et al., 2017] have been explored. RNA regulation gives a fast and tight control of output production, however, some problems with the secondary RNA structure may arise.

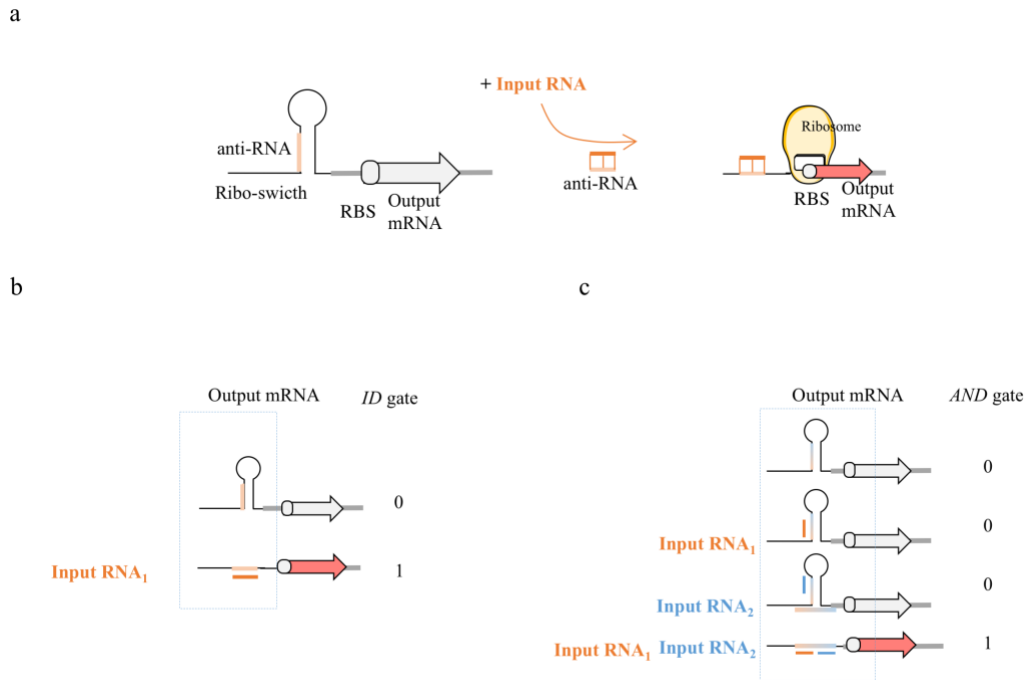


Figure 3.3 Processor computation based on different biological-elements. a) Post-transcriptional regulation. Schematic representation of RNA-inducible riboswitches, forming an RNA stem-loop blocking the ribosome to attach the RNA sequence, when an external molecule is present it generates a conformational change enabling the binding of ribosomes and its translation. b) *Identity* logic circuit. One input RNA molecule is necessary to produce a conformational change in the stem loop and enable the translation of the output mRNA. c) *AND* logic circuit. The presence of two input RNA molecules at the same time are necessary to produce a conformational change in the stem loop and enable the translation of the output mRNA. Adapted from [Green et al., 2017].

3.1.4 Devices based on signalling pathways regulations

Signalling pathways are natural systems that translate external signals to control intracellular cellular functions. Computational devices can be built modulating some key elements of a signalling pathway, for instance, regulating the expression of some MAP kinase proteins in response to external inputs [Furukawa & Hohmann, 2015] or using a the receptor-antigen recognition system, as depicted in Figure 3.4 [Kochenderfer & Rosenberg, 2013; C. Y. Wu et al., 2015]. Signalling pathways modulations are optimal to control information flow and modifying them to produce fast responses, being useful for applications regarding temporal resolution.

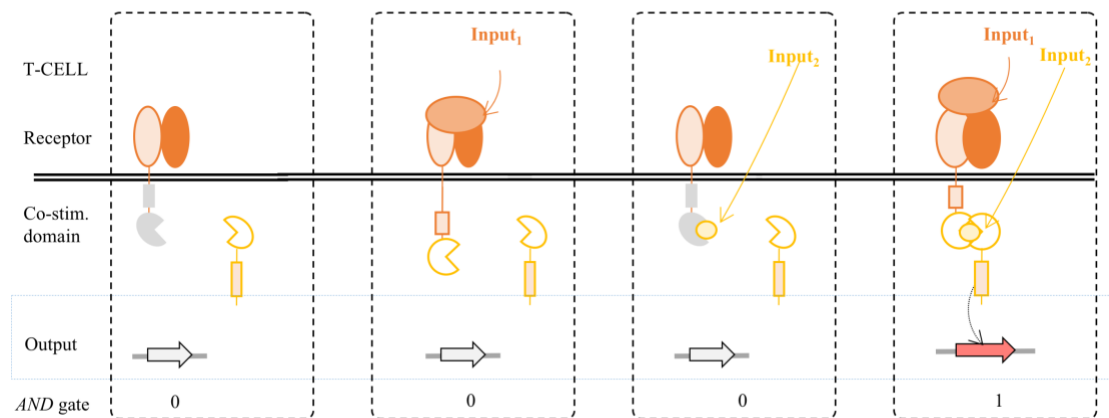


Figure 3.4 Processor computation based on different biological-elements. Signalling pathways. Schematic representation of the strategy for an *AND* logic circuit developed by Wu et al. through splitting the chimeric antigen receptors (CARs) elements into two different peptides that could be assembled in an inducible manner. Adapted from [C. Y. Wu et al., 2015].

3.1.5 Devices based on multicellular computation

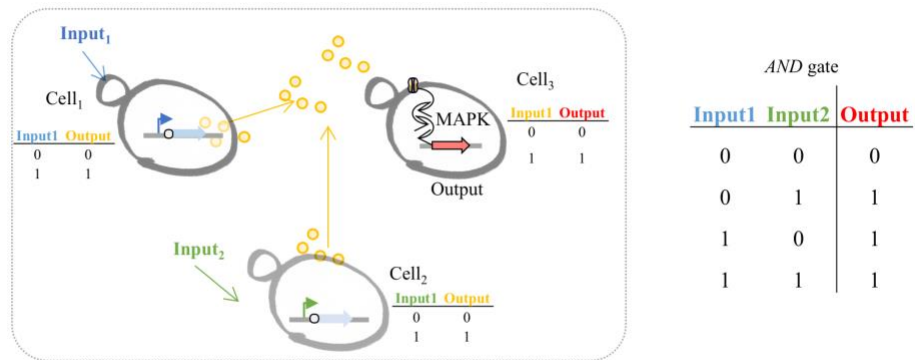
Up until now, we have presented different biological embodiments implementing lower-order logic gates. In electronics, it is described that any complex computation could be implemented by the combination of several logic gates, defining a functionally complete set [Savant et al., 1991]. Unfortunately, this approach fails when applying synthetic biology principles. Embedding large and sophisticated synthetic gene circuits into cellular organisms demands for a large set of orthogonal parts properly connected [Morey et al., 2012; F. Wu et al., 2014], drowning cellular metabolism [M Carbonell-Ballester et al., 2016] and inducing inappropriate host genetic interactions [Tan et al., 2009] and most remarkable, once circuits are engineered, its reusability to create higher-order circuits, as stated in electronics, remains a challenge [Regot et al., 2011]. To overcome these limitations, a new approach based on the multicellular implementation of computational devices has been explored (Figure 3.5).

Implementing computational devices in multicellular consortia, i.e. using different engineered strains, allows simplifying the synthetic genetic circuits (Figure 3.5a). As a result, the number of required orthogonal parts is diminished, the associated metabolic

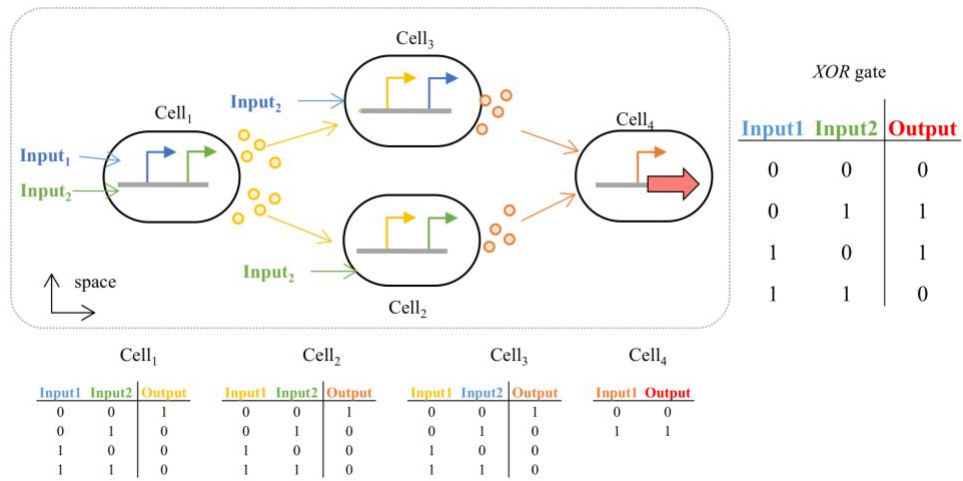
cost is reduced and the host genetic interactions are minimized [Regot et al., 2011]. Nevertheless, allocating different tasks in different cells demands for cellular connection, as wires do in electronics and the growth in the same environment of the different cell types. When performing complex computational devices both the number of different cell types and the number of wires scales up, limiting the scalability of the device [Kwok, 2010]. Physical separation of the different cell types, i.e. spatial distribution in a 2D surface, offers the possibility to combine multiple engineered cells without suffering the negative growth competition effects (Figure 3.5b). Still, the connection of multiple functional modules with wires limit their scalability [Tamsir et al., 2011], denoting that for higher-order logic gates chemical wires without cross-talk are needed [Canton et al., 2008; Macía et al., 2012].

Alternatively, combining multicellular distributed computation [Regot et al., 2011], spatial segregation [Tamsir et al., 2011] and the breakdown of complex logics by the combination of a functionally complete set of logic gates has been demonstrated extremely useful for implementing high complex devices [Macia et al., 2016]. In the general design (Figure 3.5c), a particular logic circuit is composed of M different multicellular consortia allocated in physically isolated chambers, i.e. $\{\psi_1, \psi_2 \dots \psi_M\}$. Each consortium contains two different cell layers: The Input Layer (IL) and the Output Layer (OL) encoding the output “1s” codified in the truth table of the logic computation. The IL senses external inputs and secretes a wiring molecule according to a particular internal logic, *Identity* or *NOT*. Next, the secreted wiring molecule is mixed in the medium implementing the *OR* function implicitly. Then, the OL , consisting on a single cell type that responds to the wiring molecule, produces the device output according to a *NOT* logic, i.e. the output molecule is produced only in the absence of the wiring molecule. Therefore, the final output could be easily implemented by the physical connection of the different chambers when the output is a secreted molecule, e.g. hormone. Noteworthy, only one wire is needed and scalability is afforded by the ability to detect extracellular signals with *Identity* and *NOT* logics. However, stability is compromised due to the consortia negative competition growth effects [Amoyel & Bach, 2014; Kwok, 2010].

a



b



c

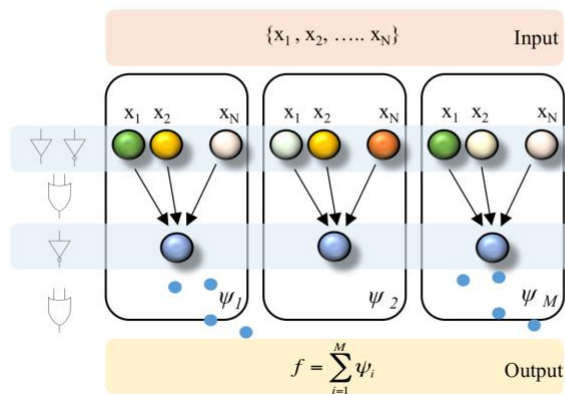


Figure 3.5 Processor computation based on different biological-elements. a) Schematic representation of distributed computation in different engineered cell types. Adapted from [Regot et al., 2011]. b) Schematic representation of an *XNOR* gate by communicating differently engineered *E. coli* cells performing *NOR* and *Identity* gates. Adapted from [Tamsir et al., 2011]. c) Schematic approach in which engineered cells are divided into sequential chambers. Adapted from [Macia et al., 2016].

3.2 Objectives

Efforts in the development of standardized architectures enabling devices to integrate multiple signals and responding to programmed rules have extensively been afforded. However, despite the advantages presented by multicellular computation and spatial segregation, the experimental evidence for complex computational devices are far from being easy to implement in a standard and reliable way, thus, compromising the real development of end-user applications.

We aim to design and systematically built simple, robust and scalable multicellular computational devices by using a new multicellular embodiment in which cells are located in a 2D surface in a very specific geometrical arrangement.

The *specific objectives* addressed within this section are:

- Computation can be implemented by the modulation of a *Carrier Signal*, that flows through a 2D surface, in response to external inputs, emulating transistor-modules.
- Any arbitrary device performing complex computations can be implemented into a multi-branch topology, in which each branch behaves as a multi-base transistor.
- Experimentally validate the multi-branch architecture by building a library of engineered *E. coli* strains.

3.3 Design of a transistor-like modules

Considering that computation is, on its essence, a matter of information processing [Harder, 1959], our approach encodes information in the concentration of a unique biological signal, the carrying signal (*CS*) [Basu et al., 2005; Waters & Bassler, 2005]. We envisioned the creation of our devices in a 2-dimensional surface where *CS* is produced in a specific location, diffused along the surface, and could interact with different modulatory elements properly distributed alongside the surface. The main role of these modulatory elements relies on performing *CS* modulations: by allowing or blocking its diffusion. The specific spatial arrangement of modulatory elements codifies the device computational complexity.

Gaining insights from electronics, devices were designed based on transistors-like modules, the basic elements of analogue and digital computation. Electronic transistors use electric fields to control the flow of current between the emitter and the collector terminals [Savant et al., 1991]. The electron flow is influenced by the base element, modulating it, depending on its ability to conduct electric signals (Figure 3.6a). Furthermore, our approach takes inspiration from printed electronics [Khan et al., 2015; Tong et al., 2018], exploring the ability to draw 2D cellular devices behaving as transistor elements. As represented in Figure 3.6b-c, we have implemented the transistor-like architecture by the combination of different engineered cell types. Namely, the Emitter Cell (*EC*) secretes *CS*, which diffuses along the 2D surface and is modulated by Base Cells (*BC*), to be finally detected by Collector Cells (*CC*). It is worth mentioning that in this approach, part of the computational complexity is encoded in the spatial arrangement of the modulatory elements instead of in the genetic circuitry of each cell type.

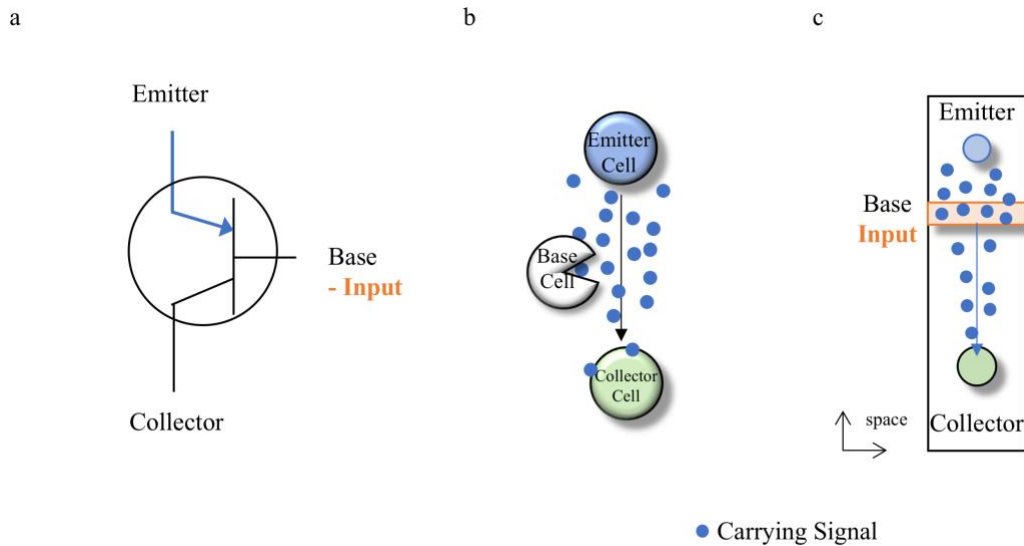


Figure 3.6 Schematically representation of a transistor-like architecture. **a)** Electronic transistor architecture. The emitter supplies the electron flow, which is collected in the collector. In between, the base is able to regulate the electron flow. **b)** Transistor-like architecture mapped into cellular elements. *CS* signal is produced and secreted in the *EC* cells, diffuse through and meets the modulatory element *BC*. *CC* cells detect *CS* signal producing the final output. **c)** Transistor-like architecture representation on top of a 2D surface. *CS* signal is produced on the top by the *EC* and diffuses through the 2D surface meeting the modulatory element in between and the *CC* cells at the bottom.

To experimentally validate our approach, a library of *E. coli* engineered cells were built. More specifically, we took profit from the natural cell-to-cell communication system involved in bacterial quorum sensing [Nelson & Hastings, 1979]. *CS* is encoded in the bacterial *3OC6HSL* acyl-homoserine lactone. Hence, Emitter Cells express constitutively the LuxI autoinducer synthase, producing the autoinducer 3OC6-homoserine lactone, which can diffuse across cell membranes [Eberhard et al., 1981; Engebrecht & Silverman, 1984]. Therefore, Collector Cells are based on the *LuxR-3OC6HSL* transcription activation complex: when *3OC6HSL* signal reaches a critical activation threshold it is bound the LuxR receptor protein triggering the operon transcription [Stevens et al., 1994]. As a *proof-of-principle*, we have characterized our devices by expressing a fluorescent protein, e.g. green fluorescent protein (GFP), as an output.

Modulatory elements were implemented in a library of Base Cells responding to device inputs. *BC* were engineered with the ability to modulate, either positively or negatively, *3OC6HSL* concentrations by expressing the *aiiA* degradation enzyme, an enzyme that

degrades *3OC6HSL* [Dong, 2000]. Negative Base Cells, i.e. BC^- , block the flow of *3OC6HSL* in the presence of the external input as a result of the induction of *aiiA*. Whereas in positive Base Cells, i.e. BC^+ , *3OC6HSL* flow is allowed in the presence of the external input since the expression of *aiiA* is repressed by them. It is worth mentioning that BC^+ genetic architecture involves a genetic *NOT* logic thanks to the $\text{LacI/P}_{\text{Lac}}$ repressor gene [Elowitz & Leibier, 2000]. In our approach, anhydrotetracycline (aTc) and arabinose (ara) were used as the external inputs. Detailed cellular genetic architecture is described in Table 3.2.

3.4 Design and characterization of a 2D surface

The 2D surface envisioned as the cellular computation support platform must ensure the reproducibility and serial production of cellular circuits. Surface characteristics must guarantee: i) bacterial cell growth, ii) signal diffusion, and iii) fluorescence measurements. Despite there are multiple substrates that can be used, a combination of an LB-agar solid surface together with a paper strip [Struss et al., 2010] was chosen because satisfies the previous requirements. Additionally, we have developed a set of cellular inks for each cell type from Table 3.2 to draw the different elements into the 2D surface. Cellular inks contain the i) cell type, ii) nutrients and iii) agar as a thickener for ensuring cellular deposition on top of the surface. The combination of the 2D surface together with cellular inks enables to design and draw cellular devices. Further details on the 2D surface composition and cellular inks' recipe are described in the **Methodology** section.

To validate our methodology, firstly, we characterized the 2D surface in terms of cellular growth and signal diffusion.

3.4.1 Cellular growth

Cellular growth could not be monitored via Optical Density [Carbonell et al., 2002; Koch, 1970] due to the paper surface characteristics'. To quantify cellular growth, cells were engineered with the constitutive expression of a red fluorescent protein (RFP). RFP is

expressed downstream a weak promoter to prevent cells for an additional metabolic burden. Detailed genetic constructs are summarized in Table 3.2.

The first set of experiments were devoted to analyse and monitor cellular growth by means of RFP expression. Figure 3.7 shows the temporal evolution of RFP levels depicting that the monitoring of the RFP fluorescent protein could serve as an indicator of cellular growth.

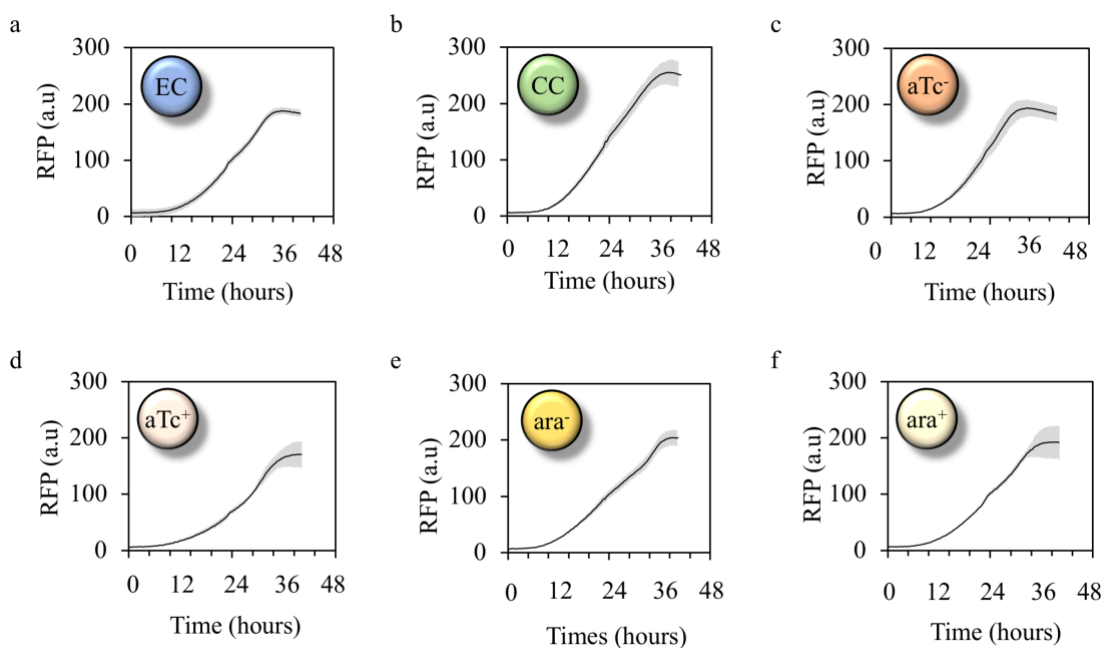


Figure 3.7 Cellular growth monitoring from RFP expression levels in the 2D surface. 0.5 μ L of cellular inks from Table 3.2 were deposited in the 2D paper surface and incubated at 37°C for 40h. Fluorescent measurement levels were taken every 30 minutes. The error bars shown in the figures are the standard deviation of three independent experiments. **a)** Emitter Cell. **b)** Collector Cell. **c)** aTc^- Base Cell. **d)** aTc^+ Base Cell. **e)** ara^- Base Cell. **f)** ara^+ Base Cell.

3.4.2 Carrying Signal diffusion

To assess *CS* diffusion through the 2D surface, a circuit composed by the *EC* and *CC* was built. An *EC* cellular ink dot was deposited in one end of the paper strip separated 5mm away for an array of *CC* dots (Figure 3.8 Bottom). *CS* diffusion was determined by measuring GFP levels in the array of *CC*. Experimental results shown in Figure 3.8 indicate that *EC* can secrete *CS*, which efficiently diffuses through the 2D surface and can be detected by *CC* at a large distance, i.e. 25 mm. *CS* signal depicts a characteristic diffusion profile where it decays with distance.

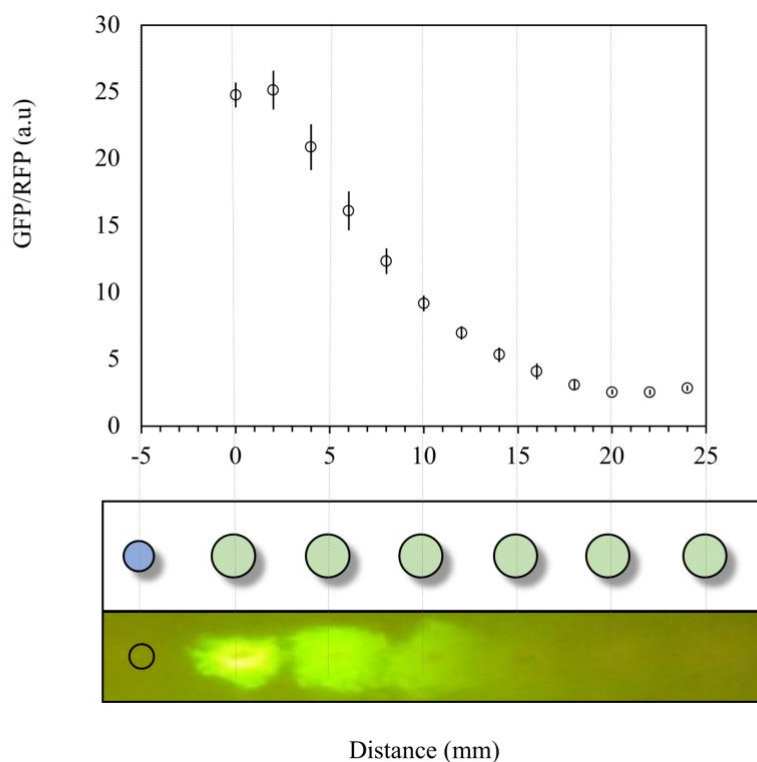


Figure 3.8 *CS* diffusion profile through the 2D surface. **Bottom.** Schematic representation of the experimental setup. The blue circle represents *EC* whereas the green circles correspond to *CC*. The image shows the paper strip with the GFP fluorescence from *CC* along to x-axis (mm). **Top.** 0.5 μ L of *EC* and *CC* cellular inks were deposited on the 2D surface and incubated at 37°C for 24 hours. GFP/RFP measurements were obtained according to **section 3.9.6** and plotted along the x-axis. The error bars shown in the figures are the standard deviation of three independent experiments.

Departing from *CC* GFP expression levels it was possible to quantify the concentration of *CS* implemented by *3OC6HSL* molecules. Firstly, it was necessary to experimentally determine the relationship between GFP expression levels and *3OC6HSL* concentration (Figure 3.9a). Afterwards, the experimental values were fitted to a Hill equation (Eq. 3.1) and the concentration of *3OC6HSL* along the surface, i.e. along the x-axis, was obtained.

$$GFP/RFP = \alpha_{3OC6HSL} + \frac{k_0 \cdot [3OC6HSL]^n}{k_1 + [3OC6HSL]^n} \quad \text{Eq. 3.1}$$

The gradient of the concentration profile of *3OC6HSL* associated with a diffusion process through the 2D surface is observed in Figure 3.9b.

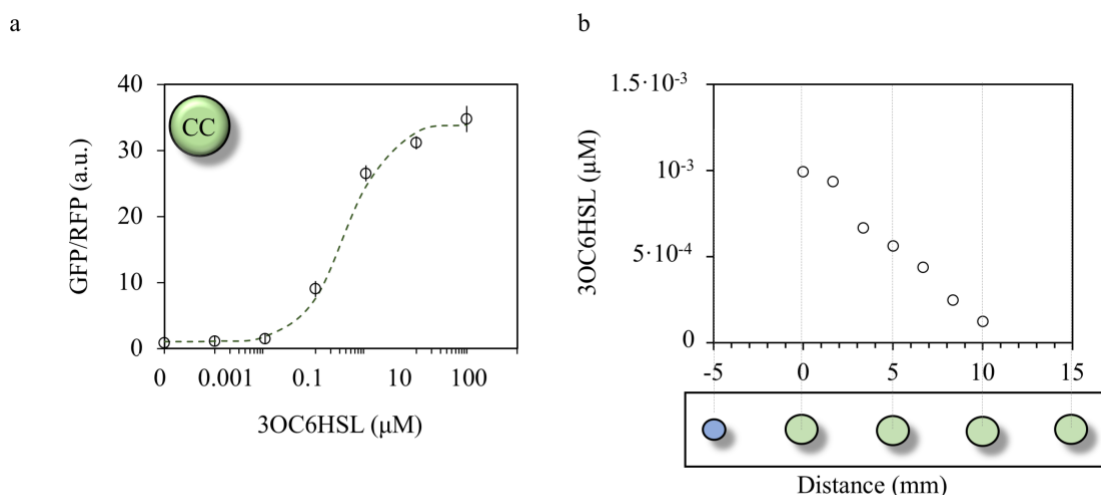


Figure 3.9. *3OC6HSL* diffusion profile characterization a) *CC* response to *3OC6HSL* concentrations ranging from 100 μM to 0.001 μM. 1 μL of *CC* cellular ink was incubated at 37°C for 24h with fluorescent measurements every 30 minutes. GFP measurement levels were normalized by RFP according to the methodology described in section 3.9.6. Dots correspond to experimental values and the dashed line to the mathematical fitting according to Eq. 3.1. The error bars are the standard deviation of three independent experiments. *Matlab R2016a* least-squares analysis software was used for fitting the parameters to experimental results. Parameter values obtained were: are $\alpha_{AHL} = 1$, $k_0 = 33$ 1/M, $k_1 = 4 \cdot 10^7$ M and $n=1$. b) **Bottom.** Schematically representation of the experimental setup for *EC* and *CC* circuit. The blue circle represents *EC* whereas the green circles correspond to *CC*. 0.5 μL of *EC* and *CC* cellular inks were deposited on the 2D surface and incubated at 37°C for 24 hours. GFP/RFP measurements were obtained according to section 3.9.6 and plotted along the x-axis. *3OC6HSL* concentration diffusion profile along 2D surface up to a 10 mm distance for an incubation time of 24h at 37°C.

3.5 Transistor-like device for CS modulation

Base Cells were designed to modulate CS in response to external inputs. To analyse the modulatory capacity of BC several circuits were built by placing the BC elements, forming a horizontal band, between EC and CC. The experimental setup is depicted in Figure 3.10.

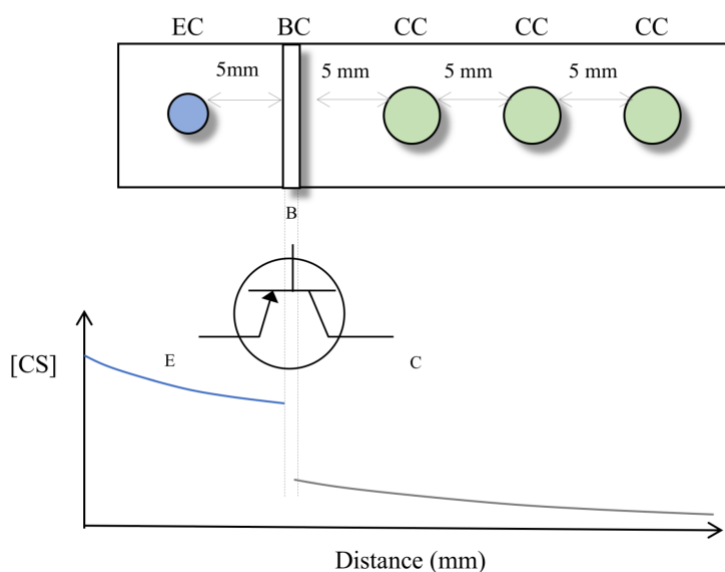


Figure 3.10 Experimental setup of a transistor-like circuit. Top. Schematic representation of the paper drawn transistor-like architecture. An EC cellular ink dot (blue circle) separated 5 mm above BC (white band) followed by several CC dots (green circles) separated 5 mm each. **Bottom.** Schematic representation of a CS diffusion profile along the 2D surface by the modulatory BC.

We analysed four different modulatory BC responding to inputs aTc and ara. Experimental results in Figure 3.11 displays the ratio of GFP/RFP relative to its maximum value, which corresponds to the CC response in the absence of modulatory elements between EC and CC cells. Negative modulatory BC, i.e. ara^- and aTc^- , reduce the *3OC6HSL* flow when external signals decrease (Figure 3.11a and Figure 3.11b respectively). Whereas positive modularity BC correspond to ara^+ and aTc^+ (Figure 3.11c and Figure 3.11d respectively) increase the *3OC6HSL* flow across the circuit when external arabinose or aTc input signals are present. Experimental results demonstrate a continuous modulation on the CS flow in response to different input concentrations.

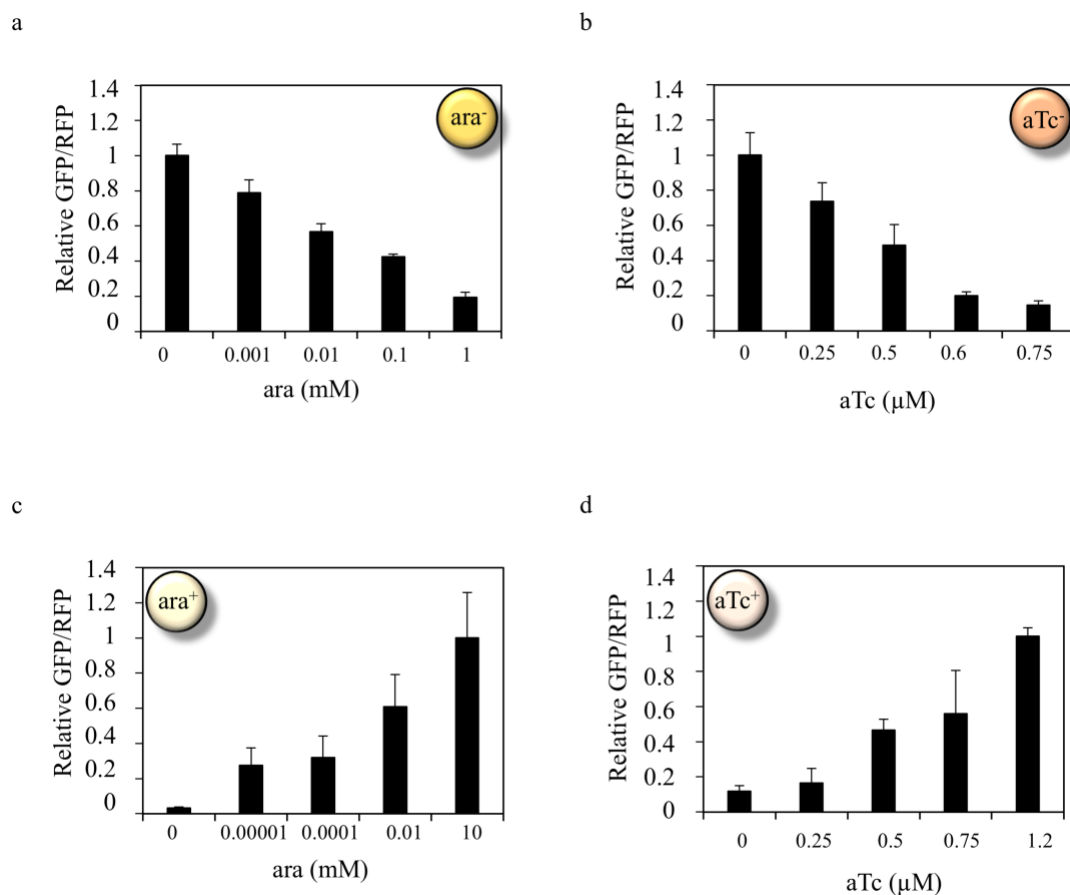


Figure 3.11 Transistor-like device for *3OC6HSL* modulation. Input signals were streaked into the 2D surface. 0.5 μ L of cellular inks were deposited as depicted in Figure 3.10 for each modulatory BC. Circuits were incubated for 24h at 37°C and fluorescence levels were obtained from the surface scan. Average fluorescent measurements of the first two CC cellular inks dots were obtained using *Matlab* image analysis. Normalized GFP values were obtained according to section 3.9.6. Data are shown as means \pm SD from three independent experiments. **a)** *ara*⁻ modulatory BC **b)** *aTc*⁻ modulatory BC **c)** *ara*⁺ modulatory BC **d)** *aTc*⁺ modulatory BC.

3.6 Logic computation based on a multi-branch topology

Concerning the scale-up of our transistor-like circuits, we have explored a general methodology allowing to map any arbitrary logic computation in a specific geometrical topology. A logic function involving N inputs and one output can be described by the so-called truth table and mathematically designated with the Boolean expression (f). Systematically applying Boolean algebra rules, f can be expressed as a minimal

combination of *ID*, *NOT*, *OR*, and *AND* binary operators in the canonical form. Thus, any arbitrary Boolean function with N inputs has the following general expression:

$$\begin{aligned} f = & [\varphi_{11}(x_1) \text{ AND } \varphi_{12}(x_2) \cdots \text{ AND } \varphi_{1N}(x_N)] \\ & \text{OR } [\varphi_{21}(x_1) \text{ AND } \varphi_{22}(x_2) \cdots \text{ AND } \varphi_{2N}(x_N)] \\ & \cdots \text{OR} [\varphi_{M1}(x_1) \text{ AND } \varphi_{M2}(x_2) \cdots \text{ AND } \varphi_{MN}(x_N)] \end{aligned} \quad \text{Eq. 3.2}$$

or in a compact form:

$$f = \sum_{i=1}^M \left[\prod_{j=1}^N \varphi_{ij}(x_j) \right] \quad \text{Eq. 3.3}$$

In which Σ represents the *OR* operator and Π the *AND* operator. The function φ_{ij} is either an *Identity* function, i.e. $\varphi_{ij} = 1$ if $x_j = 1$, or a *NOT* function, i.e. $\varphi_{ij} = 1$ if $x_j = 0$. N represents the number of different inputs and M is the maximum number of terms present in the Boolean function, always satisfying $M \leq 2 \cdot N - 1$ [Bender & Williamson, 2005]. Moreover, the expression of a Boolean function f can be minimized by the systematic application of standard rules of simplification, such as the so-called Karnaugh maps [Karnaugh, 2013] or the Quine-McCluskey algorithm [McCluskey, 1965].

Figure 3.12a-b illustrates one of the possible methods for Boolean function minimization, the Karnaugh maps. In Figure 3.12a a truth table is represented and, departing from that, the Karnaugh graphic map is built (Figure 3.12b). It consists of a lattice formed by 2^N squares corresponding to all possible input combinations in the truth table. From that, squares are filled with the output accordingly to each input combination. Since we are focused on *mindterms* [Hill & Peterson, 1981], subsequently groups of adjacent squares with a 1 inside are formed, i.e. ψ_i . These groups must contain 1, 2, 4 or 8 squares. Within a group, the logic product of the inputs that do not change is considered. Then the minimized Boolean function (Figure 3.12b) is obtained by adding all groups $f = \sum_{i=1}^M \psi_i$. This formalism can be easily translated into the multi-branch topology (Figure 3.12c). In this topology, each input combination associated with output 1, i.e. ψ_i , is codified by a

multi-base transistor module, implementing the Π operator. Concretely, at one end of the branch, the EC is placed whereas the CC is placed at the other end. In between, different bands containing modulatory BC are present. Logic inputs “1”, i.e. *Identity*, in the truth table are encoded with BC^+ , allowing CS diffusion only if the input is present. On the contrary, logic inputs “0”, i.e. *Not*, are encoded in BC^- , allowing CS diffusion only when the input is absent. The output of the device is obtained by the combination of the CS flow from the different branches, i.e. Σ operator, encoded by placing a single CC dot within the branch intersection.

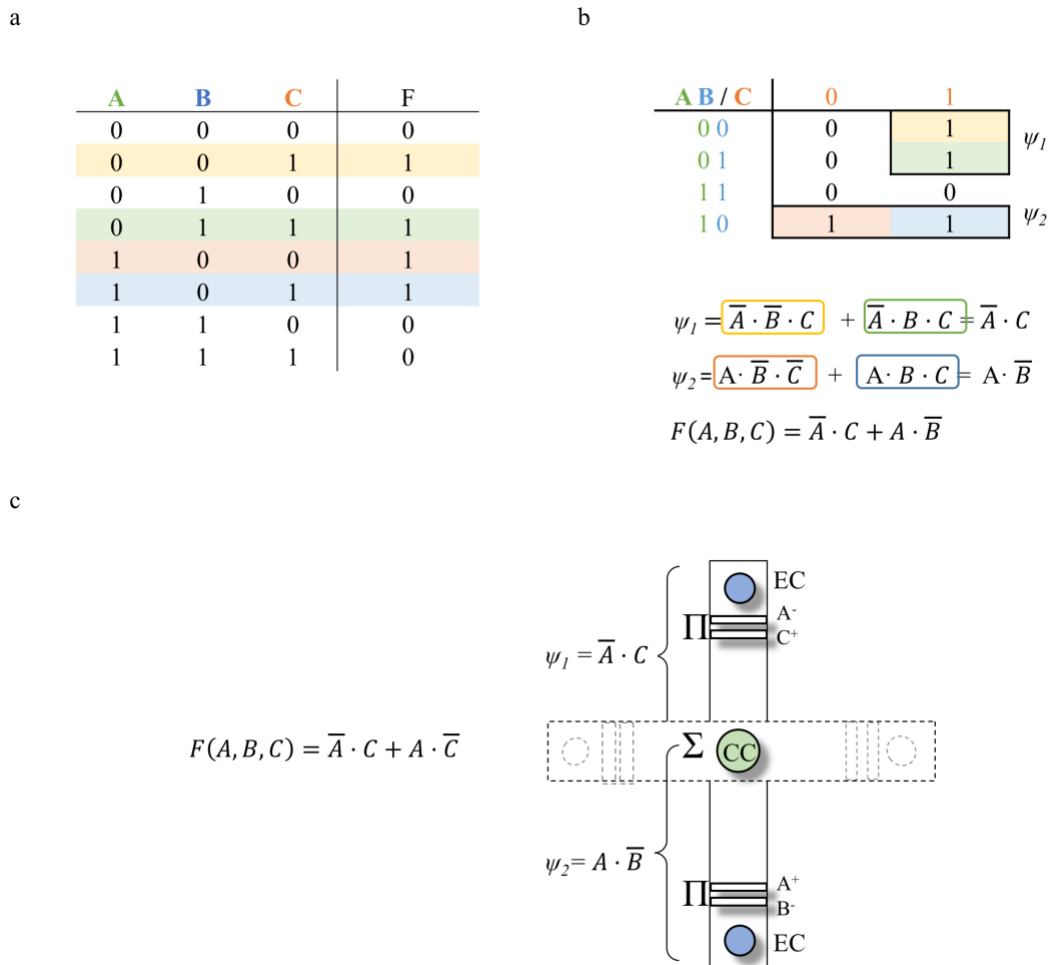


Figure 3.12 Multi-branch approximation for logic computation. a) Three-input one-output logic computation represented in a truth table. All input combinations with a 1 as an output, i.e. *mindterms*, are highlighted in different colours. b) Karnaugh map of the three-input one-output logic function. Within a group, firstly, for each square, the combination of inputs is obtained. Then, only the non-changing inputs are considered to the final minimized Boolean function. c) General multi-branch topology for implementing complex logic computations based on a transistor-like topology. In each branch, a multi-base transistor

module is placed and the CS signal is collected in the middle of the branches. The blue circle represents EC whereas the green circle corresponds to CC . The white-bands correspond to the modulatory BC .

The multi-branch approach allows scaling-up computational complexity without incrementing device complexity. The number of accessible functions has been analysed with respect to the elements of the multi-branch approach, i.e. branches and modulatory BC . For circuits responding to N inputs the maximum size of the modulatory BC library is $2 \cdot N$, i.e. two types of modulatory elements: BC^+ and BC^- for each input, and the maximum number of branches is 2^{N-1} , i.e. using the Karnaugh map minimization from Figure 3.12b, corresponds to the number of groups in the case of no adjacent squares containing a “1”.

Figure 3.13 shows the analysis of the number of accessible functions for 2-,3- and 4-input logic gates. The number of accessible functions is significantly larger than the topological complexity determined in terms of the number of branches. The maximum number of functions for a given number of inputs N corresponds to 2^{2^N} . For instance, the multi-branch topology limits the maximum number of BC per branch to the number of detectable inputs, i.e. 2 BC for 2-input logic gates, 3 BC for 3-inputs logic gates or 4 BC for 4-inputs logic gates. Besides, in the worst scenario, up to 2^{2^4} functions can be implemented with 8 branches and 4 modulatory BC per branch.

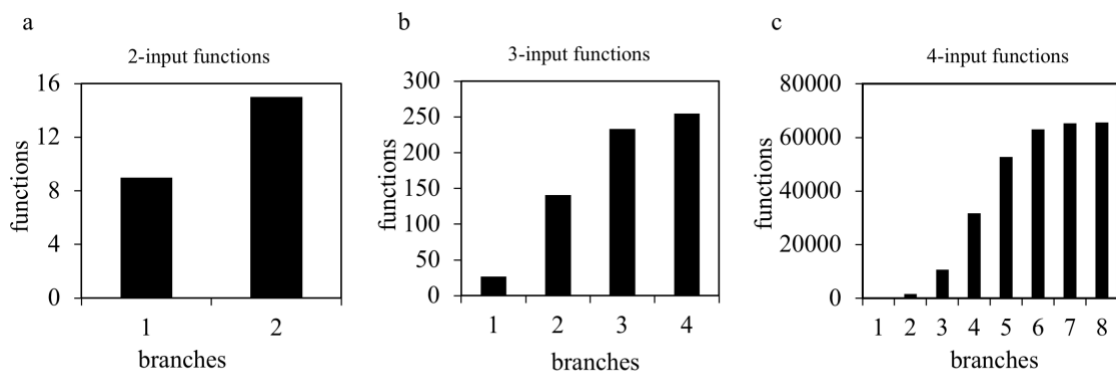


Figure 3.13 Relationship between the number of logic functions and topological complexity. **a)** Number of branches for two-input logic functions. **b)** Number of branches for three-input logic functions. **c)** Number of branches for four-input logic functions.

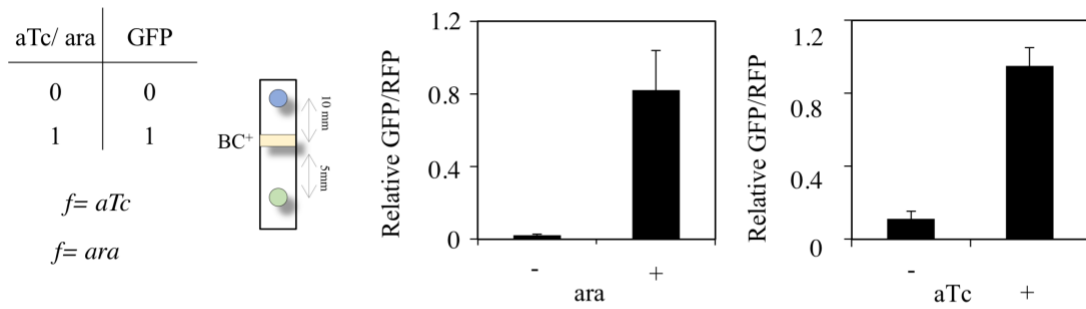
3.7 Experimental validation of two-inputs multi-branch topology

To experimentally validate the multi-branch topology approach, we have implemented a set of logic gates using the characterized transistor-like modules from **section 3.5**. For instance, some examples for two-inputs one-output logic gates have been experimentally implemented. Experimental results, in **Figure 3.14**, display the ratio of GFP/RFP relative to its maximum value, which corresponds to the *CC* response in the absence of modulatory elements between *EC* and *CC* cells.

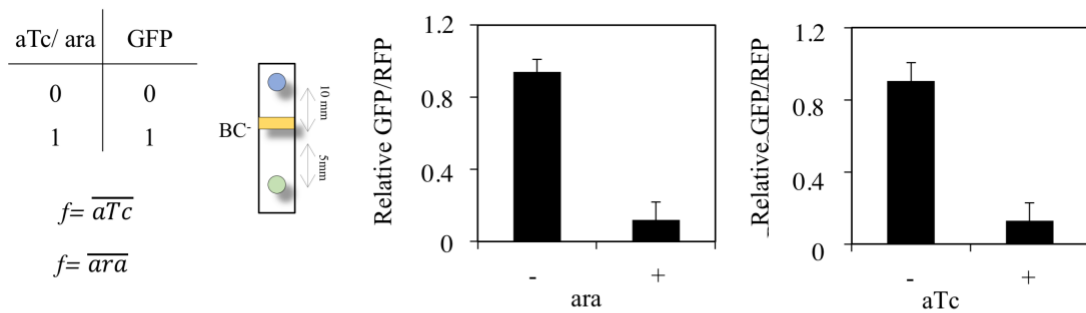
The *Identity* gate is accomplished by the positive modulatory *BC*, i.e. BC^+ , and the *NOT* gate with the negative modulatory *BC*, i.e. BC^- . Therefore, a single branch with the *BC* placed in a band manner codifies both logic gates. **Figure 3.14a-b** show the experimental results of the *Identity* gates for two different inputs. **Figure 3.14c-d** show the experimental results for the *NOT* gates.

For two-input logic gates the coexistence of two or more modulatory *BC* is required. The minimized Boolean function of the *AND* gate denotes the logic product of the *Identity* inputs ($f = ara \cdot aTc$). Hence, it is implemented in a single branch with the two positive modulatory elements, each one responding to the two different external inputs, in consecutive bands after the *EC* (**Figure 3.14e**). The minimized Boolean function of the *OR* gate accounts for the *Identity* combination of both input signals ($f = ara + aTc$). Therefore, it is implemented in two branches, in one branch is placed the positive modulatory element for *ara* input, and in the other branch the positive modulatory element for *aTc* input (**Figure 3.14f**).

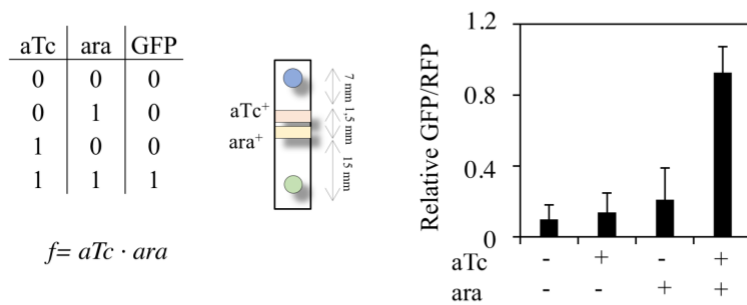
a



b



c



d

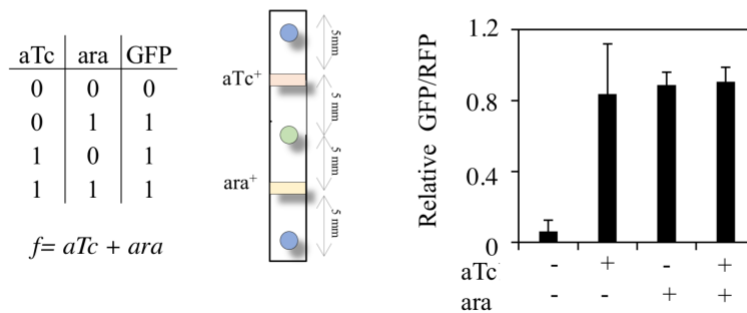


Figure 3.14 Experimental implementation of logic gates based on the multi-branch approach. For each logic gate the experimental setup containing the relative geometrical position and the experimental results are shown. Input signals were streaked into the 2D surface according to $[ara^+] = 0.1 \text{ mM}$, $[ara^-] = 0$

M, $[aTc^+] = 1.2 \mu\text{M}$ and $[aTc^-] = 0 \mu\text{M}$. $0.5 \mu\text{L}$ of cellular inks were deposited as depicted in each specific geometric topology. The blue circle represents *EC* whereas the green circle corresponds to *CC*. The coloured-bands correspond to the modulatory *BC*. Circuits were incubated for 24h at 37°C and fluorescence levels were obtained from the surface scan. Average fluorescent measurements of the *CC* cellular ink dot were obtained using *Matlab* image analysis. Normalized GFP values were obtained according to **section 3.9.6**. Data are shown as means \pm SD from three independent experiments. **a)** *aTc ID* gate with aTc^+ . **b)** *aTc NOT* gate with aTc^- . **c)** *ara ID* gate with ara^+ . **d)** *ara NOT* gate with ara^- . **e)** *ara* and *aTc AND* gate with aTc^+ and ara^+ . **f)** *ara* and *aTc OR* logic with aTc^+ and ara^+ .

3.8 Discussion

Implementing transistor-like elements allows to encode computation in a unique and diffusible signal, i.e. *Carrier Signal*, avoiding the so-called wiring problem accounting for the inherent cross-talk when using several chemical wires [Canton et al., 2008; Macía et al., 2012]. Depositing different cell types in separated spatial locations avoids negative growth competition effects which have revealed to challenge device stability and reproducibility [Tamsir et al., 2011]. Thanks to the use of 2D surface the *Carrier Signal* encoded into *3OC6HSL* molecules can diffuse, be modified and collected. Moreover, *3OC6HSL* flow modulations by the presence of external inputs allowed to perform logic computations. The translation of computational complexity from genetic complexity to geometric complexity, much easier to implement, is undoubtedly one of the highlights of this new methodology. Although the present work has been dedicated towards digital computation, the ability of external signals to tune *3OC6HSL* in a continuous manner opens the door towards analogic computation. Furthermore, inspiration gained from printed electronics permits the design and implementation of an automated cellular ink deposition hypothesising, for instance, the use of 3D printers [Balasubramanian et al., 2019; Pan et al., 2019; Schaffner et al., 2017].

The multi-branch topology based on transistor-like modules permits to systematically implement devices performing logic computations. In detail, we have validated our approach by designing and building some two-input logic gates. Therefore, we have experimentally demonstrated that modifying the transistor-module geometry functions

involving one or two branches with either one or two modulatory *BC* per branch could be built.

Although the present approach encompasses a novel design framework of digital circuits and further hypothesized analogue, some concerns regarding scalability must be mentioned. *CS* flow modulation by external inputs has been accurately chosen for optimizing output response. However, envisioning the use of application-driven inputs must demand a prior characterization of modulatory elements in order to properly select geometrical distances. For instance, a mathematical formalization of *3OC6HSL* degradation by *aiiA* together with its relative levels characterization exploiting relative promoter strength [Kelly et al., 2009] would enable to fine-tune geometrical setup, i.e. distances and volumes. Further work should be devoted within that line for the improvement of the experimental setup of the multi-branch approach.

Furthermore, besides our system has been implemented for four modulatory elements, using two input signals, future work should be devoted to scaling towards more inputs and its experimental validation. It is evident, that device output must be selected according to the intended function. Engineered fluorescent proteins with fast-maturation [Pédélecq et al., 2006; Shcherbakova et al., 2012] or degradation tags [Andersen et al., 1998] would be explored for optimizing time-scale resolution. Despite there are so many questions to address our results suggest that the potential of this new methodology for creating cellular devices is enormous.

3.9 Methodology

3.9.1 Strains, media and growth conditions

Top10 *E. coli* strain was used for cloning and expression experiments (*F*- *mcrA* Δ (*mrr*-*hsdRMS*-*mcrBC*) ϕ 80*lacZ* Δ *M15* Δ *lacX74* *nupG* *recA1* *araD139* Δ (*ara-leu*)7697 *galE15* *galK16* *rpsL*(*StrR*) *endA1* λ -). Construct containing TetR promoter were expressed in ZN1 strain (*LacIq* *PN25-tetR* *SpR* *F*- *endA1* *glnV44* *thi-1* *recA1* *relA1* *gyrA96* (*NacR*) *deoR* *nupG* Φ 80*dlacZ* Δ *M15* Δ (*lacZYA*-*argF*) *U169*, *hsdR17*(*rK*- *mK*+), λ -), containing the constitutively expression of TetR negative regulator.

E. coli were grown in Lysogeny Broth (LB) at 37 °C and selected with the appropriate antibiotics corresponding to the transformed plasmid. Antibiotics were purchased from Sigma and used at the following concentration: chloramphenicol: 35 μ g/ml, ampicillin: 50 μ g/ml.

Bacterial strains were preserved in LB glycerol 20% (v/v) at -80 °C. Single colonies obtained from streaked glycerol stocks were inoculated and the cells were grown overnight at 37 °C with shaking (200 revolutions per minute (rpm)). Overnight cultures were diluted into fresh LB (1/100 dilution) and grown for 5 hours until reaching an exponential OD of 0.3.

3.9.2 Cellular inks

Thickener solution containing Lysogeny Broth (Sigma Aldrich, USA) with 3% agar (Sigma Aldrich, USA) was boiled for solution dissolving. After cooling ~50 °C, properly antibiotic selection and cell cultures were added to obtain each cellular ink according to the cell library in Table 3.2.

- Modulatory Base cells cellular ink was obtained from mixing 2 parts of cell culture with 1 part of the thickener solution.

- Emitter cells cellular ink was obtained from mixing 1 part of cell culture with 1 part of the thickener solution.
- Collector cells cellular ink was obtained from mixing 1 part of cell culture with 1 part of the thickener solution.

0,5 μL of each cell-type cellular ink was deposited in the 2D surface according to the different topologies allowing computation.

3.9.3 2D Surface

Experiments were performed in petri dishes (Nunc, ThermoFisher Scientific, USA) pouring 20 ml of LB broth with 1,5 % agar (Sigma Aldrich, USA) supplemented with the antibiotic and the appropriate inducers before depositing the paper strips to print the circuit. The support-based paper was Discovery A4 white paper with 75g/m² rigidity and 80 g/m² opacity.

For inducers arabinose (L-(+)-Arabinose 98%, Sigma Aldrich, USA) and aTc (N Anhydrotetracycline 98%; Cayman Chemical Company, USA) were used.

For Collector Cell synthetic *3OC6HSL* (N-[γ -ketocaproyl]-L-homoserine lactone; Cayman Chemical Company, USA).

3.9.4 Molecular cloning and parts

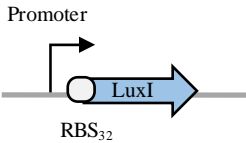

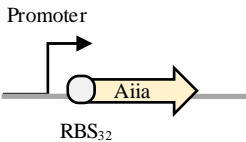


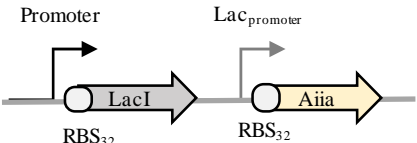
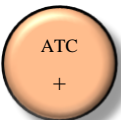

Construction of the genetic sensors by cloning was carried out using the Biobrick assembly method and parts from the Spring 2018 iGEM distribution (<http://parts.igem.org>). DNA sequences are detailed in Table A. 3.

Name	Part Registry Code	Plasmid
Terminator	BBa_B0014	pSB1C3
Medium RBS	BBa_B0032	pSB1C3
Constitutive promoter 1	BBa_J23100	pSB1C3
Constitutive promoter 2	BBa_J23105	pSB1C3
aTC- inducible promoter	BBa_R0040	pSB1C3
Arabinose-inducible promoter	BBa_I0050	pSB1C3
pLac-inducible promoter	BBa_R0011	pSB1C3
LacI protein	BBa_C0012	pSB1C3
aiiA synthetase	BBa_C0060	pSB1C3
LuxI	BBa_C0061	pSB1C3
LuxR receptor protein	BBa_R0060	pSB1C3
Lux inducible promoter	BBa_R0061	pSB1C3
Red Fluorescent Protein	BBa_E1010	pSB1C3
Green Fluorescent Protein	BBa_E0040	pSB1C3

Table 3.1 Biobricks used in this study.

3.9.5 Cell library

In this case study, a transistor-like architecture is designed so three main elements mimicking transistor's emitter, base and collector have to be implemented, each of them being embedded in a different biological engineered construct. All the constructs analysed in this chapter were built by combining the genetic parts described in Table 3.1 using 3A assembly. Table 3.2 shows the genetic structures of the different constructs. Biobrick cloning was performed using an assembly kit (Ginkgo Bioworks, USA). All constructs were included in the Biobricks high copy number plasmid (pSB1AC3) and were transformed using a chemical method. Sanger sequencing confirmed all genetic constructs. Plasmid maps are detailed in Table A. 4.

Construct	Genetic Structure	Strain
Emitter Cell		
		
	B0014 + PTET + B0032 + C0061 B0014 + J23105 + B0032 + E1010 + B0014	Top10
Base Cells		
		
	B0014 + R0040 + B0032 + C0060 B0014 + J23105 + B0032 + E1010 + B0014	Zn1
	B0014 + I0050 + B0032 + C0060 B0014 + J23105 + B0032 + E1010 + B0014	Top10
		
	B0014 + R0040 + B0032 + C0012 + B0014+ R0011 + B0032 + C0060 B0014 + J23105 + B0032 + E1010 + B0014	Zn1
	B0014 + I0050 + B0032+ C0012 + B0014+ R0011 + B0032 + C0060 B0014 + J23105 + B0032 + E1010 + B0014	Top10
Collector Cell		

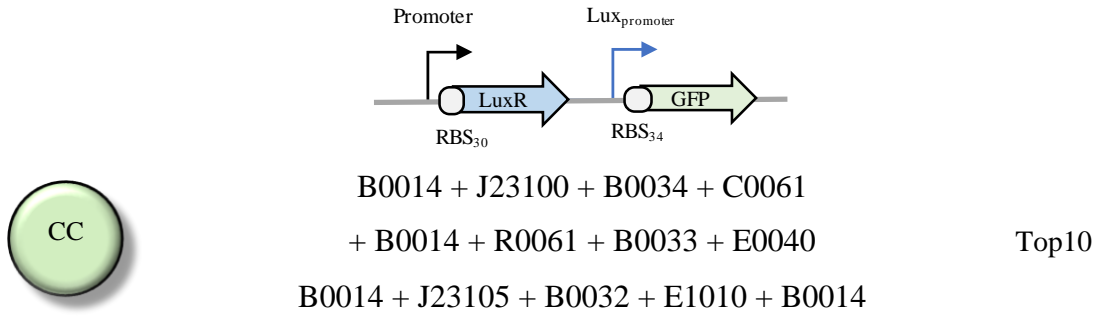


Table 3.2 Transistor-like modules genetic constructs.

3.9.6 Fluorescence assays for gene expression determination

Cellular growth was monitored by means of a constitutively RFP expression whereas circuit output gene expression was monitored by quantification of GFP expression levels. The bacterial cultures were incubated and induced on a Synergy MX microplate reader (BioTek Instruments, USA). RFP and GFP surface scan measurements were obtained after the incubation of the different circuits at 37 °C. Conditions for fluorescence measurements of the red fluorescent protein (RFP) were: excitation: 578±9 nm, emission: 616±9 nm, with a gain of 50.

GFP and RFP measurement data were analysed by a self-customized *Matlab analysis toolbox*. A 21x21 grid was obtained from Synergy MX microplate reader surface scan. Normalized GFP measurements were obtained from the region comprising the first and second *CC* cellular inks, i.e. 7x3 pixels. Blank correction, i.e. *CC* cellular ink without *EC* nor *BC* cellular inks, was performed after cellular growth correction. GFP was computed accordingly to Eq. 3.4.

$$\Phi = \frac{\langle GFP(S) \rangle - \langle GFP(B) \rangle}{\langle RFP(S) \rangle - \langle RFP(B) \rangle} \quad \text{Eq. 3.4}$$

$\langle GFP(S) \rangle$ and $\langle RFP(S) \rangle$ represent the surface mean of the grid containing the *CC* cellular inks, whereas $\langle GFP(B) \rangle$ and $\langle RFP(B) \rangle$ stands for the mean of the blank region.

Figure 3.15 summarizes the procedure for obtaining Φ measurements. Figure 3.15a is the sketched pattern representing an experimental setup from the abovementioned experiments. Figure 3.15b-c are the result of the Synergy MX microplate reader surface scan for RFP and GFP, respectively. Figure 3.15d-e represent horizontal average data along the y-axis of three individual experiments after blank correction, as well as the mean and the std. Figure 3.15 shows the RFP normalized measurement along y-axis. Red-dashed lines depict positional information of the first two *CC* cellular inks dots. Within this region, final GFP measurement was obtained from GFP average data. For modulatory elements characterization, GFP/RFP relative levels are calculated. The geometrical topology described in Figure 3.10, where no modulatory bands are placed between *CS* and *CC*, is described as the experimental positive control. In this scenario, *CC* receives the maximum *CS* signal. Subsequent analysis on *CS* modulations, by means of either positive or negative modulatory *BC* cells, is described as relative GFP/RFP.

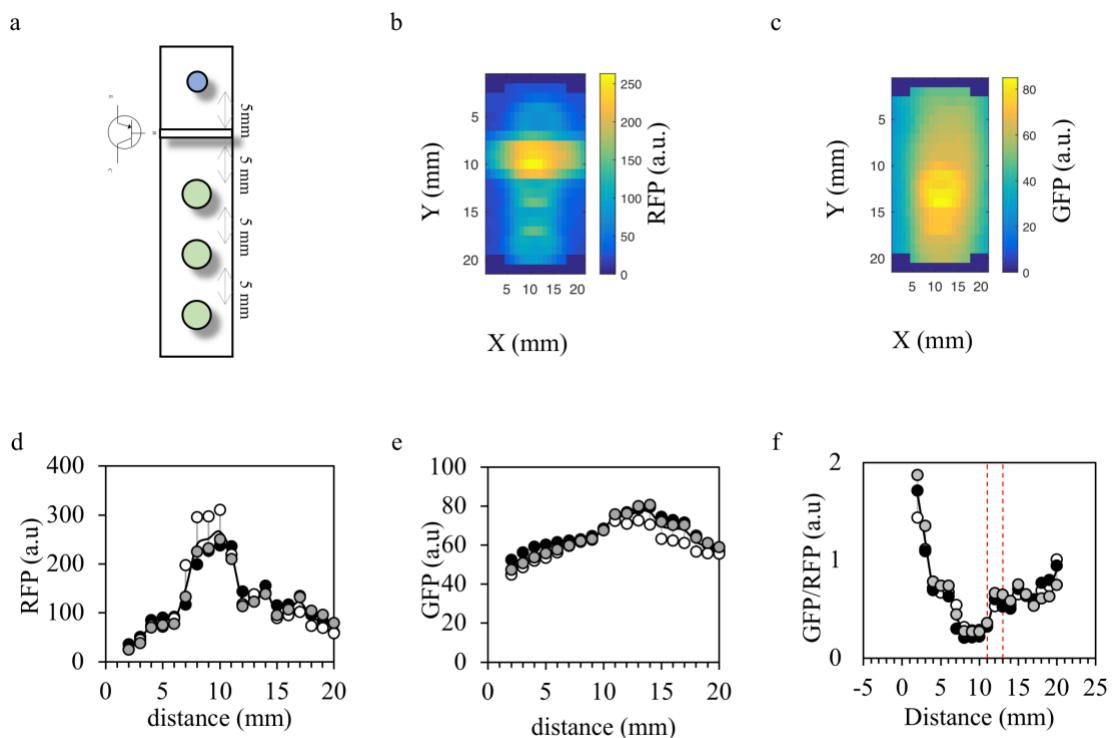


Figure 3.15 Graphical representation of the Φ measurements obtained from the fluorescence surface scan. a) Paper strip experimental setup of transistor-like computation. **b)** RFP scan measurement of the whole paper strip, represented with *Matlab* software. **c)** GFP scan measurement of the whole paper strip, represented with *Matlab* software. **d)** RFP measurement representation along the y-axis (mm). **e)** GFP measurement representation along y-axis (mm). **f)** Φ from Eq. 3.4 representation along the y-axis (mm).

CHAPTER 4

Living devices with time-dependent responses:

Plug-and-play multicellular circuits with time-dependent dynamic responses

Working on the design and construction of living biomedical devices claims on the study and analysis of extracellular signal detection followed by signal integration to perform desired responses. Therefore, this chapter focuses on how sensed signals can be integrated to produce non-trivial responses for a desired biomedical application, i.e. Diabetes Mellitus. *S. cerevisiae* was used as *proof-of-concept* to analyse how a proper configuration of multicellular circuits allow to tune its response along with the introduction of analogue complex responses.

Dr. Javier Macia and I have done this work in collaboration with the *Cell Signalling Research Group* (Arturo Urrios, David Canadell, Francesc Posas and Eulalia de Nadal) as a part of the research project “Distributed computation applications in biological systems for the study and application in Diabetes Mellitus” funded by Centre per a la Innovació de la Diabetis Infantil (CIDI) - Fundació Sant Joan de Déu (2012-2017) and MINECO (2015-2017) “Aproximaciones desde la biología de sistemas y sistémica en el diseño de circuitos celulares para la homeostasis de la glucemia en diabéticos”.

Particularly, the theoretical framework design, mathematical modelling and theoretical analysis of device tunable response were developed by Dr. Javier Macia and myself. Cellular engineering, the experimental implementation and data analysis was developed in the *Cell Signalling Research Group*. As a result, the research main achievements described in this chapter have been published in [Urrios & Gonzalez-Flo et al., 2018].

4 LIVING BIOMEDICAL DEVICE WITH TIME-DEPENDENT RESPONSES

4.1 Analogue responses for biomedical applications

Synthetic biology studies have the potential to create biologically engineered devices for a wide range of applications. In general, biological devices rely on a synthetic genetic circuit composed of basic heterologous control components that fine-tune transgene expression in response to particular exogenous or endogenous signals [Nandagopal & Elowitz, 2011]. Up until now, we have explored the ability of engineered living devices to use the intrinsic cellular machinery to sense extracellular signals, and how we can apply genetic engineering to tune its activation threshold and dynamic range. Particularly, modifying the activation threshold of a specific cellular sensor opens the door on the design of application-driven biosensors with pre-defined operating ranges. Therefore, allowing to hypothesize the development of new and more efficient alternative treatments for health problems [Folcher & Fussenegger, 2012; Warren C. Ruder, Ting Lu, 2011; W. Weber & Fussenegger, 2012] and to re-design the field of biomedical devices and theranostics. The emergence of living technologies combining both cells and electromechanical devices are projected to overcome the current detection limitations. Relevant is the use of cellular sensors to detect pathological biomarkers putting the manifest the design of novel biomedical devices able to detect biological substrates. In that line, integrating sensorial information from one or diverse biomarkers could help on the diagnose and treatment of complex diseases. Putting efforts on designing cellular devices with the ability to integrate extracellular information in a logical fashion ease to speculate its use for diagnosis. Relevant is the need to identify the cellular machinery responsible for extracellular signal detection and couple biosensor design together with engineered cellular computation capabilities. Consequently, devices intended for disease diagnosis or follow-up should be engineered to depict a readable, standard, and quantifiable output. On the other hand, if a device application has been envisaged to treat a particular disease, the accurate selection of the output molecule, e.g. hormone, drug, or enzyme, should be addressed.

However, medical applications require complex responses that occur with high precision and specific analogue dynamics and that have a predictable logic in response to external or internal signals. As a consequence, the building of high-order networks, including sequential [Kramer et al., 2005] or feedback control systems [Tigges et al., 2010; Tsimring et al., 2010], is still a major challenge in synthetic biology due to the emergence of additional constraints associated with the complexity of genetic circuits that compromise their viability [Kwok, 2010]. Concerning society-driven applications claims for the need for fine-tuning graded responses and puts in manifest the lack of developed tools for the rational design of circuits implementing analogue computations [Daniel et al., 2013; Purcell & Lu, 2014].

An alternative to the use of single cell circuits for biological computation is the use of multicellular consortia. Computation based on multicellular devices has revealed to be extremely useful for implementing complex logic circuits [Macía et al., 2012; Regot et al., 2011; Tamsir et al., 2011]. However, this approach has not been systematically applied either in analogue nor time-dependent circuits. The development of cellular devices envisioned for biomedical applications is still in the early development phase. Besides the selection of the physiological signals encoding both input and output, efforts should be done in identifying the proper device dynamics for a particular application. Hence, limiting the scalability of such devices. As a particular case of study, we would highlight the dynamics of insulin secretion for glycaemia regulation in healthy subjects. Physiological blood glucose levels are maintained within a normoglycaemia range by the secretion of insulin, at high glucose levels, or glucagon, at low ones [Association, 2010]. Indeed, the secretion of the insulin hormone is governed by a pulsatile temporal dynamics [Nan-Kuang Yau & Liang-Wey Chang, 1995; Polonsky et al., 1988; S. H. Song et al., 2002]. Thus, a device able to detect extracellular glucose levels and secrete insulin hormones could potentially be applied for glucose homeostasis maintenance in diabetic patients [Callejas et al., 2013; Xie et al., 2017; Ye et al., 2011]. However, since glucose homeostasis demands a fine-tune control of blood glucose levels, i.e. blood glucose levels should be maintained between a narrow range to avoid severe health problems [Kalra et al., 2013], device dynamics should offer tight control of insulin secretion in terms of device operating range and sensitivity.

4.2 Objectives

We aim to design and build multicellular devices performing complex dynamic responses using physiologic-based signals, e.g. glucose.

The *specific objectives* addressed within this section are:

- Design a sensor layer able to discriminate between low and high glucose concentrations and an effector layer expressing and secreting hormones enabling the restoration of glycaemia, i.e. insulin and glucagon.
- Design a modulator layer enabling the modulation of the output to perform analogue response.

4.3 The use of hexose transporter promoters serves to create cells able to detect and respond to different extracellular glucose levels.

Glycaemia regulation in healthy mammalian organisms relies on the balance between insulin and glucagon secretion in response to different glucose levels. To mimic this natural behaviour in a multicellular synthetic device, we considered two minimal circuits, one responsible for insulin secretion and the other for glucagon secretion. Therefore, each multicellular device, represented in Figure 4.1, has i) a sensor layer comprising the sensor cells detecting different glucose ranges and secreting a wiring molecule, ii) effector cells that produce a glucose-balancer output, i.e. insulin or glucagon, in response to the wiring molecule and iii) modulator cell that in response to an external signal modify the communication between sensor and effector cells by altering the levels of the wiring molecule.

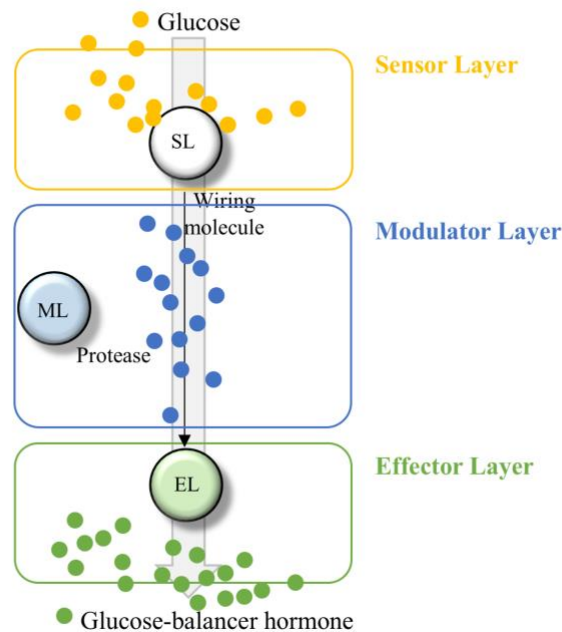


Figure 4.1 Schematically representation of the multicellular device comprising three layers. Cells in the Sensor Layer (*SL*) detect extracellular glucose levels and respond by secreting a wiring molecule. The Modulatory Layer (*ML*) is comprised by a cell type that secretes a protease that degrades the wiring molecule, which is finally collected in the Effector Layer (*EL*), that in response to the wiring molecule secretes glucagon or insulin accordingly.

For the experimental implementation of our devices, we have used *Saccharomyces cerevisiae* as a model organism, because yeast is an excellent workbench to explore different theoretical designs. Particularly, the *S. cerevisiae* pheromone pathway was manipulated to establish the connection between layers [Macia et al., 2016; Regot et al., 2011]. Yeast can reproduce sexually through a signalling pathway. Following this process, two haploid cells combine to form a diploid cell. Yeast secretes to the extracellular environment signal molecules, i.e. pheromones a and α , attracting them to their mates, which in turn are able to detect the mating signals and activate a signalling pathway cascade, which ends in the activation of mating genes and cell cycle arrest [Bardwell, 2005]. Figure 4.2 represents schematically the different signalling cascade proteins involved in the activation of the *FUS1* promoter (P_{FUS1}) under the presence of α -factor. In detail, downstream P_{FUS1} genes would be expressed in the presence of mating α -factor pheromone [Macia et al., 2016; Regot et al., 2011].

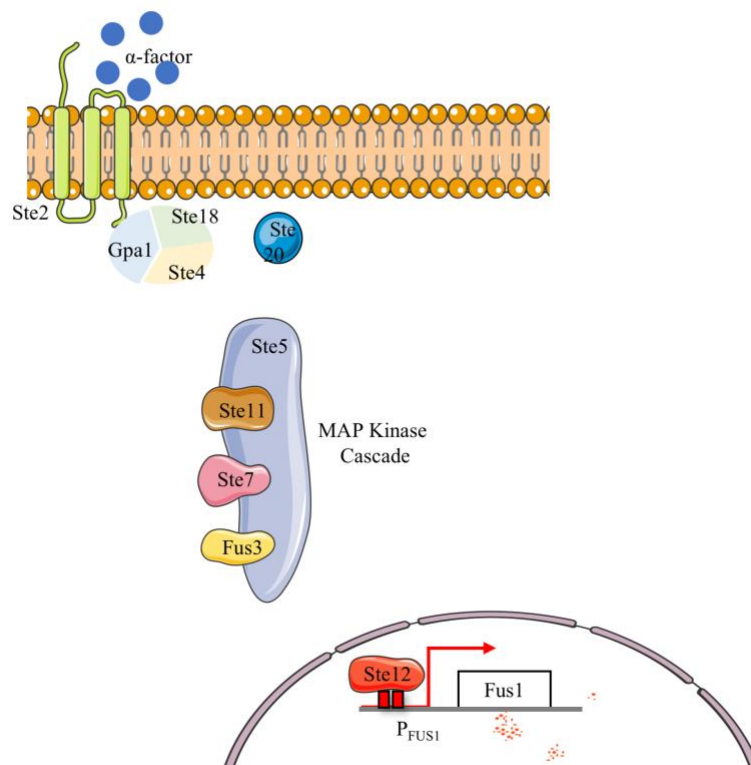


Figure 4.2 α -factor pheromone pathway. Mating pheromone-induced cell cycle arrest in budding yeast is mediated by the *FUS3* MAP kinase pathway. Pheromone binding to its cognate seven transmembrane receptor promotes the activation of the mating response MAP kinase cascade via the *STE2* protein kinase.

Subsequently, nuclear translocation of the MAP kinase FUS₃ facilitates the expression of the FUS₁ promoter.

To build a set of sensor cells that respond to a range of glucose levels, the natural capabilities of yeast to sense environmental glucose levels and to adjust the expression of genes encoding hexose transporters (*HXT*) to maximize glucose uptake was exploited [J. H. Kim et al., 2013; Özcan & Johnston, 1999]. Several genetic constructs were built in which the expression of the pheromone α -factor from *S. cerevisiae* (α Sc) was under the control of different *HXT* promoters, i.e. *HXT*₁, *HXT*₂, *HXT*₃, *HXT*₄ and *HXT*₇. This α Sc is the wiring molecule that permits communication between different cells in the consortia (Figure 4.3a). Different strains containing the *HXT* promoters upstream the α Sc sequence were engineered, therefore α Sc could be secreted in response to different glucose concentrations. Detailed cellular genotypes are related in Table 4.3. The α Sc level was indirectly quantified using a reporter cell that sensed α Sc and subsequently expressed a green fluorescent protein (GFP) under the control of the pheromone inducible *FUS*₁ promoter, the α Sc-reporter cell, i.e. cell α Sc:GFP from Table 4.3. Figure 4.3a shows the α Sc-reporter cell relationship between synthetic α Sc and GFP signal for an incubation time of 4 hours.

Cells containing the engineered *HXT* promoters fused to α Sc synthetic constructs were incubated together with α Sc-reporter cells in the presence of several extracellular glucose levels for 4 hours to ensure a robust GFP signal. GFP fluorescence was then analysed using flow cytometry. Experimental results shown in Figure 4.3b indicate that cells containing the *HXT*₁ construct increase the production of α Sc in response to an increase in glucose levels, behaving as a high glucose sensor, which would be designated as an *Identity* logic. On the other hand, cells containing *HXT*₃ display α Sc production that was independent of the extracellular glucose levels. In contrast, cells containing either *HXT*₂, *HXT*₄ or *HXT*₇ act as glucose repressible systems, since α Sc production is repressed in response to an increase in the concentration of glucose following a *NOT* logic. Therefore, engineered cells with *HXT*₁ and *HXT*₇ were designated as the *in vivo* glucose sensors able to discriminate between high and low glucose levels.

To improve the efficiency of the glucose sensors two copies of the construct containing the *HXT* promoter with the α Sc sequence were introduced into each cell. Therefore, obtaining two Sensor Layer cells corresponding to the *HIGH-glucose sensor* cell i.e. cell *HXT1:: α Sc* from Table 4.3, and the *LOW-glucose sensor* cell, i.e. cell *HXT7:: α Sc* from Table 4.3. Then, secretion of the wiring molecule by the new *HIGH* and *LOW* -glucose sensor cells was assessed by incubating them in the presence of different glucose levels together with the α Sc-reporter cells for 4 hours. Figure 4.3c shows the transfer function relating the levels of the output GFP fluorescent with glucose levels.

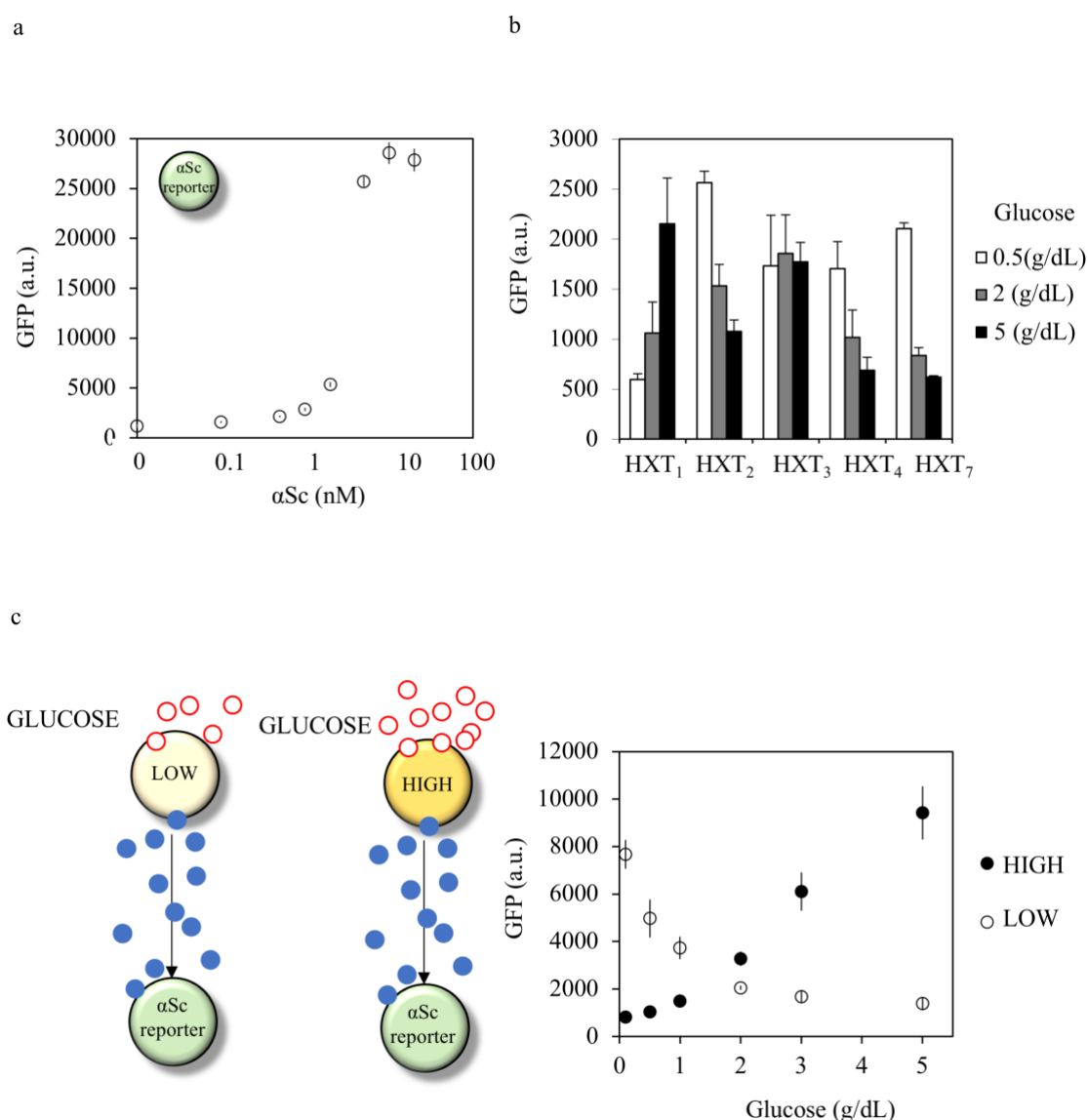
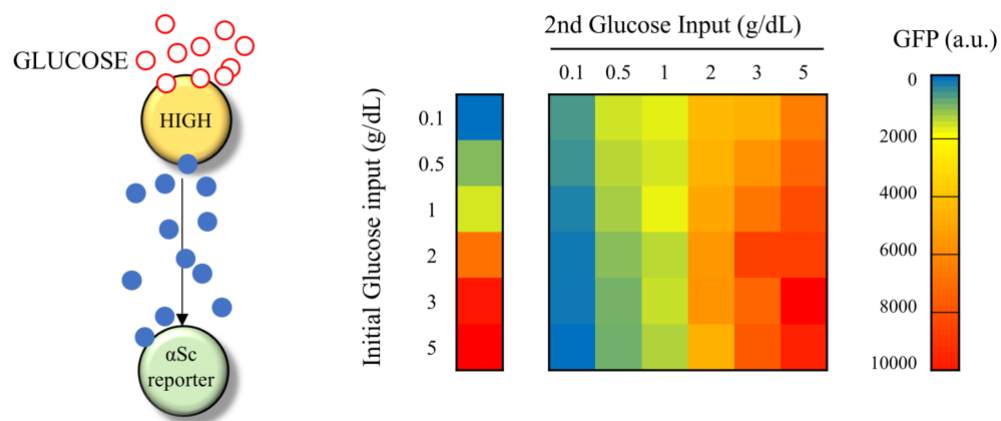


Figure 4.3 Design and characterization of glucose sensor cells. a) α Sc-reporter cells were incubated with different concentrations of α Sc, i.e. 0.01, 0.1, 0.5, 1, 2, 5, 10, or 20 nM, for 4 h. GFP fluorescence (a.u.) was then analysed using flow cytometry. Dots correspond to experimental values. The error bars

shown in the figures are the standard deviation of three independent experiments. **b)** *MATa W303* cells were modified to express *aSc* under the control of different *HXT* promoters: *HXT*₁, *HXT*₂, *HXT*₃, *HXT*₄ and *HXT*₇. Cells were incubated together with *aSc-reporter* cells with a cellular proportion of 2:1 for 4 h in three different glucose concentrations i.e. 0.5, 2 or 5 g/dL. GFP fluorescence (a.u.) of *aSc-reporter* cells was analysed using flow cytometry. Data are shown as means \pm SD from three independent experiments. **c)** *HIGH* and *LOW* -glucose sensor cells were incubated together with *aSc-reporter* cells with a cellular proportion of 2:1 for 4 h in the presence of different concentrations of glucose, i.e. 0.1, 0.5, 1, 2, 3 or 5 g/dL. Black dots correspond to experimental values of the *HIGH*-glucose sensor cells and white dots correspond to experimental values of the *LOW*-glucose sensor cells. The error bars shown in the figures are the standard deviation of three independent experiments.

Additionally, it was tested whether the sensor cells retained memory of previous glucose states or not. *HIGH* and *LOW* -glucose sensor cells were grown in the presence of different glucose concentrations for 2 hours. The cell supernatants were then collected, and the cells were washed and incubated with the above different glucose levels again for an additional 2 hours. Therefore, *aSc-reporter* cells were incubated with the cell supernatants and GFP-fluorescence was then assessed using flow cytometry. Experimental results shown in Figure 4.4 depict that neither of the glucose sensors displayed a strong dependence on the previous glucose states although some minor differences were observed specially between extreme conditions. Experimental results pointed out that *aSc* production by sensors cells mainly depends on the extracellular glucose concentration and not so much on their previous glucose state. Thus, permitting the re-engineer use of *HXT* promoters to create sensor cells responding to different glucose levels.

a



b

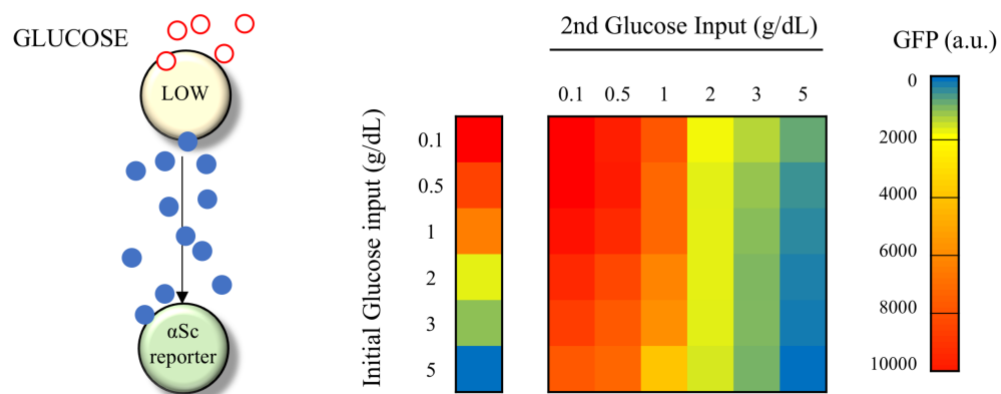


Figure 4.4 Design and characterization of glucose sensor cells. a-b) *HIGH* and *LOW* -glucose sensor cells were incubated in different concentrations of glucose i.e. 0.1, 0.5, 1, 2, 3 or 5 g/dL for 2 h. The cell supernatants were collected and cells were washed, re-diluted in fresh media containing the above different glucose concentrations and incubated for a further 2 h. After 2 h the cell supernatants were again collected. All supernatants were analysed by incubation with *αSc-reporter* cells for 4 h and subsequent measurement of GFP using flow cytometry. Data are shown as mean from three independent experiments.

4.4 Implementation of different minimal circuits to produce hormones in a glucose-dependent manner.

To create a circuit able to produce different hormones in response to the presence of the wiring molecule from the sensor cells, the *Insulin* and *Glucagon* -effector cells were engineered by placing under the control of the *FUS₁* promoter the insulin and glucagon genes. To obtain the extracellular secretion of insulin a modified version of an insulin

analogue precursor (IAP) with a short C-chain (EWK) fused to the pre-pro-leader sequence of α -factor for efficient secretion in yeast [Kjeldsen et al., 2002] was expressed under the *FUS1* promoter. Analogously, for glucagon expression, glucagon was fused to the pre-pro-leader sequence of α -factor. Therefore, obtaining the *Insulin-effector* cell, i.e. α Sc:GCG from Table 4.3, and *Glucagon-effector* cell, i.e. α Sc:GCG from Table 4.3.

For their characterization, *Insulin* and *Glucagon* -effector cells were incubated with different levels of synthetic α Sc for 1 hour and insulin and glucagon levels in the supernatant were then quantified using specific ELISA kits (see **Methodology** for further details). Output levels of insulin and glucagon with respect to synthetic α Sc levels are shown in Figure 4.5a-b respectively. In the absence of α Sc, neither insulin nor glucagon was detected, whereas, upon addition of α Sc, cells produced and secreted insulin or glucagon that accumulated in the media.

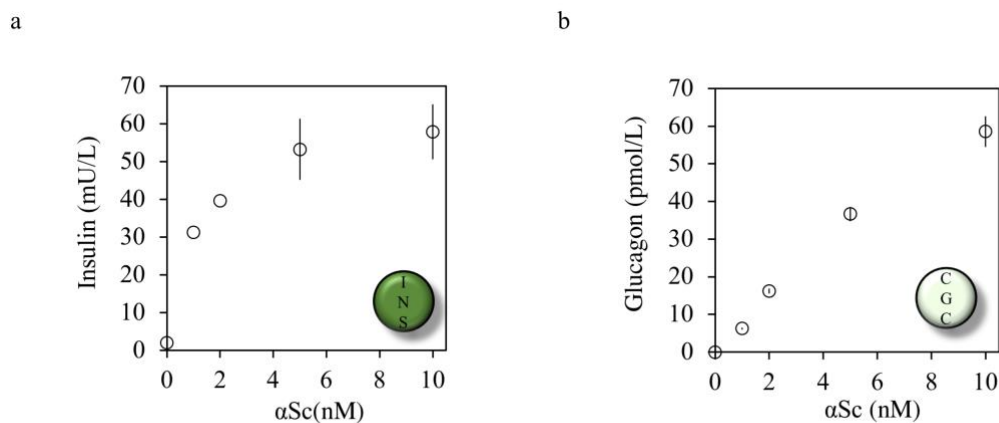
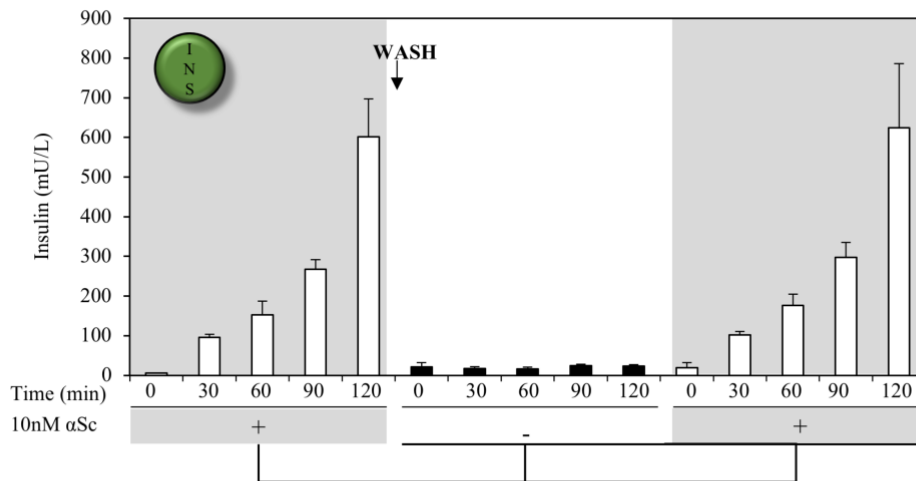


Figure 4.5 Characterization of output cells. a) *Insulin-effector* cells and b) *Glucagon-effector* cells were incubated with different levels of α Sc, i.e. 0, 1, 2, 5, or 10 nM for 1 h. Cell supernatants were then collected and insulin or glucagon levels were analysed using ELISA. Dots correspond to experimental values. The error bars shown in the figures are the standard deviation of three independent experiments.

Moreover, *Insulin* and *Glucagon-effector* dynamic response to α Sc was analysed following a kinetic experiment. Insulin and glucagon accumulation was quantified when *effector* cells were shifted from a media containing the wiring molecule into new media without α Sc (Figure 4.6). In this setup, glucagon and insulin levels were detectable after 30 minutes of induction. Furthermore, when shifting from a media without α Sc, *effector* cells ceased to secrete insulin or glucagon unless α Sc was readed to the medium. Hormone

secretion by these cells therefore did not depend on previous exposure to extracellular αSc , but depended solely on the presence of currently available extracellular αSc . Altogether suggesting that the αSc signal can be transformed into different biological outputs depending on the presence of different *effector* cells in the cell culture.

a



b

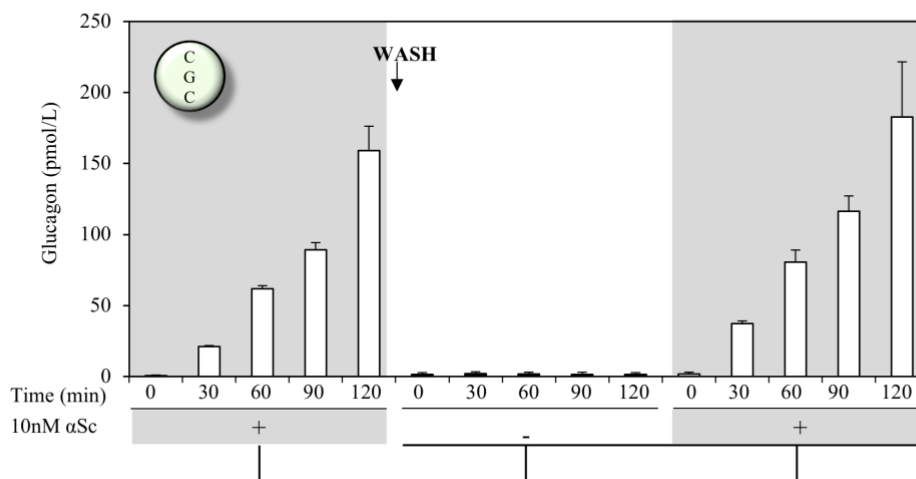


Figure 4.6 Response of the effector cells in the alternate presence or absence of αSc wiring molecule.

a) Insulin-effector cells and b) Glucagon-effector cells were exposed to 10 nM of αSc and cell supernatants were collected every 30 min over 120 min. Cells were washed, re-diluted and re-incubated for a further 120 minutes in media without αSc (black bars) or with 10 nM of αSc (white bars). Insulin and glucagon were detected in the supernatants using ELISA. Data are shown as means \pm SD from three independent experiments.

To build a circuit that produces insulin in response to high glucose levels, *HIGH-glucose sensor* cells and *Insulin-effector* cells were cultured together. Analogously, for glucagon

production at low glucose levels, *LOW-glucose sensor* cells and *Glucagon-effector* cells were combined in a second multicellular consortium (Figure 4.7a). Both consortia were independently incubated with different glucose levels for 1 hour, and insulin and glucagon production were then measured. Experimental results in Figure 4.7b show the relationship between glucose and insulin and glucagon outputs. Interestingly, the *HIGH-glucose-consortium* secretes insulin at high glucose levels (>2 g/dL), while glucagon was produced at low glucose concentrations (<2 g/dL) with the consortia involving the *LOW-glucose sensor cells*. These results indicate that the sensor cell mainly drives the input-to-output relationship in multicellular consortia whereas the biological output is produced by the effector cell.

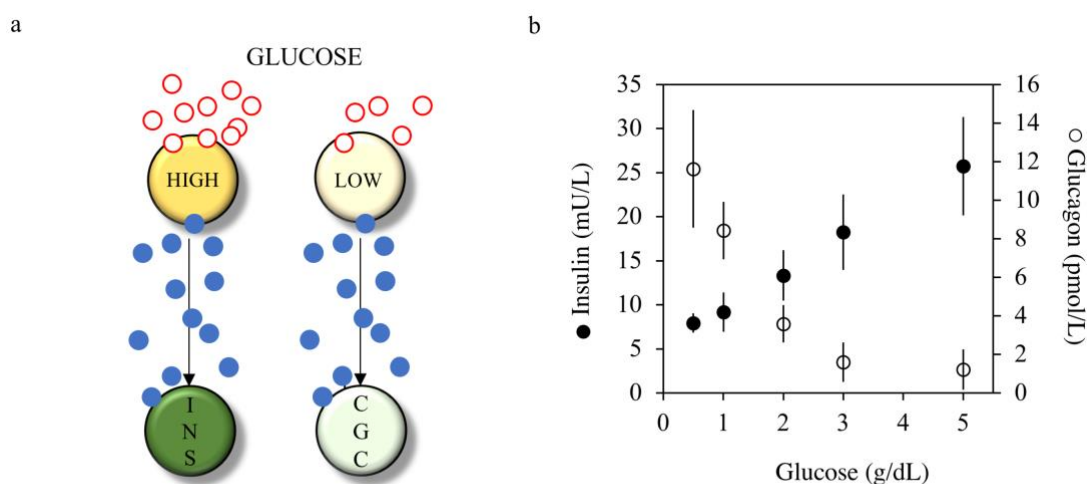


Figure 4.7 Design and implementation of multicellular consortia for glucose-responsive devices. a) Multicellular consortia for glucose-mediated insulin and glucagon production. *HIGH-glucose-consortium* consisted of *HIGH-glucose* sensor cells incubated together with *Insulin-effector* cells, using *aSc* as a wiring molecule. Similarly, the *LOW-glucose-consortium* the *LOW-glucose sensor* cells with *Glucagon-effector* cells using *aSc* as a wiring molecule. Simultaneous use of both circuits required physical segregation to prevent crosstalk. **b)** *HIGH* and *LOW-glucose-consortium* in a cellular ratio of *sensor:effector* cells of 2:1 were exposed to different glucose levels, i.e. 0.1, 0.5, 1, 2, 3 or 5 g/dL, for 1 h. Cell supernatants were collected, and secreted hormones were detected using ELISA. Black dots correspond to experimental values of the *HIGH-glucose consortium* and white dots correspond to experimental values of the *LOW-glucose consortium*. The error bars shown in the figures are the standard deviation of three independent experiments.

While both cellular consortia could produce insulin or glucagon in response to the extracellular levels of glucose, the potential application of the cellular devices requires their adaptability to constant changes in glucose levels. To assess their dynamic response to glucose the consortia were shifted from high to low glucose scenarios several times and accumulated insulin and glucagon were measured from the supernatant. Experimental results shown in Figure 4.8 depict that both consortia produced insulin or glucagon as expected according to the external glucose level, from as early as 30 minutes during a 2 hours incubation. For each 2 hours incubation, insulin or glucagon production was independent of the glucose level of the previous incubation. A small leakiness in the *HIGH-glucose-consortium* during the initial 30 minutes of incubation with low glucose was observed. Thus, suggesting the feasibility to implement minimal synthetic circuits able to produce hormones in response to fluctuating glucose levels.

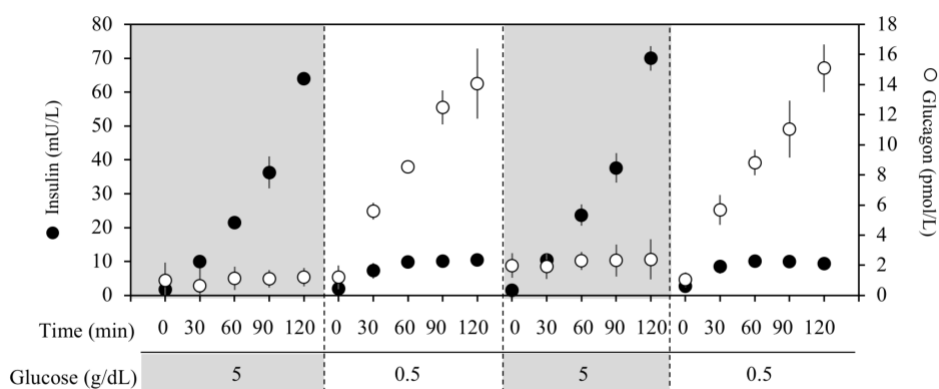


Figure 4.8 Design and implementation of multicellular consortia for glucose-responsive devices. Both *HIGH* and *LOW-glucose-consortium* were initially exposed to 5 g/dL glucose and cell supernatants were taken every 30 min for 120 min. The cells were then diluted, shifted to media containing 0.5 g/dL glucose, and supernatants were taken every 30 min over a further 120 min incubation. The cells were then diluted again, shifted back to medium containing 5 g/dL glucose for another 120 min incubation, and subsequently shifted to medium containing 0.5 g/dL glucose for a further 120 min incubation. Supernatant samples were taken as above. Hormones in the supernatants were assessed using the corresponding ELISA kit. Data are shown as means \pm SD from three independent experiments.

4.5 The affinity and sensitivity of circuits can be tuned by modulating extracellular wiring molecule levels

The possibility of tuning device sensitivity and affinity could be extremely useful for biomedical applications. In general, fine-tuning involves modification of the properties of gene promoters through genetic manipulations [Alper et al., 2005; Bakke et al., 2009; Brewster et al., 2012; Nevoigt et al., 2006]. By contrast, in a multicellular approach, tuning could be achieved by modulating the total amount of a wiring molecule such as αSc in the medium. In the present case, this modulation can be achieved in two ways: i) by adjusting the population of sensor cells or ii) by the addition of *Bar1Sc*, a specific protease that degrades αSc [MacKay et al., 1988]. In both cases, additional genetic engineering is not required.

To explore these scenarios, we developed a mathematical model that, based on the experimental response of each individual cell type, the affinity and sensitivity of the device were analysed depending on the cell population and the *Bar1Sc* concentration. The response of our device was analysed with a minimal mathematical model in which the internal details of the underlying network of biological responses were not included. Since the signalling time scale for external cues is very short compared with that for protein production, we applied the rapid equilibrium approach in the mathematical model [Ingalls, 2012]. This approach considers a separation of time scales in such a way that the fastest process reaches the steady state almost instantaneously compared with the slowest process. Based on these assumptions, the production of αSc in response to glucose can be described by:

$$\frac{d\alpha Sc}{dt} = N_{HXT} \cdot f(G) - K_{Bar1Sc} \cdot Bar1^{Sc} \cdot \alpha Sc - \delta_{\alpha Sc} \alpha Sc \quad \text{Eq. 4.1}$$

where N_{HXT} is the population of sensor cells over time and $\delta_{\alpha Sc}$ is the degradation rate of αSc , which can be neglected in a 1 hour simulation [Hoffman-Sommer, 2012]. Here, $f(G)$ describes the relationship between the rate of αSc production and the glucose concentration G , which depends on the specific *HXT* promoter. Finally, *Bar1Sc* is the

concentration of the protease added into the medium that degrades αSc with a kinetic constant $K_{Bar1Sc} = 0.5 \text{ s}^{-1}$ (data from [Jin et al., 2011]). In this model, the general expression for $f(G)$ is described by the Hill-like function:

$$f(G) = \gamma_{HXT} \cdot \left[\frac{1 + (\beta_{HXT} \cdot G)^{n_{HXT}}}{1 + (\omega_{HXT} \cdot G)^{n_{HXT}}} \right] \quad \text{Eq. 4.2}$$

The parameters γ_{HXT} , β_{HXT} , ω_{HXT} and n_{HXT} are specific for each promoter type, i.e. *HXT1* or *HXT7*. A standard logistic model describes the growth of the cell population. However, for short periods, below two doubling times, the logistic growth model can be approximated to an exponential model:

$$\frac{dN_{HXT}}{dt} = r_{HXT} \cdot N_{HXT} \cdot \left(1 - \frac{N_{HXT}}{K} \right) \approx r_{HXT} \cdot N_{HXT} \quad \text{Eq. 4.3}$$

with a duplication rate r_{HXT} . Here N_{HXT} is the number of cells and K is the carrying capacity.

Introducing Eq. 4.1 and Eq. 4.2 into Eq. 4.3 we obtain the relationship between Glucose (G) and αSc defining the *HIGH-glucose sensor cell* and *LOW-glucose sensor cell*:

$$\frac{d\alpha Sc}{dt} = r_{HXT} \cdot N_{HXT} \cdot \gamma_{HXT} \cdot \left[\frac{1 + (\beta_{HXT} \cdot G)^{n_{HXT}}}{1 + (\omega_{HXT} \cdot G)^{n_{HXT}}} \right] - K_{Bar1Sc} \cdot Bar1^{Sc} \cdot \alpha Sc - \partial_{\alpha Sc} \alpha Sc \quad \text{Eq. 4.4}$$

Finally, the production of the output, i.e. insulin or glucagon, is described by:

$$\frac{dX}{dt} = g_x(\alpha Sc) \cdot N_X \quad \text{Eq. 4.5}$$

where N_X is the population of effector cells producing X (i.e. insulin or glucagon), depending on the specific circuit. Similar to sensor cells, effector cells grow according to:

$$\frac{dN_x}{dt} \approx r_x \cdot N_x \quad \text{Eq. 4.6}$$

The $g(\alpha Sc)$ function defines the dependence between the ratio of synthesis of the output X with respect to the concentration of the wiring molecule (αSc). This function is described according to a Hill-like dependence:

$$g_x(\alpha Sc) = \gamma_x \cdot \left[\frac{1 + (\kappa_{HXT} \cdot \alpha Sc)^{n_x}}{1 + (\varphi_{HXT} \cdot \alpha Sc)^{n_x}} \right] \quad \text{Eq. 4.7}$$

Introducing Eq. 4.6 and Eq. 4.7 into Eq. 4.5 we obtain the relationship between αSc and the output, i.e. insulin or glucagon, defining the *Insulin-effector* cell and *Glucagon-effector* cell:

$$\frac{dX}{dt} = r_x \cdot N_x \cdot \gamma_x \cdot \left[\frac{1 + (\kappa_{HXT} \cdot \alpha Sc)^{n_x}}{1 + (\varphi_{HXT} \cdot \alpha Sc)^{n_x}} \right] \quad \text{Eq. 4.8}$$

The model parameters were fitted to reproduce the experimental relationship between glucose and insulin for the *HIGH-glucose-consortium* and the relationship between glucose and glucagon for the *LOW-glucose-consortium*. *Matlab R2016a* least-squares analysis software was used for fitting the parameters. Model parameters are depicted in Table 4.1 for sensor cells and in Table 4.2 for effector cells. We used the highest output expression, i.e. 5 g/dL glucose for the *HIGH-glucose-consortium* and 0.5 g/dL for the *LOW-glucose-consortium*, as a reference value to calculate the relative output change. Relative output expression for both experimental and model fitting are depicted in Figure 4.9a for both consortia. Furthermore, the fitted mathematical model could predict the accumulated insulin and glucagon levels from the abovementioned glucose dynamic response from Figure 4.8. Of note, as shown in Figure 4.9b, the model properly predicted the accumulation of insulin and glucagon at high and low glucose concentrations, respectively. Relative output change was assessed by normalizing by the highest output expression. However, these predictions were less accurate for insulin accumulation at very low glucose levels possibly due to the threshold of experimental sensitivity.

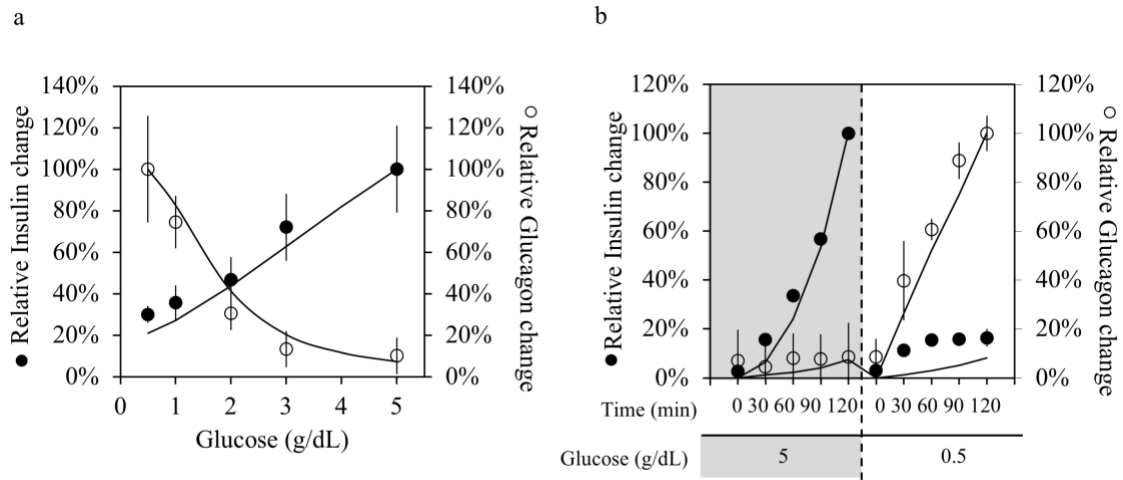


Figure 4.9 Mathematical model fitting. **a)** The model parameters were fitted to reproduce the experimental relationship between glucose concentrations and insulin or glucagon from Figure 4.7. Black dots correspond to experimental values of the *HIGH-glucose consortium* and white dots correspond to experimental values of the *LOW-glucose consortium*. The error bars shown in the figures are the standard deviation of three independent experiments. The solid lines are the theoretical results for both circuits. Relative output change was calculated by considering the maximum expression of insulin (5 g/dL) and the maximum of glucagon (0.5 g/dL) as the reference value for each cellular consortium. Correlation coefficients are $R^2 = 0.98$ for insulin and $R^2 = 0.98$ for glucagon fittings. **b)** Time-course of insulin and glucagon accumulation when the circuits were exposed to a high glucose level (5 g/dL) for 120 minutes and then shifted to lower glucose (0.5 g/dL) for a further 120 minutes. Black dots correspond to experimental values of the *HIGH-glucose consortium* and white dots correspond to experimental values of the *LOW-glucose consortium*. The error bars shown in the figures are the standard deviation of three independent experiments. The solid lines are the mathematical model predictions. Relative output change was calculated by considering the maximum expression of insulin and the maximum of glucagon as the reference value.



Parameter	γ	β	ω	\mathbf{n}	\mathbf{r}	$KBarI^{Sc}$	∂_{aSc}
Units	(nM/s)	(1/nM)	(1/nM)		(1/nM)	(1/s·nM)	(1/s·nM)
	$5 \cdot 10^{-4}$	1.113	$5.4 \cdot 10^{-2}$	1.7	$\log(2)/90$	30	$3.3 \cdot 10^{-1}$
	0.1	0	2.78	1.7	$\log(2)/90$	30	$3.3 \cdot 10^{-1}$

Table 4.1 Model parameters for Sensor Cells. Parameters used to fit the experimental results to Eq. 4.4.



Parameter	γ	κ	ρ	n	r
Units	(nM/s)	(1/nM)	(1/nM)		(1/nM)
	0.41	64.03	0.83	0.9	$\log(2)/90$
	0.9	10.38	0.93	1.6	$\log(2)/90$

Table 4.2 Model parameters for Effector Cells. Parameters used to fit the experimental results to Eq. 4.8.

In order to explore the tunability offered by the cellular consortia and to test the reliability of the mathematical model, different circuits containing different ratios of the *HIGH-glucose sensor* cells and the *Insulin-effector* cells (1:1, 2:1 and 4:1, respectively) were assessed. Therefore, the parameter N for both sensor and effector cells was adjusted to each cellular proportion. Simulations were done in the absence of *Bar1Sc*. Remarkably, the ratio of *sensor:effector* cells 2:1 was considered as the reference ratio, and percental changes in insulin levels relative to this ratio were obtained. Experimental and model predictions are shown in Figure 4.10a. The model predictions (solid lines) showed good agreement with the experimental data (dots) properly capturing the dynamics. Moreover, it was assessed whether insulin production could be altered in the presence of different concentrations of *Bar1sc* protease. In these experimental setup, *HIGH-glucose sensor* cells and *Insulin-effector* cells were mixed with a ratio of 2:1 and *Bar1sc* protease was added. Both experimental results and model predictions are shown in Figure 4.10b. The model predicted the observed reduction in insulin production in the presence of increasing amounts of *Bar1sc*.

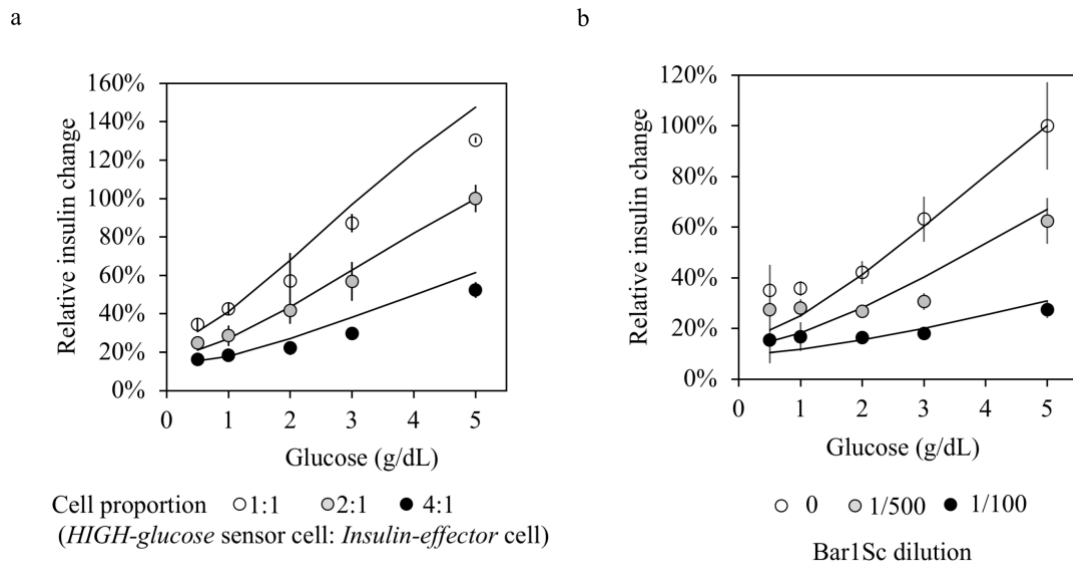


Figure 4.10 Fine-tune of *HIGH-glucose-consortium*. **a)** *HIGH-glucose sensor* cells were mixed with *Insulin-effector* cells using different proportions of *sensor:effector* cells 1:1 (black dots), 2:1 (grey dots) or 4:1 (white dots) and were incubated with different amounts of glucose, i.e. 0.1, 0.5, 1, 2, 3 or 5 g/dL, for 1 h. Insulin in supernatants was assessed using an ELISA kit. Dots correspond to experimental values. The error bars shown in the figures are the standard deviation of three independent experiments. The solid lines are the model predictions with correlation coefficients $R^2 = 0.91$ for 1:1 circuit, $R^2 = 0.92$ for 2:1 circuit and $R^2 = 0.92$ for 4:1 circuit. Cell proportion of *sensor:effector* cells 2:1 was considered as the reference value. Relative insulin change was obtained by dividing insulin levels by the maximum insulin level in the 2:1 ratio. **b)** *HIGH-glucose sensor* cells were mixed with *Insulin-effector* cells with a 2:1 ratio in the presence of different dilutions of *Bar1Sc*: 0 (white dots), 1/500 (grey dots) or 1/100 (white dots) and were incubated in different glucose concentrations, i.e. 0.1, 0.5, 1, 2, 3 or 5 g/dL, for 1 h. Supernatants were analysed using an ELISA kit. Dots correspond to experimental values. The error bars shown in the figures are the standard deviation of three independent experiments. The solid lines are the model predictions with correlation coefficients $R^2 = 0.96$ for 0 circuit, $R^2 = 0.83$ for 1/500 circuit and $R^2 = 0.81$ for 1/100 circuit, respectively. Relative insulin change was obtained by dividing insulin levels by the maximum insulin level without *Bar1Sc*.

Modulations in cellular proportion or *Bar1Sc* protease allow to modify the levels of the αSc wiring molecule and therefore would allow to tune the main features of the glucose sensor, i.e. sensitivity (σ) and affinity ($K_{0.5}$). In order to explore how the main features can be tuned by the modulation of αSc we simulated multiple consortia configurations involving either different cellular proportion ratios or the addition of *Bar1Sc* protease. To control population growth the *in silico* experiments were performed within a semi-continuous embodiment [Ed. Malek, 1964]. Every 90 minutes, which approximately

corresponds to the average cellular doubling time, from experimental results, a volume $v = V_0 / \mu$ was removed from the culture and replaced by the same amount of fresh medium with glucose, to maintain the volume (V_0), the extracellular glucose concentration and the optical density constants. In the following equation, μ is the dilution fraction:

$$\mu = \frac{OD_{HXT:\alpha Sc} + OD_{\alpha Sc:INS}}{OD_{HXT:\alpha Sc}^0 + OD_{\alpha Sc:INS}^0} \quad \text{Eq. 4.9}$$

where $OD_{HXT:\alpha Sc}$ and $OD_{\alpha Sc:INS}$ are the optical density values measured every 90 minutes, and $OD_{HXT:\alpha Sc}^0$ and $OD_{\alpha Sc:INS}^0$ are the initial optical densities of each cell type in the initial state of the multicellular consortia. The accumulated output was measured after each dilution. We then considered multiple combinations of sensor cells and the presence of different concentration of *BarISc*. For each combination, affinity and sensitivity were calculated. Circuit's affinity was determined by calculating the $K_{0.5}$, the concentration of glucose that results in 50% of the maximal insulin accumulation. Circuit's sensitivity was defined as the relationship between the increase in insulin (*Ins*) and the increase in glucose levels (*G*), i.e. $\frac{dIns}{dG}$.

To evaluate the dependence between the sensitivity and the specific multicellular configuration of the circuit, a large number of combinations of cellular proportion and *BarISc* were computationally analysed. Simulations were performed over 600 minutes. Every 90 min, a volume v of the cellular culture was replaced with the same amount of fresh medium containing a similar glucose concentration and different concentrations of *BarISc*. For illustrative purposes, Figure 4.11a shows the evolution of the insulin accumulation measured after medium replacement versus time for a given circuit. A maximum in insulin accumulation was reached after 600 minutes. Actually, after 600 minutes, all circuits analysed reached its maximum level of insulin. Interestingly, when plotting the maximum accumulated insulin for each specific glucose value a linear dependence between glucose and the maximal insulin is observed. As an example, Figure 4.11b shows this linear dependence for three different consortia configurations. Therefore, allowing to characterize the sensitivity of each circuit with a single value, i.e. $\frac{dIns}{dG}$. Figure 4.11c shows the sensitivity with respect to each particular circuit configuration for a large

number of cellular proportion and *Bar1Sc* dilution. Whereas sensitivity increased when the circuits contained more sensor cells, the reduction in *aSc* levels brought about by the addition of *Bar1Sc* generated a dramatic decrease in the sensitivity.

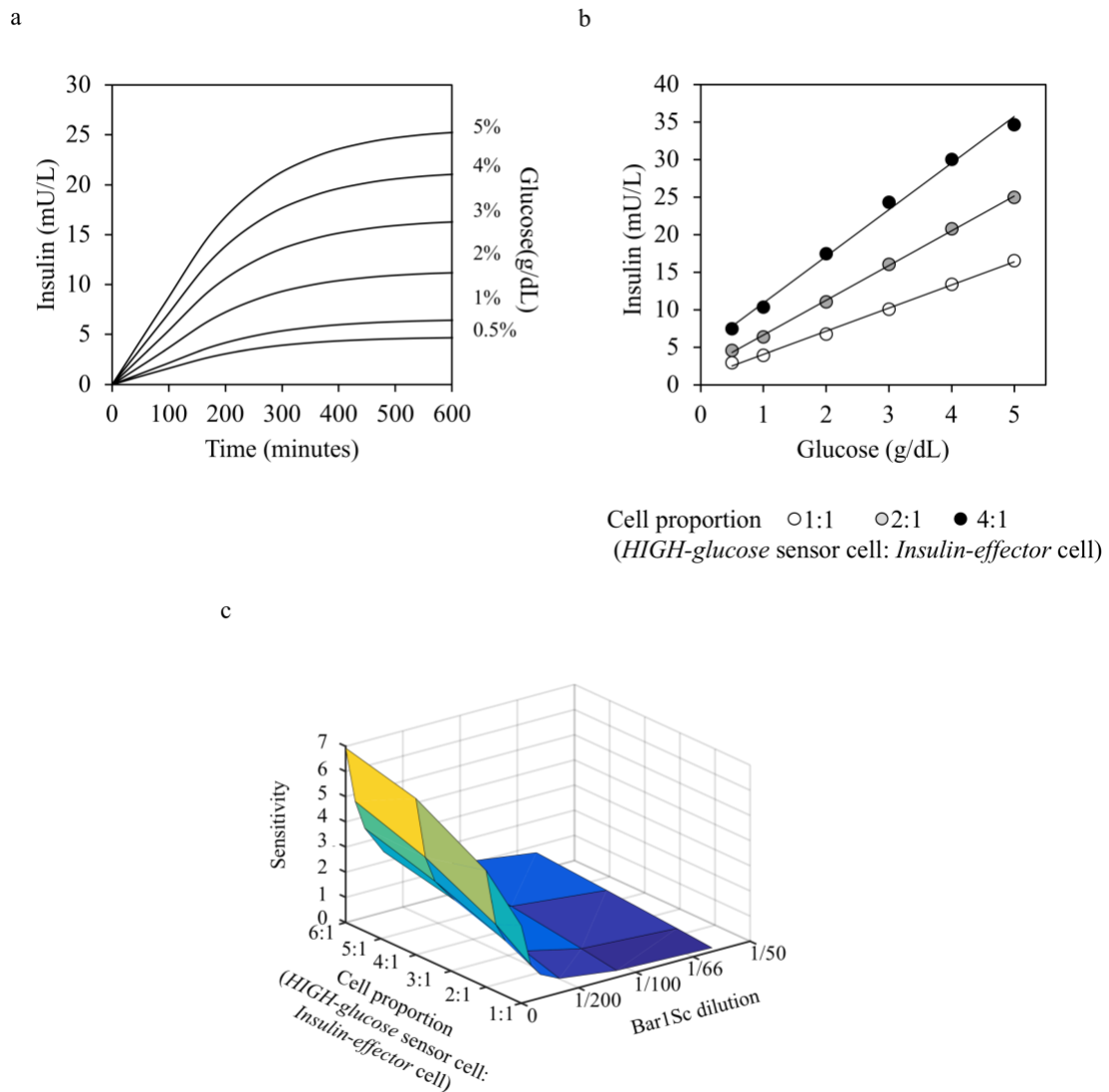


Figure 4.11 Fine-tune of a circuit's sensitivity. **a)** Dependence between accumulated insulin and glucose. Temporal evolution in a semi-continuous embodiment of accumulated insulin in a circuit 1:1. Insulin values were recorded after each dilution. **b)** Insulin values calculated after 600 minutes at different glucose concentrations for three different configurations. Dots correspond to the predicted accumulated insulin and the solid line to the linear correlation with a correlation coefficient of R^2 (1:1) = 0.997, R^2 (2:1) = 0.999 and R^2 (4:1) = 0.995. **c)** Mathematical prediction of the relationship between the sensitivity of the circuits containing different amounts of *HIGH-glucose sensor cells* and different amounts of *Bar1Sc*.

To determine the affinity of each circuit, we performed the same computational simulations in a semi-continuous device during 600 minutes for a larger range of glucose concentrations, until reaching the maximal insulin expression levels (Figure 4.12a). The affinity of a given circuit can be determined by calculating the $K_{0.5}$ values, the higher the affinity, the lower $K_{0.5}$. For each specific circuit configuration, once the maximum insulin levels were reached, the glucose concentration $K_{0.5}$ was determined. Figure 4.12b shows the relationship between $K_{0.5}$ and the circuit's configuration. Likewise to the previous results, in the absence of *Bar1Sc*, the affinity increased with an increase in the number of sensor cells. However, upon addition of *Bar1Sc* a smooth transition toward lower affinities, i.e. a higher $K_{0.5}$, was observed.

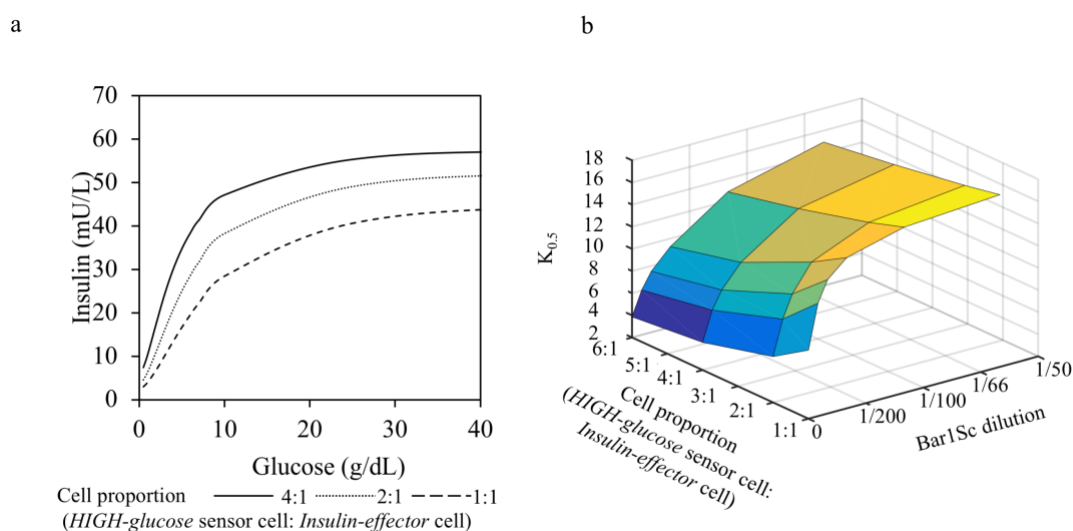


Figure 4.12 Fine-tune of a circuit's affinity. **a)** Transfer function of accumulated insulin. Computational determination of the transfer function of accumulated insulin versus a large range of glucose with the consortia configurations. **b)** Mathematical prediction of the relationship between the $K_{0.5}$ values of the circuits containing different amounts of *HIGH-glucose sensor* cells and different amounts of *Bar1Sc*.

4.6 Implementation of a time-dependent single pulse behaviour by multicellular consortia.

A multicellular approach allows the adjustment of different sensor main features without additional genetic manipulation. However, our simple design using only two cell types, i.e. sensor and effector cells, cannot generate time-dependent responses that are of interest to many potential applications. We, therefore, explored the ability of multicellular devices

to perform time-dependent responses, and more specifically, to display single pulse dynamics. In general, this behaviour plays a fundamental role at the core of many natural systems, resulting in time-regulated responses in the cell [Levine et al., 2013]. For example, pancreatic hormone secretion, i.e. secretion of insulin and glucagon, exhibits a single pulse dynamic [Nan-Kuang Yau & Liang-Wey Chang, 1995; Polonsky et al., 1988; S. H. Song et al., 2002]. In order to elucidate whether multicellular devices can mimic these natural dynamic responses, we designed a more complex device including a feed-forward loop. Feed-forward loops (*FFL*) are recurring topological motifs present in biological networks [Balázsi et al., 2005; Milo et al., 2002]. There are different configurations of these abundant motifs, which are plastic structures able to implement multiple dynamics [Macía et al., 2009; Milo et al., 2002; Widder et al., 2012]. Specifically, we implemented a particular type of one of these configurations, the canonical three-node Type I Incoherent Feed-forward Loop (*II-FFL*) [Mangan et al., 2006]. This topology involves three nodes; an input, a modulator, and an output node (Figure 4.13a) where the input and the modulator nodes directly control the output production. In turn, the modulator node is controlled by the input, which introduces an additional indirect control of the output. The input directly activates both the output and the modulator nodes, while the modulator represses the output.

To implement this feedforward circuit (Figure 4.13b), the input node was composed of two different cell types, *HIGH-glucose* sensor cells and a new cell type that produces the α -factor from *Candida albicans* (αCa) under the HXT_1 promoter, *HIGH- αCa* , i.e. *HXT1: αCa* cell from Table 4.3. The input node composed of *HIGH-glucose* sensor cells and *HIGH- αCa* cells secretes αSc and αCa simultaneously in response to an increase in the presence of extracellular glucose. On one hand, αSc directly induces the synthesis of insulin in the output node, activating the *Insulin-effector* cells, whereas αCa stimulates a new cell type that secretes the *Bar1Sc* protease, the *Modulator* cell, i.e. *$\alpha Ca:Bar1Sc$* cell from Table 4.3, and thereby inhibits insulin production in the output node.

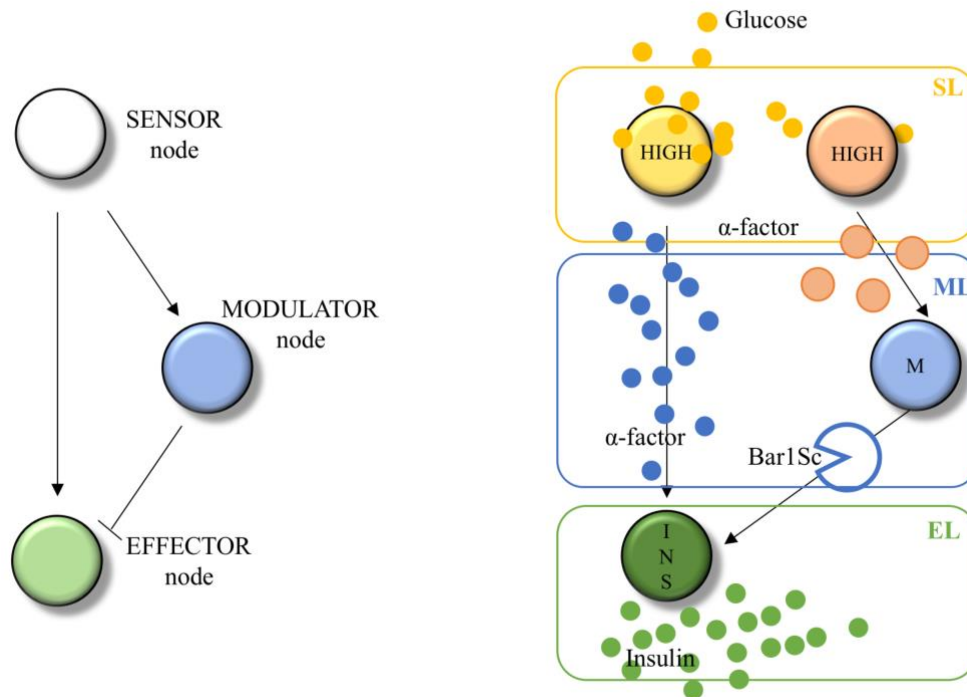


Figure 4.13 Single pulse dynamics in multicellular circuits. a) Schematic diagram of a Type I incoherent feed-forward loop motif. The sensor node activates the output node and the modulator node, which in turn represses the output node. b) Experimental implementation of a feed-forward circuit. The sensor node was implemented by a consortium involving *HIGH-glucose* sensor cell and *HIGH-αCa* cells. The output node was implemented by the *Insulin-effector* cell. The modulator node was implemented by the *Modulator* cell type.

Therefore, it was necessary to test and characterize the new cell types: the *HIGH-αCa* and the *Modulator* cell. The *αCa-reporter* cell, i.e. cell *αCa:GFP* from Table 4.3, is a reporter cell that when sensing *αCa* expresses a green fluorescent protein (GFP). Figure 4.14a shows the *αCa-reporter* cell relationship between synthetic *αCa* and GFP signal for an incubation time of 4 hours. Moreover, crosstalk between *αCa* and *αSc* wiring molecules was analysed together with the ability of *Bar1Sc* degradation upon *αCa*. Each *α-factor* reporter cell was exposed either to a high concentration of synthetic *αSc*, *αCa*, or *Bar1Sc* (Figure 4.14b-c).

Experimental results shown in Figure 4.14b for the *αCa-reporter* cell depicts that *αCa* was not degraded by *Bar1Sc* and did not show crosstalk with the *αSc-receptor* cell whereas, in Figure 4.14c, the *αSc-reporter* cell gets activated with *αSc* but no with either *αCa* and

$\alpha Sc + Bar1Sc$. Therefore, *HIGH- αCa* induced the production of αCa in response to an increase in extracellular glucose, analysed by *HIGH- αCa* and αCa -reporter cell. In Figure 4.14d the relationship between glucose levels and GFP levels by αCa -reporter is shown. The modulatory effect on αSc by the *Modulator* cell, expressing the *Bar1Sc* protease in response to αCa was assessed by culturing the *Modulator* cell with the αSc -reporter cell with a fixed concentration of synthetic αSc and increasing levels of αCa . Figure 4.14e shows the modulatory effect of αSc levels via the reduction of the GFP from the αSc -reporter cell with increasing levels of αCa .

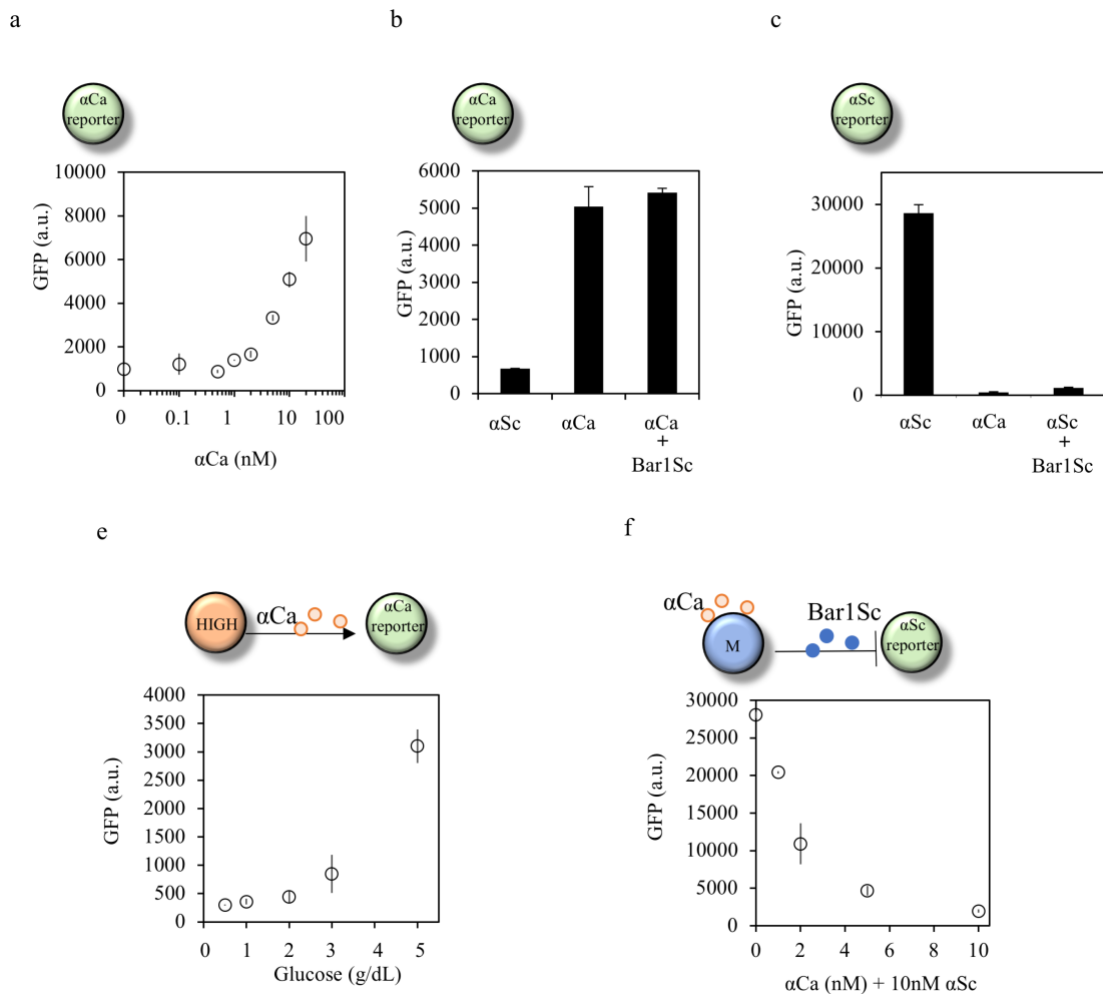


Figure 4.14 Characterization of *HIGH- αCa* cell type and the *Modulator* cell. **a)** αCa -reporter cells were incubated with different levels of αCa , i.e. 0.01, 0.1, 0.5, 1, 2, 5, 10 or 20 nM, for 4 h. Mean GFP fluorescence (a.u.) of αCa -reporter cells was then analysed using flow cytometry. Dots correspond to experimental values. The error bars shown in the figures are the standard deviation of three independent experiments. **b)** αCa -reporter cells were incubated for 4 h with 10 nM of αSc , 10 nM of αCa or a combination of 10 nM αCa and an excess concentration of purified *Bar1Sc*. GFP fluorescence (a.u.) of αCa -reporter cells was then analysed using flow cytometry. Data are shown as means \pm SD from three

independent experiments. **c)** *aSc-reporter* cells were incubated for 4 hours with 10 nM of *aSc*, 10 nM of *aCa* or 10 nM of *aSc* together with an excess concentration of purified *ScBar1Sc*. GFP fluorescence (a.u.) of *aSc-reporter* cells was analysed using flow cytometry. Data are shown as means \pm SD from three independent experiments. **d)** Transfer function of *HIGH-aCa*. *HIGH-aCa* cells were mixed with *aCa-reporter* cells and incubated for 4 hours with different glucose concentrations, i.e. 0.1, 0.5, 1, 2, 3 or 5 g/dL. GFP fluorescence (a.u.) of *aCa-reporter* cells was analysed using flow cytometry. Dots correspond to experimental values. The error bars shown in the figures are the standard deviation of three independent experiments. **e)** *Modulatory* cells were mixed with *aSc-reporter* cells and incubated for 4 h with 10 nM of *aSc* and different levels of *aCa*, i.e. 0, 1, 2, 5 or 10 nM. GFP fluorescence (a.u.) of *aSc-reporter* cells was analysed using flow cytometry. Dots correspond to experimental values. The error bars shown in the figures are the standard deviation of three independent experiments.

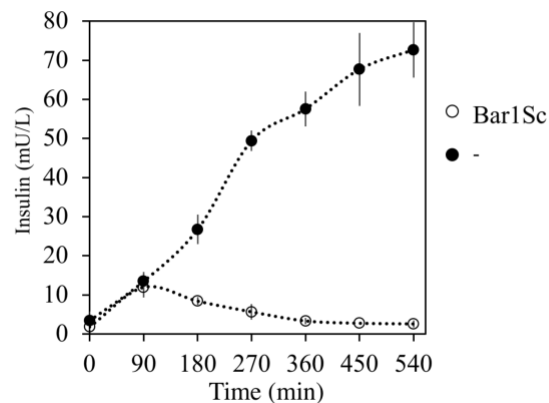
Initially, the response of the *IFFL* device in the absence of the *Modulatory* cell was tested by assaying the production of insulin by the *HIGH-glucose* sensor cells and *Insulin-effector* cells over 9 hours incubation in high glucose in a semi-continuous setup, in which the culture was diluted by half every doubling time (Figure 4.15a). The addition of purified *Bar1Sc*, after the first 90 min of incubation, caused a clear decrease in insulin production and suggested that a decrease in the extracellular wiring molecule levels generated a single pulse response in insulin production.

A remaining question was whether the same effect could be achieved by the production of *Bar1Sc* by an engineered cell within the device. *HIGH-glucose sensor* cells and *Insulin-effector* cells were mixed with different amounts of *Modulatory* cells and insulin levels were assessed as before. In the absence of extracellular *aCa*, the circuit responded similarly to its response in the absence of *Modulatory* cells. In contrast, when *aCa* was added after 90 minutes, the insulin levels decreased depending on the number of *Modulatory* cells, indicating that *Bar1Sc* production by these cells could alter the communication between sensor and effector cells, inducing a single pulse response (Figure 4.15b).

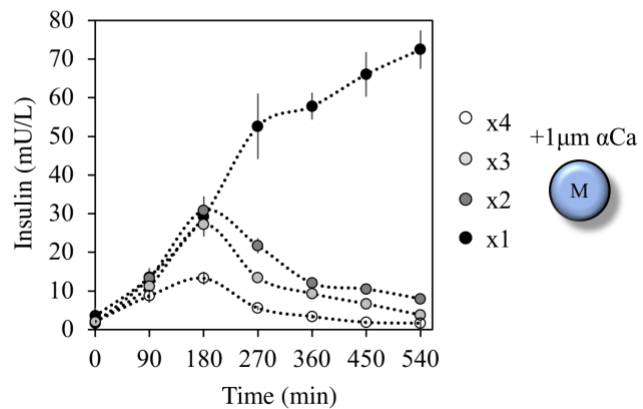
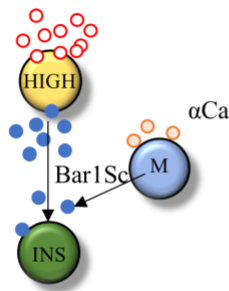
Finally, the response of the fully assembled synthetic device was evaluated (Figure 4.15c). To implement a single pulse behaviour without adding an external modulator (*aCa*), the *HIGH-aCa* cells, a cell type that produces *aCa* in response to increased glucose levels, was combined with the above-described consortium. To modulate the amplitude of the

output response different amounts of *HIGH- α Ca* cells were added. Cells were cultured together in high glucose for 9 hours and insulin was quantified. In the presence of lower amounts of *HIGH- α Ca* cells, there was a progressive accumulation of insulin over time. By contrast, higher concentrations of *HIGH- α Ca* cells led to a single pulse response. Therefore, the specific circuit's configuration determines the total amount, i.e. the dose, of insulin produced in response to a physiological signal such as glucose. Of note, an excessive induction of the modulator node prevented insulin production possibly caused by an excess of the *Bar1Sc* that degraded α Sc. These results showed that multicellular consortia can generate complex time-dependent analogue responses. Addition of a modulation module that generated delayed production of a repressor completely changed the preconfigured response of the circuit from that of a simple behaviour into that of a time-dependent circuit with a single pulse behaviour.

a



b



c

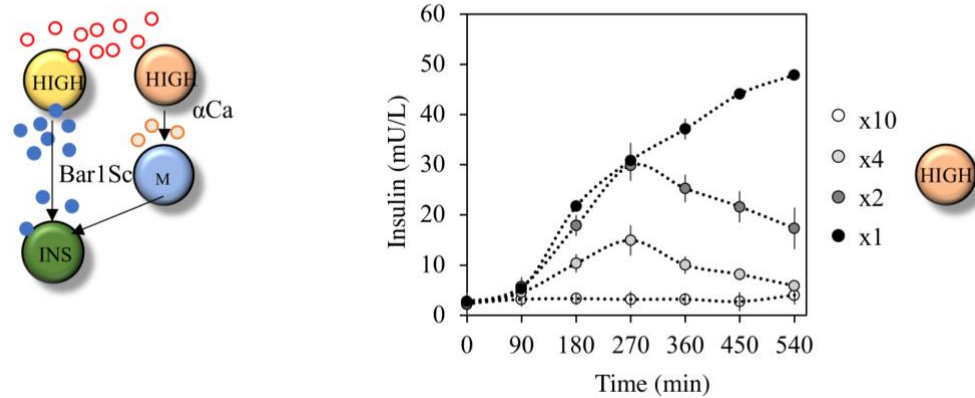


Figure 4.15 Characterization of different elements in a circuit with a feed forward loop to generate a single pulse response. **a)** *HIGH*-glucose sensor cells and *Insulin-effector* cells (in the proportion 2:1) were cultured together in 5 g/dL glucose for 9 h. The culture was diluted every doubling time in fresh media containing 5 g/dL glucose and cell supernatants were collected. *Bar1Sc* was added (white dots) or not (black dots) after the first 90 min of incubation. The insulin level was assessed using ELISA. Dots correspond to experimental values and the error bars shown in the figures are the standard deviation of three independent experiments. **b)** *HIGH*-glucose sensor cells and *Insulin-effector* cells were grown with different amounts of *Modulatory* cells (1x to 4x) for 9 h in 5 g/dL glucose. Synthetic *αCa* (1 μM) was added after 90 min. Insulin levels were assessed using ELISA. All these experiments were conducted in a semi-continuous setup. Dots correspond to experimental values. The error bars shown in the figures are the standard deviation of three independent experiments. **c)** Single pulse dynamics in multicellular circuits. *HIGH-αCa* cells were mixed in different proportions with *HIGH*-glucose sensor cells, *Insulin-effector* cells and *Modulatory* cells in the presence of 5 g/dL of glucose for 9 h. When cells duplicated, the culture was diluted with fresh media containing 5 g/dL glucose to maintain a constant optical density. All these experiments were conducted in a semi-continuous setup. Insulin in the supernatant was measured using an ELISA kit. Dots correspond to experimental values and the error bars shown in the figures are the standard deviation of three independent experiments.

4.7 Discussion

In this chapter, we addressed how extracellular sensed signals could be integrated to produce non-trivial responses for a particular biomedical application. We have designed a multicellular embodiment in which each particular layer, represented by different engineered cell types, could detect biological signals, discriminate between different physiological conditions, and respond according to a non-trivial logic. The experimental

implementation carried in *Cell Signalling Research Group* by engineering *S. cerevisiae* model organism achieved the extracellular glucose discrimination between high and low glucose levels, coupled with the production of insulin or glucagon accordingly. Moreover, output response was modulated by implementing a device with single pulse behaviour. These results reinforce the idea that synthetic biology can offer a new framework for the development of *in vivo* biomedical devices that can complement or even substitute devices based on electronic or electro-mechanical technology. Second, our results demonstrate that devices based on multicellular consortia are flexible and tuneable. Device characteristics, i.e. sensitivity (σ) and affinity ($K_{0.5}$), can be adjusted with the proper modulation of the molecule responsible for the connection between layers, without the need for additional cell engineering. Experimental results and the development of a mathematical model describing the cellular consortium allow for the *in silico* exploration of the circuit's main features; demonstrating the tunability of the sensitivity and affinity in two different ways: by adjusting the initial concentration of the cells involved in the layers, or by the addition of an external biochemical compound that degrades the wiring molecule, e.g. *Bar1Sc*. Thus, the inclusion of an additional cell type makes possible to modulate the levels of the wiring molecule and accordingly, the behaviour of a circuit. The modularity of our device allowed to re-design it and emulate an *IFFL* motif, that together with the introduction of a temporal-delay in the production of *Bar1Sc*, generates a complex time-dependent analogue response. The implementation of single pulse circuits based on *FFL* architectures allows for the synthesis and release of hormones or other molecules of interest in response to physiological signals in a predetermined dose. The total dosage released, i.e. the pulse area, is an analogue magnitude and can be tuned by properly defining the circuit's configuration. In our case of study, the physiological input was glucose and the hormone released was insulin, but this approach can be easily applied to other signal and molecules. Noteworthy is that depending on the configuration of the multicellular elements' device response suffers a radical-transformation: from a simple behaviour into that of a time-dependent circuit with a single pulse behaviour.

However, when hypothesizing the use of our device for an *in vivo* application some important drawbacks arouse. Remarkably are the activation thresholds of the *HXT*

glucose-promoters defining the thresholds of hyper and hypoglycaemia for yeast model organism. Although explored the ability of the multicellular consortia to modify the device affinity, i.e. $K_{0.5}$ parameter, by increasing or diminishing the levels of αSc , experimental results are much more above the levels of humans' hyperglycaemia and hypoglycaemia. Another important drawback arouses concerning device stability. Although demonstrating the flexibility in the device response occasioned by the different cellular proportions of the multicellular consortium components, changes in cellular proportion along time, for instance due to negative competition growth effects [Amoyel & Bach, 2014; Kwok, 2010], would have a direct effect on device affinity and sensibility. Besides the ability of yeast model organism to sense physiological signals, perform non-trivial responses and secrete, via the pheromone pathway, insulin and glucagon, both physiological hormones must be further processed to be fully functional. Future work should be devoted to analyse and design the device dynamics considering the physiological scenario ensuring the proper detection of the regulable analyte and its corresponding output to decipher device characteristics for its optimal response.

4.8 Methodology

4.8.1 Experimental methodology

4.8.1.1 Engineered yeast cell library and cell growth conditions




Yeast *W303* cells (*ade2-1 his3-11,15 leu2- 3,112 trp1-1 ura3-1 can1-100*), complete genotype and information of each yeast strain is related in Table 4.3. Cells were grown overnight in rich media containing 2 g/dL glucose at 30 °C, and were then spun down and resuspended in rich media containing the specific glucose concentration required for each experiment.

Sensor layer cells are designed to produce αSc in the presence of different glucose concentrations. These cells are MAT α yeast cells in which MF α 1 and MF α 2 α -factor mating pheromone genes were deleted to avoid endogenous α -factor expression. The

STE3 receptor was also deleted to prevent mating with MATa cells within the circuit. The MFa1 gene is expressed the different HTX promoters (pRS406-PHXTX-MFa1).

Modulator layer cells are designed to express the protease *Bar1Sc* in the presence of α Sc. These cells are MATa yeast cells in which BAR1 gene was deleted. These cells express the *S. cerevisiae* protease Bar1 under the control of the *PFIG1* inducible promoter (pRS406-P_{FIG1}-Bar1). Upon addition of α SC these cells secrete the protease Bar1 in the media.

Effector layer and Reporter cells are designed to express GFP, insulin or glucagon in the presence of α Sc or α Ca. These cells are MATa yeast cells in which BAR1 and STE2 genes were deleted. These cells contain GFP, α -insulin or α -glucagon in the FUS1 gene locus under its promoter (fus1::GFP-KanMX) for the *C. albicans* reporter cell pheromone receptor (CaSTE2). mCHERRY inserted in the ENO1 locus. Constitutive mCherry intensity allows distinguishing these cells from mCherry-negative cells once mixed together.

Cell	Name	Genotype*
Sensor layer		
	HXT2-Sc	<i>MATa ste3::HIS3 mfa1::LEU2 mfa2::KanMX</i> <i>pRS406-P_{HXT2}-MFa1</i>
	HXT3-Sc	<i>MATa ste3::HIS3 mfa1::LEU2 mfa2::KanMX</i> <i>pRS406-P_{HXT3}-MFa1</i>
	HXT4-Sc	<i>MATa ste3::HIS3 mfa1::LEU2 mfa2::KanMX</i> <i>pRS406-P_{HXT4}-MFa1</i>









	HXT1- α Sc	<i>MATa ste3::HIS3 mfa1::LEU2 mfa2::KanMX</i> <i>pRS406-P_{HXT1}-MFα1 pRS404-P_{HXT1}-MFα1 ENO1-YFP-</i> <i>HphNT</i>
	HXT7- α Sc	<i>MATa ste3::HIS3 mfa1::LEU2 mfa2::KanMX</i> <i>pRS406-P_{HXT7}-MFα1 pRS404-P_{HXT7}-MFα1</i>
	HXT1- α Ca	<i>MATa ste3::HIS3 mfa1::LEU2 mfa2::KanMX</i> <i>pRS424-P_{HXT1}-CaMFα1</i>
Modulator layer		
	Bar1Sc	<i>MATa bar1::NatNT ste2:: caste2-HphNT far1::LEU2</i> <i>pRS406-P_{FIG1}-ScBar1 ENO1-iRFP-KanMX</i>
Effector layer		
	α Sc-INS	<i>MATa bar1::NatNT far1::URA3</i> <i>pRS404-P_{FUS1}-αINS ENO1-mCHERRY-KanMX</i>
	α Sc -GCG	<i>MATa bar1::NatNT far1::URA3</i> <i>pRS404-P_{FUS1}-αGCG ENO1-mCHERRY-KanMX</i>
Reporter cells		
	α Sc-GFP	<i>MATa bar1::HIS3</i> <i>P_{FUS1} -GFP-KanMX ENO1-mCHERRY-HphNT</i>
	α Ca-GFP	<i>MATa bar1::HIS3 ste2::URA3 yIP</i> <i>P_{TDH3}-CaSTE2-TRP P_{FUS1}-GFP-KanMX ENO1-mCHERRY-</i> <i>HphNT</i>

Table 4.3 Yeast strains used in this study. * Strain background W303 (ade2-1 his3-11,15 leu2-3,112 trp1-1 ura3-1 can1-100). “.” represent genotype deletions. *pRS406* is the URA3 integrative vector and *pRS404* the TRP1 integrative vector.

4.8.1.2 Experimental characterization of the engineered cells

Reporter cells were grown to mid-exponential phase, diluted to $OD_{660} = 0.2$, and then treated with different inputs (synthetic *S. cerevisiae* α -factor, synthetic *C. albicans* α -factor). Samples were incubated for 4 h at 30 °C and analysed using flow cytometry. For consortium involving sensor and effector cells both cells were mixed in a media containing different glucose concentrations, ranging from 0.5 g/dL to 5 g/dL. Effector cells were grown to mid-exponential phase and diluted to an $OD_{660} = 0.1$, whereas sensor cells were grown at different initial OD_{660} depending on the specific cellular ratio (*sensor:effector*) of $OD_{660} = 0.1, 0.2$ or 0.4 .

4.8.1.3 Experimental characterization of *IFFL* consortia

For the consortia involving sensor and effector cells were grown to mid-exponential phase, diluted to $OD_{660} = 0.2$ for the *HIGH-glucose* sensor cell and to $OD_{660} = 0.1$ for the *Insulin-effector* cell. *Modulatory* cell was added in different proportions by diluting its OD_{660} to 0.1, 0.2, 0.3 or 0.4. The final *IFFL* configuration comprises the *HIGH-glucose* sensor cell diluted to $OD_{660} = 0.2$, the *Modulatory* cell to $OD_{660} = 0.2$ and the *Insulin effector* cell to $OD_{660} = 0.1$. The *HIGH- α Ca* cell was grown to mid-exponential phase and then diluted to $OD_{660} = 1, 0.4, 0.2$ or 0.1 for each specific cell ratio. Mixed cells were grown for 9h at 30°C in a media containing high glucose (5 g/dL). Every time cells doubled the culture was diluted with fresh media with 5 g/dL of glucose to keep optical density constant.

4.8.1.4 Fluorescence measurements using flow cytometry

All of the experiments requiring flow cytometry were analysed as follows: samples were diluted in phosphate-buffered saline (PBS) with 1X cyclohexamide and analysed using flow cytometry (BD LSRFortessa). A total of 10000 cells were collected from each sample. Constitutive mCherry fluorescence (*ENO1::mCherry*) of *α Sc-reporter* and *α Ca-reporter* cells was used to differentiate them from other cells in the consortia when mixed.

Specific emission in the fluorescence channel was measured versus autofluorescence (PerCP-Cy5-5-A channel for GFP and PerCP-Cy7 channel for mCherry). Mean GFP fluorescence was calculated using *FlowJo software*. Data are expressed as mean fluorescence (in arbitrary units).

4.8.1.5 Insulin and glucagon production and measurements

Yeast *W303 MATa* cells were transformed with *pRS406-PFUS1- α INS* or *pRS406-PFUS1- α GCG*. *PFUS1- α INS* expressed a modified version of an insulin analogue precursor (IAP) with a short C-chain (EWK) fused to the pre-pro-leader sequence of α -factor for efficient secretion in yeast [Bakke et al., 2009; Kjeldsen et al., 2002] under a pheromone inducible promoter. *PFUS1- α GCG* expressed a modified version of glucagon fused to the pre-pro-leader sequence of α -factor for efficient secretion in yeast under a pheromone inducible promoter. Insulin and glucagon presence in the supernatant of cells were quantified using specific ELISA kits. Insulin was measured using the Merckodia Iso-Insulin ELISA kit according to the manufacturer's protocol. Glucagon was measured using the Merckodia Glucagon ELISA kit) according to the manufacturer's protocol.

4.8.1.6 Protease purification

Yeast *W303* cells were modified to express the *S. cerevisiae Bar1* protease gene (*Bar1Sc* in this study) under the control of the *GAL1* promoter (*pRS406-PGAL1-Bar1Sc*). Cells were grown overnight in synthetic media containing 2% raffinose and were then diluted to OD₆₆₀ = 0.8 in synthetic media containing 2% galactose to induce protease expression. After 4 h incubation, the supernatant was collected and concentrated using 10 kDa Centrifugal Filter Units (Amicon Ultra). Filtered products were stored at -20 °C. Synthetic Pheromones. The synthetic pheromones *C. albicans* α -factor mating pheromone (GFRLTNFGYFEPG) (α Ca) and *S. cerevisiae* α -factor mating pheromone (WHWLQLKPGQPMY) (α Sc) were synthesized by the peptide synthesis facility (UPF) in free dithiol form. The peptides were diluted in H₂O to a final concentration of 3 mM and stored at -20 °C.

4.8.2 Mathematical modelling methodology

Ordinary Differential Equations (ODEs) describing the *HIGH-glucose sensor* cell (Eq. 4.4) and the *Insulin-effector* cell (Eq. 4.8) with experimental fitted model parameters from Table 4.1 and Table 4.2 have been integrating with the Runge–Kutta method order 4 in *Matlab R2016a software*. For sensitivity and affinity analysis predictions have been carried in a semi-continous embodiment consisting of a total time of 600 min with media replacement according to Eq. 4.9 to maintain the volume (V_0), the extracellular glucose concentration and the optical density constants. Cell proportion was modelled considering the different Optical Densities of sensor cell in Eq. 4.3 and *BarISc* dilutions in Eq. 4.1.

CHAPTER 5

Deciphering living device closed-loop performance:

Implantable cellular devices for diabetes mellitus treatment

The aim of this chapter is to *in silico* explore the potential applicability of cellular devices for diseases treatment. In particular, we focused on the effects of implanting engineered cellular devices for glycaemia regulation in Type I Diabetic Mellitus patients.

The work presented along this chapter is enclosed in a project from *Fundació La Marató de TV3* (2017-2020) entitled “Encapsulated Synthetic Cellular Circuits to Restore Glycemic Control in Type 1 Diabetes” in which we aim to *in vivo* treat diabetic mouse model with encapsulated cells to restore glycaemia. The project was done in collaboration with our group from Universitat Pompeu Fabra in charge of designing and modelling the synthetic gene circuits producing insulin hormone, the group of *Cell Signalling* from Institut de Recerca Biomedica de Barcelona in charge of engineering the eukaryotic cells and performing the *in vitro* experiments, the group *NanoBioCel* from Universidad del País Vasco developed the cellular encapsulation and viability analysis of the reconstituted cellular implants to be finally implanted in diabetic mouse models in Hospital Sant Joan de Déu de Barcelona.

5 DECIPHERING LIVING DEVICE CLOSED-LOOP PERFORMANCE

5.1 Cellular devices for Diabetes Mellitus treatment

Living biomedical devices can be designed to act as a read-out of a pathophysiologic state [Courbet et al., 2015] or as a control device when the output regulates the system input. When accounting for physiological regulatory devices, in addition to the internal architecture of the living device, i.e. sensor, transducer and, actuator modules, its close-loop execution must be considered as the fourth module. In **chapter 4**, we have explored the ability of multicellular devices to respond to different glucose levels in an analogue-mode by secreting insulin or glucagon, mimicking the physiology of glucose regulation and the use of these cellular devices has been hypothesized for treating Diabetes Mellitus. Physiological glucose levels in healthy subjects are comprised between 140 mg/dL and 60 mg/dL [Association, 2010], which correspond to the normoglycaemia state. Unbalanced glucose levels are defined either being above or below normoglycaemia, i.e. hyperglycaemia or hypoglycaemia. Although there are numerous glucose disruptors, in particular, food intake, physical exercise or other factors such as stress, sleep or hormones, pancreatic cells act as a sensor detecting abnormal blood glucose states and secreting the glucose-balancers hormones insulin and glucagon. Insulin acts diminishing blood glucose levels by promoting glucose cellular uptake, contrarily glucagon acts stimulating glucose release [Nussey S, 2001]. Diabetes mellitus is a disorder caused by unbalanced blood glucose levels due to defects in insulin secretion or loss of insulin sensibility [Association, 2010]. Diabetes mellitus therapies rely on the external administration of insulin hormone and the proper control of food ingestion for balancing blood glucose levels. Besides, being insulin therapy the major treatment it has a major impact on diabetes mellitus patients' quality of life. Research lines endeavours β -cell islet transplantation or stem-cells regeneration [Bouwens et al., 2013; Robertson, 2010; Fan Zhang & Tzanakakis, 2019] or the possibility of controlling the patient's immune system to stop the destruction of pancreatic islets [Actobiotics, 2020; Lichtman et al., 2012], but accomplishing very little success.

Noticeable is the impact of technologies on palliative treatments. Figure 5.1 summarizes the advances done in the field of diabetes management. From the very first insulin syringes and insulin pump (1960s) to the actual technologies seeking an electro-mechanic artificial pancreas.

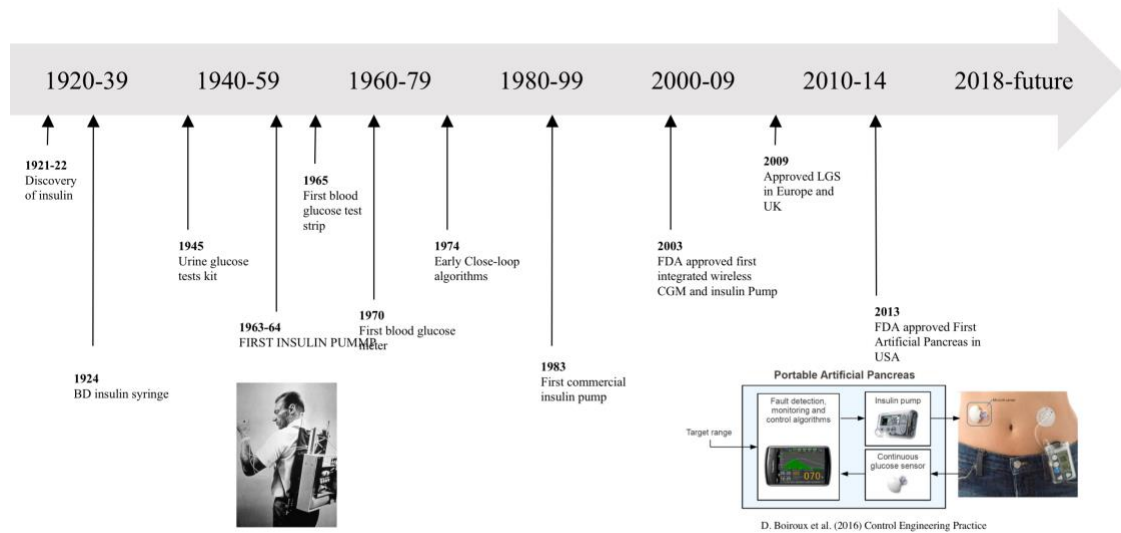


Figure 5.1 Historical evolution of diabetes management milestones. Adapted from [Shah et al., 2014].

The very first discovery of insulin hormone at the beginnings of 1990s together with the first blood glucose detectors launched important advances. Despite numerous technological advances, diabetic patients' daily life is still based on monitoring glucose levels and having a fine-tune control of insulin injection. The insulin pump has clear advantages by the accurate delivery of insulin without the need for injections and had also revealed benefits on glucose physiology. However, episodes of severe low blood glucose levels [Kalra et al., 2013] are still a major drawback [Karges et al., 2017]. Efforts are devoted to the creation of autonomous regulation of blood glucose levels. As a result, different strategies seek the development of an artificial device accounting for automated insulin secretion. Among all, the electromechanical Artificial Pancreas (AP) is leading the research area. An AP is composed of a continuous glucose monitor device, a computer algorithm predicting the amount of insulin needed to restore normoglycaemia and a pump to inject insulin into the bloodstream. Up to now the FDA has approved the very first electromechanical device fully envisioned to act as an artificial pancreas [MiniMed 670G System], however, it still relies upon user assessment on insulin delivery.

Nevertheless, a very recent clinical trial incorporating a fully closed-loop algorithm [S. A. Brown et al., 2019] achieved a 6-month glucose regulation in 112 type 1 diabetes mellitus patients with no serious hypoglycaemic events. Despite the numerous advantages arising from the AP, the invasiveness of the device (Figure 5.1) accounts for a negative impact on patients' life. Patients are concerned about the associated problems of wearing and carrying the device components as well as the patient-device interaction through catheters. To tackle this need, strategies based on drug delivery or non-invasiveness artificial pancreas have been broadly explored based on the use of nanoparticles or using synthetic biology approaches. In general, any glucose-stimulated insulin delivery system, mimicking β -cells behaviour, should be addressed to ensure an automated closed-loop regulation, i.e. without patient supervision, based on i) constant glucose monitoring and ii) drug administration, altogether acting in an intelligent closed-loop fashion.

In this context, interesting strategies within the field of nanoparticles, i.e. solid particles in the size of nanometres, are based on glucose-responsive materials such as glucose oxidase nanoparticles [Duan et al., 2018; Zhao et al., 2016], Concanavalin A protein [Bauri et al., 2018; Yin et al., 2011] or Phenylboronic acid (PBA) allowing to obtain glucose-sensitive particles due to their versatile chemical structures [Zhao et al., 2013]. Specifically, insulin was quickly released from nanoparticles as the glucose concentration increased due to conformational changes in the nanoparticle structure. Furthermore, it is worth mentioning an intelligent delivery system based on a micron needles patch was designed to release insulin in response to the hypoxic microenvironment in a hyperglycaemic state [Yu et al., 2015]. Despite showing very promising results, hypoxia is a secondary effect from hyperglycaemic state and may occur in non-hyperglycaemic scenarios. More sophisticated glucose-regulated insulin device was accomplished by synthesized artificial pancreatic β -cells (A β Cs) [Z. Chen et al., 2018] by a combination of inner small liposomal vesicles (ISVs) and outer large vesicle (OLV). Insulin was incorporated in ISVs mimicking the storage granules inside β -cells and under hypoglycaemic conditions ISVs fuses OLV triggering insulin exocytosis. All in all, nanoparticles strategies account for a rapid release of insulin when high blood glucose scenarios are faced, but with a limited insulin cargo.

Synthetic biology and more specifically the field of biosensors envisioned glucose homeostasis restoration by engineering eukaryotic cells, with the ability to *in situ* produce and secrete glucose-regulator factors. The field has envisioned either the use of engineered patients' cells [Jaén et al., 2017] or laboratory workhorse eukaryotic cells [Shao et al., 2017; Xie et al., 2016; Ye et al., 2011]. The very first attempt of genetic engineering applied to diabetic dogs accomplished a long-term efficacy, i.e. up to 8 years, glycaemia regulation. In this case, a glucokinase protein was constitutively expressed in skeletal muscle cells [Jaén et al., 2017]. Else ways, allotransplantation of genetically engineered eukaryotic cells, encapsulated in alginate beads and implanted in mice either intraperitoneal or subcutaneously, allowed glycaemia regulation. Effectiveness of alginate beads microencapsulation has been demonstrated upon a variety of different input-signals triggering drug response [Bojar et al., 2018; Shao et al., 2017; Ye et al., 2011] or by inducing different glucose-modulators, such as glucagon-like peptide-1 [Bojar et al., 2018; Shao et al., 2017; Ye et al., 2011].

Despite the enormous achievements in glycaemia restoration, in general, most existing synthetic biology approaches rely on the genetic transcriptional control of insulin delivery and accordingly demand for larger periods for glycaemia regulation. Most of the generated cellular devices operated in isolation without any interference with the desired application or are programmed responding to external input signals, therefore not properly responding to the demanded signals, i.e. glucose concentrations, putting in evidence the difficulty of the strategy. Hence, we claim that developing a platform enabling the design and test of glucose-regulated insulin production devices in a closed-loop environment would allow adapting living device performance upon physiological needs. The medical application demands for an analogue protein expression dynamic with high precision and predictable logic in response to external glucose signals. Therefore, devices should offer a fast temporal dynamic emulating the physiological glucose homeostasis. These types of devices could potentially be applied for glucose homeostasis maintenance in diabetic patients. Indeed, the secretion of these pancreatic hormones is governed by pulsatile dynamics [Nan-Kuang Yau & Liang-Wey Chang, 1995; Polonsky et al., 1988; S. H. Song et al., 2002] and the development of synthetic devices able to mimic this natural behaviour is still a challenge.

5.2 Objectives

We aim to explore *in silico* strategies for glycaemia regulation in Type 1 diabetic patients using a glucose-insulin simulator.

The *specific objectives* addressed in this chapter are:

- Characterize the ability of implanting engineered cellular devices to regulate glycaemia in diabetic organisms.
- Design *in silico* new strategies for glycaemia regulation based of feed-restriction patterns.
- Combine implanted cellular devices with feed-restriction patterns.

5.3 The virtual organism: Glucose insulin meal simulator

An *in silico* description of glucose and insulin metabolism would serve as the platform to test novel strategies for glycaemia regulation: the virtual organism. In this context, the mathematical model developed by Dalla Man *et al.* [Dalla Man et al., 2007], based on the acquisition of data from experiments involving NMR or PET technologies concerning glucose and insulin metabolism, describes the dynamics of glucose and insulin fluxes upon meal ingestion. As a result, the *in silico* description of glucose plasma concentration of healthy subjects was obtained (Figure 5.2). The description of the glucose and insulin fluxes for a Type 1 diabetic patients is described in the UVA/PADOVA Type 1 Diabetes Simulator S2008 [Kovatchev et al., 2009], where β -cell insulin secretion from Dalla Man *et al.* has been removed and replaced by an external insulin supply (the red module in Figure 5.2). To describe this process, a subcutaneous insulin infusion module should be considered. It is worth mentioning that in S2013 [Dalla Man et al., 2014] glucagon kinetics secretion and action models have been incorporated into the simulator.

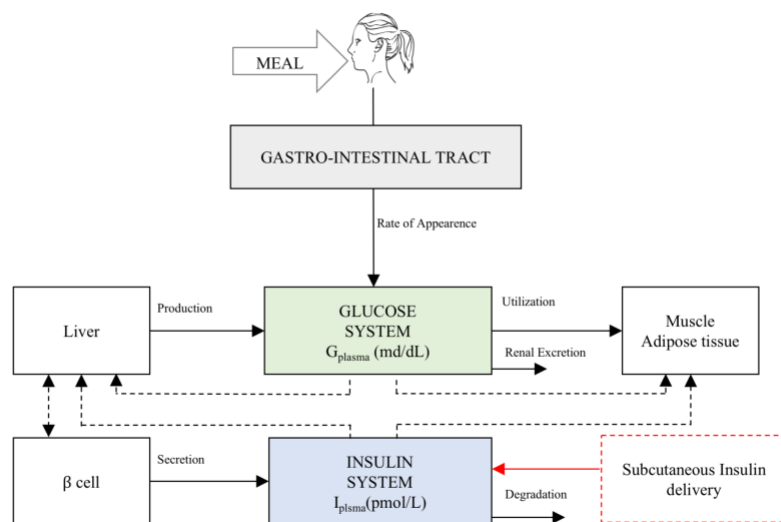


Figure 5.2 Schematically representation of the Glucose-insulin meal simulator. The mathematical model developed in [Dalla Man et al., 2007] contemplates the measured glucose and insulin plasma concentrations, i.e. Glucose G and Insulin I , and the glucose fluxes, i.e. Glucose rate of appearance, Glucose production, Glucose utilization, Glucose renal excretion and Insulin secretion and degradation. The red-dashed box replaces the β -cell compartment accounting for insulin secretion in T1DM patients. Adapted from [Dalla Man et al., 2007] and [Kovatchev et al., 2009].

The model described in Dalla Man *et al.* [Dalla Man et al., 2007] considers the glucose and insulin plasma concentrations as well as the different fluxes of glucose. More specifically, the glucose subsystem is composed by a two-compartment model, concerning the glucose uptake, i.e. diminish of glucose concentration, and the glucose creation, i.e. increase of glucose concentration, by the main organs involved in glucose and insulin metabolism tissues and organs. On the other hand, the insulin subsystem also consists of a two-compartment model, the first representing the liver and the second the plasma.

From the above-mentioned glucose subsystem, the most important parameters are the endogenous glucose production, glucose rate of appearance and glucose utilization. *Endogenous glucose production* in the liver represents the breakdown of glycogen when the blood glucose levels are low and is assumed to be linearly dependent on glucose concentration, portal insulin concentration and a delayed insulin signal. *Glucose rate of appearance* accounts for the glucose absorbed in the intestinal tract after meal ingestion. Intestinal absorption describes the transit through the stomach, represented as a two-compartment model accounting for solid and triturated phases [Hellström et al., 2006]. In this system, glucose is moved to the gut and distributed in plasma as the flux of rate of appearance. Plasma glucose can decrease due to *renal excretion* or *glucose utilization*. Insulin-independent utilization occurs in the brain and erythrocytes and is assumed constant, whereas insulin-dependent utilization follows a Michaelis-Menten kinetics in muscles and adipose tissues [Yki-Jarvinen et al., 1987]. In the *in silico* health subject, *β -cell insulin secretion* is described by static and dynamic components. The dynamic component likely represents the release of promptly releasable insulin and is proportional to the rate of increase of glucose concentration through a parameter called dynamic β -cell responsivity.

5.4 Experimental construction and characterization of cellular devices for insulin production

Within the context of the project “Encapsulated Synthetic Cellular Circuits to Restore Glycaemic Control in Type 1 Diabetes” from *Fundació La Marató de TV3*, cellular

implants able to produce insulin were experimentally built and characterized *in vitro* [Canadell, D *et al*, *unpublished data*] by the *Cell Signalling Group* headed by Dr. Francesc Posas (IRB). Experimental results allowed for a realistic mathematical description of insulin production devices. This section describes the experimental construction, characterization and mathematical modelling of engineered eukaryotic cells with the ability to produce insulin in the presence of extracellular glucose to be further *in silico* analysed in the T1DM patient. Figure 5.3 summarizes the procedure enclosed in this chapter.

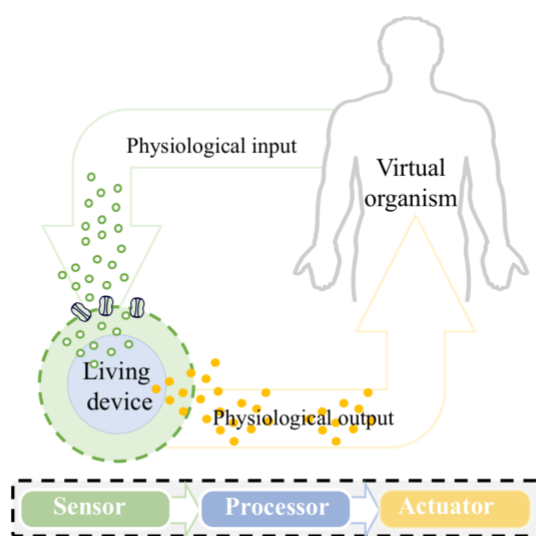


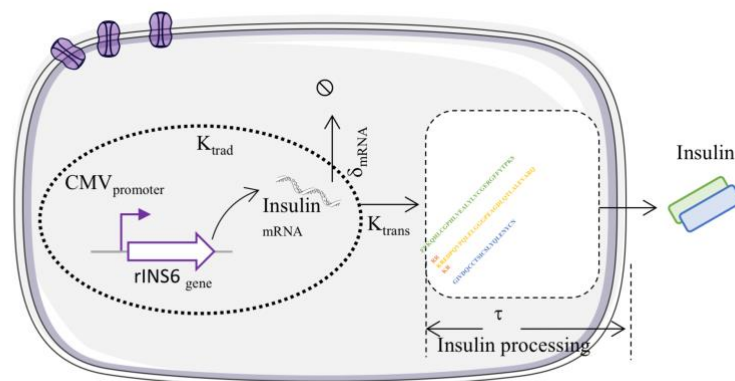
Figure 5.3 Schematically representation of a cellular device implanted in the organism simulator. Cellular device parts are represented in a coloured legend. A physiological input, e.g. glucose, is sensed by the sensor module (green). After some internal processes done by the processor module (blue) a physiological output is secreted by the actuator module (yellow). Particularly in the presented approach the secreted output molecule, i.e. insulin, directly regulates the concentration of the device input, i.e. glucose, behaving as a closed-loop system.

Cellular devices were engineered in HEK293T cell type with the ability to produce insulin following two different approaches for insulin gene regulation. The first strategy consists of a constitutive expression of the insulin gene downstream the CMV promoter, a widely used constitutive promoter for mammalian cells [Foecking & Hofstetter, 1986]. The second strategy comprises the glucose-dependent expression of insulin regulated by the Thioredoxin interacting protein promoter (TXNIP) [Kanari *et al.*, 2013].

To produce a fully functional insulin hormone, a modified version of insulin, rINS6 [Hay & Docherty, 2003], was used due to the inability of HEK293T cells to process human insulin because the endopeptidases PC₂ and PC_{3/1} responsible of C-peptide cleavage are only present in endocrine cells [M. Weiss et al., 2000]. rINS6 is a Rat1-furin insulin version in which endopeptidases sites flanking C-peptide in proinsulin DNA sequence were engineered to be further recognized by furin protease. Furin protease is ubiquitously expressed in HEK293T cells. In order to test insulin functionality, an insulin action test was performed. An Akt phosphorylation assay [M. Lu et al., 2012] demonstrated that insulin was fully functional. To characterize the dynamics of the different analysed promoters a multicistronic vector was build containing the desired promoter upstream of the secreted embryonic alkaline phosphatase (SEAP), acting as a reporter, together with the modified furin-insulin. SEAP is a widely used reporter in the study of promoter activity or gene. HEK293T were transfected and obtained stable cell lines trough Sleeping beauty transposon system [Mátés et al., 2009].

As a result, two engineered HEK293T cell lines were obtained able to produce insulin either constitutively or in a glucose-dependent manner. Figure 5.4 shows a schematic representation of the two genetically engineered cell lines.

a



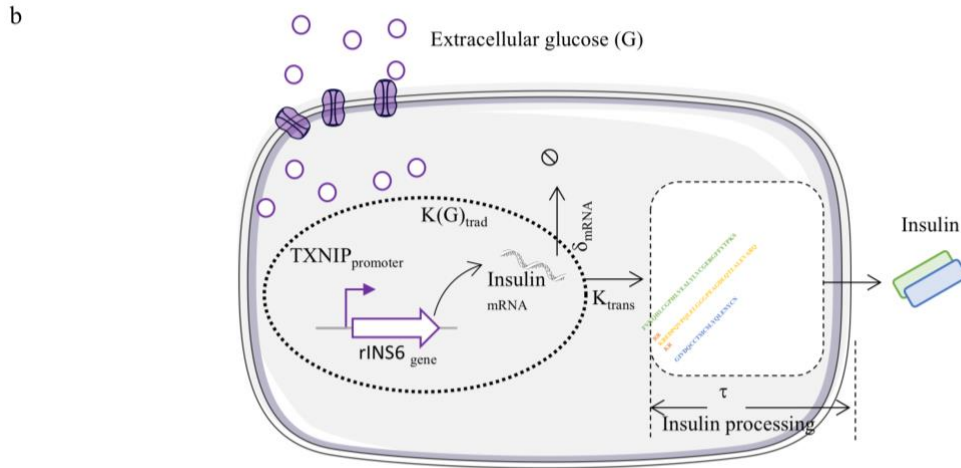


Figure 5.4 Schematically representation of insulin expression living devices. a) Engineered cell constitutively expressing insulin. The expression of the insulin gene (rIns6) is triggered by the constitutive CMV promoter. The rIns6 mRNA is transcribed with a rate variable K_{trad} and degraded at a rate ∂_{mRNA} . The mRNA is translated into the pre-pro-insulin protein with a rate K_{trans} , which is finally processed by the C-peptide cleavage to be finally secreted. **b)** Engineered cell production insulin in a glucose-dependent manner. The expression of the insulin gene (rIns6) is triggered by the glucose-regulated TXNIP promoter. The rIns6 mRNA is transcribed with a rate variable K_{trad} and degraded at a rate ∂_{mRNA} . The mRNA is translated into the pre-pro-insulin protein with a rate K_{trans} , which is finally processed by the C-peptide cleavage to be finally secreted.

A mathematical model describing the secretion of insulin was developed representing the processes described Figure 5.4a for the constitutive expression of insulin and in Figure 5.4b for the glucose-regulated insulin expression. Our models have been formulated as a set of Ordinary Differential Equations (ODEs).

Secretion dynamics can be described by the following equations:

The insulin mRNA production is described as:

$$\frac{dmRNA}{dt} = K_{trad} - \partial_{mRNA} \cdot mRNA(t) \quad \text{Eq. 5.1}$$

Where K_{trad} is the transcription rate and ∂_{mRNA} represents the degradation rate of $mRNA$. For constitutive cells, the ratio of $mRNA$ synthesis is described by the parameter K_{trad}

which is assumed constant. On the opposite, the activity of glucose-dependent promoter TXNIP, $K_{trad}(G)$, is described according to:

$$K_{trad}(G) = \gamma \cdot \frac{Glucose^n}{K_{0.5} + Glucose^n} \quad \text{Eq. 5.2}$$

The insulin secretion rate $\frac{dInsulin}{dt} = u(t)$ is described according:

$$u(t) = K_{trans} \cdot mRNA(t - \tau_{ins}) \cdot N \quad \text{Eq. 5.3}$$

Where K_{trans} is the insulin translation rate, τ_{ins} is the insulin processing time N the number of cells.

5.4.1 Glucose-promoter regulation

In order to characterize the response of the TXNIP promoter SEAP gene was placed under the TXNIP regulatory promoter, in tandem with rINS6. SEAP acts as a secretable reporter [Yang et al., 1997] and allows for a rapid and cheap quantification using a chemiluminescence SEAP Reporter Gene Assay Kit.

Glucose-dependent cells were grown during 16 h at 36 mg/dL of glucose. Then, cell cultures were shifted to media with different glucose concentrations, i.e. 36 mg/dL, 90 mg/dL, 200 mg/dL and 450 mg/dL. SEAP activity was measured at several time points for 9 hours, and experimental data is shown in Figure 5.5a. Figure 5.5b shows the relationship between SEAP levels and the different glucose concentrations corresponding to the kinetic time point = 8 hours. The dependence between SEAP levels and glucose concentrations was fitted to the Hill equation Eq. 5.4.

$$SEAP(G) = \gamma \cdot \frac{Glucose^n}{K_{0.5} + Glucose^n} \quad \text{Eq. 5.4}$$

Here γ corresponds to the relative dynamic range, n the Hill coefficient and $K_{0.5}$ is the concentration of external glucose that gives the half-maximal response. From that, *Matlab R2016a* least-squares analysis software was used for fitting the parameters to the Hill expression. Fitted parameters are $\gamma = 1.95 \cdot 10^{-6}$ 1/hours, $K_{0.5} = 104$ mg/dL and $n = 2$.

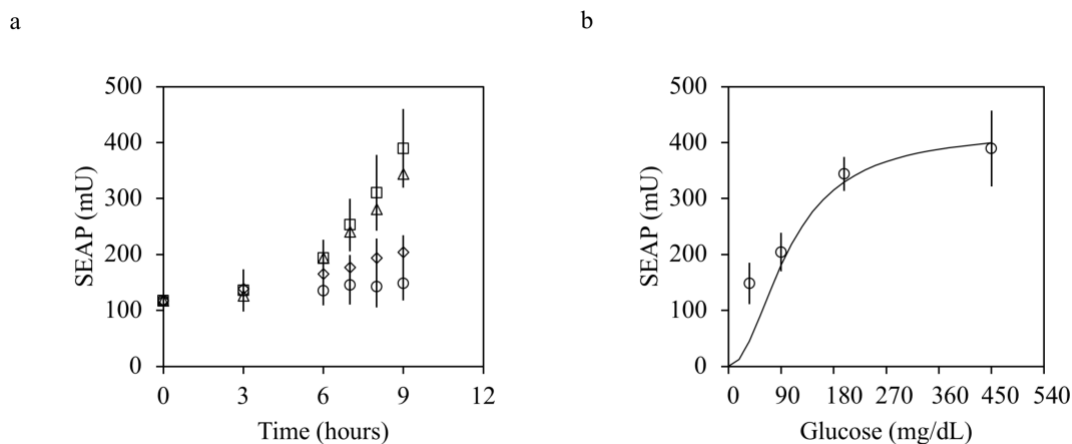


Figure 5.5 Glucose-dependent SEAP expression of TXNIP-rINS6-SEAP cells. **a)** Glucose-dependent kinetics at different glucose concentrations. Cell cultures were shifted from 36 mg/dL glucose to media containing 36 mg/dL, 90 mg/dL, 200 mg/dL and 450 mg/dL glucose. SEAP activity was measured at several time points for 9 h. SEAP activity was measured using a reporter gene assay kit. Squares: 450 mg/dL, triangles: 200 mg/dL, rhombus 90 mg/dL and circles 36 mg/dL. The error bars correspond to the standard deviation of three independent experiments. **b)** Relationship between SEAP and glucose concentrations after 8 h of induction. SEAP activity at time point $t = 8$ h was plotted according to each specific glucose media. White dots represent experimental values and the error bars correspond to the standard deviation of three independent experiments. The solid line corresponds to the fitted Eq. 5.4 using *Matlab R2016a* least-squares analysis software with a correlation coefficient $R^2 = 0.98$.

5.4.2 mRNA degradation rate

To experimentally measure the insulin mRNA degradation rate, Real Time RT-PCR was performed in glucose-dependent insulin producer cells and ΔC_t method [Kozera & Rapacz, 2013] allowed to calculate mRNA fold-change. Therefore, two different experimental setups were performed. Firstly, cells were grown during 16 h at 36 mg/dL glucose and then shifted to 450 mg/dL glucose (Figure 5.6a). In the second experiment, cells grow for 16 hours at 450 mg/dL glucose and then shifted to 36 mg/dL glucose (Figure 5.6b). From both experiments, cellular extracts were taken every 3 hours and

mRNA fold change was calculated. A degradation rate of $\delta_{mRNA} = 0.4$ 1/hours was determined from experimental data.

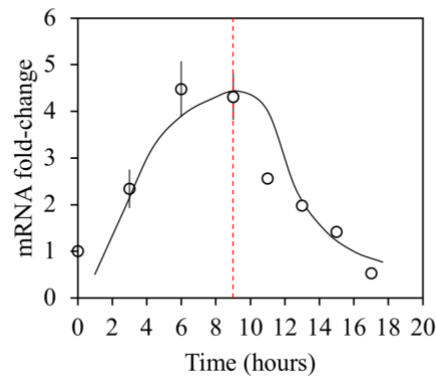


Figure 5.6 rINS6 mRNA dynamics measured with Real Time RT-PCR. Glucose-dependent insulin producer cells were shifted from a low glucose media of 36 mg/dL to a high glucose media of 450 mg/dL for 9 h. The red dashed line indicates the time point glucose was shifted from 450 mg/dL to of 36 mg/dL back again. Cellular extracts were taken every 3 hours to extract RNA and analyse the fold change of mRNA using Real Time RT-PCR. White dots represent experimental values and the error bars correspond to the standard deviation of three independent experiments. Solid line corresponds to the fitted Eq. 5.1 using *Matlab R2016a* least-squares analysis software with a correlation coefficient $R^2 = 0.92$.

5.4.3 Insulin translation rate and Insulin processing delay

Insulin translation rate was obtained from [Tang & Sambanis, 2003]. To determine the insulin secretion rate, i.e. μ_{ins} , in the glucose-dependent insulin producer cell, cellular culture was grown at 36 mg/dL glucose for 12 hours, afterwards the media was changed to high glucose concentration, i.e. 450 mg/dL, and maintained during 12h more. Insulin levels were measured every 4h using a mouse insulin ELISA KIT [Mercoxia Insulin ELISA]. Figure 5.7a shows the experimental levels of insulin. The same experiment was carried with the constitutive insulin secretion cells. (Figure 5.7b). It is worth mentioning that glucose-dependent insulin producer cells exhibit a significant delay before insulin accumulation that is not observed in constitutive cells. We hypothesized that this delay is due to the processing time required for insulin transcription, translation, processing and secretion once the glucose-dependent promoter has been activated at high glucose levels.

From this data it was possible to estimate the insulin processing delay, which is $\tau_{ins} = 4.5$ hours.

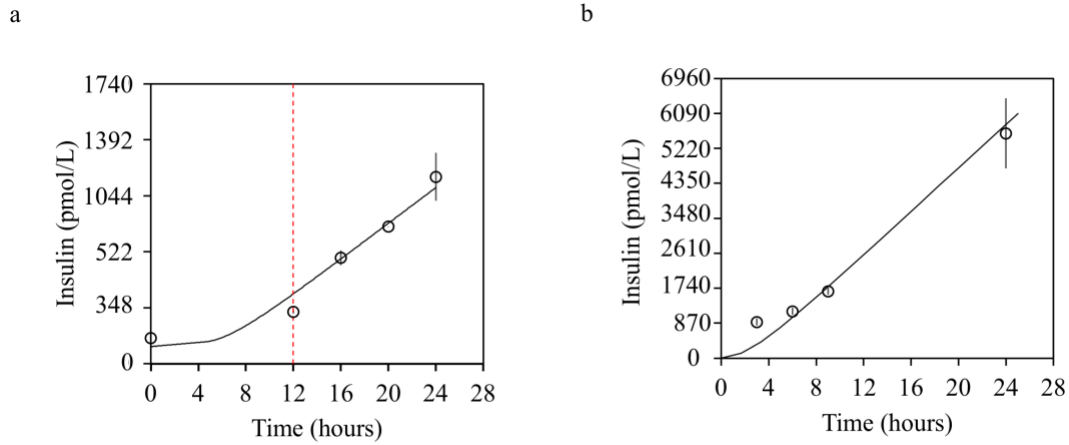


Figure 5.7 Insulin expression profiles for CMVp-rINS6 and TXNIPp-rINS6 cells. a) Accumulated insulin for the glucose-dependent insulin producer cells. Cells were grown in low glucose media, i.e. 36 mg/dL, during 12 h and shifted to a high glucose scenario, i.e. 450 mg/dL, during 12 h more. Accumulated insulin levels were measured by taking the supernatant every 4 h using a mouse insulin ELISA KIT. White dots represent experimental values and the error bars correspond to the standard deviation of three independent experiments. The solid line corresponds to fitted Eq. 5.3 using *Matlab R2016a* least-squares analysis software with a correlation coefficient $R^2 = 0.97$. **b)** Accumulated insulin for the constitutive producer cells. Cells were grown during 24 h and accumulated insulin levels were measured by taking the supernatant every 4 h using a mouse insulin ELISA KIT. White dots represent experimental values and the error bars correspond to the standard deviation of three independent experiments. The solid line corresponds to fitted Eq. 5.3 using *Matlab R2016a* least-squares analysis software with a correlation coefficient $R^2 = 0.99$.

Table 5.1 summarizes model parameters for both constitutive and glucose-dependent insulin producer cells. Using these parameters and Eq. 5.1 and Eq. 5.3 it is possible to theoretical describe the experimental results and predict insulin dynamics in the *in silico* virtual patient.

Process	Parameter	CMV	TXNIP	Units
Transcription rate	K_{trad}	$4.608 \cdot 10^{-5}$	$\gamma = 1.95 \cdot 10^{-6}$ $K_{0.5} = 104$ $n=2$	1/hours mg/dL
mRNA degradation	$\hat{\sigma}_{mRNA}$		0.4	1/hours
Translation rate	K_{trans}		0.9	1/hours
Insulin processing delay	τ_{ins}		4.5	hours
Insulin production rate	μ_{ins}	$1.74 \cdot 10^{-4}$	$3.13 \cdot 10^{-5}$	pmol/ L·cell·hour

Table 5.1 Model parameters. Equations Eq. 5.1, Eq. 5.2 and were fitted to experimental values to obtain the parameters describing insulin secretion dynamics for both the constitutive and glucose-dependent cellular devices.

5.5 3D space definition for Diabetes Mellitus diagnosis criteria

To measure implant efficiency for glycaemia regulation in the *in silico* T1DM patients it is necessary to define a diagnostic criterion. The World Health Organisation (WHO) has established different key indicators for Diabetes Mellitus diagnosis [Association, 2010; Kalra et al., 2013] summarized in Table 5.2.

	Diabetic Criteria (WHO)
Fasting glycaemia test (<i>FT</i>): Hyperglycaemia	≥ 126 (mg/dL)
Oral glucose tolerance test (<i>OGTT</i>): Hyperglycaemia	After 2 hours ≥ 200 (mg/dL)
Random glucose test (<i>RT</i>): Hyperglycaemia	>140 (mg/dL)
Random glucose test (<i>RT</i>): Hypoglycaemia	< 60 (mg/dL)

Table 5.2 Glucose test for T1DM diagnosis. Extracted from World Health Organisation.

Fasting Glycaemia Tests consists on measuring plasma glucose levels after 8 hours of food and drink starvation, whereas the Oral Glucose Tolerance Test consists on the administration of a high glucose dose (75g) and measure plasma glucose levels after 2 hours. Furthermore, highest and lowest plasma glucose values were measured after the

Oral Glucose Tolerance Test to assess for the hyper and hypoglycaemic scenarios., i.e. Random Glucose Test.

In order to assess the effects of different cellular implants in the *in silico* T1DM patient, we have established a novel measurement integrating the criteria summarized in Table 5.2. A 3-dimensional space is settled considering the Fasting Glycaemia Test (*FT*), the Oral Glucose Tolerance Test (*OGTT*) and Random Glucose Test (*RT*).

$$P(FT, OGGT, RT) \in \mathbb{R}^3 \quad \text{Eq. 5.5}$$

Within this 3D space, we have defined a sub-region that simultaneously fulfil the criteria of Table 5.2. The sub-region defines the normoglycaemia scenario, which is entitled *Health Glucose Behaviour Region*. Its Cartesian Coordinates defining the *xyz*-volume are defined by Eq. 5.6.

$$\text{Health Glucose Behaviour Region } (x, y, z) = \begin{cases} OGGT & 60 \leq x \leq 200 \\ FT & 60 \leq y \leq 126 \\ RT & 60 \leq z \leq 140 \end{cases} \quad \text{Eq. 5.6}$$

The analysis of the implanted cellular devices' is accomplished by calculating plasma glucose levels for *FT*, *OGGT* and *RT*. The ability to regulate glycaemia by the implanted cells is quantified by the Glycaemia Restoration Index, considering the distance between the values of *OGTT*, *FT* and *RT* and the *Health Glucose Behaviour Region*. As a matter of exemplification, Figure 5.8 shows three different T1DM virtual patients with three different implants. Virtual patient₁ and virtual patient₃ coordinates lie outside the *Health Glucose Behaviour Region* whether coordinates for the virtual patient₂ are within the defined region, meaning that the implant for the virtual patient₂ restores normoglycaemia. Notice that virtual patient₃ is above the hypoglycaemia limits for the Random Glucose Test. Hypoglycaemia scenarios must be prevented because of the severe death risk associated with hypoglycaemic episodes [Kalra et al., 2013]. Therefore, the Glycaemia Restoration Index must contain how far is the virtual patient from the *Health Glucose Behaviour Region* and if any of the coordinates is below any defined hypoglycaemia threshold from Table 5.2.

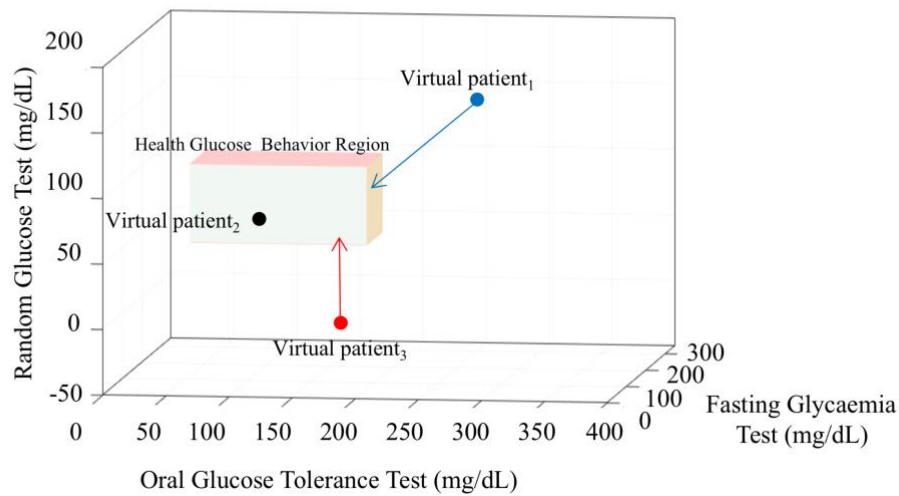


Figure 5.8 3D space for Fasting Glycaemia Test, Oral glucose Tolerance Test and Random Glucose Test. Coloured cuboid, from Eq. 5.6, represents the *Health glucose behaviour region*. The blue, red and black dot coordinates are defined by the values of *FT* and *OGTT* and *RT* resulting from the computational simulation of different implants in a virtual diabetic patient. The arrows represent the distance between the patient glycaemia and the *Health Glucose Behaviour Region*.

The Glycaemia Restoration Index (GRI) is a novel metric defining the ability of cellular implants to restore normoglycaemia in the *in silico* T1DM patients considering: i) the distance between the T1DM to the *Health Glucose Behaviour Region* and ii) the relative positional information with respect the *Health Glucose Behaviour Region*. Therefore, allowing to discriminate between the different devices' performances seen in Figure 5.8. To do so, we must compute the minimal Euclidean distance between the 3D point and all the faces of the *Health Glucose Behaviour Region*. The 3D cuboid is defined by 3 planes: *xy*-plane is shown in Figure 5.9a, the *yz*-plane in Figure 5.9b and the *zx*-plane in Figure 5.9c. Each plane consists of two faces, one for the upper limit values, i.e. positive, and the other for the lower limit values, i.e. negative.

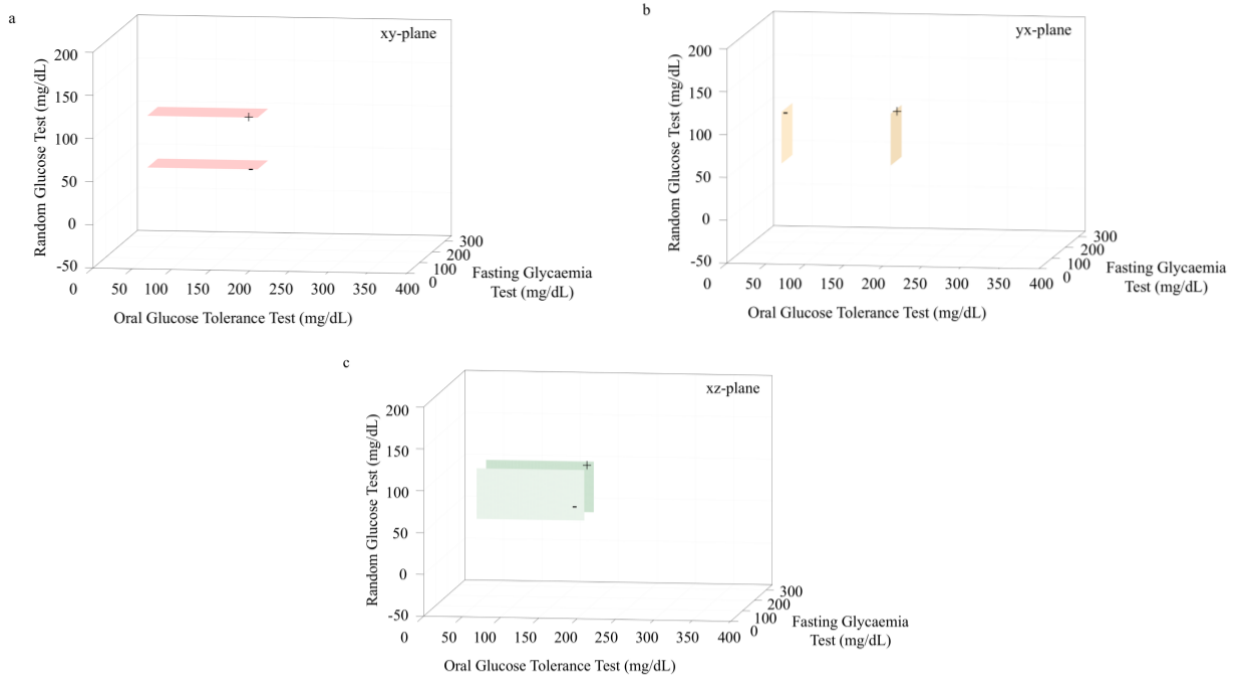


Figure 5.9 3D space for Fasting Glycaemia Test, Oral glucose Tolerance Test and Random glucose Test. **a)** *xy*-plane with positive face corresponding to the upper limit of Fasting Glycaemia and Oral Glucose Tolerance Test from Eq. 5.6. and negative face corresponding to the lower limit of Fasting Glycaemia Test and Oral Glucose Tolerance Test from Eq. 5.6. **b)** *yz*-plane with positive face corresponding to the upper limit of Random Glucose Test and Oral Glucose Tolerance Test from Eq. 5.6. and negative face corresponding to the lower limit of Random Glucose Test and Oral Glucose Tolerance Test from Eq. 5.6. **c)** *xz*-plane with positive face corresponding to the upper limit of Random Glucose Test and Fasting Glycaemia from Eq. 5.6. and negative face corresponding to the lower limit of Random Glucose Test Fasting Glycaemia from Eq. 5.6.

For all three planes we must compute the distance between the virtual patient 3D point and the positive and negative faces according to:

$$D_{ij}^{\pm} = n_{ij}^{\pm} \otimes (p_0^{\pm} - p) \quad \text{Eq. 5.7}$$

for $ij = xy, yz$ and zx -plane

Where n_{ij}^{\pm} is the normal vector of the plane ij , p_0^{\pm} is a plane point and p stand for the 3D coordinates of each T1DM. However, for each plane, three different scenarios are found when analysing the relative position of the virtual patient. Particularly, Figure 5.10,

graphically shows the three possible scenarios for the xy -plane. In Figure 5.10a the virtual patient (p) is above xy^+ and xy^- because the Euclidean distance to the positive plane is the smallest whereas in Figure 5.10b the point p is below xy^+ and xy^- faces because the Euclidean distance to the negative plane is, in this case, the smallest. Remarkably in Figure 5.10c the point p is between xy^+ and xy^- faces because both Euclidean distances are smaller than the distance between the two faces.

Thus, computing the distances to the positive and negative faces for each plane allow us to obtain the positional information and define the minimum distance between the 3D coordinate point and the faces of the cuboid according to:

$$\begin{aligned}
 D_{ij} &= D_{ij}^+ && \text{if } D_{ij}^+ < D_{ij}^- \\
 D_{ij} &= D_{ij}^- && \text{if } D_{ij}^+ > D_{ij}^- \\
 D_{ij} &= 0 && \text{if } D_{ij}^+ < d_{<+,->} < D_{ij}^-
 \end{aligned}
 \tag{Eq. 5.8}$$

for $ij=xy, yz$ and zx -plane

The informational position for each plane allows to compute the GRI as the minimum average distance of the three different planes according to:

$$GRI = \begin{cases} +\frac{1}{3} \cdot (D_{xy} + D_{yz} + D_{xz}) & \text{if } D_{ij}^- > D_{ij}^+ \\ -\frac{1}{3} \cdot (D_{xy} + D_{yz} + D_{xz}) & \text{if } D_{ij}^- < D_{ij}^+ \end{cases}
 \tag{Eq. 5.9}$$

for $ij=xy, yz$ and zx -plane

Where D_{xy} , D_{yz} and D_{xz} are computed according to Eq. 5.7 and Eq. 5.8. The negative term accounts for glycaemia values below the defined hypoglycaemia threshold and corresponds to the scenario where $D_{ij}^- < D_{ij}^+$. Remarkably, for the virtual patient₁ in Figure 5.10d the $GRI > 0$, for virtual patient₂ the $GRI < 0$ and for virtual patient₃ = 0.

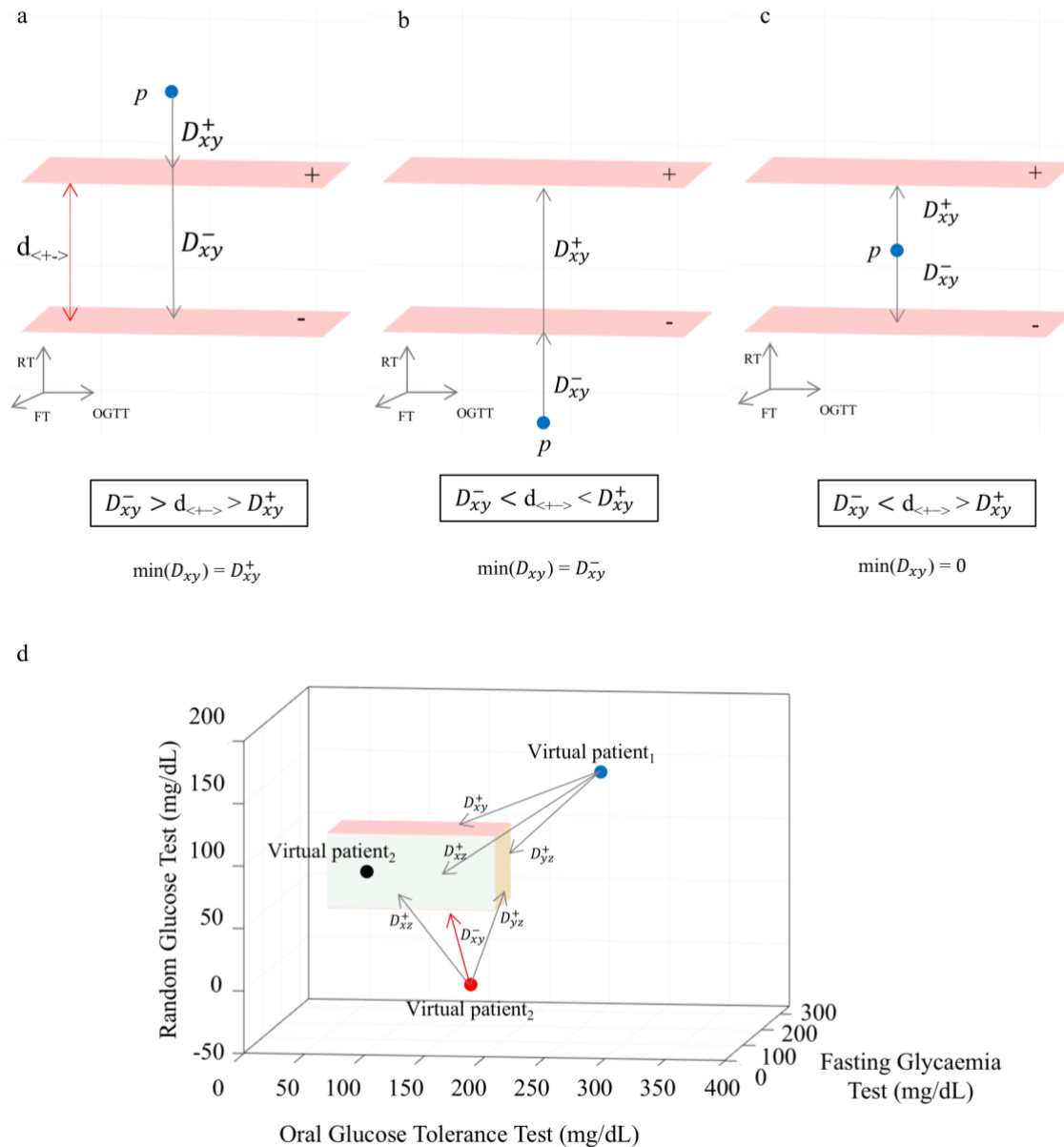


Figure 5.10 3D space for xy -plane and virtual patient p . xy -plane with positive face corresponding to the upper limit of Fasting Glycaemia and Oral Glucose Tolerance Test from Eq. 5.6. and negative face corresponding to the lower limit of Fasting glycaemia test and Oral Glucose Tolerance Test from Eq. 5.6. The blue dot corresponds to the 3D for the virtual patient. D_{xy}^+ corresponds to the Euclidean distance between the point p and the positive face computed with Eq. 5.7 and D_{xy}^- corresponds to the Euclidean distance between the point p and the negative face computed with Eq. 5.7. $d_{<+,->}$ corresponds to the Euclidian distance between the two faces, i.e. positive and negative. **a)** Scenario where the point p is below the positive face with $D_{xy}^+ < D_{xy}^-$ **b)** Scenario where the point p is above the positive face with $D_{xy}^+ > D_{xy}^-$ **c)** Scenario where the point p is between the two faces. **d)** 3D space for Fasting Glycaemia Test, Oral glucose

Tolerance Test and Random Glucose Test. Coloured cuboid, from Eq. 5.6, represents the *Health glucose behaviour region*. The blue, red and black dot coordinates are defined by the values of *FT* and OGTT and *RT* resulting from the computational simulation of a given implant in a virtual diabetic patient. The arrows represent the distance between the patient glycaemia and the *Health glucose behaviour region*. The red arrow indicates that the virtual patient₂ is below the negative face in the *xy*-plane.

5.6 *In silico* analysis of cellular implants in T1DM patients

In this section, we focus on the feasibility of implanting the engineered insulin producer cells in the *in silico* T1DM patient. Enclosed in the project “Encapsulated Synthetic Cellular Circuits to Restore Glycemic Control in Type 1 Diabetes” engineered insulin producer cells follow an encapsulation process to be further subcutaneously implanted in diabetic mice models. Cellular encapsulation is done by means of alginate microcapsules [Ye et al., 2011; Ausländer et al., 2014; Xie et al., 2016]. Cell viability analysis was performed in order to determine the biomaterials, capsule design, size and cell density. Encapsulation procedure and analysis was carried by the group of *Biomaterials and Nanomedicine* in UPV-EHU [*unpublished data*]. Experiments reveal that the optimal conditions enabling a 40 days’ performance of the engineered cells upon extracellular glucose detection and insulin secretion is a bead embodiment made of Alginate-poly-(l-lysine)-alginate with <400-500> μm radius and a cellular density of a $\varphi = 5 \cdot 10^6$ cell/mL.

To that end, we have modified the model of Dalla Man *et al.* [Dalla Man et al., 2007] by introducing a new set of equations describing the insulin production of the engineered cells from Canadell *et al.* [*Canadell. D et al, unpublished data*]. Engineered cells were considered to be subcutaneously implanted. Eq. 5.10 and Eq. 5.11 from Magni *et al.* [Magni et al., 2007] account for the perfusion of subcutaneous insulin:

$$\frac{dS_1}{dt} = -(K_{a1} + K_d) \cdot S_1(t) + u(t) \quad \text{Eq. 5.10}$$

$$\frac{dS_2}{dt} = -K_d \cdot S_1(t) + K_{a2} \cdot S_2(t) \quad \text{Eq. 5.11}$$

Eq. 5.10 represents the amount of nonmonomeric insulin in the subcutaneous space and Eq. 5.11 the monomeric insulin. $u(t)$ represents the ratio of exogenous insulin administration. Nonmonomeric insulin is partly transformed into monomeric insulin with absorption rate constants k_{a1} and k_d respectively; therefore, monomeric insulin is finally absorbed with rate constant k_{a2} .

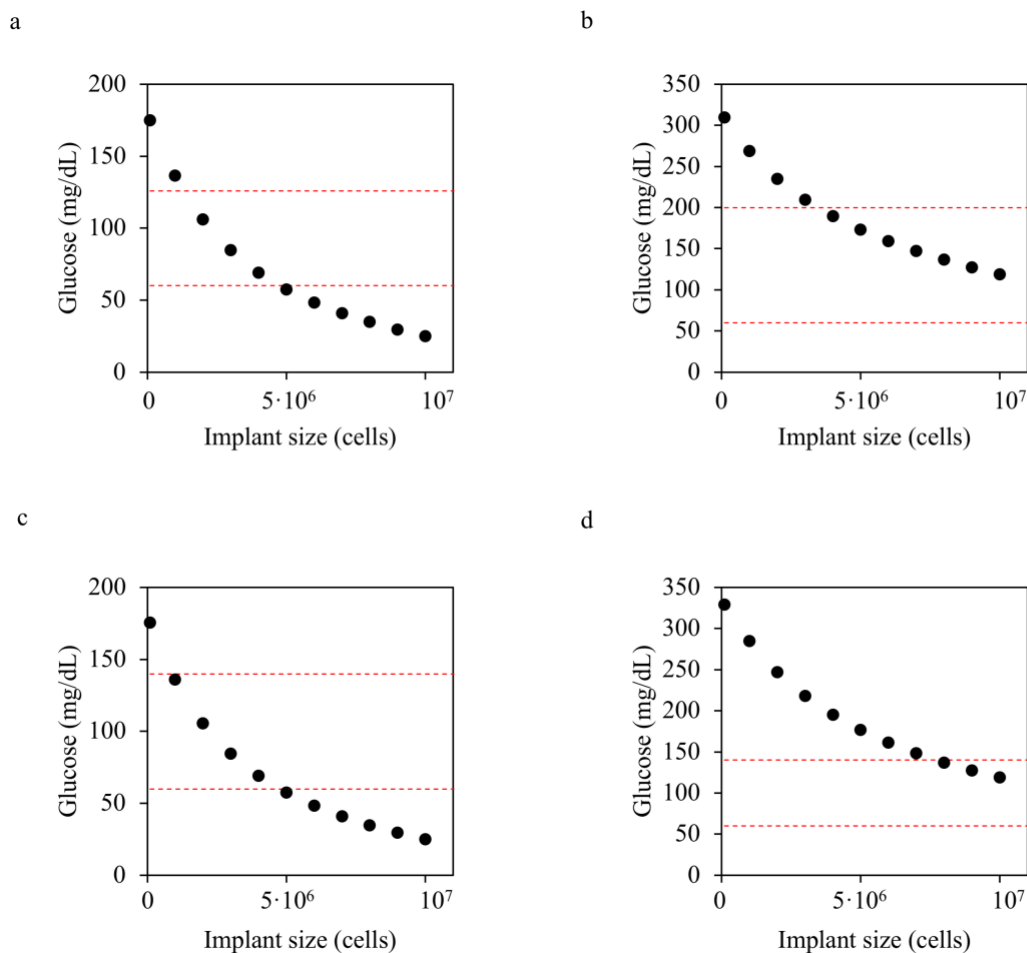
Departing from these equations, the term $u(t)$ in Eq. 5.10 has been replaced by the insulin supply from engineered cells (Eq. 5.3). Furthermore, in equation (3) from Dalla Man *et al.* [Dalla Man *et al.*, 2007], an additional term must be placed to account for the infusion rate of monomeric insulin to plasmatic insulin. The implant insulin supply can be modulated with the total number of encapsulated engineered cells conferring the device implant, i.e. term N in Eq. 5.3. Prior to the *in vivo* treatment with the encapsulated cellular implants, we have performed an *in silico* analysis for each cellular device to decipher its ability to restore glycaemia. For each specific cellular implant, i.e. constitutive and glucose-regulated insulin production, the Glycaemia Restoration Index (GRI) has been computed considering different implant sizes, i.e. implants that contain different amounts of engineered cells.

5.6.1 Cellular implants based on constitutive insulin production for glycaemia regulation in T1DM patients

To assess the effect of the engineered cells with constitutive insulin secretion for glycaemia regulation several implants containing different quantities of cells were simulated in the *in silico* T1DM patient. Equations describing the T1DM virtual patient Dalla Man *et al.* [Dalla Man *et al.*, 2007] together with the Ordinary Differential Equations describing the dynamics of the constitutive insulin production (Eq. 5.1 and Eq. 5.2) with model parameters from Table 5.1 have been integrated with the Fourth Order-Runge Kutta Method in *Visual Basic software*.

Computational results from the previously defined tests are shown in Figure 5.11. Values for Fasting Glycaemia Test are shown in Figure 5.11a and Oral Glucose Tolerance Test is shown in Figure 5.11b. Random Glucose Test was analysed within a time window of 24

hours after the *OGTT*. Maximum and minimum plasma glucose concentrations are shown in Figure 5.11c-d respectively. For each plot, red dashed lines depict the plasma glucose concentrations defining normoglycaemia. As figures show, there is a strong dependence between glycaemia levels and implant size. An optimal implant size has to lead glycaemia levels as close as possible or within the normoglycaemia region in all the different tests. Figure 5.11e shows the locations of *OGTT*, *FT* and *RT* tests in the 3D representation with respect to the *Health glucose Behaviour Region*. The blue dot corresponds to the *in silico* T1DM patient without an implant, and subsequent white dots correspond to different T1DM patients with increasing implant sizes. The red dot corresponds to the implant size fulfilling the criteria of Table 5.2.



e

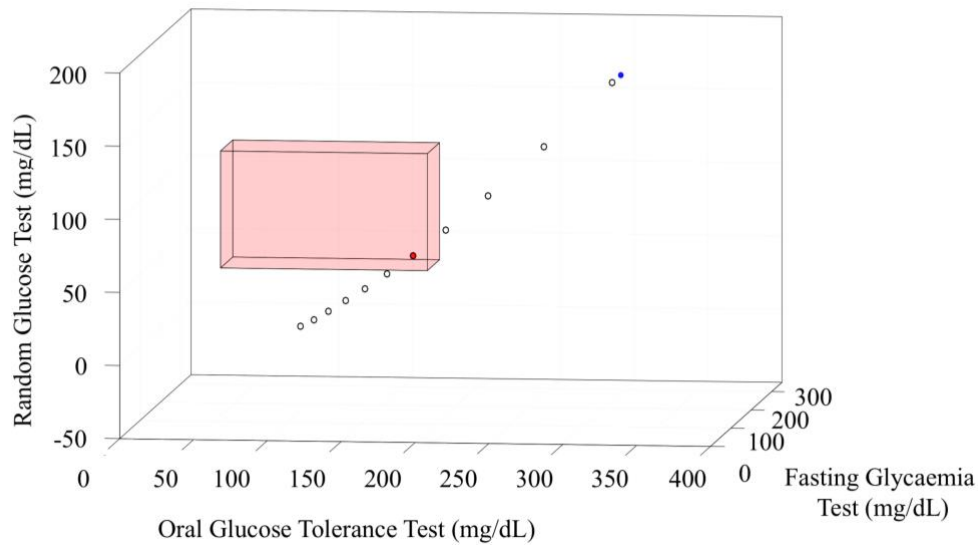


Figure 5.11 Plasma glucose levels for T1DM patients with different implants sizes constitutively producing insulin. Plasma glucose calculation for several T1DM patients with different implant sizes. **a)** Fasting Glycaemia Test was assessed by computing plasma glucose levels after an 8 h time period. Fasting glycaemia levels are plotted for each specific implant size. **b)** Oral Glucose Tolerance Test was computed considering an intake of 75 g and measuring plasma glucose levels in the following 2 h for each different implant size configuration. **c-d)** Higher glycaemia and Lower glycaemia for Random Glucose Test are calculated within a time window of 24 h after the *OGTT*. **e)** 3D representation of Fasting glycaemia test, *OGTT* and Random Glucose test for different implant sizes. Each dot corresponds to a T1DM patient with a different implant size of the constitutive insulin production implant. The blue dot corresponds to the T1DM virtual patient without an implant, the red dot corresponds to the T1DM virtual patient with an implant lying inside the *Health Glucose Behaviour Region*.

To obtain the relationship between implant size and its ability for plasma glucose levels regulation, the Glycaemia Restoration Index was computed according to Eq. 5.9 and normalized by the GRI corresponding to the T1DM patient without an implant. Consequently, higher GRI, i.e. close to 1 or -1, correspond to bad glycaemia regulation, whereas GRI close to 0 indicate good glycaemia regulation. Notably, $GRI < 0$ indicate the presence of episodes of hypoglycaemia. These situations must be prevented because of a severe death risk associated with hypoglycaemic episodes [Kalra et al., 2013].

Figure 5.12 shows the normalized distance allowing describing the implant impact in glycaemia regulation. Worst implant performance, i.e. near $GRI \sim 1$, is associated with

low implant size. As implant size increases associated GRI decreases up to 0 for implant size = $4 \cdot 10^6$ cells.

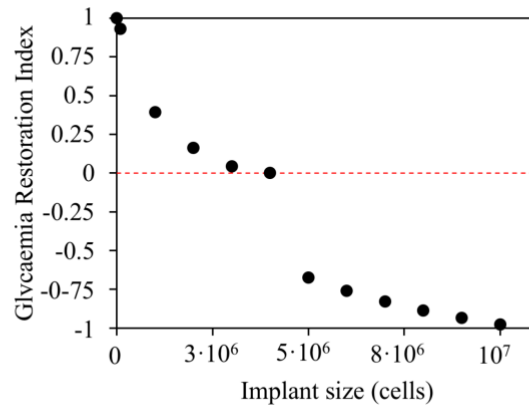


Figure 5.12 Evolution of glycaemic regulation based on constitutive insulin producer implants versus implant size. Glycaemia restoration index is computed as the minimal Euclidean distance between each 3D coordinate corresponding to a T1DM patient with different sizes of the constitutive insulin production implant and the faces of the *Health glucose behaviour region* according to Eq. 5.9. Computed values are normalized by the GRI corresponding to the T1DM patient without an implant.

In order to show the ability of the different implant sizes for plasma glucose regulation several simulations considering cellular implants with diverse GRI were considered. The computational procedure was: i) simulations compute a first starvation period of 8 hours corresponding to fasting glycaemia test, represented between time = -8 h to 0 h. At time 0 h, a glucose ingestion of 75 grams is simulated to perform the oral glucose tolerance test. Figure 5.13a represents the glycaemic response curves after glucose intake for the different implant sizes associated to positive, zero or negative GRIs. As figure shows, there is a strong dependence between glycaemia regulation and implant size, which correlates with the different plasma insulin levels depicted in Figure 5.13b. Computational results indicate that despite it is possible to define an implant size for optimal glycaemia regulation, the time required to recover the pre-prandial glucose levels is larger than health patients.

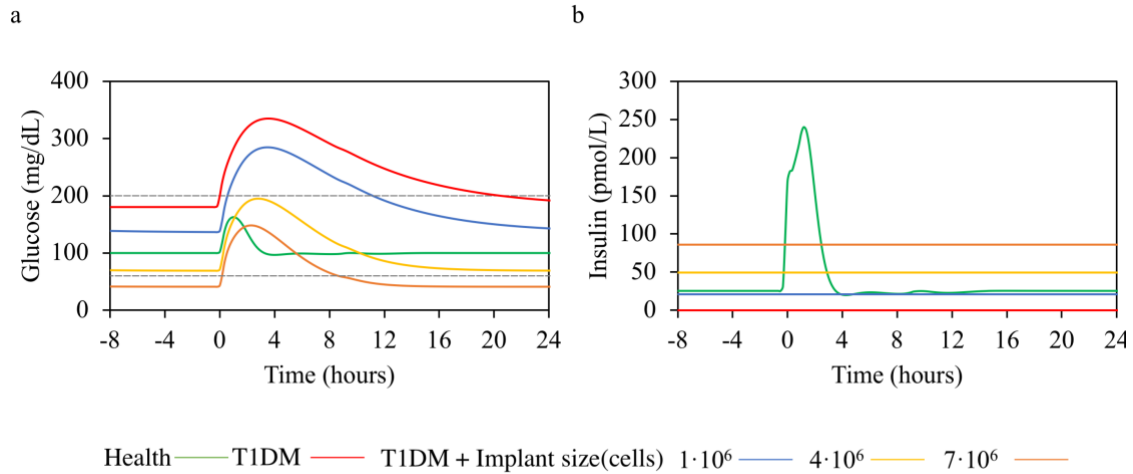


Figure 5.13 Dependence between plasma glucose and insulin with implant size. Plasma levels for the Fasting glycaemia test have been calculated for the time interval between -8 h and 0 h. At time $t = 0$ h the Oral glucose tolerance test consisting on the ingestion of 75 g of glucose is simulated up to a total time window of 24 h. The green line corresponds to the Health subject, the red to the T1DM without implant, the blue to T1DM with an implant size of $1 \cdot 10^6$ cells (GRI= -0.4), the yellow to T1DM with an implant size of $4 \cdot 10^6$ cells (GRI=0) and the orange to T1DM with an implant size of $7 \cdot 10^6$ cells (GRI=-0.8). **a)** Plasma glucose values. The dashed lines represent the hyperglycaemic and hypoglycaemic thresholds. **b)** Plasma insulin values.

5.6.2 Cellular implants based on glucose-dependent insulin production for glycaemia regulating in T1DM patients

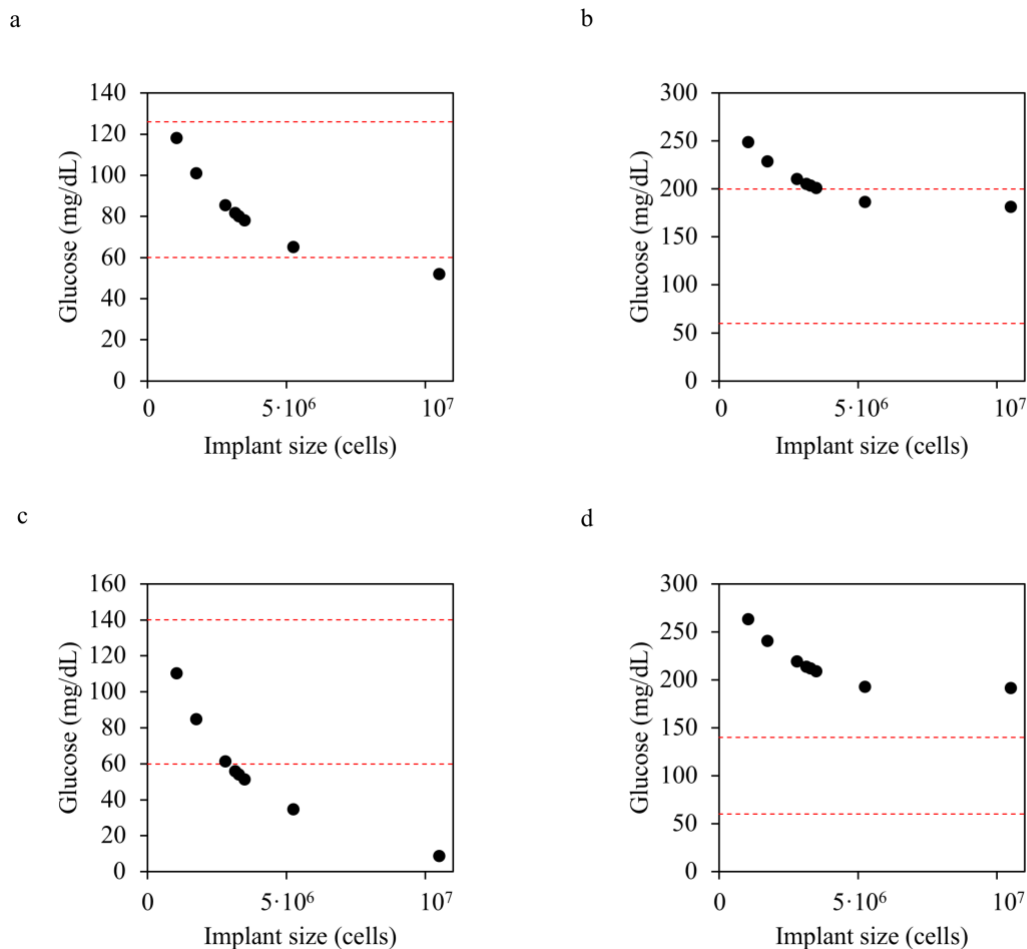
Subcutaneous implants with engineered cells able to produce insulin in a glucose-dependent manner require the detection of subcutaneous glucose levels. Eq. 5.12 extracted from *Magni et al.* [Magni et al., 2007] measures subcutaneous glucose concentration with a time delay, i.e. T_s , between plasma and subcutaneous space.

$$\frac{dG_s}{dt} = -\frac{1}{T_s}G_s(t) + \frac{1}{T_s} \cdot G(t) \quad \text{Eq. 5.12}$$

Where $G_s(t)$ is the input glucose concentration in Eq. 5.2. To assess the effects of implant size in plasma glucose regulation several simulations with different implant sizes for Fasting glycaemia Test, Oral Glucose Tolerance Test and Random Glucose test were

performed. Equations describing the T1DM virtual patient Dalla Man *et al.* [Dalla Man *et al.*, 2007] together with the Ordinary Differential Equations describing the dynamics of the constitutive insulin production (Eq. 5.1, Eq. 5.2 and Eq. 5.3) with model parameters from Table 5.1 have been integrated with the Fourth Order-Runge Kutta Method in *Visual Basic software*.

Computational results are shown in Figure 5.14a-d. In each plot, red dashed lines account for the plasma glucose concentrations defining the normoglycaemia region. Figure 5.14e shows the 3D space. Noticing that despite several implant sizes values are close to the *Health Glucose Behaviour Region*, none of them satisfies the three defined criteria.



e

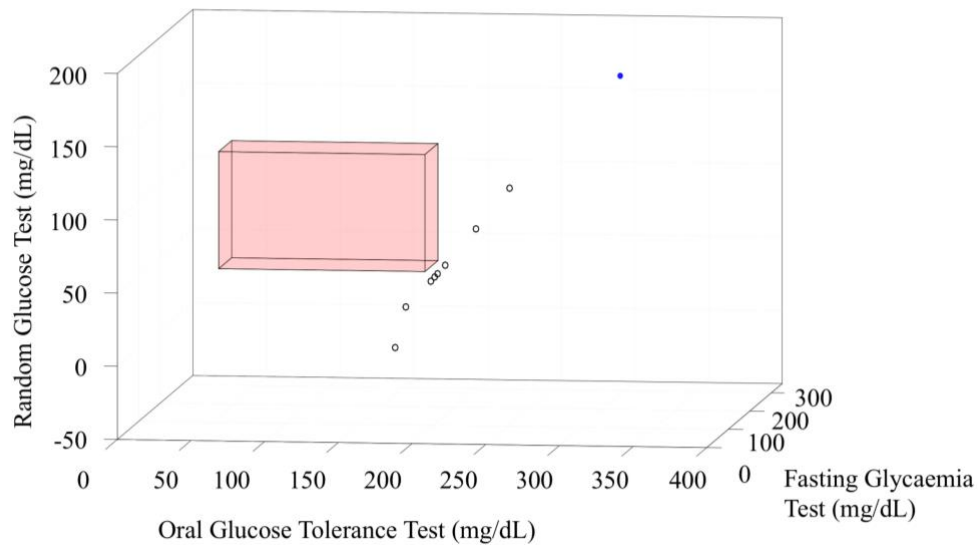


Figure 5.14 Dependence between plasma glucose levels with different implant sizes of glucose-dependent producer cells. Plasma glucose calculation for several T1DM patients with different implant sizes. **a)** Fasting Glycaemia Test was assessed by computing plasma glucose levels after an 8 h time period. Fasting glycaemia levels are plotted for each specific implant size. **b)** Oral Glucose Tolerance Test was computed considering an intake of 75 g and measuring plasma glucose levels in the following 2 h for each different implant size configuration. **c-d)** Higher glycaemia and Lower glycaemia for Random Glucose Test are calculated within a time window of 24 h after the *OGTT*. **e)** 3D representation of Fasting glycaemia test, *OGTT* and Random Glucose test for different implant sizes. Each dot corresponds to a T1DM patient with different sizes of the glucose-dependent insulin production implant. The blue dot corresponds to the T1DM virtual patient without an implant.

Figure 5.15 depicts the computed GRI with respect to the implant size. As the figure shows, increasing implant size provides better glucose regulation but beyond a critical size, i.e. $2.8 \cdot 10^6$ cells, glycaemia regulation presents hypoglycaemic episodes, i.e. $GRI < 0$, that must be prevented.

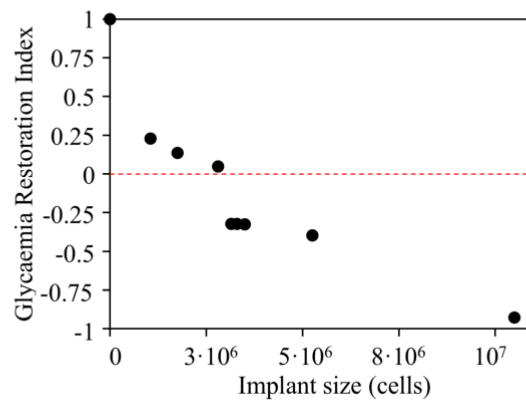


Figure 5.15 Evolution of glycaemic regulation based on glucose-dependent insulin producer implants versus implant size. Glycaemia restoration index is computed as the minimal Euclidean distance between each 3D coordinate corresponding to a T1DM patient with different sizes of the glucose-dependent insulin production implant and faces of the *Health glucose behaviour region* according to Eq. 5.9. Computed values are normalized by the distance corresponding to the T1DM patient without an implant.

Figure 5.16 represents the glycaemic response curves after an initial time period of fasting glycaemia, i.e. time = - 8 h to 0 h, and a glucose intake of 75g at time 0 h, i.e. Oral glucose tolerance test, for the different implant sizes associated to different GRI. Interestingly, the glycaemic response curves from Figure 5.16a shows a proper fasting glycaemia regulation for all of the simulated implant sizes. However, when analysing the dynamics in the *OGTT* the different implants display either the regulation of the higher or the lower glycaemia levels. Notice a delay in insulin accumulation (Figure 5.16b), compared with the health patient, which can be a limiting factor in the use of this type of approach for optimal glucose regulation in diabetic patients.

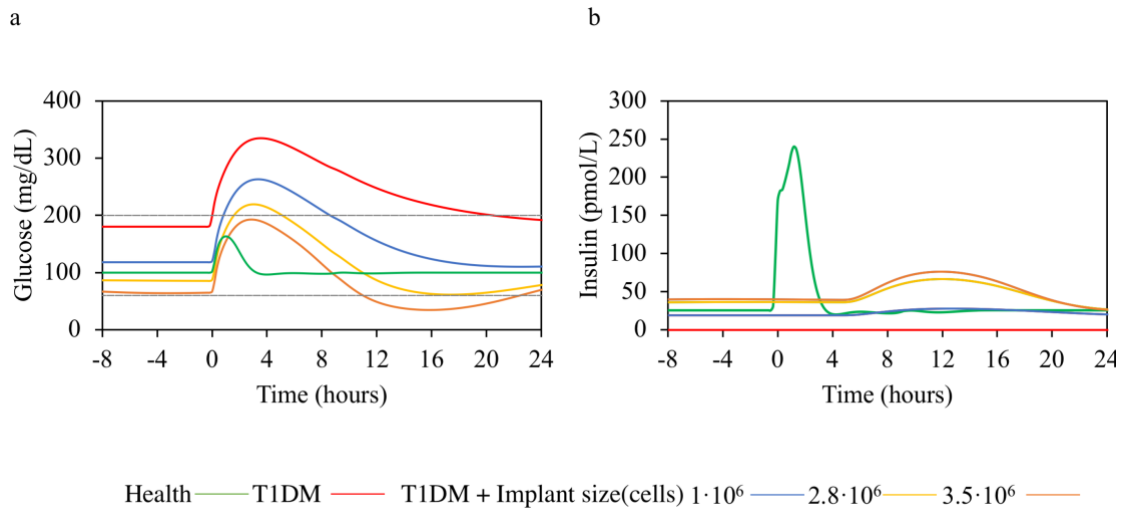


Figure 5.16 Dependence between plasma glucose and insulin with implant size. Plasma levels for the Fasting glycaemia test have been calculated for the time interval between -8 h and 0 h. At time $t = 0$ h the Oral glucose tolerance test consisting on the ingestion of 75 g of glucose is simulated up to a total time window of 24 h. The green line corresponds to the Health subject, the red to the T1DM without an implant, the blue to T1DM with an implant size of $1 \cdot 10^6$ cells (GRI= -0.2), the yellow to T1DM with an implant size of $2.8 \cdot 10^6$ cells (GRI~0) and the orange to T1DM with an implant size of $3.5 \cdot 10^6$ cells (GRI=-0.3).
a) Plasma glucose values. The dashed lines represent the hyperglycaemic and hypoglycaemic thresholds.
b) Plasma insulin values.

5.7 *In silico* daily life meal ingestion simulations

Moreover, the efficiency of cellular devices to regulate glycaemia in T1DM patients was implemented in a daily life meal routine. A 24 hours simulation accounting for breakfast at 9 a.m. (45 g), lunch at 2 p.m. (75 g) and dinner at 8 p.m. (75 g) was considered. Different implant sizes were implemented for both cellular devices. Figure 5.17a-b show the plasma glucose and insulin levels for the constitutive insulin production cellular implant and in Figure 5.17c-d for the glucose-dependent insulin production cellular implant. For both implant types' cellular sizes with positive, negative and 0 GRI have been considered.

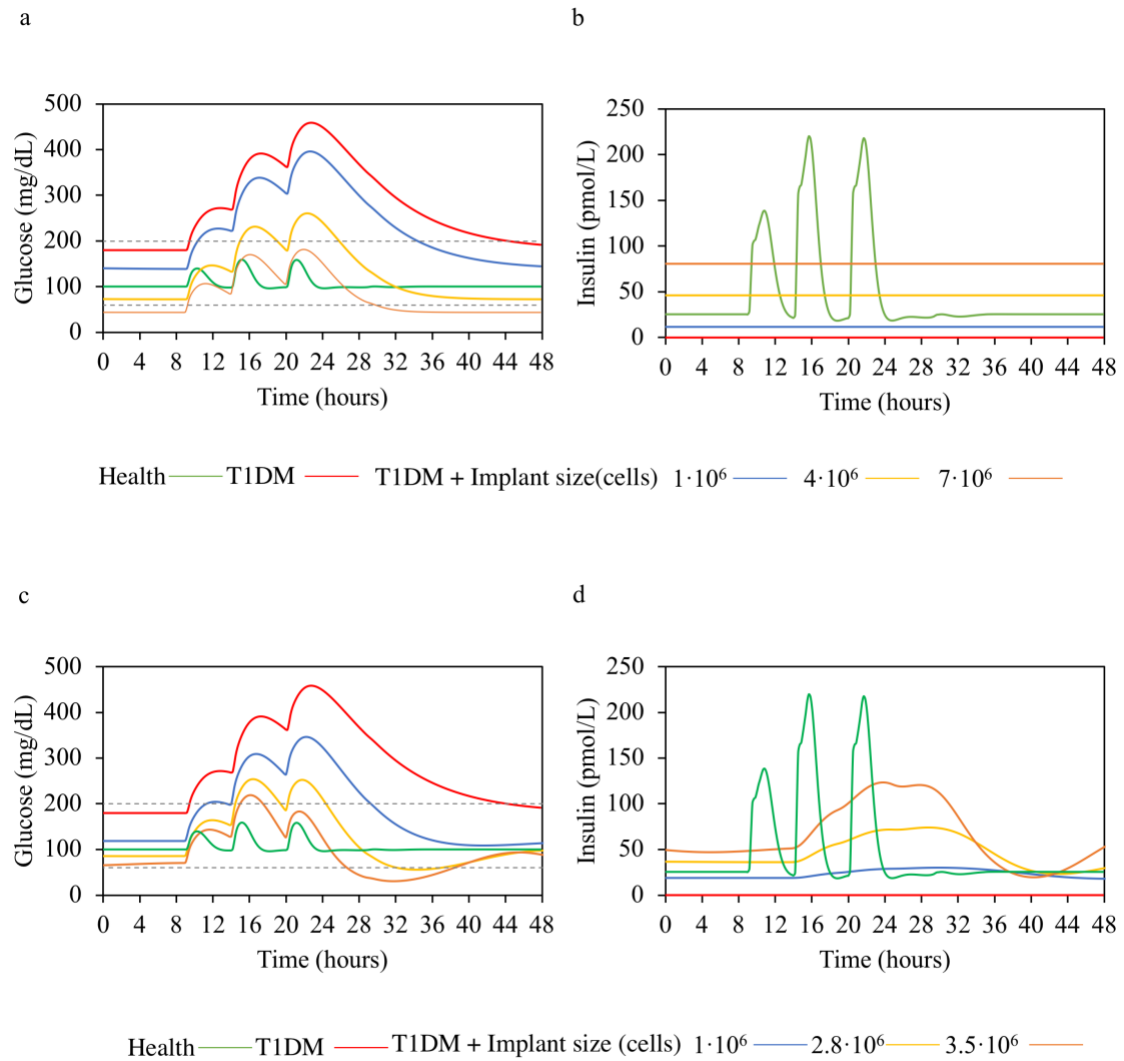


Figure 5.17 Three meal ingestion plasma glucose and insulin levels with respect to implant size. Three meal ingestion consisting on 45 g at 9 a.m., 70 g at 2 p.m. and 70 g at 8 p.m. **a-b)** Constitutive insulin production cellular implants. The green line corresponds to the Health subject, the red to the T1DM without an implant, the blue to T1DM with an implant size of $1 \cdot 10^6$ cells (GRI= -0.4), the yellow to T1DM with an implant size of $4 \cdot 10^6$ cells (GRI=0) and the orange to T1DM with an implant size of $7 \cdot 10^6$ cells (GRI=-0.8). **a)** Plasma glucose values. The dashed lines represent the hyperglycaemic and hypoglycaemic thresholds. **b)** Plasma insulin values. **c-d)** Glucose-dependent insulin production cellular implant. The green line corresponds to the Health subject, the red to the T1DM without an implant, the blue to T1DM with an implant size of $1 \cdot 10^6$ cells (GRI= -0.2), the yellow to T1DM with an implant size of $2.8 \cdot 10^6$ cells (GRI~0) and the orange to T1DM with an implant size of $3.5 \cdot 10^6$ cells (GRI=-0.3). **c)** Plasma glucose values. The dashed lines represent the hyperglycaemic and hypoglycaemic thresholds. **d)** Plasma insulin values.

Despite constitutive insulin producer cells showed a glycaemia restoration, i.e. GRI=0, with an implant size of $4 \cdot 10^6$ cells, notice the effect of plasma glucose accumulation after

several meal ingestions (Figure 5.17a). The cumulative glucose effect is observed in all three simulated implant sizes for the constitutive insulin producer implant correlating with the different plasma insulin levels shown in Figure 5.17b. Moreover, plasma glucose levels depict a longer postprandial recovery time when comparing with the health subject.

Computational glycaemia levels for the T1DM with the glucose-dependent insulin production cellular implants showed a reduction on both glucose cumulative effect and the time required to recover pre-prandial glucose levels (Figure 5.17c). However, a delayed insulin secretion is shown in the cumulative plasma insulin levels (Figure 5.17d). We have observed that delayed insulin compromises the optimization of the maximum and minimum glucose levels for the *OGTT* in Figure 5.16, however, for a daily meal routine the delayed secretion helps on the reduction of the cumulative glucose levels due consecutive ingestions, nonetheless implants with a $GRI < 0$ depict severe postprandial hypoglycaemia scenario.

5.8 Time Restriction Feed for glycaemia optimization

Computational simulations revealed that the delays in insulin secretion from the glucose-dependent implants are critical and can compromise its use for optimal glucose regulation due to the risk to induce hypoglycaemic episodes. In order to improve glucose regulation by preventing hypoglycaemia scenarios we have explored a novel approach, alternative to genetic engineering, based on the combination of cellular implants and time restriction feed patterns.

We have hypothesized if a proper feed modulation could benefit from the delayed subcutaneous insulin secretion. T1DM subjects should regulate very tightly the combination of food ingestion together with external insulin injection and exercise to regulate plasma glucose levels. For that reason, we have envisioned if a proper distribution of both, time and food ingestion, during an entire day could improve glycaemia regulation. To that end, we have developed an Evolutionary Algorithm (EA) enabling to optimize a meal pattern, i.e. time and food consumption, minimizing the episodes of hyper and hypoglycaemia.

An Evolutionary Algorithm (AE) [Eiben & Smith, 2003; Sloss & Gustafson, 2019] uses evolution and Darwin's natural selection of survival of the fittest to explore the solutions for complex problems. Applying the concepts of natural evolution, AE, works as an optimization algorithm by applying the concept of fitness evaluation, fittest selection, replication and, mutation. Figure 5.18 represents the different steps of an AE.

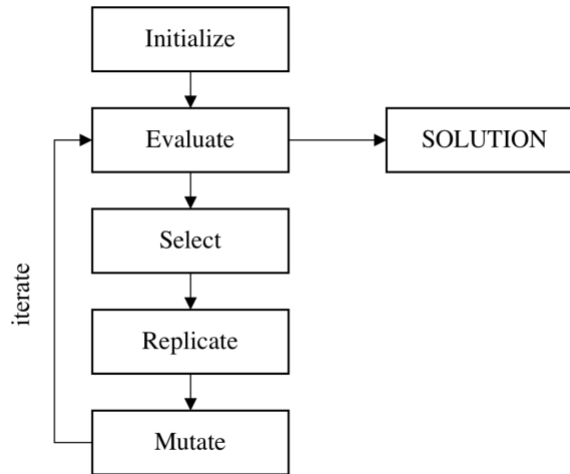


Figure 5.18 Schematically representation of the Evolutionary Algorithm procedure for time restriction feed optimization.

First, we created a virtual population of *Z in silico* T1DM patients following random feeding patterns, i.e. the total amount of glucose intake has been organized in several meals randomly distributed during the day. In detail, feeding patterns are defined by the meal food consumption σ_i (in grams) and mealtime ω_i (in hours).

We considered up to 6 different meals per day, with a total ingestion of $\theta = 185$ grams of glucose [Dalla Man et al., 2007]. The intake of each meal is randomly distributed according to a uniformly random distribution, but the total amount of food consumption θ during the day is constant and identical for each patient. Hence:

$$\theta = \sum_{i=1}^6 \sigma_i \quad \text{Eq. 5.13}$$

Time-periods of meal ingestion, i.e. ω_i , are selected according to a uniformly random distribution restricted to daylight hours considering starvation periods during the night according to:

$$\omega_i \in [\mu_{morning}, \mu_{night}] \quad \text{Eq. 5.14}$$

where $\mu_{morning}$ and μ_{night} are settled to 7 a.m. and 11 p.m. hours respectively.

Once this first generation of patients has been defined an iterative loop begins. In each generation, T1DM patients with its corresponding meal pattern are evaluated for an entire day (24 hours) and plasma glucose concentrations are calculated, from that maximum, i.e. G_H , and minimum plasma glucose levels, i.e. G_L , are obtained.

Second, we defined a fitness function that accounts for the quality of glucose regulation. This fitness function has been defined to penalize episodes of hyper and hypoglycaemia.

Fitness function F_n of a patient n is defined as:

$$F_n(\sigma_i, \omega_i) = H(G_L - G_{target}) \cdot \min |G_L - G_{target}| \cdot \min(G_H) \quad \text{Eq. 5.15}$$

Where G_{target} is the minimal glucose concentration accessible by the patient. $H(G_L - G_{target})$ is the Heaviside function:

$$H(G_L - G_{target}) = \begin{cases} 1 & \text{if } G_L \leq G_{target} \\ 0 & \text{if } G_L > G_{target} \end{cases} \quad \text{Eq. 5.16}$$

This definition penalizes hyperglycaemia and prevents hypoglycaemia, i.e. $G_L < G_{target}$.

Patients are labelled according to its fitness function $F_n(\sigma_i, \omega_i)$. Afterwards, the population is sorted according to its fitness evaluation, from the best to the worst fitness function. Next step considers that only individuals with better fitness, i.e. m fittest patients consisting of the 25% of the Z individuals, would be replicated for the next generation.

The new Z - m individuals are created by replicating the existing m patients according to the roulette wheel method, i.e. we generate a uniformly random number $r \in [0,1]$ and patient m will be replicated if $r \leq p(m, t)$.

$$p(m, t) = \frac{F_n}{\sum_{n=1}^m F_n} \text{ for } t \in [1, \infty] \quad \text{Eq. 5.17}$$

After replication, some variability is introduced in the Z - m individuals by random mutations in the feed pattern. Mutations are defined as small changes in the optimization parameters σ_i or ω_i .

Mutations in σ_i are done in terms of a food exchanged (λ) between two different meal in the same day. First, two different meals, a and b are randomly selected according to a uniformly random distribution. Second, λ is determined as a 25% of σ_a . The amount λ is subtracted from σ_a and added to σ_b .

$$\theta (\text{grams}) = (\sigma_a - \lambda \cdot \sigma_i, \sigma_b + \lambda \cdot \sigma_i) \quad \text{Eq. 5.18}$$

On the other hand, mutations in ω_i are implemented randomly selecting a meal i and selecting a new time-period according uniformly random distribution satisfying the criteria from Eq. 5.14.

Once replicated and mutated the meal patterns for the next generation, i.e. $t + 1$, the algorithm simulates the *in silico* T1DM patients with its associated feeding patterns and again patient's glycaemia is calculated and fitness function is evaluated. Iterations will finish when finding a meal pattern with minimum plasma glucose levels satisfying $-10\% \cdot G_{target} < G_L < +10\% \cdot G_{target}$ and the minimal G_H below the hyperglycaemia threshold, i.e. 200 mg/dL. Figure 5.19a-b show the show G_H and G_L evolution during algorithm iterations, respectively. Random mutations together with fittest survival enables to explore the landscape of optimal solutions.

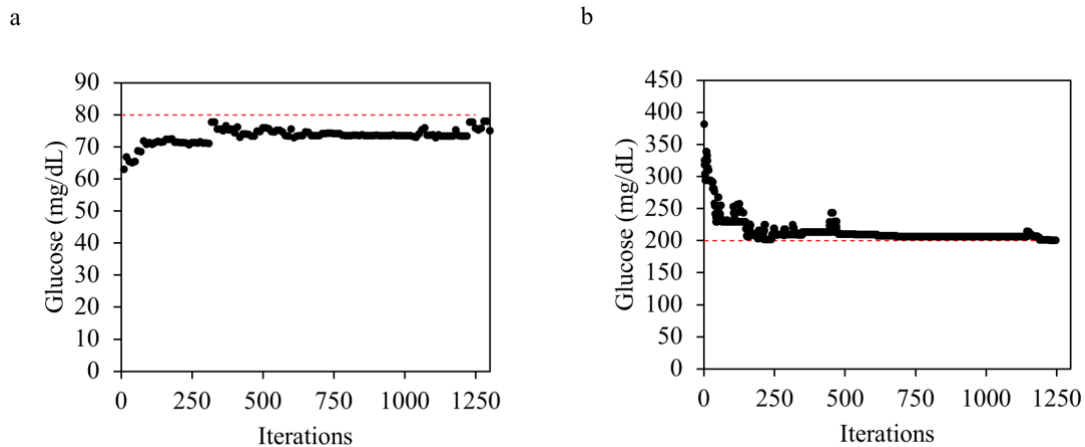


Figure 5.19 Maximum and minimum plasma glucose levels evolution during algorithm iterations. A population of $Z=100$ T1DM patients have been optimized with $G_{target} = 85$ mg/dL. **a)** Minimum plasma glucose levels. **b)** Maximum plasma glucose levels.

5.8.1 Time Restriction Feed Algorithm for T1DM patients

TRF algorithm was applied to the *in silico* T1DM patient. A population of 100 T1DM patients was used to optimize the meal pattern with minimum glucose levels $G_{target} = 85$ mg/dL and minimizing the maximum glucose levels. Plasma glucose for a random feeding pattern, i.e. corresponding to the generation 0 in the AE, was calculated for both health and T1DM subjects (Figure 5.20a). The random feeding pattern shows 6 different meals with very diverse plasma glucose peaks corresponding to each meal ingestion. Surprisingly, the TRF-optimized feeding pattern converges into 4 different meals (Figure 5.20b). Interestingly, very different amount of glucose is observed in the different meal ingestions, and so is depicted in the plasma glucose simulation for the health patient (green line in Figure 5.20b), however, for the T1DM patient glucose levels for each ingestion depict similar plasma glucose levels after food ingestion, i.e. around 350 mg/dL. The TRF-optimized feeding pattern suggests that a proper distribution of the total amount of food per day in amount and time plays a relevant role in glycaemia restoration without the addition of exogenous insulin. However, tying patients' life into a very strict feeding routine.

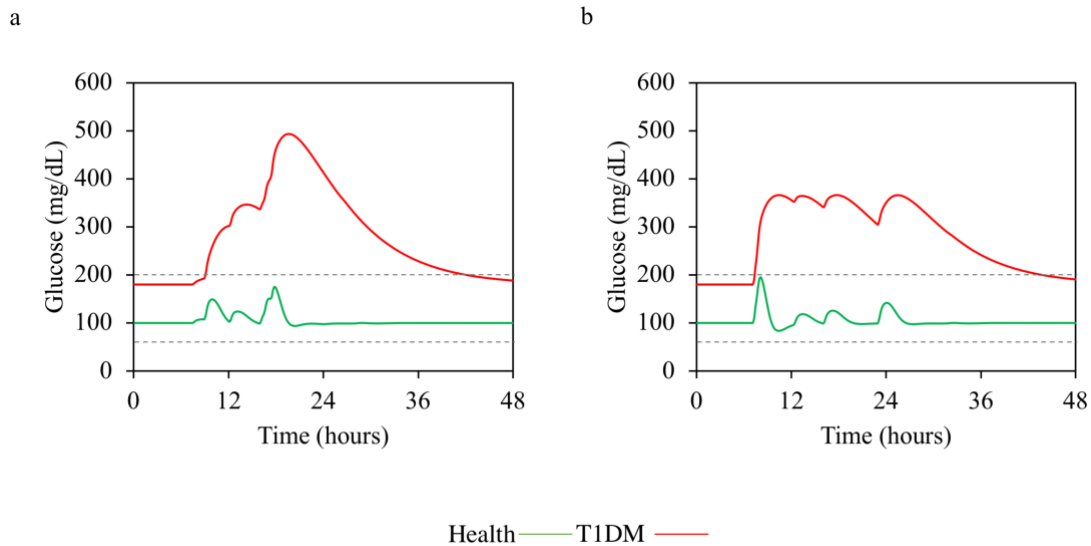


Figure 5.20 Plasma glucose levels for random and optimized feeding patterns. The green line corresponds to the Health subject and the red to the T1DM without an implant. **a)** Random feed pattern. Meal₁ {7 a.m., 8.14 g}, Meal₂ {9 a.m., 52 g}, Meal₃ {12 p.m., 27 g}, Meal₄ {4 p.m., 29 g}, Meal₅ {5 p.m., 26 g}, Meal₄ {11 p.m., 42 g}. **b)** T1DM TRF-optimized feed pattern Meal₁ {7 a.m., 87 g}, Meal₂ {12 p.m., 20 g}, Meal₃ {4 p.m., 30 g}, Meal₄ {11 p.m., 22 g},

5.8.2 Time Restriction Feed Algorithm for T1DM patients with cellular implants

Previous results demonstrated that the use of optimized TRF patterns has a significant impact on glycaemia regulation, even in the absence of cellular implants. In this section, we explored the combination of the TRF algorithm in T1DM patients with the glucose-dependent cellular implants. More specifically the TRF algorithm has been applied to a population of 100 T1DM patients with the glucose-dependent insulin producer cellular implant with a GRI ~ 0 (Figure 5.15) to optimize the meal pattern with minimum glucose levels $G_{target} = 85$ mg/dL and minimizing the maximum glucose levels.

Once the algorithm has optimized the TRF pattern for the glucose-dependent insulin producer cellular implants, the optimized TRF pattern has also been applied to the health subject, the T1DM and the T1DM with a constitutive implant, and plasma glucose levels have been obtained (Figure 5.21).

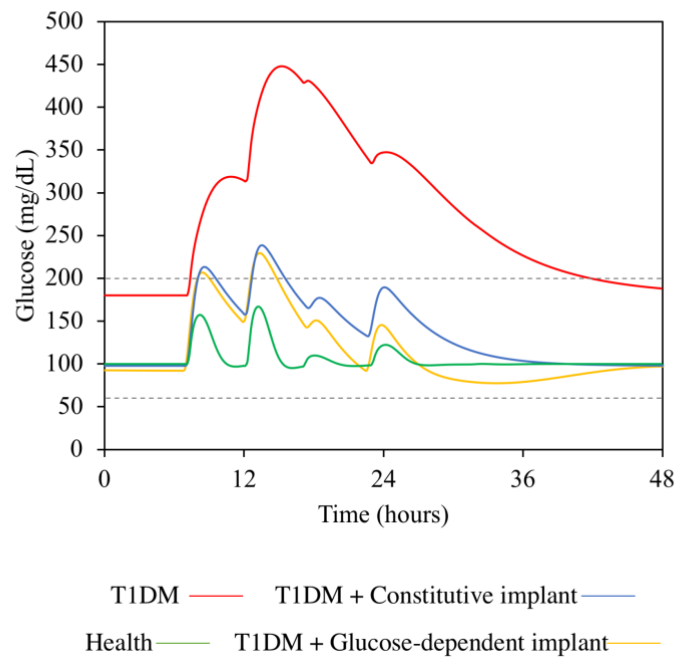


Figure 5.21 Glycaemia evolution applying the optimized TRF pattern for the glucose-dependent implant. TRF pattern corresponding to iteration = 1300. The green line corresponds to the Health subject, the red to the T1DM without an implant, the blue to T1DM with constitutive implant and the yellow to T1DM with glucose-dependent implant. Meal₁ {7 a.m., 67 g}, Meal₂ {12 p.m., 80 g}, Meal₃ {5 p.m., 17 g}, Meal₄ {11 p.m., 27 g}.

The TRF-optimized pattern showed the convergence to 4 different meals with higher food intake in the first and second meals and lower glucose intake in the third and fourth meals. When comparing the T1DM patient without an implant (red line) with T1DM with an implant (blue and yellow lines) a significant reduction of maximum plasma glucose levels is achieved as well as the time spent above the hyperglycaemia threshold when combined both the TRF and implants. Delayed insulin secretion effect allows decreasing the plasma glucose accumulation due to consecutive meals as well as the postprandial glucose when comparing the glucose-dependent implant with the constitutive implant. Neither the constitutive nor the glucose-dependent implants face a hypoglycaemic scenario.

Moreover, TRF-optimized pattern was applied for three entire days in order to explore possible accumulation of plasma glucose (Figure 5.22a). Additionally, some perturbations

were introduced to assess cellular implant robustness. More specifically perturbations shown in Figure 5.22b-c consist of the elimination of either the second or third meal, respectively, for the simulated second day. In Figure 5.22d the last meal of the last simulated day, i.e. the third day, was eliminated.

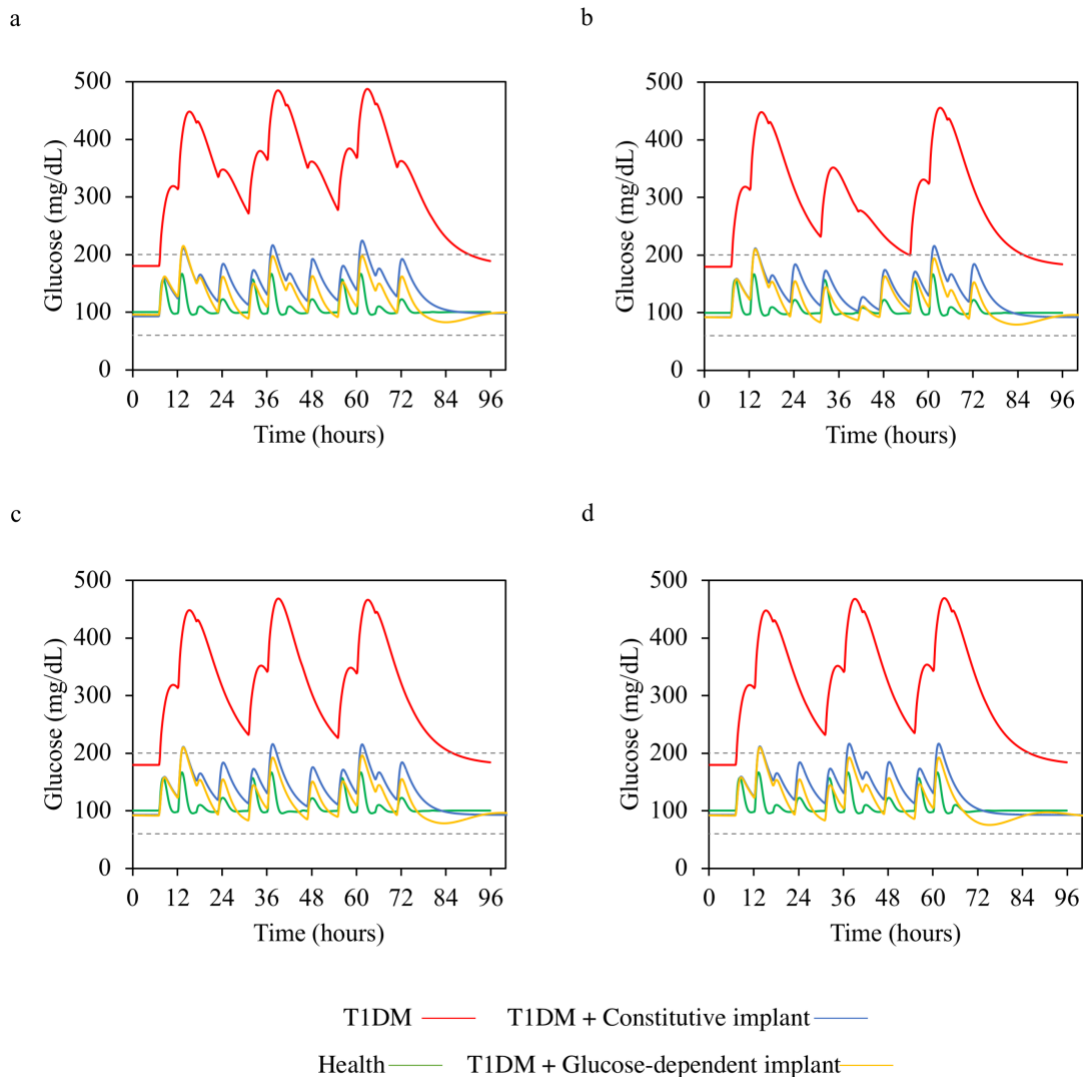


Figure 5.22 Glycaemia evolution applying the glucose-dependent implant TRF-optimized pattern for three days. The green line corresponds to the Health subject, the red to the T1DM without an implant, the blue to T1DM with constitutive implant and the yellow to T1DM with glucose-dependent implant. Optimized feed pattern Meal₁ {7 a.m., 67 g}, Meal₂ {12 p.m., 80 g}, Meal₃ {5 p.m., 17 g}, Meal₄ {11 p.m., 27 g}. **a)** Three days of simulation following the same optimized feed pattern **b)** First- and third-days simulation following the optimized feed pattern, for the second day Meal₂ = 0 g. **c)** First- and third-days simulation following the optimized feed pattern, for the second day Meal₃ = 0 g. **d)** First- and second-days simulation following the optimized feed pattern, Meal₄ of the third day = 0 g.

Figure 5.22a shows a cumulative effect of plasma glucose levels for the T1DM with constitutive implant, however, the T1DM with glucose-dependent implant shows a slightly better glucose regulation for both second and third simulation days. In Figure 5.22b-c show no significant impact on plasma glucose levels when skipping neither a large nor a small meal during the second simulation day. Furthermore, nocturnal hypoglycaemia is not faced when skipped the last meal of the day in the third simulated day for the glucose-dependent (Figure 5.22d).

5.9 Discussion

Enclosed in the project “Encapsulated Synthetic Cellular Circuits to Restore Glycaemic Control in Type 1 Diabetes” the potential use of cellular implants able to produce insulin, in a constitutive or glucose-dependent manner, has been explored. Cellular implants performance relies on the combination of i) engineered synthetic gene circuit, ii) cellular encapsulation and iii) implantation. The design of cellular implants for biomedical applications should follow the *design-build-test-learn* cycle together with a combination of experimental and computational tools. Computational tools allowed to simulate a closed-loop scenario enabling to decipher device characteristics for response optimization.

Our analysis departs from the experimental results of Canadell *et al.* [Canadell, D *et al*, *unpublished data*], in which two different engineered eukaryotic cells able to produce and secrete insulin from either a constitutive or glucose-dependent manner were constructed and characterized. We formalized a mathematical model describing both cellular dynamics. Afterwards, we implemented a computational model describing the glucose dynamics in T1DM patients, according to the model developed by Cobelli and co-workers [Dalla Man *et al.*, 2007]. The combination of the mathematical model describing the glucose-insulin dynamics in diabetic patients together with the models describing the dynamics of the engineered eukaryotic cells allowed to *in silico* explore the potential use of cellular implants to regulate glycaemia in diabetic patients. To quantitative evaluate the effect of cellular implants in glycaemia regulation, we defined a novel metric based on the diabetes mellitus diagnosis criteria from the World Health Organization (WHO).

Our computational results exhibited that glycaemia regulation is strongly dependent on the implant size, i.e. the number of engineered implanted cells, with comparable implant size, i.e. cells or mL of implanted alginate beads, with previous research studies [Xie et al., 2016]. Surprisingly, cellular implants based on a constitutive insulin production showed a better glucose restoration when compared to glucose-dependent cellular devices. Nonetheless, the ability of constitutive insulin secretion to regulate glycaemia has achieved very promising results. In Jaen *et al.* [Jaén et al., 2017] the engineering of skeletal muscles with a constant insulin production allowed to restore glycaemia for an 8-years follow up in diabetic dogs. However, glycaemia restoration by a constant insulin supply would face some drawbacks due to glucose-disruptors such as feeding, exercise or unbalanced hormones. Therefore, the ability to modulate insulin secretion according to plasma glucose levels had been further hypothesized. However, neither previous research studies [Xie et al., 2016] nor our engineered glucose-dependent cellular devices exhibit a proper glycaemia restoration, putting the manifest the difficulty of engineering cellular devices with the ability to mimic β -pancreatic cells.

Our computational results suggest that, for the glucose-dependent implants, the temporal delay required for insulin production in response to changes in glucose levels, combined with implant size, has a major impact in glycaemia regulation. As a consequence of these delays, when optimizing hyperglycaemia device faces severe hypoglycaemia scenarios which should be avoided due to higher death risk factors. Despite constitutive insulin expression revealed to be easily optimized for plasma glucose regulation, when facing several consecutive glucose ingestions, glucose-dependent implants enable an accurate adjustment of insulin secretion lowering both postprandial glucose levels and the time to recover normoglycaemia.

To counterbalance delays in insulin secretion we demonstrated that glycaemia regulation by glucose-dependent implants could be improved when combined with time restriction feed patterns (TFR). To define the optimal TFR we developed an evolutionary algorithm, based on Darwinian evolution rules, that determines the amount of food per meal and the ingestion time, minimizing hyperglycaemia and preventing hypoglycaemic scenarios.

Altogether, we have created an *in silico* closed-loop platform comprising a glucose-insulin meal simulator and the computational description of cellular devices based on the *in vitro* characterization of engineered eukaryotic cells. Nonetheless, although hypothesizing the need of balancing implant insulin production according to current glucose plasma needs, the model describing the glucose-insulin dynamics does not include the effect of non-insulin mediated glucose consumption due to physical exercise [SyLOW et al., 2017], limiting the platform potential. Overall, we have demonstrated that a combination of experimental evidence together with *in silico* computational simulations in a closed-loop scenario allows for a powerful framework concerning the design of living biomedical devices.

CHAPTER 6

Discussion and Conclusions

6 DISCUSSION AND CONCLUSIONS

6.1 Living biomedical devices from intrinsic cellular components

Synthetic biology has moved forward developing novel strategies to address biomedical problems applying engineering principles to biology. A rational assembling of pre-characterized modules composed of biological substrates has been envisioned as a powerful tool to build complex living devices. Within that line, the field of theranostics envisaged the development of personalized biomedical devices allowing to diagnose, monitor or treat complex medical problems from a technological point of view [Crawley et al., 2014; Jeelani et al., 2014; Kojima et al., 2015]. On the other hand, living technologies had revealed that the use of biological substrates, by its own or in combination with electro-mechanical components, allowed to overcome the limitations when developing electronic sensors [Bedau et al., 2010; Froese, 2014]. Clear is the relevance of biological organisms detecting, processing and responding to intra- and extracellular information and allowing its survival in challenging environmental conditions [Owicki & Wallace Parce, 1992]. Hence, the use of cellular components for sensing would help on the detection of disease markers.

The engineering of cellular organisms, and more specifically bacteria, for detection of biological signals [Khalil & Collins, 2010; Pan et al., 2019; Wan et al., 2019] is based on the engineering biology modularity principle. New biosensors can be assembled by combining different biological parts from different species in a host cell. In this way, intrinsic cellular machinery able to detect extracellular environments [Selifonova et al., 1993] is exploited and rewired to create novel devices. Despite the enormous potential to detect a broad range of extracellular or intracellular signals, the major drawback to be faced is the adaptation of the biosensor performance to satisfy the specific application detection requirements [Van Der Meer et al., 2004]. More specifically, requirements rely on the operating range (γ), sensitivity (σ), dynamical range and affinity ($K_{0.5}$). Although different methods for tuning biosensor responses have been explored [Ang et al., 2013; Max Carbonell-Ballesteros et al., 2014; Y. Chen et al., 2018; M. S. Lu et al., 2012; Shopera

et al., 2015; B. Wang et al., 2015] there is a need for the development of methodologies to modify biosensor features so that they can satisfy the demands of specific applications in a predictable way. To address this issue, in **chapter 2**, we have developed a general mathematical model for Two-Component-Biosensors based on the *3OC6HSL-LuxR-pLux* system [Fuqua et al., 1994], relating the abundance of the receptor protein (R_T) with the main biosensor features, i.e. γ and $K_{0.5}$. Moreover, our model also captures the biosensor region exhibiting the maximal input/output relative change, i.e. sensitivity (σ), which defines the optimal region of the biosensor to work with. The relation with the operating range and receptor abundance had also been defined.

Our approach aims to help on the design of biosensors working on the desired operating range with specific affinity requirements. Thus, a library of biosensors working with different receptor abundances is required to determine model parameters a_1 , b_0 and b_1 . Once these parameters are fixed with the specific complex [*signal-receptor-operator*], the mathematical model allows predicting biosensor transfer function and its main features based on the relative receptor protein abundance. To be more precise, a library of varying-strength expressions systems, e.g. constitutive promoters with different strengths, RBS with different efficiencies or inducible promoters, have been characterized in terms of their relative receptor protein abundance [Kelly et al., 2009]. Using model equations γ and $K_{0.5}$ are calculated and the relationship between input and output is predicted. Experimental results show that variations in the relative amount of receptor protein impacts on $K_{0.5}$ parameter independently of the specific genetic system used to produce the receptor protein, but no significant variation is found in γ , thus allowing to shift the operating range towards greater or lower input signals, and hence adapting the biosensor response towards the required needs. More specifically, in the particular case of study, the relationship observed between the activation threshold, i.e. $K_{0.5}$, and the receptor protein, i.e. LuxR, permits to modify the activation threshold of the *3OC6HSL-pLux* biosensor up to two orders of magnitude. Our mathematical model allows to design biosensors to perform specific features without its prior construction only by the promoter characterization using readable fluorescent outputs and hence, minimizing experimental workload.

Although this study is focused on the experimental validation of the *3OC6HSL-LuxR-pLux* system [Fuqua et al., 1994], the developed mathematical model pursue the description of all inducible TCB. With our approach, we aim to overcome the limitations faced when applying TCB for real-need problems [Mahr & Frunzke, 2016; Merulla & Van Der Meer, 2016; A. J. Meyer et al., 2019; Fuzhong Zhang et al., 2012] and serve as a design tool for further biosensors' applications based on novel metabolic transducers [Voyvodic et al., 2019].

Once sensorial information is gained from the sensor module, further analysis or integration is required to generate non-trivial responses either in the analogue or digital context. On that line, the use of a multicellular implementation for computational devices has revealed as extremely useful for complex circuits [Regot et al., 2011; Tamsir et al., 2011] because each component is implemented in a different cellular type. This embodiment is appealing because simplifies the genetic engineering required [Morey et al., 2012; F. Wu et al., 2014], minimizes the emergence of unexpected interactions with the host cell [M Carbonell-Ballesteros et al., 2016], diminishes inappropriate host genetic interactions [Tan et al., 2009] and reduces significantly the metabolic burden associated to foreign genes [M Carbonell-Ballesteros et al., 2016]. Furthermore, depositing the different cell types in different spatial locations avoid negative growth competition effects which have revealed to challenge device stability and reproducibility [Kwok, 2010] [Amoyel & Bach, 2014].

In chapter 3 we have codified computation into a unique information signal, namely *3OC6HSL* from *E. coli*, and implemented devices performing digital computation. The approach relies on the construction of different engineered cell types with the ability to i) secrete, ii) modify and iii) detect the information signal. After an initial characterization of the different engineered cellular modules, we have experimented with the far-reaching scalability introduced with the 2D geometrical topology. Introducing cellular modules and space enables to translate higher-order complex functions within the particular space configuration rather than in genetic engineering. Therefore, the ability to implement different device responses rely on re-arranging the device modules and opens the door of a new vision of cellular computation.

We have implemented some examples of two-inputs one-output logic computations, for instances devices involving one or two modulatory *BC* in one or two different branches. Scaling-up the number of functions does not necessarily imply scaling up the complexity of our design, therefore, for 4-input logic functions, in the worst scenario, the geometrical multi-branch approach enables to perform up to 2^{2^4} functions with 8 branches and 4 modulatory *BC* per branch.

In our approach signal detection is mediated by its promoter transcriptional activation expressing the *aiiA* degradation enzyme with and *Identity* or *NOT* logic. It is worth mentioning that the *NOT* logic is easily implemented thanks to the *LacI/P_{Lac}* repressor gene. Therefore, identification of input-detection transcriptional promoters would allow our multi-branch approach to recognize complex scenarios resulting as the combination of several signals. Despite our approach has been experimentally tested for 2 well-studied input signals, an appropriate input detection and coupled with the operating range selection for a specific application would enable, for instance, to detect toxic environmental conditions [Joshi et al., 2009; Paitan et al., 2004; Saeidi et al., 2011] or disease-related signals [Anderson et al., 2006].

Moreover, efforts were done into the development of an experimental setup foreseeing the automation and reproducible production of printable computation circuits. Therefore, serving as a fingerprint in the field of cellular computation. Hence, future work should be devoted scaling towards application-based inputs that together with a printing approach reinforces the scalability, standardization and automatization of the proposed multi-branch design. Moreover, hypothesising the exploration of the printable ability on different substrates, as suggested in an artistic fashion, for instance, the *Vienna Textile Lab* or *Ginko Bioworks* to use bacteria dyes to textile materials, for a futurable broad field of applications.

On the other hand, in **chapter 4**, we have demonstrated that multicellular devices could be applied for biomedical applications offering flexible and tuneable analogue responses. Fundamental characteristics of sensor devices such as sensitivity and affinity can be adjusted with proper modulation of the carrying information signal flow, either by

incrementing the number of producer cells or modulator cells, without the need for additional cell engineering. By the proper re-formulation of the different multicellular modules, both simple input-output responses and complex dynamics, i.e. a pulsatile response, can be implemented.

Overall, the codification of sensorial information in a unique signal molecule, independent on the cellular type, allowed translating the computation in the modulation of the signal flow rather than in the different modules made of higher complex synthetic circuits. Following the engineering of biology approach, we have reformulated the use of communication molecules, for instance, bacterial quorum sensing and yeast mating pheromones, to encode both digital or analogue computation.

As a *proof-of-principle*, *S. cerevisiae* was engineered to detect a physiological signal, i.e. glucose, and produce a therapeutic molecule as an output, e.g. insulin and glucagon hormones. Thus, we have transferred the ability of pancreatic cells to a eukaryotic organism. Even though we have engineered a modular device with the ability to perform either simple or complex responses in response to high or low glucose concentrations, these devices have some limitations. Mainly, the operating range of the yeast glucose-responsive promoters differ three orders of magnitude from the human physiological ones, the multicellular circuits were sensitive to changes in cellular proportion and the insulin and glucagon produced need further postprocessing to be fully functional. Although reinforcing the idea that synthetic biology can offer a new framework for the development of *in vivo* biomedical devices complementing or even substituting devices based on electronic or electro-mechanical technology, a deeper analysis on device performance considering the specific application should be done. More specifically, in diabetes mellitus pathophysiology, device would constantly monitor plasma glucose levels and respond producing an output when detecting abnormal glucose concentrations. When glucose is above normoglycaemia the device should produce insulin to lower glucose values, on the other hand when glucose is below normoglycaemia the device should produce glucagon to increase glucose levels. In general, a living device operating in disease conditions should constantly monitor circulating disease-relevant metabolites,

process abnormal concentrations and coordinate the production and release of the specific output acting in a closed-loop process.

6.2 *In silico* closed-loop living biomedical device performance

We have considered the closed-loop implementation of cellular devices as the fourth-functional module of a living biomedical device to be analysed. In **chapter 5**, we have studied the regulation of plasma glucose by the ability of different cellular devices to secrete insulin. In this scenario, the device output, i.e. insulin hormone, has a direct regulation on the device input, i.e. glucose. In diabetes mellitus, closed-loop device dynamics must guarantee the regulation of plasma glucose between normoglycaemia levels. Engineered cells with the ability to produce insulin when glucose levels are above normoglycaemia would allow restoring plasma glucose levels, as insights gained through **chapter 4**, and previous research studies demonstrated that further cell encapsulation and implantation into diabetic organisms effectively control glycaemic levels for several days [Shao et al., 2017; Xie et al., 2016]. However, some limitations of these studies rely on how engineered cells produce insulin secretion by indirect measurement of glucose levels, for instance via cell membrane depolarization [Xie et al., 2016] or external activation with red-light [Shao et al., 2017]. Overall, claiming the need to establish a framework enabling the study of glucose-regulating living devices.

We have based our analysis in the *in silico* glucose-insulin simulator [Dalla Man et al., 2007] to serve as the platform for the *design-build-test* of cellular devices regulating glucose homeostasis. First, it was necessary to establish a new metric allowing to classify the cellular device performance and categorize the different device characteristics with its ability to regulate glycaemia. In that sense, our study was based on the well-established WHO criteria for diabetes mellitus.

Therefore, we have mathematically modelled two *in vitro* engineered and characterized cellular devices with the ability to i) secrete insulin in a constitutive manner or ii) glucose-regulated insulin secretion. The experimental approach was based on the ability of *HEK293T* cells to detect extracellular glucose [Kanari et al., 2013] and secrete an active

insulin hormone [Hay & Docherty, 2003] followed by cellular encapsulation and subcutaneous implantation.

Despite glucose-regulated insulin secretion is postulated as an autonomous mechanism for glucose homeostasis, constitutive insulin expression showed a better glucose restoration when compared to the glucose-dependent device. Within this particular dynamic, we have found that an insulin secretion time delay, an intrinsic characteristic exhibited by the chosen cellular type, accounts for a negative impact on glucose restoration, driving to hypoglycaemia scenarios. Therefore, we have explored the possibility of applying feed pattern modulations to benefit from implant delayed insulin secretion. Diet is a well-known disruptor for diabetes pathophysiology [Hajiaghaalipour et al., 2015; Russell et al., 2016] but also its had been explored in other high-society impact illness [Stower, 2019].

We have based our analysis in the optimization of dietary habits for plasma glucose regulation based on the recommended ingestion of carbohydrates rather than on the particular food. An evolutionary algorithm based on Darwinian Evolution allowed to optimize time and food consumption to find a time-restriction feed (TRF) diet. Hence, a combination of approaches based on implantable cellular insulin delivery together with TRF pattern results on a greater plasma glucose regulation therapy. Additionally, TRF therapy should also further be explored with already existing techniques such as insulin therapy, i.e. insulin injection or insulin pump. Overall, we have demonstrated that a combination of experimental evidence together with *in silico* computational simulations in a closed-loop scenario allows for a powerful platform to design application-based living biomedical devices.

6.3 Final considerations

The present PhD thesis hypothesized the use of biological elements to rationally design standard, robust and reliable biomedical living devices enabling the fine-tune management of closed-loop applications. By using a modular approach, we have analysed the four main functional-modules of a living biomedical device: i) the sensor module,

where the signal detection is done, ii) the processor module, where the external information is processed according to a pre-defined rule, iii) the actuator module, where the processed information is transformed into an output of interest and the iv) closed-loop performance, the embodiment of the living biomedical device into the real-application scenario. We have identified some of the limitations arising when applying synthetic biological approaches into living technologies and established some blueprints for adapting engineering approaches to biomedical applications. In that line, we have studied how to sense, integrate and respond to signals of interest re-engineering the cellular machinery from different experimental model organisms, i.e. *E. coli*, *S. cerevisiae*, mammalian *HEK293*, and applying mathematical tools. We have shown that device operating ranges can be tuned by re-engineering bacteria's two-component-sensors or with a multicellular approach, where information is codified in a unique signal. Moreover, this codification has exploited to accomplish either analogue or digital responses. However, the multicellular approach demands the physical separation in 2D of the engineered cellular types. To do so, one explored scenario is the development of a 2D surface or cellular encapsulation. Despite, the novelty of both approaches, further exploration should be addressed or even combined, for instance, cellular encapsulation would offer the possibility to isolate the different modules of a multicellular device. It is clear that the manufactured 2D surface would be considered as a diagnosis or monitoring platform, however, should be re-designed for treatment purposes. In that line, efforts should be done in the characterization of the suitable cellular embodiment, as the use of patients' cells [Jaén et al., 2017; Kochenderfer & Rosenberg, 2013], sophisticated 3D biocompatible devices [Bhattacharjee et al., 2016; Derakhshanfar et al., 2018] or the encapsulation of engineered cells [Xie et al., 2016]. And more important, evidencing the need to design cellular devices for closed-loop applications combining both experimental and computational approaches.

6.4 Main research findings

Objective 1: Explore the ability to create a living biomedical device using intrinsic cellular components.

Objective 1.1. Upon sensor module.

- We have designed a mathematical tool allowing to design biosensors architecture based on natural two-component systems to act in a pre-defined operating range.
- Our mathematical model describes the relationship between relative receptor abundance and biosensor key parameters: affinity, operating range, sensitivity.
- Our mathematical model allows defining the biosensors operating range in terms of relative receptor abundance.
- Our experimental results based the *E. coli* 3OSCHL-LuxR two component systems validate the proposed mathematical modelling.

Objective 1.2. Upon transducer module.

- We have developed a multicellular approximation encoding information in the modulation of a diffusible signal which contains three-main modules.
- Biological computation, either digital or analogue, was achieved by integrating multiple input signals in both *E. coli* and *S. cerevisiae* model organisms.
- Digital computation is accomplished by introducing a 2D surface and the geometrical arrangement of the engineered cell types as new computational elements.
- Digital computation is encoded in a multi-branch approximation enabling to map systematically any arbitrary digital computation.
- Digital computation was experimentally validated using *E. coli* model organism and using ara and aTc as signal inputs.
- Analogue computation was developed in a liquid environment with the co-existence of three engineered *S. cerevisiae* cell types.
- Analogue computation response is modulated, i.e. affinity and sensitivity, by the relative proportions of multicellular modules.

- Analogue computation allows to switch towards non-trivial dynamics, i.e. pulsatile-time response, modifying the modules composition.

Objective 1.3. Upon actuator module.

- We have developed a multicellular approximation able to detect and produce physiological signals in *S. cerevisiae*.
- A sensor layer detects different glucose concentrations.
- An effector layer produces and secretes insulin and glucagon hormones according to the detected inputs.

Objective 2: Explore the performance of the biomedical device in a close-loop scenario.

Objective 2.1. Upon biomedical device dynamics.

- We have developed an *in silico* platform enabling to test device performance in terms of plasma glucose regulation in diabetic organisms.
- Constitutive implant dynamics enable plasma glucose regulation.
- Time delay exhibited by the glucose-dependent cellular limits the glycaemia regulation either optimizing maximum or minimum plasma glucose levels.

Objective 2.2. Upon the patient daily-life routines.

- We have developed an *in silico* feed pattern optimizing plasma glucose regulation in diabetic organisms.

SCIENTIFIC PUBLICATIONS

During the three-year period of work within the Synthetic Biology for Biomedical Applications Lab the research main achievements were summed up on different research publications.

Eva Gonzalez-Flo, Maria Elisenda Alaball, Javier Macia. (2020). Two-component biosensors: unveiling the mechanisms of predictable tunability *ACS Synthetic Biology*, <https://doi.org/10.1021/acssynbio.0c00010>

Urrios*, **E. Gonzalez-Flo***, D. Canadell, E. de Nadal, J. Macia, and F. Posas. (2018). Plug-and-Play Multicellular Circuits with Time-Dependent Dynamic Responses. *ACS Synthetic Biology*, vol. 7, no. 4, pp. 1095–1104. <https://doi.org/10.1021/acssynbio.7b00463>

*Equal contribution.

BIBLIOGRAPHY

- Abramson, A., Caffarel-Salvador, E., Khang, M., Dellal, D., Silverstein, D., Gao, Y., Frederiksen, M. R., Vegge, A., Hubálek, F., Water, J. J., Friderichsen, A. V., Fels, J., Kirk, R. K., Cleveland, C., Collins, J., Tamang, S., Hayward, A., Landh, T., Buckley, S. T., ... Traverso, G. (2019). An ingestible self-orienting system for oral delivery of macromolecules. *Science*, *363*(6427), 611–615. <https://doi.org/10.1126/science.aau2277>
- Actobiotics. (2020). *Products / ActoBio*. <https://actobio.com/Home/Products>
- Ajikumar, P. K., Xiao, W. H., Tyo, K. E. J., Wang, Y., Simeon, F., Leonard, E., Mucha, O., Phon, T. H., Pfeifer, B., & Stephanopoulos, G. (2010). Isoprenoid pathway optimization for Taxol precursor overproduction in *Escherichia coli*. *Science*, *330*(6000), 70–74. <https://doi.org/10.1126/science.1191652>
- Alloush, H. M., Anderson, E., Martin, A. D., Ruddock, M. W., Angell, J. E., Hill, P. J., Mehta, P., Smith, M. A., Smith, J. G., & Salisbury, V. C. (2010). A bioluminescent microbial biosensor for in vitro pretreatment assessment of cytarabine efficacy in leukemia. *Clinical Chemistry*, *56*(12), 1862–1870. <https://doi.org/10.1373/clinchem.2010.145581>
- Alper, H., Fischer, C., Nevoigt, E., & Stephanopoulos, G. (2005). Tuning genetic control through promoter engineering. *Proceedings of the National Academy of Sciences of the United States of America*, *102*(36), 12678–12683. <https://doi.org/10.1073/pnas.0504604102>
- Amaro, F., Turkewitz, A. P., Martín-González, A., & Gutiérrez, J. C. (2011). Whole-cell biosensors for detection of heavy metal ions in environmental samples based on metallothionein promoters from *Tetrahymena thermophila*. *Microbial Biotechnology*, *4*(4), 513–522. <https://doi.org/10.1111/j.1751-7915.2011.00252.x>
- Amoyel, M., & Bach, E. A. (2014). Cell competition: How to eliminate your neighbours. In *Development (Cambridge)* (Vol. 141, Issue 5, pp. 988–1000). Oxford University Press for The Company of Biologists Limited. <https://doi.org/10.1242/dev.079129>
- Andersen, J. B., Sternberg, C., Poulsen, L. K., Bjørn, S. P., Givskov, M., & Molin, S. (1998). New unstable variants of green fluorescent protein for studies of transient
-

- gene expression in bacteria. *Applied and Environmental Microbiology*, 64(6), 2240–2246. <https://doi.org/10.1128/aem.64.6.2240-2246.1998>
- Anderson, J. C., Clarke, E. J., Arkin, A. P., & Voigt, C. A. (2006). Environmentally controlled invasion of cancer cells by engineered bacteria. *Journal of Molecular Biology*, 355(4), 619–627. <https://doi.org/10.1016/j.jmb.2005.10.076>
- Anderson, J. C., Voigt, C. A., & Arkin, A. P. (2007). Environmental signal integration by a modular and gate. *Molecular Systems Biology*, 3(133). <https://doi.org/10.1038/msb4100173>
- Andrianantoandro, E., Basu, S., Karig, D. K., & Weiss, R. (2006). Synthetic biology: New engineering rules for an emerging discipline. *Molecular Systems Biology*, 2. <https://doi.org/10.1038/msb4100073>
- Ang, J., Harris, E., Hussey, B. J., Kil, R., & McMillen, D. R. (2013). Tuning response curves for synthetic biology. *ACS Synthetic Biology*, 2(10), 547–567. <https://doi.org/10.1021/sb4000564>
- Annaluru, N., Muller, H., Mitchell, L. A., Ramalingam, S., Stracquandano, G., Richardson, S. M., Dymond, J. S., Kuang, Z., Scheifele, L. Z., Cooper, E. M., Cai, Y., Zeller, K., Agmon, N., Han, J. S., Hadjithomas, M., Tullman, J., Caravelli, K., Cirelli, K., Guo, Z., ... Chandrasegaran, S. (2014). Total synthesis of a functional designer eukaryotic chromosome. *Science*, 344(6179), 55–58. <https://doi.org/10.1126/science.1249252>
- Association, A. D. (2010). Diagnosis and classification of diabetes mellitus. In *Diabetes Care* (Vol. 33, Issue SUPPL. 1). American Diabetes Association. <https://doi.org/10.2337/dc10-S062>
- Ausländer, D., Ausländer, S., Charpin-El Hamri, G., Sedlmayer, F., Müller, M., Frey, O., Hierlemann, A., Stelling, J., & Fussenegger, M. (2014). A synthetic multifunctional mammalian pH sensor and CO₂ transgene-control device. *Molecular Cell*, 55(3), 397–408. <https://doi.org/10.1016/j.molcel.2014.06.007>
- Baeshen, N. A., Baeshen, M. N., Sheikh, A., Bora, R. S., Ahmed, M. M. M., Ramadan, H. A. I., Saini, K. S., & Redwan, E. M. (2014). Cell factories for insulin production. *Microbial Cell Factories*, 13(1). <https://doi.org/10.1186/s12934-014-0141-0>
- Bakke, I., Berg, L., Aune, T. E. V., Brautaset, T., Sletta, H., Tøndervik, A., & Valla, S. (2009). Random mutagenesis of the P_m promoter as a powerful strategy for

-
- improvement of recombinant-gene expression. *Applied and Environmental Microbiology*, 75(7), 2002–2011. <https://doi.org/10.1128/AEM.02315-08>
- Balasubramanian, S., Aubin-Tam, M. E., & Meyer, A. S. (2019). 3D Printing for the Fabrication of Biofilm-Based Functional Living Materials. In *ACS Synthetic Biology* (Vol. 8, Issue 7, pp. 1564–1567). American Chemical Society. <https://doi.org/10.1021/acssynbio.9b00192>
- Balázsi, G., Barabási, A. L., & Oltvai, Z. N. (2005). Topological units of environmental signal processing in the transcriptional regulatory network of *Escherichia coli*. *Proceedings of the National Academy of Sciences of the United States of America*, 102(22), 7841–7846. <https://doi.org/10.1073/pnas.0500365102>
- Banica, F.-G. (2012). *Chemical sensors and biosensors : fundamentals and applications*. John Wiley & Sons Inc.
- Bardwell, L. (2005). A walk-through of the yeast mating pheromone response pathway. In *Peptides* (Vol. 26, Issue 2, pp. 339–350). Elsevier Inc. <https://doi.org/10.1016/j.peptides.2004.10.002>
- Barrangou, R., Fremaux, C., Deveau, H., Richards, M., Boyaval, P., Moineau, S., Romero, D. A., & Horvath, P. (2007). CRISPR provides acquired resistance against viruses in prokaryotes. *Science*, 315(5819), 1709–1712. <https://doi.org/10.1126/science.1138140>
- Basu, S., Gerchman, Y., Collins, C. H., Arnold, F. H., & Weiss, R. (2005). A synthetic multicellular system for programmed pattern formation. *Nature*, 434(7037), 1130–1134. <https://doi.org/10.1038/nature03461>
- Bauri, K., Nandi, M., & De, P. (2018). Amino acid-derived stimuli-responsive polymers and their applications. In *Polymer Chemistry* (Vol. 9, Issue 11, pp. 1257–1287). Royal Society of Chemistry. <https://doi.org/10.1039/c7py02014g>
- Bayer, T. S., & Smolke, C. D. (2005). Programmable ligand-controlled riboregulators of eukaryotic gene expression. *Nature Biotechnology*, 23(3), 337–343. <https://doi.org/10.1038/nbt1069>
- Becskei, A., & Serrano, L. (2000). Engineering stability in gene networks by autoregulation. *Nature*, 405(6786), 590–593. <https://doi.org/10.1038/35014651>
- Bedau, M. A., McCaskill, J. S., Packard, N. H., & Rasmussen, S. (2010). Living technology: Exploiting life's principles in technology. *Artificial Life*, 16(1), 89–97.
-

- <https://doi.org/10.1162/artl.2009.16.1.16103>
- Beggah, S., Vogne, C., Zenaro, E., & Van Der Meer, J. R. (2008). Mutant HbpR transcription activator isolation for 2-chlorobiphenyl via green fluorescent protein-based flow cytometry and cell sorting. *Microbial Biotechnology*, 1(1), 68–78. <https://doi.org/10.1111/j.1751-7915.2007.00008.x>
- Bender, E. A., & Williamson, S. G. (Stanley G. (2005). *A short course in discrete mathematics*. Dover Publications.
- Benner, S. A. (2003). Act natural. In *Nature* (Vol. 421, Issue 6919, p. 118). Nature Publishing Group. <https://doi.org/10.1038/421118a>
- Benner, S. A., & Sismour, A. M. (2005). Synthetic biology. In *Nature Reviews Genetics* (Vol. 6, Issue 7, pp. 533–543). Nature Publishing Group. <https://doi.org/10.1038/nrg1637>
- Beyer, P. (2010). Golden Rice and “Golden” crops for human nutrition. In *New Biotechnology* (Vol. 27, Issue 5, pp. 478–481). Elsevier. <https://doi.org/10.1016/j.nbt.2010.05.010>
- Bhattacharjee, N., Urrios, A., Kang, S., & Folch, A. (2016). The upcoming 3D-printing revolution in microfluidics. In *Lab on a Chip* (Vol. 16, Issue 10, pp. 1720–1742). Royal Society of Chemistry. <https://doi.org/10.1039/c6lc00163g>
- Blattner, F. R., Plunkett, G., Bloch, C. A., Perna, N. T., Burland, V., Riley, M., Collado-Vides, J., Glasner, J. D., Rode, C. K., Mayhew, G. F., Gregor, J., Davis, N. W., Kirkpatrick, H. A., Goeden, M. A., Rose, D. J., Mau, B., & Shao, Y. (1997). The complete genome sequence of Escherichia coli K-12. In *Science* (Vol. 277, Issue 5331, pp. 1453–1462). <https://doi.org/10.1126/science.277.5331.1453>
- Bojar, D., Scheller, L., Hamri, G. C. El, Xie, M., & Fussenegger, M. (2018). Caffeine-inducible gene switches controlling experimental diabetes. *Nature Communications*, 9(1). <https://doi.org/10.1038/s41467-018-04744-1>
- Bousse, L. (1996). Whole cell biosensors. *Sensors and Actuators, B: Chemical*, 34(1–3), 270–275. [https://doi.org/10.1016/S0925-4005\(96\)01906-5](https://doi.org/10.1016/S0925-4005(96)01906-5)
- Bouwens, L., Houbracken, I., & Mfopou, J. K. (2013). The use of stem cells for pancreatic regeneration in diabetes mellitus. In *Nature Reviews Endocrinology* (Vol. 9, Issue 10, pp. 598–606). <https://doi.org/10.1038/nrendo.2013.145>
- Brewster, R. C., Jones, D. L., & Phillips, R. (2012). Tuning Promoter Strength through

-
- RNA Polymerase Binding Site Design in Escherichia coli. *PLoS Computational Biology*, 8(12), e1002811. <https://doi.org/10.1371/journal.pcbi.1002811>
- Brophy, J. A., & Voigt, C. A. (2016). Antisense transcription as a tool to tune gene expression. *Molecular Systems Biology*, 12(1), 854. <https://doi.org/10.15252/msb.20156540>
- Brouns, S. J. J., Jore, M. M., Lundgren, M., Westra, E. R., Slijkhuis, R. J. H., Snijders, A. P. L., Dickman, M. J., Makarova, K. S., Koonin, E. V., & Van Der Oost, J. (2008). Small CRISPR RNAs guide antiviral defense in prokaryotes. *Science*, 321(5891), 960–964. <https://doi.org/10.1126/science.1159689>
- Brown, B. D., Gentner, B., Cantore, A., Colleoni, S., Amendola, M., Zingale, A., Baccarini, A., Lazzari, G., Galli, C., & Naldini, L. (2007). Endogenous microRNA can be broadly exploited to regulate transgene expression according to tissue, lineage and differentiation state. *Nature Biotechnology*, 25(12), 1457–1467. <https://doi.org/10.1038/nbt1372>
- Brown, S. A., Kovatchev, B. P., Raghinaru, D., Lum, J. W., Buckingham, B. A., Kudva, Y. C., Laffel, L. M., Levy, C. J., Pinsker, J. E., Wadwa, R. P., Dassau, E., Doyle, F. J., Anderson, S. M., Church, M. M., Dadlani, V., Ekhlaspour, L., Forlenza, G. P., Isganaitis, E., Lam, D. W., ... Beck, R. W. (2019). Six-month randomized, multicenter trial of closed-loop control in type 1 diabetes. *New England Journal of Medicine*, 381(18), 1707–1717. <https://doi.org/10.1056/NEJMoa1907863>
- Brun, M. A., Griss, R., Reymond, L., Tan, K. T., Piguet, J., Peters, R. J. R. W., Vogel, H., & Johnsson, K. (2011). Semisynthesis of fluorescent metabolite sensors on cell surfaces. *Journal of the American Chemical Society*, 133(40), 16235–16242. <https://doi.org/10.1021/ja206915m>
- Callejas, D., Mann, C. J., Ayuso, E., Lage, R., Grifoll, I., Roca, C., Andaluz, A., Ruiz-de Gopegui, R., Montané, J., Muñoz, S., Ferre, T., Haurigot, V., Zhou, S., Ruberte, J., Mingozzi, F., High, K. A., Garcia, F., & Bosch, F. (2013). Treatment of diabetes and long-term survival after insulin and glucokinase gene therapy. *Diabetes*, 62(5), 1718–1729. <https://doi.org/10.2337/db12-1113>
- Canton, B., Labno, A., & Endy, D. (2008). Refinement and standardization of synthetic biological parts and devices. In *Nature Biotechnology* (Vol. 26, Issue 7, pp. 787–793). <https://doi.org/10.1038/nbt1413>
-

- Carbonell-Ballester, M., Garcia-Ramallo, E., Montã Nez, R., Rodriguez-Caso, C., & Macía, J. (2016). Dealing with the genetic load in bacterial synthetic biology circuits: convergences with the Ohm's law. *Nucleic Acids Research*, *44*(1), 496–507. <https://doi.org/10.1093/nar/gkv1280>
- Carbonell-Ballester, Max, Duran-Nebreda, S., Montañez, R., Solé, R., Macía, J., & Rodríguez-Caso, C. (2014). A bottom-up characterization of transfer functions for synthetic biology designs: Lessons from enzymology. *Nucleic Acids Research*, *42*(22), 14060–14069. <https://doi.org/10.1093/nar/gku964>
- Carbonell, X., Corchero, J. L., Cubarsí, R., Vila, P., & Villaverde, A. (2002). Control of *Escherichia coli* growth rate through cell density. *Microbiological Research*, *157*(4), 257–265. <https://doi.org/10.1078/0944-5013-00167>
- Carpenter, A. C., Paulsen, I. T., & Williams, T. C. (2018). Blueprints for biosensors: Design, limitations, and applications. *Genes*, *9*(8). <https://doi.org/10.3390/genes9080375>
- Cayron, J., Prudent, E., Escoffier, C., Gueguen, E., Mandrand-Berthelot, M. A., Pignol, D., Garcia, D., & Rodrigue, A. (2017). Pushing the limits of nickel detection to nanomolar range using a set of engineered bioluminescent *Escherichia coli*. *Environmental Science and Pollution Research*, *24*(1), 4–14. <https://doi.org/10.1007/s11356-015-5580-6>
- Chan, A. Y. K. (2008). *Biomedical Device Technology: Principles and Design: Vol. Second edi.*
- Chang, H.-J. J., Voyvodic, P. L., Zuñiga, A., & Bonnet, J. (2017). Microbially derived biosensors for diagnosis, monitoring and epidemiology. *Microbial Biotechnology*, *10*(5), 1031–1035. <https://doi.org/10.1111/1751-7915.12791>
- Chang, H.-J., Mayonove, P., Zavala, A., De Visch, A., Minard, P., Cohen-Gonsaud, M., & Bonnet, J. (2018). A Modular Receptor Platform To Expand the Sensing Repertoire of Bacteria. *ACS Synthetic Biology*, *7*(1), 166–175. <https://doi.org/10.1021/acssynbio.7b00266>
- Chappell, J., Jensen, K., & Freemont, P. S. (2013). Validation of an entirely in vitro approach for rapid prototyping of DNA regulatory elements for synthetic biology. *Nucleic Acids Research*, *41*(5), 3471–3481. <https://doi.org/10.1093/nar/gkt052>
- Chen, S.-Y., Wei, W., Yin, B.-C., Tong, Y., Lu, J., & Ye, B.-C. (2019). *Development of*

-
- a Highly Sensitive Whole-Cell Biosensor for Arsenite Detection through Engineered Promoter Modifications*. <https://doi.org/10.1021/acssynbio.9b00093>
- Chen, Y., Ho, J. M. L., Shis, D. L., Gupta, C., Long, J., Wagner, D. S., Ott, W., Josić, K., & Bennett, M. R. (2018). Tuning the dynamic range of bacterial promoters regulated by ligand-inducible transcription factors. *Nature Communications*, 9(1), 1–8. <https://doi.org/10.1038/s41467-017-02473-5>
- Chen, Y. Y., Galloway, K. E., & Smolke, C. D. (2012). Synthetic biology: Advancing biological frontiers by building synthetic systems. In *Genome Biology* (Vol. 13, Issue 2, p. 240). <https://doi.org/10.1186/gb-2012-13-2-240>
- Chen, Z., Wang, J., Sun, W., Archibong, E., Kahkoska, A. R., Zhang, X., Lu, Y., Ligler, F. S., Buse, J. B., & Gu, Z. (2018). Synthetic beta cells for fusion-mediated dynamic insulin secretion. *Nature Chemical Biology*, 14(1), 86–93. <https://doi.org/10.1038/nchembio.2511>
- Chong, H., & Ching, C. B. (2016). Development of Colorimetric-Based Whole-Cell Biosensor for Organophosphorus Compounds by Engineering Transcription Regulator DmpR. *ACS Synthetic Biology*, 5(11), 1290–1298. <https://doi.org/10.1021/acssynbio.6b00061>
- Courbet, A., Endy, D., Renard, E., Molina, F., & Bonnet, J. (2015). Detection of pathological biomarkers in human clinical samples via amplifying genetic switches and logic gates. *Science Translational Medicine*, 7(289). <https://doi.org/10.1126/scitranslmed.aaa3601>
- Crawley, N., Thompson, M., & Romaschin, A. (2014). Theranostics in the growing field of personalized medicine: An analytical chemistry perspective. In *Analytical Chemistry* (Vol. 86, Issue 1, pp. 130–160). American Chemical Society. <https://doi.org/10.1021/ac4038812>
- Crick, F. (1970). Central dogma of molecular biology. *Nature*, 227(5258), 561–563. <https://doi.org/10.1038/227561a0>
- Culler, S. J., Hoff, K. G., & Smolke, C. D. (2010). Reprogramming cellular behavior with RNA controllers responsive to endogenous proteins. *Science*, 330(6008), 1251–1255. <https://doi.org/10.1126/science.1192128>
- Dalla Man, C., Micheletto, F., Lv, D., Breton, M., Kovatchev, B., & Cobelli, C. (2014). The UVA/PADOVA type 1 diabetes simulator: New features. *Journal of Diabetes*
-

- Science and Technology*, 8(1), 26–34. <https://doi.org/10.1177/1932296813514502>
- Dalla Man, C., Rizza, R. A., & Cobelli, C. (2007). Meal simulation model of the glucose-insulin system. *IEEE Transactions on Biomedical Engineering*, 54(10), 1740–1749. <https://doi.org/10.1109/TBME.2007.893506>
- Daniel, R., Rubens, J. R., Sarpeshkar, R., & Lu, T. K. (2013). *Synthetic analog computation in living cells*. <https://doi.org/10.1038/nature12148>
- Danino, T., Prindle, A., Kwong, G. A., Skalak, M., Li, H., Allen, K., Hasty, J., & Bhatia, S. N. (2015). Programmable probiotics for detection of cancer in urine. *Science Translational Medicine*, 7(289), 1–12. <https://doi.org/10.1126/scitranslmed.aaa3519>
- Derakhshanfar, S., Mbeleck, R., Xu, K., Zhang, X., Zhong, W., & Xing, M. (2018). 3D bioprinting for biomedical devices and tissue engineering: A review of recent trends and advances. In *Bioactive Materials* (Vol. 3, Issue 2, pp. 144–156). KeAi Communications Co. <https://doi.org/10.1016/j.bioactmat.2017.11.008>
- Diafa, S., & Hollenstein, M. (2015). Generation of Aptamers with an Expanded Chemical Repertoire. *Molecules*, 20(9), 16643–16671. <https://doi.org/10.3390/molecules200916643>
- Dincer, C., Bruch, R., Costa-Rama, E., Fernández-Abedul, M. T., Merkoçi, A., Manz, A., Urban, G. A., & Güder, F. (2019). Disposable Sensors in Diagnostics, Food, and Environmental Monitoring. *Advanced Materials*, 31(30), 1806739. <https://doi.org/10.1002/adma.201806739>
- Dong, Y.-H. (2000). AiiA, an enzyme that inactivates the acylhomoserine lactone quorum-sensing signal and attenuates the virulence of *Erwinia carotovora*. *Proceedings of the National Academy of Sciences*, 97(7), 3526–3531. <https://doi.org/10.1073/pnas.060023897>
- Duan, Y., Ye, F., Huang, Y., Qin, Y., He, C., & Zhao, S. (2018). One-pot synthesis of a metal-organic framework-based drug carrier for intelligent glucose-responsive insulin delivery. *Chemical Communications*, 54(42), 5377–5380. <https://doi.org/10.1039/c8cc02708k>
- Eberhard, A., Burlingame, A. L., Eberhard, C., Kenyon, G. L., Nealson, K. H., & Oppenheimer, N. J. (1981). Structural Identification of Autoinducer of *Photobacterium fischeri* Luciferase. *Biochemistry*, 20(9), 2444–2449.
-

-
- <https://doi.org/10.1021/bi00512a013>
- Ed. Malek, I. (1964). *Continuous Cultivation of Microorganisms*. Ed. Malek, I. (M. I. (ed.)). Academic Press.
- Eiben, A. E., & Smith, J. E. (2003). *Natural Computing Series Introduction to Evolutionary Computing* (G. Rozenberg & Th. Bäck A.E. Eiben J.N. Kok H.P. Spaink (eds.)). Springer-Verlag. www.springer.com/series/
- Ellis, T., Adie, T., & Baldwin, G. S. (2011). DNA assembly for synthetic biology: from parts to pathways and beyond. *Integrative Biology*, 3(2), 109–118. <https://doi.org/10.1039/c0ib00070a>
- Elowitz, M. B., & Leibler, S. (2000). A synthetic oscillatory network of transcriptional regulators. *Nature*, 403(6767), 335–338. <https://doi.org/10.1038/35002125>
- Endy, D. (2005). Foundations for engineering biology. *Nature*, 438(7067), 449–453. <https://doi.org/10.1038/nature04342>
- Engelbrecht, J. A., & Silverman, M. (1984). Identification of genes and gene products necessary for bacterial bioluminescence. *Proceedings of the National Academy of Sciences of the United States of America*, 81(13 I), 4154–4158. <https://doi.org/10.1073/pnas.81.13.4154>
- Ento, L. (2006). *Encyclopedia of sensors*. Vol. 7 (A. S. Publishers. (ed.)). Publishers., American Scientific.
- Eugenia Inda, M., Mimeo, M., & Lu, T. K. (2019). Cell-based biosensors for immunology, inflammation, and allergy. *Journal of Allergy and Clinical Immunology*, 144, 645–647. <https://doi.org/10.1016/j.jaci.2019.07.024>
- Farzadfard, F., & Lu, T. K. (2014). Genomically encoded analog memory with precise in vivo dna writing in living cell populations. *Science*, 346(6211). <https://doi.org/10.1126/science.1256272>
- Fernandez-Rodriguez, J., & Voigt, C. A. (2016). Post-translational control of genetic circuits using Potyvirus proteases. *Nucleic Acids Research*, 44(13), 6493–6502. <https://doi.org/10.1093/nar/gkw537>
- Foecking, M. K., & Hofstetter, H. (1986). Powerful and versatile enhancer-promoter unit for mammalian expression vectors. *Gene*, 45(1), 101–105. [https://doi.org/10.1016/0378-1119\(86\)90137-X](https://doi.org/10.1016/0378-1119(86)90137-X)
- Folcher, M., & Fussenegger, M. (2012). Synthetic biology advancing clinical
-

- applications. *Current Opinion in Chemical Biology*, 16(3–4), 345–354. <https://doi.org/10.1016/j.cbpa.2012.06.008>
- Friedland, A. E., Lu, T. K., Wang, X., Shi, D., Church, G., & Collins, J. J. (2009). Synthetic gene networks that count. *Science*, 324(5931), 1199–1202. <https://doi.org/10.1126/science.1172005>
- Froese, T. (2014). Bio-machine Hybrid Technology: A Theoretical Assessment and Some Suggestions for Improved Future Design. *Philosophy and Technology*, 27(4), 539–560. <https://doi.org/10.1007/s13347-013-0130-y>
- Fuentes, P., Zhou, F., Erban, A., Karcher, D., Kopka, J., & Bock, R. (2016). A new synthetic biology approach allows transfer of an entire metabolic pathway from a medicinal plant to a biomass crop. *Elifesciences.Org*. <https://doi.org/10.7554/eLife.13664.001>
- Fuqua, W. C., Winans, S. C., & Peter Greenberg², E. (1994). MINIREVIEW Quorum Sensing in Bacteria: the LuxR-LuxI Family of Cell Density-Responsive Transcriptional Regulators. In *JOURNAL OF BACTERIOLOGY* (Vol. 176, Issue 2).
- Furukawa, K., & Hohmann, S. (2015). A fungicide-responsive kinase as a tool for synthetic cell fate regulation. *Nucleic Acids Research*, 43(14), 7162–7170. <https://doi.org/10.1093/nar/gkv678>
- Garcia-Ojalvo, J., Elowitz, M. B., & Strogatz, S. H. (2004). Modeling a synthetic multicellular clock: Repressilators coupled by quorum sensing. *Proceedings of the National Academy of Sciences of the United States of America*, 101(30), 10955–10960. <https://doi.org/10.1073/pnas.0307095101>
- Gardner, T. S., Cantor, C. R., & Collins, J. J. (2000). Construction of a genetic toggle switch in *Escherichia coli*. *Nature*, 403(6767), 339–342. <https://doi.org/10.1038/35002131>
- Gibson, D. G., Young, L., Chuang, R. Y., Venter, J. C., Hutchison, C. A., & Smith, H. O. (2009). Enzymatic assembly of DNA molecules up to several hundred kilobases. *Nature Methods*, 6(5), 343–345. <https://doi.org/10.1038/nmeth.1318>
- Gil, R., Silva, F. J., Pereto, J., & Moya, A. (2004). Determination of the Core of a Minimal Bacterial Gene Set. *Microbiology and Molecular Biology Reviews*, 68(3), 518–537. <https://doi.org/10.1128/mubr.68.3.518-537.2004>
-

-
- Goffeau, A., Barrell, G., Bussey, H., Davis, R. W., Dujon, B., Feldmann, H., Galibert, F., Hoheisel, J. D., Jacq, C., Johnston, M., Louis, E. J., Mewes, H. W., Murakami, Y., Philippsen, P., Tettelin, H., & Oliver, S. G. (1996). Life with 6000 genes. *Science*, 274(5287), 546–567. <https://doi.org/10.1126/science.274.5287.546>
- Gonzalez-Flo, E., Alaball, M. E., & Macia, J. (2020). Two-Component Biosensors: Unveiling the Mechanisms of Predictable Tunability. *ACS Synthetic Biology*, acssynbio.0c00010. <https://doi.org/10.1021/acssynbio.0c00010>
- Green, A. A., Kim, J., Ma, D., Silver, P. A., Collins, J. J., & Yin, P. (2017). Complex cellular logic computation using ribocomputing devices. *Nature*, 548(7665), 117–121. <https://doi.org/10.1038/nature23271>
- Griss, R., Schena, A., Reymond, L., Patiny, L., Werner, D., Tinberg, C. E., Baker, D., & Johnsson, K. (2014). Bioluminescent sensor proteins for point-of-care therapeutic drug monitoring. *Nature Chemical Biology*, 10(7), 598–603. <https://doi.org/10.1038/nchembio.1554>
- Groth, A. C., & Calos, M. P. (2004). Phage integrases: Biology and applications. In *Journal of Molecular Biology* (Vol. 335, Issue 3, pp. 667–678). Academic Press. <https://doi.org/10.1016/j.jmb.2003.09.082>
- Guet, C. C., Elowitz, M. B., Hsing, W., & Leibler, S. (2002). Combinatorial synthesis of genetic networks. *Science*, 296(5572), 1466–1470. <https://doi.org/10.1126/science.1067407>
- Gutiérrez, J. C., Amaro, F., & Martín-González, A. (2015). Heavy metal whole-cell biosensors using eukaryotic microorganisms: An updated critical review. In *Frontiers in Microbiology* (Vol. 6, Issue FEB). Frontiers Media S.A. <https://doi.org/10.3389/fmicb.2015.00048>
- Hajiaghaalipour, F., Khalilpourfarshbafi, M., Arya, A., & Arya, A. (2015). Modulation of glucose transporter protein by dietary flavonoids in type 2 diabetes mellitus. *International Journal of Biological Sciences*, 11(5), 508–524. <https://doi.org/10.7150/ijbs.11241>
- Hakkila, K., Maksimow, M., Karp, M., & Virta, M. (2002). Reporter genes lucFF, luxCDABE, gfp, and dsred have different characteristics in whole-cell bacterial sensors. *Analytical Biochemistry*, 301(2), 235–242. <https://doi.org/10.1006/abio.2001.5517>
-

- Harder, E. L. (1959). Digital versus analog computation. *Mathematics and Computers in Simulation*, *1*(6), 298–300. [https://doi.org/10.1016/S0378-4754\(59\)80025-2](https://doi.org/10.1016/S0378-4754(59)80025-2)
- Hasty, J., McMillen, D., Isaacs, F., & Collins, J. J. (2001). Computational studies of gene regulatory networks: In numero molecular biology. In *Nature Reviews Genetics* (Vol. 2, Issue 4, pp. 268–279). Nature Publishing Group. <https://doi.org/10.1038/35066056>
- Hay, C. W., & Docherty, K. (2003). Enhanced expression of a furin-cleavable proinsulin. *Journal of Molecular Endocrinology*, *31*(3), 597–607. <https://doi.org/10.1677/jme.0.0310597>
- Hellström, P. M., Grybäck, P., & Jacobsson, H. (2006). The physiology of gastric emptying. In *Best Practice and Research: Clinical Anaesthesiology* (Vol. 20, Issue 3, pp. 397–407). <https://doi.org/10.1016/j.bpa.2006.02.002>
- Hicks, M., Bachmann, T.T., Wang, B. (2019). Synthetic Biology enables programmable cell-based biosensors. *ChemPhysChem*, *20*, 1–14.
- Hill, F. J., & Peterson, G. R. (1981). *Introduction to switching theory and logical design*. Wiley.
- Hoffman-Sommer, M. (2012). Cell-to-cell communication circuits: quantitative analysis of synthetic logic gates. *Frontiers in Physiology*, *3*, 287. <https://doi.org/10.3389/fphys.2012.00287>
- Hopfield, J. J. (1994). Physics, computation, and why biology looks so different. *Journal of Theoretical Biology*, *171*(1), 53–60. <https://doi.org/10.1006/jtbi.1994.1211>
- Hunsicker, A., Steber, M., Mayer, G., Meitert, J., Klotzsche, M., Blind, M., Hillen, W., Berens, C., & Suess, B. (2009). An RNA Aptamer that Induces Transcription. *Chemistry and Biology*, *16*(2), 173–180. <https://doi.org/10.1016/j.chembiol.2008.12.008>
- Hutchison, C. A., Chuang, R.-Y., Noskov, V. N., Assad-Garcia, N., Deerinck, T. J., Ellisman, M. H., Gill, J., Kannan, K., Karas, B. J., Ma, L., Pelletier, J. F., Qi, Z.-Q., Richter, R. A., Strychalski, E. A., Sun, L., Suzuki, Y., Tsvetanova, B., Wise, K. S., Smith, H. O., ... Venter, J. C. (2016). Design and synthesis of a minimal bacterial genome. *Science*, *351*(6280), aad6253–aad6253. <https://doi.org/10.1126/science.aad6253>
- Ideker, T., Thorsson, V., Ranish, J. A., Christmas, R., Buhler, J., Eng, J. K., Bumgarner,

-
- R., Goodlett, D. R., Aebersold, R., & Hood, L. (2001). Integrated genomic and proteomic analyses of a systematically perturbed metabolic network. *Science*, 292(5518), 929–934. <https://doi.org/10.1126/science.292.5518.929>
- Ingalls, B. (2012). *Mathematical Modelling in Systems Biology: An Introduction*.
- Isaacs, F. J., Dwyer, D. J., Ding, C., Pervouchine, D. D., Cantor, C. R., & Collins, J. J. (2004). Engineered riboregulators enable post-transcriptional control of gene expression. *Nature Biotechnology*, 22(7), 841–847. <https://doi.org/10.1038/nbt986>
- Jäckel, C., & Hilvert, D. (2010). Biocatalysts by evolution. In *Current Opinion in Biotechnology* (Vol. 21, Issue 6, pp. 753–759). Elsevier Current Trends. <https://doi.org/10.1016/j.copbio.2010.08.008>
- Jaén, M. L., Vilà, L., Elias, I., Jimenez, V., Rodó, J., Maggioni, L., Ruiz-de Gopegui, R., Garcia, M., Muñoz, S., Callejas, D., Ayuso, E., Ferré, T., Grifoll, I., Andaluz, A., Ruberte, J., Haurigot, V., & Bosch, F. (2017). Long-Term Efficacy and Safety of Insulin and Glucokinase Gene Therapy for Diabetes: 8-Year Follow-Up in Dogs. *Molecular Therapy - Methods and Clinical Development*, 6, 1–7. <https://doi.org/10.1016/j.omtm.2017.03.008>
- Jeelani, S., Jagat Reddy, R. C., Maheswaran, T., Asokan, G. S., Dany, A., & Anand, B. (2014). Theranostics: A treasured tailor for tomorrow. In *Journal of Pharmacy and Bioallied Sciences* (Vol. 6, Issue SUPPL. 1, pp. S6-8). Medknow Publications. <https://doi.org/10.4103/0975-7406.137249>
- Jefferson, C., Lentzos, F., & Marris, C. (2014). Synthetic Biology and Biosecurity: Challenging the “myths.” *Frontiers in Public Health*, 2(AUG), 115. <https://doi.org/10.3389/fpubh.2014.00115>
- Jeong, H., Tombor, B., Albert, R., Oltval, Z. N., & Barabási, A. L. (2000). The large-scale organization of metabolic networks. *Nature*, 407(6804), 651–654. <https://doi.org/10.1038/35036627>
- Jia, X., Bu, R., Zhao, T., & Wu, K. (2019). Sensitive and Specific Whole-Cell Biosensor for Arsenic Detection ENVIRONMENTAL MICROBIOLOGY crossm Downloaded from. *Aem.Asm.Org 1 Applied and Environmental Microbiology*, 85, 694–713. <https://doi.org/10.1128/AEM>
- Jin, M., Errede, B., Behar, M., Mather, W., Nayak, S., Hasty, J., Dohlman, H. G., & Elston, T. C. (2011). Yeast dynamically modify their environment to achieve better
-

- mating efficiency. *Science Signaling*, 4(186), ra54. <https://doi.org/10.1126/scisignal.2001763>
- Johns, N. I., Gomes, A. L. C., Yim, S. S., Yang, A., Blazejewski, T., Smillie, C. S., Smith, M. B., Alm, E. J., Kosuri, S., & Wang, H. H. (2018). Metagenomic mining of regulatory elements enables programmable species-selective gene expression. *Nature Methods*, 15(5), 323–329. <https://doi.org/10.1038/nmeth.4633>
- Johnson, L., Shen, A., Boyle, L., Kunich, J., Pandey, K., Lemmon, M., Hermiston, T., Giedlin, M., McCormick, F., & Fattaey, A. (2002). Selectively replicating adenoviruses targeting deregulated E2F activity are potent, systemic antitumor agents. *Cancer Cell*, 1(4), 325–337. [https://doi.org/10.1016/s1535-6108\(02\)00060-0](https://doi.org/10.1016/s1535-6108(02)00060-0)
- Joshi, N., Wang, X., Montgomery, L., Elfick, A., & French, C. E. (2009). Novel approaches to biosensors for detection of arsenic in drinking water. *Desalination*, 248(1–3), 517–523. <https://doi.org/10.1016/j.desal.2008.05.096>
- Kærn, M., Blake, W. J., & Collins, J. J. (2003). The Engineering of Gene Regulatory Networks. *Annual Review of Biomedical Engineering*, 5(1), 179–206. <https://doi.org/10.1146/annurev.bioeng.5.040202.121553>
- Kalra, S., Mukherjee, J., Ramachandran, A., Saboo, B., Shaikh, S., Venkataraman, S., Bantwal, G., & Das, A. (2013). Hypoglycemia: The neglected complication. *Indian Journal of Endocrinology and Metabolism*, 17(5), 819. <https://doi.org/10.4103/2230-8210.117219>
- Kanari, Y., Sato, Y., Aoyama, S., & Muta, T. (2013). Thioredoxin-Interacting Protein Gene Expression via MondoA Is Rapidly and Transiently Suppressed during Inflammatory Responses. *PLoS ONE*, 8(3), e59026. <https://doi.org/10.1371/journal.pone.0059026>
- Karges, B., Schwandt, A., Heidtmann, B., Kordonouri, O., Binder, E., Schierloh, U., Boettcher, C., Kapellen, T., Rosenbauer, J., & Holl, R. W. (2017). Association of insulin pump therapy vs insulin injection therapy with severe hypoglycemia, ketoacidosis, and glycemic control among children, adolescents, and young adults with type 1 diabetes. *JAMA - Journal of the American Medical Association*, 318(14), 1358–1366. <https://doi.org/10.1001/jama.2017.13994>
- Karnaugh, M. (2013). The map method for synthesis of combinational logic circuits.
-

-
- Transactions of the American Institute of Electrical Engineers, Part I: Communication and Electronics*, 72(5), 593–599.
<https://doi.org/10.1109/tce.1953.6371932>
- Kelly, J. R., Rubin, A. J., Davis, J. H., Ajo-Franklin, C. M., Cumbers, J., Czar, M. J., de Mora, K., Gliberman, A. L., Monie, D. D., & Endy, D. (2009). Measuring the activity of BioBrick promoters using an in vivo reference standard. *Journal of Biological Engineering*, 3, 1–13. <https://doi.org/10.1186/1754-1611-3-4>
- Kemmer, C., Gitzinger, M., Daoud-El Baba, M., Djonov, V., Stelling, J., & Fussenegger, M. (2010). Self-sufficient control of urate homeostasis in mice by a synthetic circuit. *Nature Biotechnology*, 28(4), 355–360. <https://doi.org/10.1038/nbt.1617>
- Khalil, A. S., & Collins, J. J. (2010). Memory elements Synthetic biology: applications come of age. *Nature Publishing Group*, 11, 367. <https://doi.org/10.1038/nrg2775>
- Khan, S., Lorenzelli, L., & Dahiya, R. S. (2015). Technologies for printing sensors and electronics over large flexible substrates: A review. *IEEE Sensors Journal*, 15(6), 3164–3185. <https://doi.org/10.1109/JSEN.2014.2375203>
- Khlebnikov, A., Risa, Skaug, T., Carrier, T. A., & Keasling, J. D. (2000). Regulatable arabinose-inducible gene expression system with consistent control in all cells of a culture. *Journal of Bacteriology*, 182(24), 7029–7034. <https://doi.org/10.1128/JB.182.24.7029-7034.2000>
- Kim, J. H., Roy, A., Jouandot, D., & Cho, K. H. (2013). The glucose signaling network in yeast. In *Biochimica et Biophysica Acta - General Subjects* (Vol. 1830, Issue 11, pp. 5204–5210). Elsevier Inc. <https://doi.org/10.1016/j.bbagen.2013.07.025>
- Kim, Y. G., & Chandrasegaran, S. (1994). Chimeric restriction endonuclease. *Proceedings of the National Academy of Sciences of the United States of America*, 91(3), 883–887. <https://doi.org/10.1073/pnas.91.3.883>
- Kjeldsen, T., Ludvigsen, S., Diers, I., Balschmidt, P., Sorensen, A. R., & Kaarsholm, N. C. (2002). Engineering-enhanced protein secretory expression in yeast with application to insulin. *Journal of Biological Chemistry*, 277(21), 18245–18248. <https://doi.org/10.1074/jbc.C200137200>
- Koch, A. L. (1970). Turbidity measurements of bacterial cultures in some available commercial instruments. *Analytical Biochemistry*, 38(1), 252–259. [https://doi.org/10.1016/0003-2697\(70\)90174-0](https://doi.org/10.1016/0003-2697(70)90174-0)
-

- Kochenderfer, J. N., & Rosenberg, S. A. (2013). Treating B-cell cancer with T cells expressing anti-CD19 chimeric antigen receptors. In *Nature Reviews Clinical Oncology* (Vol. 10, Issue 5, pp. 267–276). <https://doi.org/10.1038/nrclinonc.2013.46>
- Kojima, R., Aubeil, D., & Fussenegger, M. (2015). Novel theranostic agents for next-generation personalized medicine: Small molecules, nanoparticles, and engineered mammalian cells. In *Current Opinion in Chemical Biology* (Vol. 28, pp. 29–38). Elsevier Ltd. <https://doi.org/10.1016/j.cbpa.2015.05.021>
- Kosuri, S., & Church, G. M. (2014). Large-scale de novo DNA synthesis: Technologies and applications. In *Nature Methods* (Vol. 11, Issue 5, pp. 499–507). Nature Publishing Group. <https://doi.org/10.1038/nmeth.2918>
- Kovatchev, B. P., Breton, M., Dalla Man, C., & Cobelli, C. (2009). In silico preclinical trials: A proof of concept in closed-loop control of type 1 diabetes. *Journal of Diabetes Science and Technology*, 3(1), 44–55. <https://doi.org/10.1177/193229680900300106>
- Kozera, B., & Rapacz, M. (2013). Reference genes in real-time PCR. *J Appl Genetics*, 54(DOI 10.1007/s13353-013-0173-x PLANT), 391–406. <https://doi.org/10.1007/s13353-013-0173-x>
- Kramer, B. P., Fischer, M., & Fussenegger, M. (2005). Semi-synthetic mammalian gene regulatory networks. *Metabolic Engineering*, 7(4), 241–250. <https://doi.org/10.1016/j.ymben.2005.02.005>
- Kwok, R. (2010). Five hard truths for synthetic biology. *Nature*, 463(7279), 288–290. <https://doi.org/10.1038/463288a>
- Landrain, T., Meyer, M., Perez, A. M., & Sussan, R. (2013). Do-it-yourself biology: Challenges and promises for an open science and technology movement. *Systems and Synthetic Biology*, 7(3), 115–126. <https://doi.org/10.1007/s11693-013-9116-4>
- Lee, T., & Maheshri, N. (2012). A regulatory role for repeated decoy transcription factor binding sites in target gene expression. *Molecular Systems Biology*, 8(1), 576. <https://doi.org/10.1038/msb.2012.7>
- Levine, J. H., Lin, Y., & Elowitz, M. B. (2013). Functional roles of pulsing in genetic circuits. In *Science* (Vol. 342, Issue 6163, pp. 1193–1200). American Association for the Advancement of Science. <https://doi.org/10.1126/science.1239999>
- Levskaya, A., Chevalier, A. A., Tabor, J. J., Simpson, Z. B., Lavery, L. A., Levy, M.,

-
- Davidson, E. A., Scouras, A., Ellington, A. D., Marcotte, E. M., & Voigt, C. A. (2005). Engineering *Escherichia coli* to see light. *Nature*, *438*(7067), 441–442. <https://doi.org/10.1038/nature04405>
- Lichtman, E. I., Helfgott, S. M., & Kriegel, M. A. (2012). Emerging therapies for systemic lupus erythematosus - Focus on targeting interferon-alpha. In *Clinical Immunology* (Vol. 143, Issue 3, pp. 210–221). NIH Public Access. <https://doi.org/10.1016/j.clim.2012.03.005>
- Lienert, F., Torella, J. P., Chen, J.-H., Norsworthy, M., Richardson, R. R., & Silver, P. A. (2013). Two-and three-input TALE-based AND logic computation in embryonic stem cells. *Nucleic Acids Research*, *41*, 9967–9975. <https://doi.org/10.1093/nar/gkt758>
- Lönneborg, R., Varga, E., & Brzezinski, P. (2012). Directed evolution of the transcriptional regulator DntR: Isolation of mutants with improved DNT-response. *PLoS ONE*, *7*(1), e29994. <https://doi.org/10.1371/journal.pone.0029994>
- Lu, M. S., Mauser, J. F., & Prehoda, K. E. (2012). Ultrasensitive synthetic protein regulatory networks using mixed decoys. *ACS Synthetic Biology*, *1*(2), 65–72. <https://doi.org/10.1021/sb200010w>
- Lu, M., Wan, M., Leavens, K. F., Chu, Q., Monks, B. R., Fernandez, S., Ahima, R. S., Ueki, K., Kahn, C. R., & Birnbaum, M. J. (2012). Insulin regulates liver metabolism in vivo in the absence of hepatic Akt and Foxo1. *Nature Medicine*, *18*(3), 388–395. <https://doi.org/10.1038/nm.2686>
- Lu, T. K., & Collins, J. J. (2007). Dispersing biofilms with engineered enzymatic bacteriophage. *Proceedings of the National Academy of Sciences of the United States of America*, *104*(27), 11197–11202. <https://doi.org/10.1073/pnas.0704624104>
- Lucks, J. B., Qi, L., Whitaker, W. R., & Arkin, A. P. (2008). Toward scalable parts families for predictable design of biological circuits. *Current Opinion in Microbiology*, *11*(6), 567–573. <https://doi.org/10.1016/j.mib.2008.10.002>
- Macia, J., Manzoni, R., Conde, N., Urrios, A., de Nadal, E., Solé, R., & Posas, F. (2016). Implementation of Complex Biological Logic Circuits Using Spatially Distributed Multicellular Consortia. *PLoS Computational Biology*, *12*(2), 1–24. <https://doi.org/10.1371/journal.pcbi.1004685>
-

- Macía, J., Posas, F., & Solé, R. V. (2012). Distributed computation: The new wave of synthetic biology devices. *Trends in Biotechnology*, 30(6), 342–349. <https://doi.org/10.1016/j.tibtech.2012.03.006>
- Macía, J., Widder, S., & Solé, R. (2009). Specialized or flexible feed-forward loop motifs: A question of topology. *BMC Systems Biology*, 3(1), 84. <https://doi.org/10.1186/1752-0509-3-84>
- MacKay, V. L., Welch, S. K., Insley, M. Y., Manney, T. R., Holly, J., Saari, G. C., & Parker, M. L. (1988). The *Saccharomyces cerevisiae* BAR1 gene encodes an exported protein with homology to pepsin. *Proceedings of the National Academy of Sciences of the United States of America*, 85(1), 55–59. <https://doi.org/10.1073/pnas.85.1.55>
- Magni, L., Raimondo, D. M., Bossi, L., Dalla Man, C., De Nicolao, G., Kovatchev, B., & Cobelli, C. (2007). Model predictive control of type 1 diabetes: An in silico trial. *Journal of Diabetes Science and Technology*, 1(6), 804–812. <https://doi.org/10.1177/193229680700100603>
- Mahr, R., & Frunzke, J. (2016). Transcription factor-based biosensors in biotechnology: current state and future prospects. *Applied Microbiology and Biotechnology*, 100(1), 79–90. <https://doi.org/10.1007/s00253-015-7090-3>
- Mangan, S., Itzkovitz, S., Zaslaver, A., & Alon, U. (2006). The incoherent feed-forward loop accelerates the response-time of the gal system of *Escherichia coli*. *Journal of Molecular Biology*, 356(5), 1073–1081. <https://doi.org/10.1016/j.jmb.2005.12.003>
- Manzoni, R., Urrios, A., Velazquez-Garcia, S., De Nadal, E., Posas, F., Lia De Nadal, E., & Posas, F. (2016). Synthetic biology: insights into biological computation. *Integrative Biology (United Kingdom)*, 8(4), 518–532. <https://doi.org/10.1039/c5ib00274e>
- Martin, V. J. J., Piteral, D. J., Withers, S. T., Newman, J. D., & Keasling, J. D. (2003). Engineering a mevalonate pathway in *Escherichia coli* for production of terpenoids. *Nature Biotechnology*, 21(7), 796–802. <https://doi.org/10.1038/nbt833>
- Mascher, T., Zimmer, S. L., Smith, T. A., & Helmann, J. D. (2004). Antibiotic-inducible promoter regulated by the cell envelope stress-sensing two-component system LiaRS of *Bacillus subtilis*. *Antimicrobial Agents and Chemotherapy*, 48(8), 2888–2896. <https://doi.org/10.1128/AAC.48.8.2888-2896.2004>

- Mátés, L., Chuah, M. K. L., Belay, E., Jerchow, B., Manoj, N., Acosta-Sanchez, A., Grzela, D. P., Schmitt, A., Becker, K., Matrai, J., Ma, L., Samara-Kuko, E., Gysemans, C., Pryputniewicz, D., Miskey, C., Fletcher, B., Vandendriessche, T., Ivics, Z., & Izsvák, Z. (2009). Molecular evolution of a novel hyperactive Sleeping Beauty transposase enables robust stable gene transfer in vertebrates. *Nature Genetics*, *41*(6), 753–761. <https://doi.org/10.1038/ng.343>
- Maung, N. W., & Smolke, C. D. (2008). Higher-order cellular information processing with synthetic RNA devices. *Science*, *322*(5900), 456–460. <https://doi.org/10.1126/science.1160311>
- McAdams, H. H., & Arkin, A. (2000). Gene regulation: Towards a circuit engineering discipline. *Current Biology*, *10*(8), R318–R320. [https://doi.org/10.1016/S0960-9822\(00\)00440-1](https://doi.org/10.1016/S0960-9822(00)00440-1)
- McAdams, H. H., & Shapiro, L. (1995). Circuit simulation of genetic networks. In *Science* (Vol. 269, Issue 5224, pp. 650–656). American Association for the Advancement of Science. <https://doi.org/10.1126/science.7624793>
- McCluskey, E. J. (1965). *Introduction to the theory of switching circuits*. McGraw-Hill.
- Merulla, D., & Van Der Meer, J. R. (2016). Regulatable and Modulable Background Expression Control in Prokaryotic Synthetic Circuits by Auxiliary Repressor Binding Sites. *ACS Synthetic Biology*, *5*(1), 36–45. <https://doi.org/10.1021/acssynbio.5b00111>
- Meyer, A. J., Segall-Shapiro, T. H., Glassey, E., Zhang, J., & Voigt, C. A. (2019). Escherichia coli “Marionette” strains with 12 highly optimized small-molecule sensors. *Nature Chemical Biology*, *15*(2), 196–204. <https://doi.org/10.1038/s41589-018-0168-3>
- Meyer, S., Chappell, J., Sankar, S., Chew, R., & Lucks, J. B. (2016). Improving fold activation of small transcription activating RNAs (STARS) with rational RNA engineering strategies. *Biotechnology and Bioengineering*, *113*(1), 216–225. <https://doi.org/10.1002/bit.25693>
- Milo, R., Shen-Orr, S., Itzkovitz, S., Kashtan, N., Chklovskii, D., & Alon, U. (2002). Network motifs: Simple building blocks of complex networks. *Science*, *298*(5594), 824–827. <https://doi.org/10.1126/science.298.5594.824>
- Mimee, M., Nadeau, P., Hayward, A., Carim, S., Flanagan, S., Jerger, L., Collins, J.,
-

- Mcdonnell, S., Swartwout, R., Citorik, R. J., Bulovi, V., Langer, R., Traverso, G., Chandrakasan, A. P., & Lu, T. K. (2018). *Gastrointestinal Health*. 918(May), 915–918. <https://doi.org/10.1126/science.aas9315>.An
- Monod, J., & Jacob, F. (1961). General Conclusions: Teleonomic Mechanisms in Cellular Metabolism, Growth, and Differentiation. *Cold Spring Harbor Symposia on Quantitative Biology*, 26, 389–401. <https://doi.org/10.1101/SQB.1961.026.01.048>
- Moon, T. S., Lou, C., Tamsir, A., Stanton, B. C., & Voigt, C. A. (2012). Genetic programs constructed from layered logic gates in single cells. *Nature*, 491(7423), 249–253. <https://doi.org/10.1038/nature11516>
- Morey, K. J., Antunes, M. S., Barrow, M. J., Solorzano, F. A., Havens, K. L., Smith, J. J., & Medford, J. (2012). Crosstalk between endogenous and synthetic components - synthetic signaling meets endogenous components. In *Biotechnology Journal* (Vol. 7, Issue 7, pp. 846–855). <https://doi.org/10.1002/biot.201100487>
- Moscou, M. J., & Bogdanove, A. J. (2009). A simple cipher governs DNA recognition by TAL effectors. *Science*, 326(5959), 1501. <https://doi.org/10.1126/science.1178817>
- Mueller, S., Coleman, J. R., Papamichail, D., Ward, C. B., Nimnual, A., Futcher, B., Skiena, S., & Wimmer, E. (2010). Live attenuated influenza virus vaccines by computer-aided rational design. *Nature Biotechnology*, 28(7), 723–726. <https://doi.org/10.1038/nbt.1636>
- Mukherji, S., & Van Oudenaarden, A. (2009). Synthetic biology: Understanding biological design from synthetic circuits. In *Nature Reviews Genetics* (Vol. 10, Issue 12, pp. 859–871). <https://doi.org/10.1038/nrg2697>
- Nakamura, C. E., & Whited, G. M. (2003). Metabolic engineering for the microbial production of 1,3-propanediol. In *Current Opinion in Biotechnology* (Vol. 14, Issue 5, pp. 454–459). Elsevier Ltd. <https://doi.org/10.1016/j.copbio.2003.08.005>
- Nan-Kuang Yau, & Liang-Wey Chang. (1995). Dynamic Analysis of Insulin and Glucagon Secretion. *17th Annual International Conference of the IEEE Engineering in Medicine and Biology Society*, 1359–1360.
- Nandagopal, N., & Elowitz, M. B. (2011). Synthetic biology: Integrated gene circuits. In *Science* (Vol. 333, Issue 6047, pp. 1244–1248). <https://doi.org/10.1126/science.1207084>
-

-
- Nealson, K. H., & Hastings, J. W. (1979). Bacterial bioluminescence: Its control and ecological significance. In *Microbiological Reviews* (Vol. 43, Issue 4, pp. 496–518). American Society for Microbiology (ASM). <https://doi.org/10.1128/membr.43.4.496-518.1979>
- Nevoigt, E., Kohnke, J., Fischer, C. R., Alper, H., Stahl, U., & Stephanopoulos, G. (2006). Engineering of promoter replacement cassettes for fine-tuning of gene expression in *Saccharomyces cerevisiae*. *Applied and Environmental Microbiology*, 72(8), 5266–5273. <https://doi.org/10.1128/AEM.00530-06>
- Niederholtmeyer, H., Sun, Z. Z., Hori, Y., Yeung, E., Verpoorte, A., Murray, R. M., & Maerkl, S. J. (2015). Rapid cell-free forward engineering of novel genetic ring oscillators. *ELife*, 4(OCTOBER2015). <https://doi.org/10.7554/eLife.09771>
- Nielsen, A. A., & Voigt, C. A. (2014). Multi-input CRISPR / C as genetic circuits that interface host regulatory networks . *Molecular Systems Biology*, 10(11), 763. <https://doi.org/10.15252/msb.20145735>
- Nistala, G. J., Wu, K., Rao, C. V., & Bhalerao, K. D. (2010). A modular positive feedback-based gene amplifier. *Journal of Biological Engineering*, 4(1), 4. <https://doi.org/10.1186/1754-1611-4-4>
- Nurse, P. (2008). Life, logic and information. In *Nature* (Vol. 454, Issue 7203, pp. 424–426). Nature Publishing Group. <https://doi.org/10.1038/454424a>
- Nussey S, W. S. (2001). Endocrinology: An Integrated Approach. In *Endocrinology: An Integrated Approach*. <http://www.ncbi.nlm.nih.gov/pubmed/20821847>
- Owicki, J. C., & Wallace Parce, J. (1992). Biosensors based on the energy metabolism of living cells: The physical chemistry and cell biology of extracellular acidification. In *Biosensors and Bioelectronics* (Vol. 7, Issue 4, pp. 255–272). Elsevier. [https://doi.org/10.1016/0956-5663\(92\)87004-9](https://doi.org/10.1016/0956-5663(92)87004-9)
- Özcan, S., & Johnston, M. (1999). Function and Regulation of Yeast Hexose Transporters. *Microbiology and Molecular Biology Reviews*, 63(3), 554–569. <https://doi.org/10.1128/membr.63.3.554-569.1999>
- Paddon, C. J., Westfall, P. J., Pitera, D. J., Benjamin, K., Fisher, K., McPhee, D., Leavell, M. D., Tai, A., Main, A., Eng, D., Polichuk, D. R., Teoh, K. H., Reed, D. W., Treynor, T., Lenihan, J., Jiang, H., Fleck, M., Bajad, S., Dang, G., ... Newman, J. D. (2013). High-level semi-synthetic production of the potent antimalarial
-

- artemisinin. *Nature*, 496(7446), 528–532. <https://doi.org/10.1038/nature12051>
- Paitan, Y., Biran, I., Shechter, N., Biran, D., Rishpon, J., & Ron, E. Z. (2004). Monitoring aromatic hydrocarbons by whole cell electrochemical biosensors. *Analytical Biochemistry*, 335(2), 175–183. <https://doi.org/10.1016/j.ab.2004.08.032>
- Pan, Y., Hu, N., Wei, X., Gong, L., Zhang, B., Wan, H., & Wang, P. (2019). 3D cell-based biosensor for cell viability and drug assessment by 3D electric cell/matrigel-substrate impedance sensing. *Biosensors and Bioelectronics*, 130, 344–351. <https://doi.org/10.1016/j.bios.2018.09.046>
- Pancrazio, J. J., Whelan, J. P., Borkholder, D. A., Ma, W., & Stenger, D. A. (1999). Development and Application of Cell-Based Biosensors. *Annals of Biomedical Engineering*, 27(6), 697–711. <https://doi.org/10.1114/1.225>
- Pandi, A., Grigoras, I., Borkowski, O., & Faulon, J. L. (2019). Optimizing Cell-Free Biosensors to Monitor Enzymatic Production [Brief-report]. *ACS Synthetic Biology*, 8(8), 1952–1957. <https://doi.org/10.1021/acssynbio.9b00160>
- Pardee, K., Green, A. A., Ferrante, T., Cameron, D. E., Daleykeyser, A., Yin, P., & Collins, J. J. (2014). Paper-based synthetic gene networks. *Cell*, 159(4), 940–954. <https://doi.org/10.1016/j.cell.2014.10.004>
- Pédélecq, J. D., Cabantous, S., Tran, T., Terwilliger, T. C., & Waldo, G. S. (2006). Engineering and characterization of a superfolder green fluorescent protein. *Nature Biotechnology*, 24(1), 79–88. <https://doi.org/10.1038/nbt1172>
- Polonsky, K. S., Given, B. D., & Van Cauter, E. (1988). Twenty-four-hour profiles and pulsatile patterns of insulin secretion in normal and obese subjects. *Journal of Clinical Investigation*, 81(2), 442–448. <https://doi.org/10.1172/JCI113339>
- Purcell, O., & Lu, T. K. (2014). Synthetic analog and digital circuits for cellular computation and memory. In *Current Opinion in Biotechnology* (Vol. 29, Issue 1, pp. 146–155). Elsevier Ltd. <https://doi.org/10.1016/j.copbio.2014.04.009>
- Purnick, P. E. M., & Weiss, R. (2009). The second wave of synthetic biology: From modules to systems. *Nature Reviews Molecular Cell Biology*, 10(6), 410–422. <https://doi.org/10.1038/nrm2698>
- Rawson, D. M., Willmer, A. J., & Turner, A. P. P. (1989). Whole-cell biosensors for environmental monitoring. *Biosensors*, 4(5), 299–311. [https://doi.org/10.1016/0265-928X\(89\)80011-2](https://doi.org/10.1016/0265-928X(89)80011-2)
-

- Regot, S., MacIa, J., Conde, N., Furukawa, K., Kjellén, J., Peeters, T., Hohmann, S., De Nadal, E., Posas, F., & Solé, R. (2011). Distributed biological computation with multicellular engineered networks. *Nature*, *469*(7329), 207–211. <https://doi.org/10.1038/nature09679>
- Reski, R., Bae, H., & Simonsen, H. T. (2018). *Physcomitrella patens*, a versatile synthetic biology chassis. In *Plant Cell Reports* (Vol. 37, Issue 10, pp. 1409–1417). Springer Verlag. <https://doi.org/10.1007/s00299-018-2293-6>
- Rinaudo, K., Bleris, L., Maddamsetti, R., Subramanian, S., Weiss, R., & Benenson, Y. (2007). A universal RNAi-based logic evaluator that operates in mammalian cells. *Nature Biotechnology*, *25*(7), 795–801. <https://doi.org/10.1038/nbt1307>
- Rinken, T., & Kivirand, K. (2019). *Biosensors for Environmental Monitoring* (T. Rinken & K. Kivirand (eds.)). IntechOpen. <https://doi.org/10.5772/intechopen.73763>
- Ro, D. K., Paradise, E. M., Quellet, M., Fisher, K. J., Newman, K. L., Ndungu, J. M., Ho, K. A., Eachus, R. A., Ham, T. S., Kirby, J., Chang, M. C. Y., Withers, S. T., Shiba, Y., Sarpong, R., & Keasling, J. D. (2006). Production of the antimalarial drug precursor artemisinic acid in engineered yeast. *Nature*, *440*(7086), 940–943. <https://doi.org/10.1038/nature04640>
- Robertson, R. P. (2010). Islet transplantation a decade later and strategies for filling a half-full glass. In *Diabetes* (Vol. 59, Issue 6, pp. 1285–1291). American Diabetes Association. <https://doi.org/10.2337/db09-1846>
- Rogers, J. K., & Church, G. M. (2016). Genetically encoded sensors enable real-time observation of metabolite production. *Proceedings of the National Academy of Sciences of the United States of America*, *113*(9), 2388–2393. <https://doi.org/10.1073/pnas.1600375113>
- Røkke, G., Korvald, E., Pahr, J., Øyås, O., & Lale, R. (2014). BioBrick assembly standards and techniques and associated software tools. *Methods in Molecular Biology*, *1116*, 1–24. https://doi.org/10.1007/978-1-62703-764-8_1
- Roquet, N., Soleimany, A. P., Ferris, A. C., Aaronson, S., & Lu, T. K. (2016). Synthetic recombinase-based State machines in living cells. *Science*, *353*(6297). <https://doi.org/10.1126/science.aad8559>
- Rössger, K., Charpin-El-Hamri, G., & Fussenegger, M. (2013). A closed-loop synthetic gene circuit for the treatment of diet-induced obesity in mice. *Nature*
-

- Communications*, 4, 2825. <https://doi.org/10.1038/ncomms3825>
- Rubens, J. R., Selvaggio, G., & Lu, T. K. (2016). Synthetic mixed-signal computation in living cells. *Nature Communications*, 7(1), 1–10. <https://doi.org/10.1038/ncomms11658>
- Russell, W. R., Baka, A., Björck, I., Delzenne, N., Gao, D., Griffiths, H. R., Hadjilucas, E., Juvonen, K., Lahtinen, S., Lansink, M., Loon, L. Van, Mykkänen, H., östman, E., Riccardi, G., Vinoy, S., & Weickert, M. O. (2016). Impact of Diet Composition on Blood Glucose Regulation. *Critical Reviews in Food Science and Nutrition*, 56(4), 541–590. <https://doi.org/10.1080/10408398.2013.792772>
- Saeidi, N., Wong, C. K., Lo, T. M., Nguyen, H. X., Ling, H., Leong, S. S. J., Poh, C. L., & Chang, M. W. (2011). Engineering microbes to sense and eradicate *Pseudomonas aeruginosa*, a human pathogen. *Molecular Systems Biology*, 7, 521. <https://doi.org/10.1038/msb.2011.55>
- Sagi, E., Hever, N., Rosen, R., Bartolone, A. J., Premkumar, J. R., Ulber, R., Lev, O., Scheper, T., & Belkin, S. (2003). Fluorescence and bioluminescence reporter functions in genetically modified bacterial sensor strains. *Sensors and Actuators, B: Chemical*, 90(1–3), 2–8. [https://doi.org/10.1016/S0925-4005\(03\)00014-5](https://doi.org/10.1016/S0925-4005(03)00014-5)
- Sanger, F., & Coulson, A. R. (1975). A rapid method for determining sequences in DNA by primed synthesis with DNA polymerase. *Journal of Molecular Biology*, 94(3), 441–448. [https://doi.org/10.1016/0022-2836\(75\)90213-2](https://doi.org/10.1016/0022-2836(75)90213-2)
- Sarpeshkar, R. (2014). Analog synthetic biology. *Philosophical Transactions of the Royal Society A: Mathematical, Physical and Engineering Sciences*, 372(2012). <https://doi.org/10.1098/rsta.2013.0110>
- Sarpeshkar, Rahul. (1998). Analog Versus Digital: Extrapolating from Electronics to Neurobiology. In *Neural Computation* (Vol. 10, Issue 7, pp. 1601–1638). MIT Press Journals. <https://doi.org/10.1162/089976698300017052>
- Savant, C. J., Roden, M. S., Carpenter, G. L. (Gordon L., & Savant, C. J. (1991). *Electronic design : circuits and systems*. Benjamin/Cummings Pub. Co.
- Schaffner, M., Rühs, P. A., Coulter, F., Kilcher, S., & Studart, A. R. (2017). 3D printing of bacteria into functional complex materials. *Science Advances*, 3(12). <https://doi.org/10.1126/sciadv.aao6804>
- Schuler, M. L., Mantegazza, O., & Weber, A. P. M. (2016). Engineering C4
-

- photosynthesis into C3 chassis in the synthetic biology age. In *Plant Journal* (Vol. 87, Issue 1, pp. 51–65). Blackwell Publishing Ltd. <https://doi.org/10.1111/tpj.13155>
- Schultheiss, E., Weiss, S., Winterer, E., Maas, R., Heinzle, E., & Jose, J. (2008). Esterase autodisplay: Enzyme engineering and whole-cell activity determination in microplates with pH sensors. *Applied and Environmental Microbiology*, 74(15), 4782–4791. <https://doi.org/10.1128/AEM.01575-07>
- Schuster, R., & Holzhütter, H. G. (1994). Rapid-equilibrium Approximation applied to mathematical models of Tracer dynamics in biochemical reaction systems. *Mathematical and Computer Modelling*, 19(6–8), 241–253. [https://doi.org/10.1016/0895-7177\(94\)90196-1](https://doi.org/10.1016/0895-7177(94)90196-1)
- Selifonova, O., Burlage, R., & Barkay, T. (1993). Bioluminescent sensors for detection of bioavailable Hg(II) in the environment. *Applied and Environmental Microbiology*, 59(9), 3083–3090. <https://doi.org/10.1128/aem.59.9.3083-3090.1993>
- Shah, V. N., Shoskes, A., Tawfik, B., & Garg, S. K. (2014). Closed-loop system in the management of diabetes: Past, present, and future. *Diabetes Technology and Therapeutics*, 16(8), 477–490. <https://doi.org/10.1089/dia.2014.0193>
- Shao, J., Xue, S., Yu, G., Yu, Y., Yang, X., Bai, Y., Zhu, S., Yang, L., Yin, J., Wang, Y., Liao, S., Guo, S., Xie, M., Fussenegger, M., & Ye, H. (2017). Smartphone-controlled optogenetically engineered cells enable semiautomatic glucose homeostasis in diabetic mice. *Science Translational Medicine*, 9(387). <https://doi.org/10.1126/scitranslmed.aal2298>
- Shcherbakova, D. M., Hink, M. A., Joosen, L., Gadella, T. W. J., & Verkhusha, V. V. (2012). An orange fluorescent protein with a large stokes shift for single-excitation multicolor FCCS and FRET imaging. *Journal of the American Chemical Society*, 134(18), 7913–7923. <https://doi.org/10.1021/ja3018972>
- Shemer, B., Palevsky, N., Yagur-Kroll, S., & Belkin, S. (2015). Genetically engineered microorganisms for the detection of explosives' residues. In *Frontiers in Microbiology* (Vol. 6, Issue OCT). Frontiers Media S.A. <https://doi.org/10.3389/fmicb.2015.01175>
- Shetty, R. P., Endy, D., & Knight, T. F. (2008). Engineering BioBrick vectors from BioBrick parts. *Journal of Biological Engineering*, 2(1), 5. <https://doi.org/10.1186/1754-1611-2-5>

- Shis, D. L., & Bennett, M. R. (2013). Library of synthetic transcriptional AND gates built with split T7 RNA polymerase mutants. *Proceedings of the National Academy of Sciences of the United States of America*, *110*(13), 5028–5033. <https://doi.org/10.1073/pnas.1220157110>
- Shopera, T., Henson, W. R., Ng, A., Lee, Y. J., Ng, K., & Moon, T. S. (2015). Robust, tunable genetic memory from protein sequestration combined with positive feedback. *Nucleic Acids Research*, *43*(18), 9086–9094. <https://doi.org/10.1093/nar/gkv936>
- Singh, A., Nigam, P. S., & Murphy, J. D. (2011). Renewable fuels from algae: An answer to debatable land based fuels. *Bioresource Technology*, *102*(1), 10–16. <https://doi.org/10.1016/j.biortech.2010.06.032>
- Sinha, J., Reyes, S., & Gallivan, J. P. (2014). Erratum: Reprogramming bacteria to seek and destroy an herbicide (Nature Chemical Biology (2010) 6, (464-470)). In *Nature Chemical Biology* (Vol. 10, Issue 3, p. 239). Nature Publishing Group. <https://doi.org/10.1038/nchembio0314-239a>
- Siuti, P., Yazbek, J., & Lu, T. K. (2014). Engineering genetic circuits that compute and remember. *Nature Protocols*, *9*(6), 1292–1300. <https://doi.org/10.1038/nprot.2014.089>
- Sleator, R. D. (2014). The synthetic biology future. *Bioengineered*, *5*(2), 69–72. <https://doi.org/10.4161/bioe.28317>
- Sloss, A. N., & Gustafson, S. (2019). *2019 Evolutionary Algorithms Review*.
- Somleva, M. N., Snell, K. D., Beaulieu, J. J., Peoples, O. P., Garrison, B. R., & Patterson, N. A. (2008). Production of polyhydroxybutyrate in switchgrass, a value-added co-product in an important lignocellulosic biomass crop. *Plant Biotechnology Journal*, *6*(7), 663–678. <https://doi.org/10.1111/j.1467-7652.2008.00350.x>
- Song, S. H., Kjems, L., Ritzel, R., McIntyre, S. M., Johnson, M. L., Veldhuis, J. D., & Butler, P. C. (2002). Pulsatile insulin secretion by human pancreatic islets. *Journal of Clinical Endocrinology and Metabolism*, *87*(1), 213–221. <https://doi.org/10.1210/jcem.87.1.8181>
- Song, T., Garg, S., Mokhtar, R., Bui, H., & Reif, J. (2016). *Analog Computation by DNA Strand Displacement Circuits*. <https://doi.org/10.1021/acssynbio.6b00144>
- Speer, R., Journal, R., Speer, M. A., & Richard, T. L. (2011). Amplified insert assembly:

- an optimized approach to standard assembly of BioBrick™ genetic circuits
Amplified insert assembly: an optimized approach to standard assembly of BioBrick™ genetic circuits. In *Biological Engineering* (Vol. 5).
<https://doi.org/10.1186/1754-1611-5-17>
- Sterritt, R. M., & Lester, J. N. (1980). Interactions of heavy metals with bacteria. *Science of the Total Environment*, *The*, *14*(1), 5–17. [https://doi.org/10.1016/0048-9697\(80\)90122-9](https://doi.org/10.1016/0048-9697(80)90122-9)
- Stevens, A. M., Dolan, K. M., & Greenberg, E. P. (1994). Synergistic binding of the *Vibrio fischeri* LuxR transcriptional activator domain and RNA polymerase to the lux promoter region. *Proceedings of the National Academy of Sciences of the United States of America*, *91*(26), 12619–12623. <https://doi.org/10.1073/pnas.91.26.12619>
- Stock, A. M., Robinson, V. L., & Goudreau, P. N. (2000). Two-Component Signal Transduction. *Annual Review of Biochemistry*, *69*(1), 183–215. <https://doi.org/10.1146/annurev.biochem.69.1.183>
- Stower, H. (2019). Diet influence on cancer therapy. In *Nature Medicine* (Vol. 25, Issue 9, p. 1330). Nature Publishing Group. <https://doi.org/10.1038/s41591-019-0588-y>
- Struss, A., Pasini, P., Ensor, C. M., Raut, N., & Daunert, S. (2010). Paper strip whole cell biosensors: A portable test for the semiquantitative detection of bacterial quorum signaling molecules. *Analytical Chemistry*, *82*(11), 4457–4463. <https://doi.org/10.1021/ac100231a>
- Sylow, L., Kleinert, M., Richter, E. A., & Jensen, T. E. (2017). Exercise-stimulated glucose uptake-regulation and implications for glycaemic control. In *Nature Reviews Endocrinology* (Vol. 13, Issue 3, pp. 133–148). Nature Publishing Group. <https://doi.org/10.1038/nrendo.2016.162>
- Takahashi, M. K., Hayes, C. A., Chappell, J., Sun, Z. Z., Murray, R. M., Noireaux, V., & Lucks, J. B. (2015). Characterizing and prototyping genetic networks with cell-free transcription-translation reactions. *Methods*, *86*, 60–72. <https://doi.org/10.1016/j.ymeth.2015.05.020>
- Tamsir, A., Tabor, J. J., & Voigt, C. A. (2011). Robust multicellular computing using genetically encoded NOR gates and chemical “wiresg.” *Nature*, *469*(7329), 212–215. <https://doi.org/10.1038/nature09565>
- Tan, C., Marguet, P., & You, L. (2009). Emergent bistability by a growth-modulating

- positive feedback circuit. *Nature Chemical Biology*, 5(11), 842–848. <https://doi.org/10.1038/nchembio.218>
- Tang, S.-C., & Sambanis, A. (2003). Preproinsulin mRNA engineering and its application to the regulation of insulin secretion from human hepatomas. *FEBS Letters*, 537(1–3), 193–197. [https://doi.org/10.1016/S0014-5793\(03\)00121-2](https://doi.org/10.1016/S0014-5793(03)00121-2)
- Tavassoli, A., Lu, Q., Gam, J., Pan, H., Benkovic, S. J., & Cohen, S. N. (2008). Inhibition of HIV budding by a genetically selected cyclic peptide targeting the Gag-TSG101 interaction. *ACS Chemical Biology*, 3(12), 757–764. <https://doi.org/10.1021/cb800193n>
- Taylor, N. D., Garruss, A. S., Moretti, R., Chan, S., Arbing, M. A., Cascio, D., Rogers, J. K., Isaacs, F. J., Kosuri, S., Baker, D., Fields, S., Church, G. M., & Raman, S. (2016). Engineering an allosteric transcription factor to respond to new ligands. *Nature Methods*, 13(2), 177–183. <https://doi.org/10.1038/nmeth.3696>
- Terpe, K. (2006). Overview of bacterial expression systems for heterologous protein production: From molecular and biochemical fundamentals to commercial systems. In *Applied Microbiology and Biotechnology* (Vol. 72, Issue 2, pp. 211–222). <https://doi.org/10.1007/s00253-006-0465-8>
- Tigges, M., Déneraud, N., Greber, D., Stelling, J., & Fussenegger, M. (2010). A synthetic low-frequency mammalian oscillator. *Nucleic Acids Research*, 38(8), 2702–2711. <https://doi.org/10.1093/nar/gkq121>
- Tizei, P. A. G., Csibra, E., Torres, L., & Pinheiro, V. B. (2016). Selection platforms for directed evolution in synthetic biology. *Biochemical Society Transactions*, 44(4), 1165–1175. <https://doi.org/10.1042/BST20160076>
- Tong, G., Jia, Z., & Chang, J. (2018). Flexible Hybrid Electronics: Review and Challenges. *Proceedings - IEEE International Symposium on Circuits and Systems, 2018-May*, 1–5. <https://doi.org/10.1109/ISCAS.2018.8351806>
- Trang, P. T. K., Berg, M., Viet, P. H., Van Mui, N., & Van Der Meer, J. R. (2005). Bacterial bioassay for rapid and accurate analysis of arsenic in highly variable groundwater samples. *Environmental Science and Technology*, 39(19), 7625–7630. <https://doi.org/10.1021/es050992e>
- Tsimring, L., Hasty, J., Danino, T., Mondrago, O., Mondragón-Palomino, O., Tsimring, L., & Hasty, J. (2010). A synchronized quorum of genetic clocks. *Nature*,

-
- 463(7279), 326–330. <https://doi.org/10.1038/nature08753>
- Urgun-Demirtas, M., Stark, B., & Pagilla, K. (2006). Use of genetically engineered microorganisms (GEMs) for the bioremediation of contaminants. In *Critical Reviews in Biotechnology* (Vol. 26, Issue 3, pp. 145–164). Taylor & Francis. <https://doi.org/10.1080/07388550600842794>
- Urrios, A., Gonzalez-Flo, E., Canadell, D., De Nadal, E., Macia, J., & Posas, F. (2018). Plug-and-Play Multicellular Circuits with Time-Dependent Dynamic Responses. *ACS Synthetic Biology*, 7(4), 1095–1104. <https://doi.org/10.1021/acssynbio.7b00463>
- Vaidyanathan, P., Der, B. S., Bhatia, S., Roehner, N., Silva, R., Voigt, C. A., & Densmore, D. (2015). A Framework for Genetic Logic Synthesis. *Proceedings of the IEEE*, 103(11), 2196–2207. <https://doi.org/10.1109/JPROC.2015.2443832>
- Van Der Meer, J. R., Tropel, D., & Jaspers, M. (2004). Illuminating the detection chain of bacterial bioreporters. *Environmental Microbiology*, 6(10), 1005–1020. <https://doi.org/10.1111/j.1462-2920.2004.00655.x>
- Venkataraman, S., Dirks, R. M., Ueda, C. T., & Pierce, N. A. (2010). Selective cell death mediated by small conditional RNAs. *Proceedings of the National Academy of Sciences of the United States of America*, 107(39), 16777–16782. <https://doi.org/10.1073/pnas.1006377107>
- Voyvodic, P. L., Pandi, A., Koch, M., Conejero, I., Valjent, E., Courtet, P., Renard, E., Faulon, J. L., & Bonnet, J. (2019). Plug-and-play metabolic transducers expand the chemical detection space of cell-free biosensors. *Nature Communications*, 10(1). <https://doi.org/10.1038/s41467-019-09722-9>
- Wan, X., Volpetti, F., Petrova, E., French, C., Maerkl, S. J., & Wang, B. (2019). Cascaded amplifying circuits enable ultrasensitive cellular sensors for toxic metals. *Nature Chemical Biology*, 15(5), 540–548. <https://doi.org/10.1038/s41589-019-0244-3>
- Wang, B., Barahona, M., & Buck, M. (2014). Engineering modular and tunable genetic amplifiers for scaling transcriptional signals in cascaded gene networks. *Nucleic Acids Research*, 42(14), 9484–9492. <https://doi.org/10.1093/nar/gku593>
- Wang, B., Barahona, M., & Buck, M. (2015). Amplification of small molecule-inducible gene expression via tuning of intracellular receptor densities. *Nucleic Acids Research*, 43(3), 1955–1964. <https://doi.org/10.1093/nar/gku1388>
-

- Wang, B., & Buck, M. (2012). Customizing cell signaling using engineered genetic logic circuits. In *Trends in Microbiology* (Vol. 20, Issue 8, pp. 376–384). <https://doi.org/10.1016/j.tim.2012.05.001>
- Wang, B., Kitney, R. I., Joly, N., & Buck, M. (2011). Engineering modular and orthogonal genetic logic gates for robust digital-like synthetic biology. *Nature Communications*, 2(1), 508. <https://doi.org/10.1038/ncomms1516>
- Wang, H. H., Isaacs, F. J., Carr, P. A., Sun, Z. Z., Xu, G., Forest, C. R., & Church, G. M. (2009). Programming cells by multiplex genome engineering and accelerated evolution. *Nature*, 460(7257), 894–898. <https://doi.org/10.1038/nature08187>
- Warren C. Ruder, Ting Lu, J. J. C. (2011). Synthetic Biology Moving into the Clinic. *Science*, 333(6047), 1248–1252. <https://doi.org/10.1126/science.1133734>
- Waters, C. M., & Bassler, B. L. (2005). QUORUM SENSING: Cell-to-Cell Communication in Bacteria. *Annual Review of Cell and Developmental Biology*, 21(1), 319–346. <https://doi.org/10.1146/annurev.cellbio.21.012704.131001>
- Watson, J. D., & Crick, F. H. C. (1953). Molecular structure of nucleic acids: A structure for deoxyribose nucleic acid. *Nature*, 171(4356), 737–738. <https://doi.org/10.1038/171737a0>
- Weber, A. P. M., & Bar-Even, A. (2019). Update: Improving the efficiency of photosynthetic carbon reactions. *Plant Physiology*, 179(3), 803–812. <https://doi.org/10.1104/pp.18.01521>
- Weber, W., & Fussenegger, M. (2012). Emerging biomedical applications of synthetic biology. *Nature Reviews. Genetics*, 13(1), 21–35. <https://doi.org/10.1038/nrg3094>
- Weber, W., Schoenmakers, R., Keller, B., Gitzinger, M., Grau, T., Baba, M. D. El, Sander, P., & Fussenegger, M. (2008). A synthetic mammalian gene circuit reveals antituberculosis compounds. *Proceedings of the National Academy of Sciences of the United States of America*, 105(29), 9994–9998. <https://doi.org/10.1073/pnas.0800663105>
- Weiss, M., Steiner, D. F., & Philipson, L. H. (2000). Insulin Biosynthesis, Secretion, Structure, and Structure-Activity Relationships. In *Endotext*. MDText.com, Inc. <http://www.ncbi.nlm.nih.gov/pubmed/25905258>
- Weiss, R., Weiss, R., & Basu, S. (2002). *The Device Physics of Cellular Logic Gates*. <http://citeseerx.ist.psu.edu/viewdoc/summary?doi=10.1.1.12.1224>

-
- Westerhoff, H. V., & Palsson, B. O. (2004). The evolution of molecular biology into systems biology. In *Nature Biotechnology* (Vol. 22, Issue 10, pp. 1249–1252). Nature Publishing Group. <https://doi.org/10.1038/nbt1020>
- Widder, S., Solé, R., & Macía, J. (2012). Evolvability of feed-forward loop architecture biases its abundance in transcription networks. *BMC Systems Biology*, 6, 7. <https://doi.org/10.1186/1752-0509-6-7>
- Williams, J. W., Cui, X., Levchenko, A., & Stevens, A. M. (2008). Robust and sensitive control of a quorum-sensing circuit by two interlocked feedback loops. *Molecular Systems Biology*, 4. <https://doi.org/10.1038/msb.2008.70>
- Wimmer, E., Mueller, S., Tumpey, T. M., & Taubenberger, J. K. (2009). Synthetic viruses: A new opportunity to understand and prevent viral disease. In *Nature Biotechnology* (Vol. 27, Issue 12, pp. 1163–1172). <https://doi.org/10.1038/nbt.1593>
- Wu, C. Y., Roybal, K. T., Puchner, E. M., Onuffer, J., & Lim, W. A. (2015). Remote control of therapeutic T cells through a small molecule-gated chimeric receptor. *Science*, 350(6258), aab4077–aab4077. <https://doi.org/10.1126/science.aab4077>
- Wu, F., Menn, D. J., & Wang, X. (2014). Quorum-sensing crosstalk-driven synthetic circuits: From Unimodality to trimodality. *Chemistry and Biology*, 21(12), 1629–1638. <https://doi.org/10.1016/j.chembiol.2014.10.008>
- Xie, M., Ye, H., Wang, H., Charpin-El Hamri, G., Lormeau, C., Saxena, P., Stelling, J., & Fussenegger, M. (2016). β -cell-mimetic designer cells provide closed-loop glycemic control. *Science*, 354(6317), 1296–1301. <https://doi.org/10.1126/science.aaf4006>
- Xie, M., Ye, H., Wang, H., Hamri, G. C., Lormeau, C., Saxena, P., & Fussenegger, M. (2017). β -cell-mimetic designer cells provide closed-loop glycemic control. *Science*, 354(6317), 1296–1301.
- Xu, L., Xu, Q., Li, X., & Zhang, X. (2017). MicroRNA-21 regulates the proliferation and apoptosis of cervical cancer cells via tumor necrosis factor- α . *Molecular Medicine Reports*, 16(4), 4659–4663. <https://doi.org/10.3892/mmr.2017.7143>
- Xue, H., Shi, H., Yu, Z., He, S., Liu, S., Hou, Y., Pan, X., Wang, H., Zheng, P., Cui, C., Viets, H., Liang, J., Zhang, Y., Chen, S., Zhang, H. M., & Ouyang, Q. (2014). Design, construction, and characterization of a set of biosensors for aromatic compounds. In *ACS Synthetic Biology* (Vol. 3, Issue 12, pp. 1011–1014). American
-

- Chemical Society. <https://doi.org/10.1021/sb500023f>
- Yang, T. T., Sinai, P., Kitts, P. A., & Kain, S. R. (1997). Quantification of gene expression with a secreted alkaline phosphatase reporter system. *BioTechniques*, 23(6), 1110–1114. <https://doi.org/10.2144/97236pf01>
- Ye, H., Daoud-El Baba, M., Peng, R.-W. W., Fussenegger, M., Baba, M. D. El, Peng, R.-W. W., & Fussenegger, M. (2011). A synthetic optogenetic transcription device enhances blood-glucose homeostasis in mice. *Science*, 332(6037), 1565–1568. <https://doi.org/10.1126/science.1203535>
- Yim, H., Haselbeck, R., Niu, W., Pujol-Baxley, C., Burgard, A., Boldt, J., Khandurina, J., Trawick, J. D., Osterhout, R. E., Stephen, R., Estadilla, J., Teisan, S., Schreyer, H. B., Andrae, S., Yang, T. H., Lee, S. Y., Burk, M. J., & Van Dien, S. (2011). Metabolic engineering of *Escherichia coli* for direct production of 1,4-butanediol. *Nature Chemical Biology*, 7(7), 445–452. <https://doi.org/10.1038/nchembio.580>
- Yin, R., Tong, Z., Yang, D., & Nie, J. (2011). Glucose and pH dual-responsive concanavalin A based microhydrogels for insulin delivery. *International Journal of Biological Macromolecules*, 49(5), 1137–1142. <https://doi.org/10.1016/j.ijbiomac.2011.09.014>
- Yki-Jarvinen, H., Young, A. A., Lamkin, C., & Foley, J. E. (1987). Kinetics of glucose disposal in whole body and across the forearm in man. *Journal of Clinical Investigation*, 79(6), 1713–1719. <https://doi.org/10.1172/JCI113011>
- Yoo, S. M., Na, D., & Lee, S. Y. (2013). Design and use of synthetic regulatory small RNAs to control gene expression in *Escherichia coli*. *Nature Protocols*, 8(9), 1694–1707. <https://doi.org/10.1038/nprot.2013.105>
- You, L., Cox, R. S., Weiss, R., & Arnold, F. H. (2004). Programmed population control by cell-cell communication and regulated killing. *Nature*, 428(6985), 868–871. <https://doi.org/10.1038/nature02491>
- Younger, A. K. D., Dalvie, N. C., Rottinghaus, A. G., & Leonard, J. N. (2017). Engineering Modular Biosensors to Confer Metabolite-Responsive Regulation of Transcription. *ACS Synthetic Biology*, 6(2), 311–325. <https://doi.org/10.1021/acssynbio.6b00184>
- Yu, J., Zhang, Y., Ye, Y., DiSanto, R., Sun, W., Ranson, D., Ligler, F. S., Buse, J. B., Gu, Z., & Ho, D. (2015). Microneedle-array patches loaded with hypoxia-sensitive

-
- vesicles provide fast glucose-responsive insulin delivery. *Proceedings of the National Academy of Sciences of the United States of America*, 112(27), 8260–8265. <https://doi.org/10.1073/pnas.1505405112>
- Zhang, Fan, & Tzanakakis, E. S. (2019). *Amelioration of Diabetes in a Murine Model upon Transplantation of Pancreatic β -Cells with Optogenetic Control of Cyclic Adenosine Monophosphate*. <https://doi.org/10.1021/acssynbio.9b00262>
- Zhang, Fuzhong, Carothers, J. M., & Keasling, J. D. (2012). Design of a dynamic sensor-regulator system for production of chemicals and fuels derived from fatty acids. *Nature Biotechnology*, 30(4), 354–359. <https://doi.org/10.1038/nbt.2149>
- Zhao, L., Xiao, C., Ding, J., He, P., Tang, Z., Pang, X., Zhuang, X., & Chen, X. (2013). Facile one-pot synthesis of glucose-sensitive nanogel via thiol-ene click chemistry for self-regulated drug delivery. *Acta Biomaterialia*, 9(5), 6535–6543. <https://doi.org/10.1016/j.actbio.2013.01.040>
- Zhao, L., Xiao, C., Wang, L., Gai, G., & Ding, J. (2016). *Glucose-sensitive polymer nanoparticles for self-regulated drug delivery*. 52(49). <https://doi.org/10.1039/c6cc02202b>
- Zhou, S., Yomano, L. P., Shanmugam, K. T., & Ingram, L. O. (2005). Fermentation of 10% (w/v) sugar to D(-)-lactate by engineered *Escherichia coli* B. *Biotechnology Letters*, 27(23–24), 1891–1896. <https://doi.org/10.1007/s10529-005-3899-7>
- Zhou, W., Jimmy Huang, P. J., Ding, J., & Liu, J. (2014). Aptamer-based biosensors for biomedical diagnostics. *Analyst*, 139(11), 2627–2640. <https://doi.org/10.1039/c4an00132j>
-

ANNEX

ANNEX

A. Two-component biosensors: unveiling the mechanisms of predictable tunability

Part	DNA Sequence
J23100	ttgacggctagctcagtcctaggtacagtgctagc
J23105	tttacggctagctcagtcctaggtactatgctagc
J23114	tttatggctagctcagtcctaggtacaatgctagc
J23103	ctgatagctagctcagtcctagggattatgctagc
J23112	ctgatagctagctcagtcctagggattatgctagc
R0040	tcctatcagtgatagagattgacatccctatcagtgatagagatactgagcac
I0050	tatgacaacttgacggctacatcattcactttttcttcacaaccggcacggaactcgctcgggctggccccgggtgcattttta aatacccgcgagaaatagagttgatcgtcaaaaccaacattgcgaccgacgggtggcgataggcatccgggtggtgctca aaagcagcttcgctggctgatacgttggctctcgcgccagcttaagacgctaatacctaactgctggcggaaaagatgt gacagacgcgacggcgacaagcaaacatgctgtgacgctggcgatatcaaaattgctgtctgccaggtgatcgtgta tgactgacaagcctcgcgtaccgattatccatcggtggatggagcgcactgtaateccttccatgcgccgcagtaaca attgctcaagcagattatcgccagcagctccgaatagcgcccttccccttggccggcgttaatgatttgcccaaacaggtc gctgaaatgcggctggtgcttccatccggcgaaagaaccccgtattggcaaatattgacggccagttaagccattcat gccagtagggcgcgacgaaagtaaaccactggtgataccattcgcgagcctccggatgacgaccgtagtgatgaa tctctctggcgggaacagcaaaatatacccggctggcaaaacaattctcgtccctgattttaccaccccctgaccgc gaatggtgagattgagaatataacctttcattcccagcggctcggctgataaaaaatcgagataaccggtggcctcaatcg gcgttaaaccggccaccagatgggcattaaacgagatcccggcagcaggggatcattttgcgctcagccatactttcat actcccgcattcagagaagaaccaattgtccatattgcatcagacattgccgtcactgctgttttactggcttctcgtc aaccaaaccgtaaccccgttattaaaagcattctgtaacaaagcgggaccaaagccatgacaaaaacgcgtaacaaa agtgctataatcacggcagaaaagtcacattgattttgacggcgtcacactttgctatgcatagcattttatccataa gattagcggatcctacgtgacgcttttatcgcaactctctactgtttctccatacccgtttttgggctagc
R0061	ttgacacctgtaggatcgtacaggtataat

C0062	<p>atgaaaaacataaatgccgacgacacatacagaataattaataaaaattaaagctttagaagcaataatgatattaatcaatg cttatctgatatgactaaaatggtacattgtgaatattttactcgcgatcatttatcctcattctatggtaaactctgatatttcaa tctagataattaccctaaaaaatggaggcaatattatgatgacgctaatttaataaaaatgatcctatagtagattatttctaac tccaatcattcaccaattaattggaatattttgaaaacaatgctgtaataaaaaatctccaaatgtaattaaagaagcgaaa acatcaggtcttactcgggttagttccctattcacaaggctaacaatggcttcggaatgcttagtttgcacattcagaaa aagacaactatagatagttttttacatgcgtgtatgaacataccattaattgttccttctagttgataattatcgaaaaat aaatagcaataataaatcaacaacgatttaacaaaagagaaaaagaatgttagcgtgggcatcgaaggaaaaa gctcttgggatatttcaaaaatattaggtgcagtgagcgtactgtcactttccatttaaccaatgcgcaaatgaaactcaata caacaaccgctgccaaagtatttctaaagcaattttaacaggagcaattgattgccatactttaaaaat</p>
E1010	<p>atggcttctccgaagacggtatcaaagattcatgcgttcaaaagttcgtatggaaggtccgtaacggtcacgagttcga aatcgaaggtgaaggtgaaggtcgtccgtacgaaggtaccagaccgctaaactgaaagttaccaaggtggtccgctg ccgttcgcttgggacatcctgtccccgcagttccagtacggttccaaagctfacgttaaacaccggctgacatccggac tacctgaaactgtccttccggaaggttcaaatgggaacgtgttatgaaactcgaagacggtggtgtttaccgttaccca ggactcctcctgcaagacggtgagttcatctacaaagttaaactgcgtggtaccaacttcccgctccgacggtccggttat gcagaaaaaacatgggttgggaagctccaccgaacgtatgtaccgggaagacggtgctctgaaaggtgaaatcaaa atgcgtctgaaactgaaagacggtggtcactacgacgctgaagttaaaccacctacatggctaaaaaacgggttcagct gccgggtgcttcaaaaaccgacatcaaaactggacatcacctcccacaacgaagactacaccatcgttgaacagtagcaa cgtgctgaaggtcgtcactccaccggtgcttaataacgctgatagtctagttagatcgc</p>
B0030	attaagaggagaaa
B0034	aaagaggagaaa
B0033	tcacacaggac
B0014	<p>tcacactggctcacctcgggtggcctttctgcgtttatatactagagagagaatataaaaagccagattattaatcggctt ttttattattt</p>
PSB1AK3	<p>tactagtagcggccgctgcagtcggcaaaaaacgggcaaggtgtcaccaccctgcccttttctttaaaccgaaaag attacttcggttatgcaggttctcgtcactgactcgtcgcctcggctggtcggctgcggcgagcgggtatcagctcac tcaaaggcggtatacgggtatccacagaatcaggggataacgcaggaaagaacatgtgagcaaaaaggccagcaaaaag gccaggaaccgtaaaaaggccggttgcggcgttttccataggtcggccccctgacgagcatcaaaaaatcgac gctcaagttagaggtggcgaaaccgacaggactataaagataaccagcgtttccccctggaagctccctcgtgcgctc tctgttccgacctgccgcttaccggatacctgtccgctttctccctcgggaagcgtggcgttttctcatagctcacgct gtaggtatctcagttcgggttaggtcgttcctccaagctgggctgtgtgcacgaacccccgttcagcccagcgtgc gccttatccgtaactatcgtcttgagtccaaccggtaagacacgacttatcggcactggcagcagccactggtaacag</p>

gattagcagagcgaggatgtaggcggtgctacagagtcttgaagtggggcctaactacggctacactagaaggaca
gtatttggtatctgcgctctgctgaagccagttacctcggaaaaagagttgtagctcttgatccggcaacaaccaccg
ctggtagcgggtggttttttgttgaagcagcagattacgcgcagaaaaaaggatctcaagaagatcctttgatctttcta
cggggtctgacgctcagtggaacgaaaactcacgftaagggatttgggtcatgagattatcaaaaaggatctcacctagat
ccttttaataaaaaagtttaaatcaatctaaagtatatatgagtaaacttggctgacagctcgagtcgagtcgcaagta
gcgtaatgctctgccagtggtacaaccaattaaccaattctgattagaaaaactcatcgagcatcaaatgaaactgcaattat
tcatatcaggattatcaatacatttttgaaaaagccgttctgtaatgaaggagaaaaactcaccgaggcagttccatagg
atggcaagatcctgggtatcggctcgcgattccgactcgtccaacatcaatacaacctattaatttcccctcgtcaaaaataag
ggtatcaagtgagaaatccatgagtgacgactgaatccggtgagaatggcaaaagcttatgcatttcttccagactgtt
caacaggccagccattacgctcgtcatcaaaatcactcgcacatcaaccaaacggtatttattctgtgattgcgctgagcga
gacgaaatcgcgacgctgttaaaaggacaattacaacaggaatcgaatgcaaccggcgcaggaactgcccagcgc
catcaacaatattttcacctgaatcaggatattcttaataactggaatgctgtttcccggggatcgagtggtgagtaacc
atgcatcatcaggagtaggataaaatgcttgatggctcggagaggcataaattccgctcagccagtttagtctgacatctc
atctgtaacatcattggcaacgctacctttgcatgttccagaaacaactctggcgcacggttcccatacaatcgataga
ttgtgcacctgattgcccagcattatcgcgagccattataccatataaatcagcatccatgttgaattaatcgcggcc
tggagcaagacgttcccgttgaatatggctcataaaccccctgtattactgtttatgtaagcagacagttttattgtcatgat
gatataattttatctgtgcaatgtaacatcagagatcttgagacacaacgtggcttggtaataaatcgaacttttctgagttg
aaggatcagctcagttaccaatgcttaacagtgaggcacctatctcagcagctgtctatttcttcatccatagttgcctg
actccccgctgtagataactacgatacgggagggttaccatctggccccagtgctgcaatgataccgagaccac
gctcaccggctccagattatcagcaataaacagccagccggaagggccgagcgcagaagtggctcctgcaactttatc
cgctccatccagcttattaattgttccgggaagctagagtaagtagttccagtaatagtttgcgaacggttggccat
tgctacaggcagctggtgtcacgctcgtctgttggatggcttcatcagctccggttccaacgatcaaggcgagttacat
gatccccatgttggcaaaaaagcggttagctccttcggtcctccgatcgttgcagaagtaagttggccgcagtggtatc
actcatggttatggcagcactgcataattcttactgtcatccatccgtaagatgcttttctgtgactggtgagtactcaacc
aagtcattctgagaatagtgatgaggcgaccgagttgctcttcccggcgtcaatacgggataataaccgcccacatag
cagaacttfaaaagtgtcatcattggaaaacgttcttcggggcgaactctcaaggatcttaccgctgttgatccagtt
cgatgaaccactcgtgcaccaactgatcttcagcatctttactttcaccagcgttctgggtgagcaaaaacaggaag
gcaaaatgccgcaaaaaagggaataagggcgacacggaatgttgaatactcactcttcttttcaatattattgaagc
attatcagggttattgtctcatgagcggatacatattgaatgtatttagaaaaataaacaataggggttccgpcacatttc
ccgaaaagtgccactgacgtctaagaaccattatcatgacattaacctataaaaaataggcgtatcagaggcaga
atttcagataaaaaaatccttagcttctcgtactaaggatatttctggaattcgcggccgcttctagag

Table A. 1 Genetic parts DNA sequence.

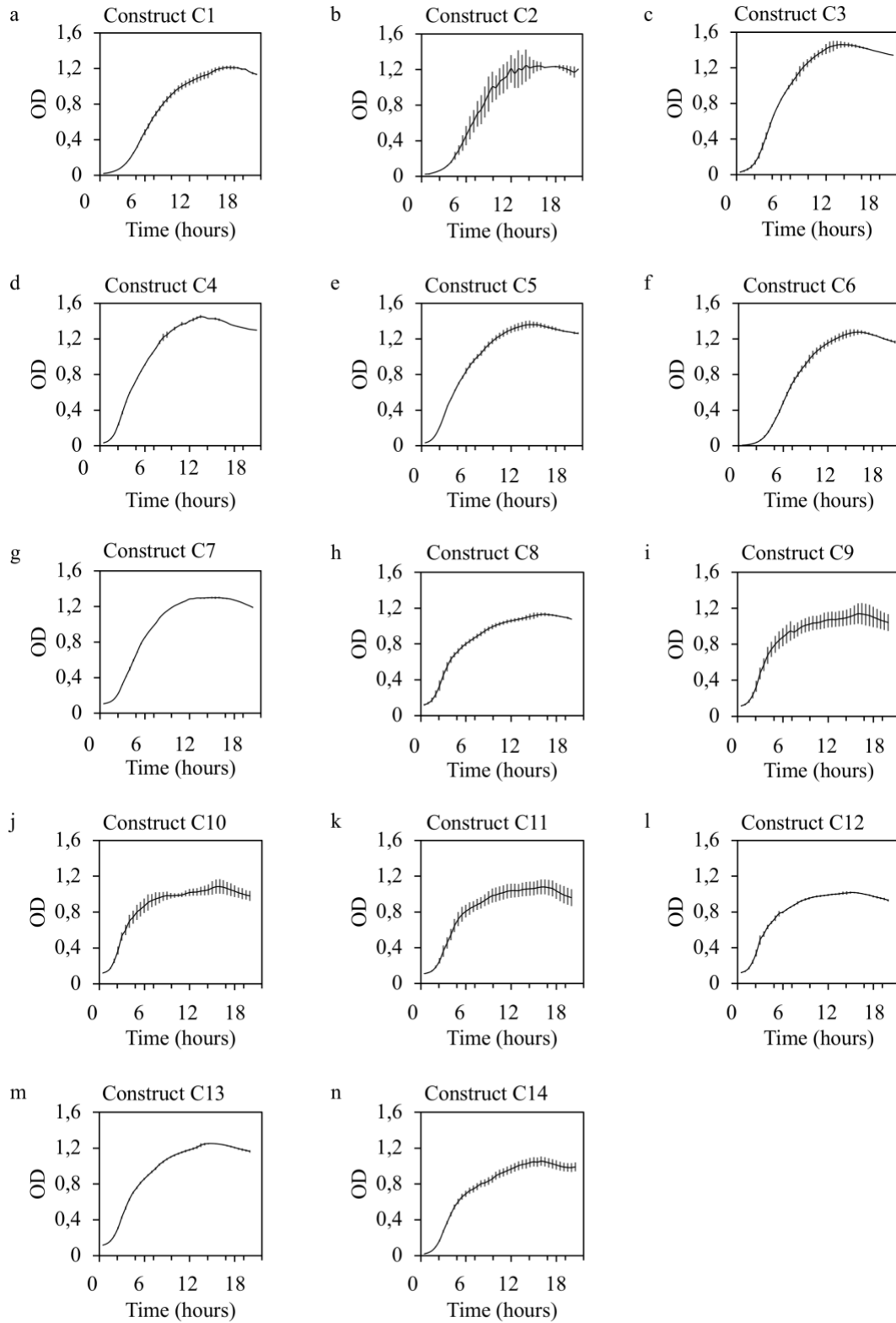


Figure A. 1 Temporal evolution of the optical density OD.

B. 2D BioPrintable Computational Circuits: modular topology for digital computation.

Part	DNA Sequence
BBa_B0014	tcacactggctcaccttcgggtgggcctttctgcgfttatatactagagagagaatataaaaagcca gattattaatccggctttttattattt
BBa_R0032	tcacacaggaaag
BBa_R0033	tcacacaggac
BBa_R0034	aaagaggagaaa
BBa_I0500	ttatgacaactgacggctacatcattcactttttctcacaaccggcacggaactcgctcgggctg gccccggtgcatttttaaataccgcgagaaatagagttgatcgtaaaaccaacattgcgaccg acggtggcgataggcatccgggtgggtgctcaaaagcagcttcgctggctgatacgttgctctc ggccagcttaagacgctaaccctaactgctggcggaaaagatgtgacagacgcgacggcga caagcaaacatgctgtgacgctggcgatatcaaaattgctgtctgccaggtgatcgctgatgta ctgacaagcctcgcgtaccggattatccatcggtggatggagcgaactcgtaacgcttccatgcg ccgcagtaacaattgctcaagcagatttatcgccagcagctccgaatagcgccttccccttgccc ggcgtaatgattgcccacaggtcgctgaaatgcggctggtgcgcttcatccgggcgaaaga accccgtattggcaaatattgacggccagttaagccattcatgccagtaggcgcgaggacgaaa gtaaacccactggtgataccattcgcgagcctccggatgacgaccgtagtgatgaatctctctg gcggaacagcaaaatatacccggctggcaaaaattctcgtccctgattttaccaccccct gaccgcgaatggtgagattgagaatataaccttcattcccagcggctcggctgataaaaaatcga gataaccgttggcctcaatcggcgtaaacccgccaccagatgggcattaaacgagtatcccgg cagcaggggatcattttgcgcttcagccatacttttcatactcccgcattcagagaagaaccaat tgtccatattgcatcagacattgccgtcactgcgcttttactggctcttctcgtacccaaaccggt accccgttattaaaagcattctgtaacaaagcgggaccaaaagccatgacaaaaacgcgtaaca aaagtgtctataatcaggcagaaaagtcacattgattttgcacggcgtcacactttgctatgc catagcattttatcataagattagcggatcctacctgacgctttttatcgcaactctctactgttctc cataaccgftttttgggctagc
BBa_J23100	ttgacggctagctcagtcctaggtacagtgtctagc
BBa_J23105	tttacggctagctcagtcctaggtactatgctagc
BBa_R0011	aattgtgagcggataacaattgacattgtgagcggataacaagatactgagcaca

BBa_R0062 acctgtaggatcgtacaggtttacgcaagaaatggtttgtatagtgaataaa

BBa_R0040 tcctatcagtgatagagattgacatccctatcagtgatagagatactgagcac

atgacagtaaagaagctttatttcgtcccagcaggtcgtgtatgttgatcattcgtctgtaatagt
acattaacaccaggagaattattagactaccggtttggtgttatctttggagactgaagaaggac
ctttttagtagatacaggtatgccagaaagtgcagtaataatgaaggcttttaacggtacattg
tcgaagggcaggtttaccgaaaatgactgaagaagatagaatcgtgaatattttaaacgggtg
gttatgagccggaagaccttctttatattattagttctcacttgcatttgatcatgcaggaggaaatg
gcgctttataaatacaccaatcattgtacagcgtgctgaatatgaggcggcgcagcatagcgaa

BBa_C0060 gaatattgaaagaatgtatattgccgaattaaactacaaaatcattgaaggtgattatgaagtcgta
ccaggagtcaattattgcatacaccaggccatactccaggcatcaatcgtatttaattgagaca
gaaaaatccggtcctgtattattaacgattgatgcatcgatacgaagagaatttgaaaaagaagt
gccatttgcgggatttgattcagaattagctttatctcaattaacgfttaaaagaagtggtgatgaa
agagaagccgattgtttctttggacatgatatagagcaggaaaggggatgtaaagtgtccctga
atatatagctgcaaacgacgaaaactacgctttagtagcttaataacgctgatagtgtagtaga
tcgc

atgactataatgataaaaaatcgatttttggcaattccatcggaggagtataaaggatttctaag
tcttcgttatcaagtgttaagcaaagacttgagtgaggacttagttgtagaaaataacctgaatcag
atgagtatgataactcaaatgcagaatattatgcttggatgatactgaaaatgtaagtgatgct
ggcgtttattacctacaacaggtgatttatgctgaaaaggttttctgaattgcttggtcaacaga
gtgctcccaaagatcctaataatagtcgaattaagtcgtttgctgtagtaaaaatagctcaagata
BBa_C0061 aataactctgctagtgaattacaatgaaactatttgaagctatatataaacacgctgttagtcaagg
tattacagaatatgtaacagtaacatcaacagcaatagagcattttaaagcgtattaaagttcctt
gtcatcgattggagacaaagaaatcatgtattaggtgataactaaatcgggtgtattgtctatgccta
ttaatgaacagtttaaaaaagcagcttaaatgctgcaaacgacgaaaactacgctttagtagctta
ataactctgatagtgtagtagatctc

atgaaaaacataaatgccgacgacacatacagaataattaataaaaattaaagcttgtagaagcaat
aatgatattaatcaatgcttattctgatatgactaaaatggtacattgtgaatattttactcgcgatcat
ttatcctcattctatggttaaatctgatatttcaatcctagataattaccctaaaaaatggaggcaatatt
BBa_C0062 atgatgacgctaatttaataaaatgatcctatagtagattattctaactccaatcattcaccatatt
tggaatataattgaaaacaatgctgtaataaaaaatcctcaaatgtaattaaagaagcgaaaacat
caggcttactcagggttagtttccctattcatcaggcctaacaatggcttcggaatgcttagtttgc
acattcagaaaaagacaactatatagatagttttttacatgcgtgatgaacataccattaattgtt

ccttctctagttgataattatcgaaaaataaatatagcaaataataaatcaacaacgatttaaccaa
aagagaaaaagaatgtttagcgtgggcatgcgaaggaaaaagctcttgggatatttcaaaaatatt
aggttgcagtgagcgtactgtcactttccatttaaccaatgcgcaaatgaaactcaatacaacaac
cgctgccaaagtatttctaaagcaatttaacaggagcaattgattgccatacttataaataataa
cactgatagtgtagtagatcac

BBa_C0012

atggtgaaatgtgaaaccagtaacgttatacagatgtcgcagagtatgccggtgtcttatacagacc
gttcccgcgtgggaaccaggccagccacgtttctgcgaaaacgcgggaaaaagtgaagcg
gcgatggcggagctgaattacattccaaccgctggcacaacaactggcgggcaaacagtcg
ttgctgattggcgttccacccagcttggcctgcacgcgccgtcgaattgtcgcggcgatt
aaatctcgcgccgatcaactgggtgccagcgtgggtgtcgcgatgtagaacgaagcggcgtc
gaagcctgtaaagcggcgggtgcacaatcttctcgcgcaacgcgtcagtggtgatcattaacta
tccgctggatgaccaggatgccattgctgtggaagctgcctgcactaatgttccggcgttatttctt
gatgtctctgaccagacacctcaacagtatttttctccatgaagacggtacgcgactgggc
gtggagcatctggtcgcattgggtcaccagcaaatcgcgctgttagcgggccattaagtctgtc
tcggcgcgtctgcgtctggctggctggcataaatatctcactcgcgaatcaaatcagccgatagcg
gaacgggaaggcgcactggagtgcatttccggtttcaacaacatgcaaatgctgaatgagg
gcatcgttcccactgcgatgctggttccaacgatcagatggcgtgggcgcaatgcgcgccatt
accgagtccgggctgcgcgttgggtgcggatatctcggtagtgggatacgcgataccgaagaca
gctcatgtatatacccgcgtaaccacatcaaacaggattttgcctgctggggcaaacaccgcg
tggaccgctgtgcaactctctcagggccaggcgggaagggcaatcagctgttcccgtctca
ctggtgaaaagaaaaaccacctggcgcaccaatacgaacccgctctcccgcgcgttggcc
gattcattaatgcagctggcacgacaggttcccactggaaaagcgggcaggctgcaaacgacg
aaaactacgctttagtagcttaataactctgatagtgtagtagatctc

BBa_E0040

atgcgtaaaggagaagaactttcactggagttgtccaattcttgtgaattagatggtgatgtaat
gggcacaaatcttctgcagtgagagggtgaaggtgatgcaacatacggaaaactacccttaa
atftatttgcaactactgaaaactacctgttccatggccaacactgtcactactttcggttatggtgtt
caatgctttgcgagataccagatcatatgaacagcatgacttttcaagagtccatgcccga
ggttatgtacaggaaagaactatattttcaagatgacgggaactacaagacacgtgctgaagtc
aagttgaaggtgatacccttgaatagaatcgagttaaaaggtattgattttaaagaagatggaaa
cattcttgacacaaattggaatacaactataactcacacaatgtatacatcatggcagacaaaca
aagaatggaatcaaagtaacttcaaattagacacaacattgaagatggaagcgttcaactagca
gaccattatcaacaaaatactccaattggcgtatggccctgtcctttaccagacaaccattacctgtc

cacacaatctgcccttcgaaagatccaacgaaaagagagaccacatggctcctcttgagttgt
aacagctgctgggattacacatggcatggatgaactatacaataataa

BBa_E1010

atggctcctccgaagacgttatcaagagttcatgcgttcaaagttcgatggaaggtccgtaa
cggtcacgagttcgaatcgaaggtgaaggtgaaggtcgtccgtacgaaggtaccagaccgc
taaactgaaagttaccaaggtggctccgtcgttgggacatcctgtccccgcagtcca
gtacggttccaaagcttacgttaaacacccggctgacatccggactacctgaaactgtcctccc
ggaaggttcaaattgggaacgtgtatgaactcgaagacgggtggtgtgtaccgttaccagga
ctcctccctgcaagacgggtgagttcatctacaaagttaaactcgtggtaccaactcccgtccga
cggtcgggttatgcagaaaaaacatgggttgggaagctccaccgaacgtatgtaccggaa
gacggtgctctgaaaggtgaaatcaaatcgtctgaaactgaaagacgggtgctactacgacg
ctgaagttaaaccacctacatggctaaaaaacgggtcagctgccgggtgcttaciaaacggac
atcaaactggacatcacctcccacaacgaagactacaccatcgttgaacagtacgaacgtgctga
aggtcgtcactccaccgggtgcttaataacgctgatagtgtagttagatcgc

Table A. 3 Genetic parts DNA sequence.

Plasmid map

Plasmid map

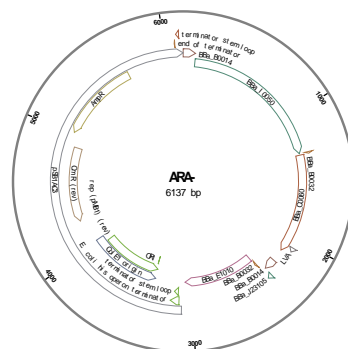
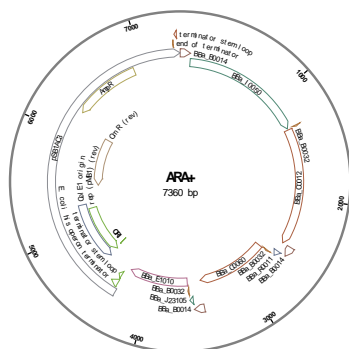
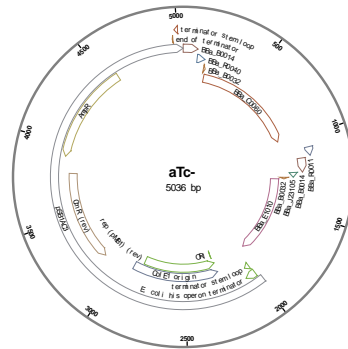
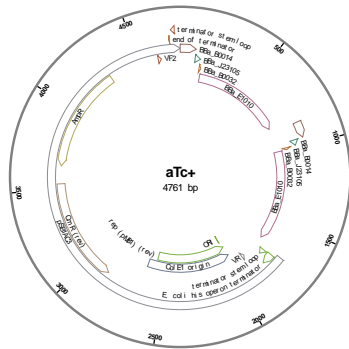
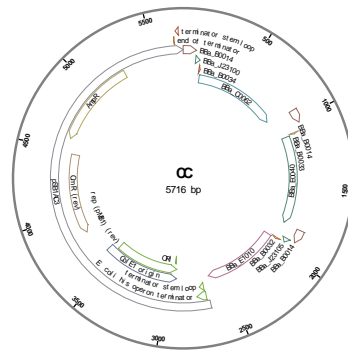
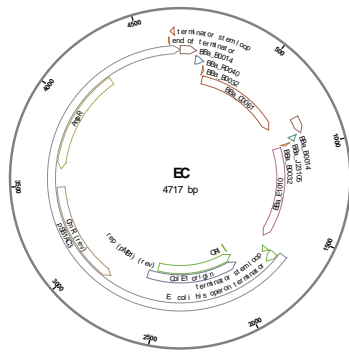


Table A. 4 Plasmid maps.

